Investigating the effects of antisense oligonucleotides on RNA editing and gene expression in SH-SY5Y cells

Ilda Qistina Sethw Hassan

School of Biological Sciences

Royal Holloway, University of London

Research thesis submitted for the degree of Doctor of Philosophy

Declaration of Authorship

I, Ilda Qistina Sethw Hassan, hereby declare that this thesis and the work presented in it is entirely my own. Where I have consulted the work of others, this is always clearly stated.

Signed: _____

Date: _____

ABSTRACT

RNA editing is a posttranscriptional modification mechanism that changes gene-specified codons. One of the main forms of RNA editing is the conversion of adenosine to inosine by the enzyme adenosine deaminase (ADAR) acting on the RNA of the GluA2 subunit of AMPA receptors. AMPA receptors (AMPARs) are a subset of ionotropic glutamate receptor composed of one or more of four subunits (GluA1-4). Incorporation of the GluA2 subunit and expression of the edited Q/R site is required to reduce calcium permeability. Deficient RNA editing has been shown to trigger significant neuron cell death in patients with motor neuron disease. Adenosine deaminase (ADAR2) exists as multiple splice variants. In one variant, the inclusion of a 120 bp AluJ cassette has been shown to reduce the catalytic activity of ADAR2. We sought to investigate the effects of specifically targeted PMOs that manipulate the alternative splicing of ADAR2 in SH-SY5Y cells and increase the expression of the more catalytically active ADAR2-AluJ exon 5a-absent isoform. Subsequently, we examined the gene expression of Pin1 and WWP2 in cells following PMO transfection, as these two proteins are known to regulate ADAR2 activity.

Our results show that the PMOs were able to induce alternative splicing events in SH-SY5Y cells, where increase in both exon skipping of the AluJ cassette and RNA editing levels was observed compared to baseline levels. Hence, the PMOs are able to manipulate RNA editing in cell lines endogenously expressing GluA2. Additionally, increased expression of the ADAR2a-AluJ exon 5a-absent isoform upregulated Pin1 gene expression, whereas WWP2 gene expression was downregulated. Hence, the ADAR2a-AluJ exon 5a-absent isoform can regulate gene expression of both Pin1 and WWP2, suggesting significant implications for their roles in neurodegenerative disorders. Taken together, our findings suggest PMO-induced changes in RNA editing can influence the gene expression of proteins regulating ADAR2-activity.

ACKNOWLEDGEMENTS

Firstly, I would like to thank my supervisor, Philip Chen, for all the help and guidance throughout my PhD. Your support has allowed me to think critically and develop my abilities as a researcher. Thank you for your endless patience. I would also like to thank Linda Popplewell and Pavlos Alifragis for the knowledge and invaluable feedback given to me throughout this process. It was a pleasure to have worked under all of your supervision.

To all official (Anila, Jade, Al, Amninder) and honorary (Marc and Leoni) members of Lab 302A, thank you for the friendship and constant motivation you have all given me. Thank you everyone for the laughs, McDonald's sessions, and car rides. Anila, for being there since our Palm Palace days all the way up until Jumeirah Lounge. To my very own Dear Mr Royal Holloway, Al, and Amninder, for being the best lads standing anyone could ever ask for. I honestly would not have survived this PhD if it weren't each and every one of you – you all believed in me when I did not believe in myself.

To Tiara, thank you for being there for me no matter what, for visiting me every year, and being such an understanding friend. Farhan, I thank you for always being a phone call away and giving me valuable advice on protocol optimisation and data analysis. I'm grateful that I can depend on you both despite the distance between us.

To Qish, Taty and Irena – thank you for cheering me up when I needed it most. I am beyond thankful that we are not only sisters, but we confide in each other as friends as well. Thanks especially to Qish for always providing me with a place to stay when I needed a weekend away.

To Dad and Ummi, thank you for the financial and emotional support you have given me. Being away from you both hasn't been easy but I am grateful for your constant visits (even meeting me halfway), making home feel a little bit closer. To Papi, thank you for the sage advice you have given me, your light-

hearted jokes (and cashew chicken), and making the time I spent writing my thesis back home a lot easier.

And finally, to my mum, Sheila Halim – I literally would not be carrying out this PhD if it weren't for you. Thank you for pushing me to where I am today, and for sharing this dream with me. You have always believed in my abilities, and you taught me that hard work and faith will get you where you want to in the end. The support you have provided me with is priceless. I dedicate this thesis to you.

ABBREVIATIONS

ADAR	adenosine deaminase
AAV	adeno-associated virus
ALS	amyotrophic lateral sclerosis
AMPA	α-amino-3-hydroxy-5-methyl-4-isoxazolepropionic acid
ANG	angiogenin
APS	ammonium persulfate
ASO	antisense oligonucleotide
BMD	Becker muscular dystrophy
CNS	central nervous system
DMD	Duchenne muscular dystrophy
DMEM	Dulbecco's modfified Eagle's media
DMSO	dimethyl sulfoxide
DNA	deoxyribonucleic acid
ECS	editing site complementary sequence
ER	endoplasmic reticulum
ESE	exon splice enhancer
ESS	exon splice silencer
fALS	familial amyotrophic lateral sclerosis
FBS	fetal bovine serum
FDA	food and drug administration

FTD	frontotemporal dementia
FUS	fused in sarcoma
GWAS	genome-wide association studies
IFN	interferon
ISE	intron splice enhancer
ISRE	interferon-sensitive response element
ISS	intronic splice silencer
LBD	ligand-binding domain
LNA	locked nucleic acid
MND	motor neuron disease
MOE	methoxy-ethyl
mRNA	messenger RNA
NGS	next-generation sequencing
NLS	nuclear localization signal
NMDA	N-methyl-D-aspartate
OPTN	optineurin
PBS	phosphate buffered saline
PCR	polymerase chain reaction
PDL	poly-D-lysine
PMO	phosphorodiamidate morpholino oligonucleotide
PS	phosphorothioate
qRT-PCR	quantitative reverse transcriptase PCR

RIPA	radio immunoprecipitation assay
RNA	ribonucleic acid
RT-PCR	reverse transcriptase PCR
sALS	sporadic amyotrophic lateral sclerosis
SMA	spinal muscular atrophy
SNP	single nucleotide polymorphism
SOD1	superoxide dismutase 1
TAE	tris-acetate-EDTA buffer
TARDBP	TAR DNA-binding protein
TARP	transmembrane AMPA receptor regulatory proteins
TBS	tris buffered saline
TEMED	tetramethylethyldiamine
TM	transmembrane

Table of Contents

TABLE OF FIGURES

TABLE OF TABLES

CHAPTER 1 INTRODUCTION

1.1 α-AMINO-3-HYDROXY-5-METHYL-4-ISOXAZOLEPROPRIONIC ACID (AMPA) RECEPTORS

1.1.1 INTRODUCTION

Synaptic plasticity can be regulated at the presynaptic side by modifying the efficacy of neurotransmitter release, or on the postsynaptic side by changing the density, types, and properties of neurotransmitter receptors. AMPA receptors (AMPARs) are the primary ionotropic glutamate receptors that mediate fast excitatory synaptic transmission in mammalian brain. AMPARs are tetrameric assemblies of highly homologous subunits encoded by four different genes, GluA1-4 (Wisden & Seeburg, 1993). The trafficking of AMPARs into and out of synapses is highly dynamic and undergoes regulation by various post-translational modifications that occur on their C-terminal domains. The regulated trafficking of AMPARs is a key mechanism underlying activity-induced changes in synaptic transmission (Shepherd & Huganir, 2007).

1.1.2 AMPA RECEPTOR STRUCTURE

AMPARs are mainly impermeable to Ca^{2+}, exhibit remarkably fast kinetics, and mediate fast synaptic transmission. These functional properties rely on the subunit composition and alterations induced by alternative splicing events. The subunits GluA1-GluA4 can exist as homomeric or heteromeric tetramers in distinctive stoichiochemistries, determining channel function and synaptic trafficking. Each subunit is made up of roughly 900 amino acids and weigh approximately 105 kDa. Subunits GluA1-GluA4 share 68-74% amino acid sequence identity and comprise of four hydrophobic domains; M1, M3 and M4 transverse the domain, while M2 enters the lipid bilayer as a re-entrant loop

which makes up part of the channel pore (Santos, Carvalho, Caldeira, & Duarte, 2009) (Figure 1.1).

The ligand-binding domain (LBD) is divided into S1 and S2 segments by the transmembrane (TM) segments (Figure 1.1). Ligand binding to this domain initiates conformational modifications that are transduced to the TM segments and activate the channel gates opening. The N-terminus, the LBD, and ion-channel domain are involved in separate and interdependent subunit-subunit interactions. The C-terminal of the S2 does not play a direct role in agonist binding. The C-terminal is expressed in two isoforms – flip and flop – due to alternative RNA splicing. The alternative splice cassette is located at the C-terminal end of the loop between M3 and M4. Even though these isoforms only differ by a few amino acids, this results in AMPA receptors with distinctive desensitisation and endoplasmic reticulum (ER) export kinetics (Santos et al., 2009).

RNA editing, a process that involves enzymatic deamination of ribonucleotides in pre-spliced mRNA, is a regulator of AMPA receptor permeability (Bass, 2002). Glutamine to arginine (Q/R) editing in the M2 region regulates calcium permeability and channel rectification in the ion channel pore region of the GluA2 subunit. This editing process also affects the endoplasmic reticulum retention of the subunit (Shepherd & Huganir, 2007). Editing of an arginine (R) codon to a glycine (G) codon, which occurs in the S2 loop of GluA4, modifies resensitisation kinetics, where edited G forms recover faster from desensitisation (Shepherd & Huganir, 2007). Little is known regarding the regulation of these splicing and editing events. In neurons, alternative splicing is regulated by neuronal activity, such as the GluN1 subunit splicing of the NMDA receptor (Mu, Otsuka, Horton, Scott, & Ehlers, 2003). However, it is still unclear whether neuronal activity regulates AMPAR subunit editing or splicing.

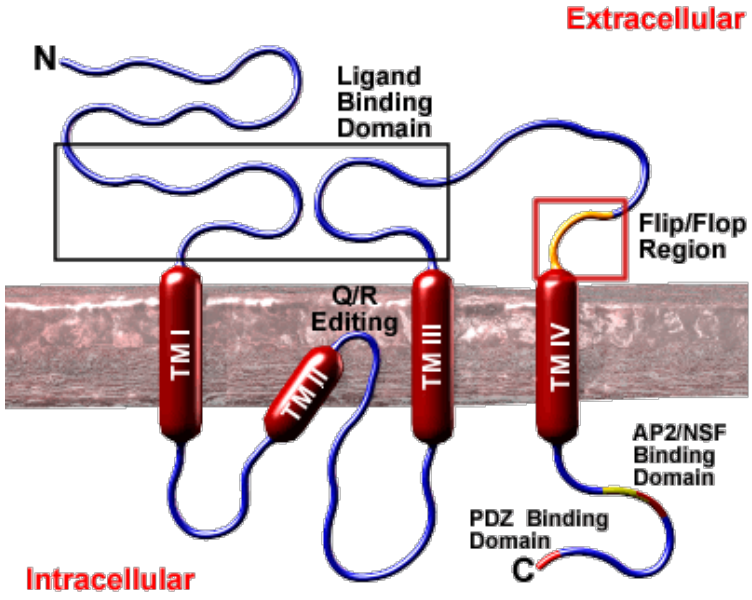

Figure 1.1 AMPA receptor structure.

Structure of the GluA2 subunit. The subunit illustrates the structural properties of the AMPA receptor subunits. The N-terminus is extracellular while the C-terminus is intracellular. Splice variation occurs in the 'Flip/Flop' region, resulting in two variants for each gene sequence. The C-terminus contains binding regions for various intracellular proteins. Figure retrieved from: **http://www.bristol.ac.uk/synaptic/receptors/ampar/**.

1.1.3 THE GLUA2 SUBUNIT

The ability of Ca^{2+} to enter the cell through the AMPARs is determined by the GluA2 subunit, which is preferentially incorporated into the receptor (Sans et al., 2003). AMPARs made up of subunits GluA1, GluA3 and GluA4 are highly permeable to Ca^{2+}, whilst GluA2-containing AMPARs have profoundly decreased permeability to Ca^{2+} (Burnashev et. al., 1992). Since most AMPARs are hetero-oligomers that consist of GluA1/GluA2 or GluA2/GluA3 subunits, they are thus Ca^{2+}-impermeable (Wright & Vissel, 2012).

Most mature GluA2 protein contains an arginine residue (R) within the re-entrant M2 membrane loop region at amino acid residue position 607 in place of the genomically encoded glutamine (Q) (Sommer, Kohler, Sprengel, & Seeburg, 1991). This alteration is the outcome of hydrolytic editing of a single adenosine base in the pre-mRNA to an inosine by the adenosine deaminase enzyme ADAR2 (Higuchi et al., 1993) (Figure 1.2). This Q/R editing is specific to the GluA2 subunit; more than 95% of GluA2 mRNA transcripts are edited in postnatal brain (Isaac, Ashby, & McBain, 2007). This editing is vital for brain function as revealed by premature death and neurological dysfunctions as early-onset epilepsy of mice heterozygous for an editing-deficient GluA2 allele and $ADAR2^{-/-}$ mice as well (Bassani, Valnegri, Beretta, & Passafaro, 2009). Interactions between the GluA2 subunit and its intracellular and extracellular partners such as transmembrane AMPA receptor regulatory protein (TARP) and PDZ proteins (protein molecules that recognise short motifs at the C-terminus) have been shown to be critical in determining AMPAR functions at the synapse, including trafficking, some forms of synaptic plasticity, and the formation and maturation of dendritic spines (Bassani et al., 2009).

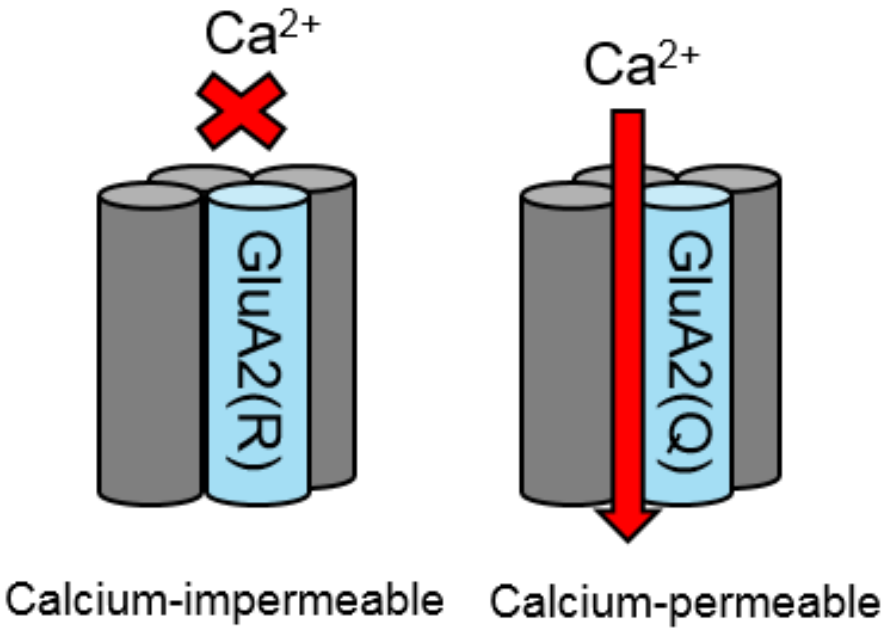

Figure 1.2 Schematic diagram of the GluA2 structure.

AMPA receptors containing edited GluA2 are impermeable to Ca^{2+} (left). AMPA receptors containing unedited GluA2 and lacking GluA2 are Ca^{2+}-permeable (right).

1.2 RNA EDITING

1.2.1 OVERVIEW

The term “RNA editing” was first conceived in 1986 to refer to the process of uridine residue insertion into mitochondrial mRNA in trypanosomes encoding cytochrome oxidase subunit II (Benne et al., 1986). The term is now used to describe insertion, deletion, as well as conversion of one base to another. Uridine to cytidine conversion through amination is rare and has only been discovered in the transcript encoding Wilms’ tumour susceptibility gene in mammals. The removal of an amine group, known as deamination, is most common and takes place on several bases within DNA or RNA; adenosine to inosine (A-to-I) and cytosine to uracil (C-to-U) (Hogg et. al., 2011). A-to-I editing modifies the information content of the RNA molecule, as inosine favourably base pairs with cytidine, causing the translational machinery to interpret inosine as guanosine (G). The three-dimensional structure of the dsRNA, which determines its RNA-binding protein interactions, is also altered due to the addition or removal of bulges formed by mismatched base pairs (Zinshteyn & Nishikura, 2010).

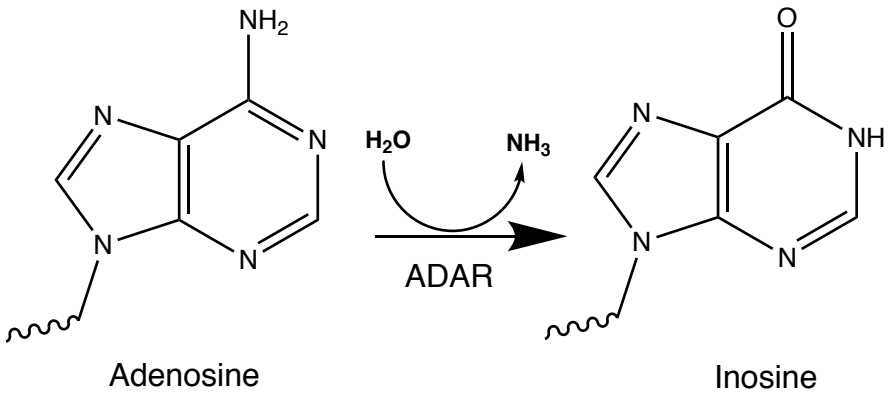

Figure 1.3 Adenosine deamination.

ADAR enzymes catalyse A-to-I hydrolytic deamination, where an adenosine loses an amine group and is converted to inosine.

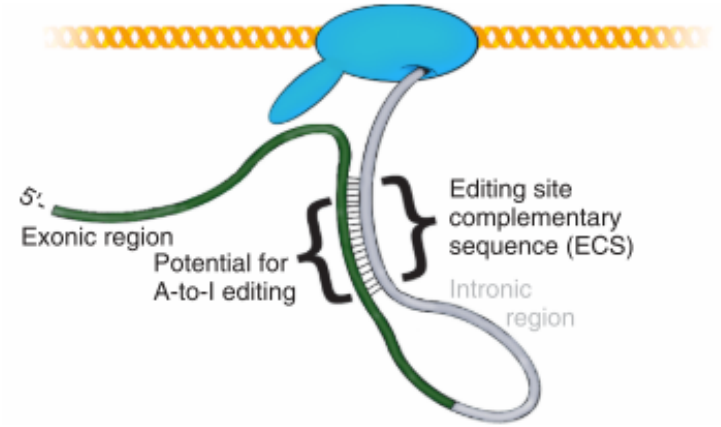

Figure 1.4 Formation of the double-stranded structure required for editing by ADAR.

mRNAs form the double-stranded structure required for ADAR editing due to the incorporation of the editing-site complementary sequence (ECS) in the intronic region, allowing base-pairing with the exonic region. Stretches of imperfectly base-paired dsRNA in precursor mRNA (pre-mRNA) are then formed, suitable for potential ADAR A-to-I editing. Figure adapted from Wulff and Nishikura (2010).

A-to-I conversion is catalysed by the enzyme family adenosine deaminase (ADAR) acting on RNA (Figure 1.3). In this process, ADARs were initially recognised to unwind dsRNA in *Xenopus laevis* embryo extracts, showing a different migration pattern when electrophoresised on a native polyacrylamide gel (Bass & Weintraub, 1987). The dsRNA was modified as such that up to half of the adenosine residues were deaminated to inosines (Bass & Weintraub, 1988).

Three structurally related ADARs (ADAR1 to ADAR3) have been identified in mammals (Kwak & Kawahara, 2005). ADAR1 and ADAR2 are expressed in most tissues and recognise the adenosine residue to be edited through the duplex structure that is formed between the editing site and its editing site complementary sequence (ECS), which is located downstream of the pre-mRNA intron (Higuchi et al., 1993) (Figure 1.4). ADAR3 is thought to be catalytically inactive and is only expressed in the brain (Hogg et al., 2011).

1.2.2 STRUCTURAL FEATURES OF ADAR

ADARs are modular proteins that share a common domain architecture comprising of several amino-terminal dsRNA binding domains (dsRBDs), which make direct contact with dsRNA substrates, and a carboxy-terminal catalytic deaminase domain (Figure 1.5a) (Mannion, Arieti, Gallo, Keegan, & O'Connell, 2015). Each dsRBD (three in ADAR1 and two in ADAR2 and ADAR3) contains an α-β-β-α topology made up of roughly 70 amino acids, where the two α helices are packed alongside a three-stranded anti-parallel β sheet. The dsRBDs are thought to synergistically act together, thus increasing the specificity and affinity for dsRNA targets (Tomaselli et al., 2013).

The *ADAR1* gene was mapped to the locus of c1q21.1-21.2 in humans at a size of ~30 Kbp (Weier, George, Greulich, & Samuel, 1995). ADAR1 is made up of two different isoforms: a 150 kDa protein (ADAR1 p150) which is induced by interferon (IFN) and a 110 kDa protein (ADAR1 p110) that is expressed constitutively (Figure 1.5b). ADAR1p150 initiates translation on exon 1A (AUG1) while ADAR1p110 starts from exon 2 (AUG296) (Patterson & Samuel, 1995) (Figure 1.5b). The different isoforms are caused by alternative splicing in exon 1. Exon 1A contains an IFN-inducible promoter with a 12-bp IFN-stimulated response element (ISRE), thus generating a transcript coding for the longer ADAR1p150 isoform. Transcripts that encode ADAR1p110 are generated from different promoters located within exon 1B, 1C, and exon 2 (C. X. George & Samuel, 1999). Since both exons 1B and 1C do not contain translation initiation sites, translation starts at codon AUG296 located in exon 2. Other alternative splicing events identified within exon 7 generates variants that contain either exon 7a or 7b (Figure 1.6). Exon 7a contains 26 amino acids that are not found in exon 7b (Yong Liu, George, Patterson, & Samuel, 1997). (Figure 1.6) Additionally, exon 7a is present in ADAR1p110 transcripts whilst exon 7b is found in ADAR1p150 transcripts (Cyril X. George, Wagner, & Samuel, 2005).

A feature that is exclusive to ADAR1 is the presence of Z-DNA binding domains (ZBDs) at the N-terminus (Figures 1.5a and b). The Zα domain is

found only in ADAR1p150 while the Zβ domain can be found in both ADAR1p110 and ADAR1p150. Only the Zα domain has Z-DNA/RNA binding capacity. Even though the functional importance of the ZBDs in ADAR1 is unclear, Zα domain-containing proteins have been associated with the type I IFN response pathway. The Zα domain is also vital for ADAR1p150 localisation to cytoplasmic stress granules resulting from the activation of type I IFN-induced stress (Mannion et al., 2015).

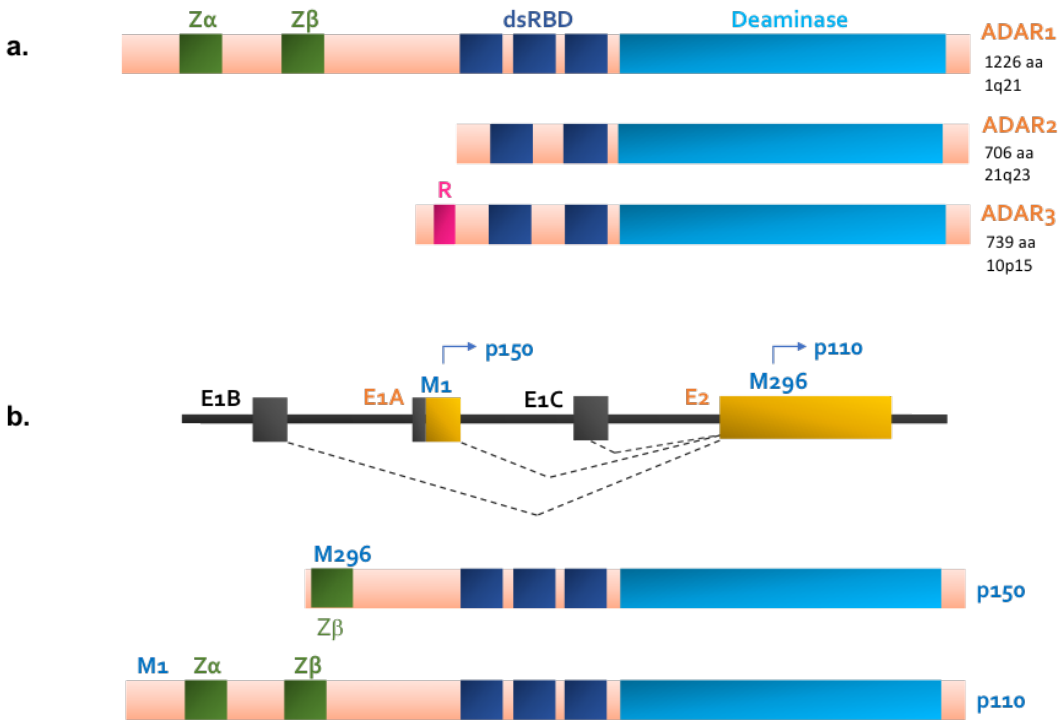

Figure 1.5 Structure of ADAR1, ADAR2, and ADAR3.

a) Indicated are the two Z-DNA binding domains (ADAR1), the dsRNA binding domains (dsRBDs). the arginine-rich, ssRNA binding domain (R domain), and the deaminase domain. The amino acid lengths and chromosomal location are shown. b) Two translation products of ADAR1. Exons E1A (IFN/ds-RNA inducible) and E1B AND E1C (constitutive) are spliced to exon 2 at approximately the same junction. Exon 1A incorporates the Met start codon for the 1226-aa ORF that specifies the IFN/dsRNA inducible p150 protein, Exons 1B and 1C do not comprise of an AUG start codon. The second AUG start codon found in exon 2 initiates translation of the 931-aa encoding ADAR1 p110 protein. Figure adapted from Maas *et. al.* (2006).

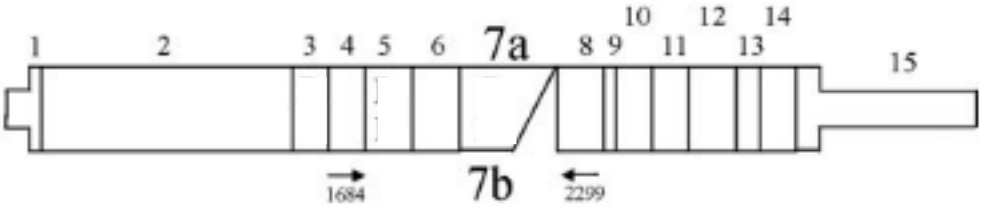

Figure 1.6 Differential expression of ADAR1 exon splice variants.

Schematic structure of the two ADAR1 exon 7 splice variants, designated as 7a and 7b, Exon 7a corresponds to the full-length 74-aa version of the mouse exon 7. Exon 7b lacks 26 aa encoded by the 3' end of exon 7a as a result of alternative splicing. Figure taken from George *et al*, 2005.

The human *ADAR2* human gene spans a size of ~153 Kbp. While the promoter responsible for ADAR2 expression has not been functionally characterised, a putative promoter region upstream of a recently identified exon was described for both human *ADAR2* and mouse *Adar2* gene. This promoter contains a TATA box sequence and binding sites for nuclear factor kappa-light-chain-enhancer of activated B cells (Nf-κ B) and Specificity Protein 1 (SP1). Subsequently, ADAR2 localisation into the cell nuclei is directed by importin α1, α4, and α5. ADAR2 can form homodimers and heterodimers with ADAR1. Dimerisation of ADAR2 appears to be vital for editing activity, although whether or not this interaction is mediated by dsRNA is still uncertain (Tomaselli et al., 2013).

Recombinant ADAR3 has been shown to bind to both dsRNA and ssRNA *in vitro*. Site-directed mutagenesis of ADAR3 revealed that it binds ssRNA through an arginine/lysine-rich domain (R-domain) positioned in the N-terminus, similar to that of ADAR2 (Figure 1.5a). This domain is essential for determining the subcellular localisation of ADAR3 and acts as an NLS. The importin alpha-1 factor KPNA2 interacts with this R-domain to promote nuclear import of ADAR3. ADAR3 remains in its monomeric form, partly explaining its lack of editing function. Hence, its function is still unknown, although its ability to bind to ss- and dsRNAs suggests a regulatory function over ADAR1 and ADAR2. ADAR3 can in fact contest for dsRNA substrates, which inhibits binding of the other ADAR enzymes (Mannion et al., 2015).

1.2.3 ADAR2

ADAR2 is an 80-kDa nuclear protein containing two ds-RNA binding domains (dsRBDs) in the amino-terminal region, and an adenosine deaminase domain near the carboxyl terminus, is responsible for most A-to-I editing modifications occurring in mammals (Feng et. al., 2006). It is a nuclear protein and has been shown to localise to the nucleolus in a dynamic manner (Dawson et. al., 2003). In cells transfected with plasmids that encode editable transcripts, ADAR2 was found to re-localise to the nucleoplasm where it carries out editing of the transcripts (Desterro et al., 2003). The nuclear localisation sequence (NLS) for ADAR2 has been recently discovered. Two NLS elements are positioned nearby each other in the amino terminus, adjacent to the first dsRBD (Behm, Wahlstedt, Widmark, Eriksson, & Öhman, 2017). Nuclear localisation requires the interaction between importin-α and ADAR2.

Whilst ADAR2 has been found to act as the primary editor of non-repetitive coding regions, the extent of variation of RNA editing caused by ADAR enzyme expression is not well-understood. Coding sites in over 8000 Gentoype-Tissue Expression (GTEx) samples revealed that ADAR2 expression in non-repetitive coding sites accounted for 25% of variation in RNA editing. This is in contrast to ADAR1 expression at the same sites, which accounted for only 6% of total variation (Tan et al., 2017). *In vivo* ADAR2 targets were determined by examining multiple adult tissues from wild-type and $Adar^{-/-}$ $Gria2^{R/R}$ mice. The results showed that ADAR2-deficient mice had lower than average editing levels compared to wild type tissues. A total of 976 sites were discovered to be edited by ADAR2 in mice (Tan et al., 2017).

The reliance of ADAR1 and ADAR2 on each other varies from tissue to tissue. ADAR1 and ADAR2 performed comparable roles in the brain, whereas ADAR1 was the dominant editing enzyme in the liver, thymus and spleen, perhaps due to the lower expression levels of ADAR2 in non-brain tissues. Clustering analysis further revealed that the editing sites can be divided into five main regulatory groups that differ in their tissue-specific dependencies on

ADAR1 and ADAR2. Notably, the dependency of most of the sites on the editing enzymes varies from tissue to tissue (Tan et al., 2017).

ADAR2 undergoes posttranslational modification. It can be phosphorylated at the N-terminus by an unknown kinase, before becoming a substrate for Pin1 (peptidylprolyl cis/trans isomerase, NIMA-interacting 1) (Marcucci et al., 2011). Proline isomerisation of ADAR2 is essential for nuclear retention of ADAR2. In the absence of Pin1, ADAR2 is unstable and is present in the cytoplasm. Accumulation of ADAR2 in the cytoplasm allows it to interact with WWP2, a ligase that results in the subsequent degradation of ADAR2 (Marcucci et al., 2011). Hence, Pin1 is a positive regulator for ADAR2 while WWP2 plays a negative role on ADAR2 regulation. Another protein that was found to be a negative regulator for ADAR2 is aminoacyl TRNA synthetase complex interacting multifunctional protein 2 (AIMP2) (Tan et al., 2017). AIMP2 overexpression caused a significant decline in editing at over 1500 sites and a reduction in both ADAR1 and ADAR2 protein levels, signifying that AIMP2 promotes ADAR1 and ADAR2 enzyme degradation (Tan et al., 2017).

ADAR2 activity is also known to affect the expression of certain genes. For instance, knockdown of ADAR2 reduces RNA editing of glioma-associated oncogene 1 (GLI1), where decreased editing is found in cell lines from the cerebellar tumour medulloblastoma (Shimokawa et al., 2013). The introduction of edited GLI1 into medullablastoma cells confers a smaller increase in cellular growth compared to non-edited GLI1, indicating that RNA editing of GLI1 is a regulatory mechanism in tumourigenesis (Shimokawa et al., 2013). RNA editing can also effect protein stability of NOVA-1, a brain-specific regulator of alternative splicing (Irimia et al., 2012). Edited isoforms of NOVA-1 showed increased protein stability, increasing protein half-life and presumably increasing global NOVA-1 activity (Irimia et al., 2012).

Recent reports have shown that incomplete nuclear localisation and lower ADAR2 levels are observed in the nucleus of immature neurons (Behm et al., 2017). Editing levels of several sites were found to increase *in vivo* during mouse brain development (Wahlstedt et. al., 2009) and *in vitro* during rat neuron maturation (Orlandi et al., 2011). However, a parallel increase of ADAR

expression levels was not always found (Wahlstedt et al., 2009). The precise molecular regulation of ADAR2 activity and expression remains unclear.

1.2.4 ALTERNATIVE SPLICING OF ADAR2

Alternative splicing refers to a regulated process during gene expression which results in a single gene encoding multiple proteins. During this process, certain exons located in a gene may be included or excluded from the final, processed mRNA of that gene, resulting in protein isoforms with differing peptide sequences and thus chemical and biological functions (Black, 2003). Data from The International Genome Sequencing Consortium predicted that >50% of human genes are subjected to alternative splicing (Brett et. al., 2002). Various types of alternative splicing include exon skipping, intron retention, alternative 5' or 3' splice sites, mutually exclusive exons, mutually exclusive 5' or 3' untranslated regions (UTRs), and tandem UTRs (E. T. Wang et al., 2008).

Nine splice sites have been discovered in human ADAR2 pre-mRNA thus far (Table 1.1). Alternative splicing at these sites occurs independently, which results in dozens of ADAR2 spliced isoforms, making it challenging to analyse tissue-specific and developmental stage-dependent properties of these splice variants *in vivo* (Solomon et al., 2013). Five of these splicing events affect ADAR2 catalytic function (Li et al., 2015). The inclusion of exon 1a between exon -1 and exon 1 results in an N-terminal extension of 28 amino acids, including seven arginine (R)/lysine (K) residues (Slavov & Gardiner, 2002). The inclusion of exon 0, located between exon -1 and exon 1, results in the addition of 49 amino acids at the N-terminus (Maas & Gommans, 2009). The functional properties and relative protein abundance of these two ADAR2 isoforms have yet to be determined.

Authors	Alternative splice site	Effect on ADAR2 transcript	Effect on ADAR2 protein	Effect on catalytic activity
Gerber *et. al.*, 1997	5-6	Inclusion of exon 5a	Insertion of AluJ cassette in the catalytic domain	Decreased
Lai *et. al.*, 1997	9	Truncates 3' end of the coding region	Replacement of 29 C-terminal residues with 2 amino acids	None
Rueter *et. al., 1999*	1-2	Addition of 47 nt to 5' end of exon 2	Generation of a 9 kDa protein	Decreased
Slavov and Gardiner, 2002	-1-1	Inclusion of exon 1a	28- amino acid N-terminal extension	Unknown
Kawahara *et. al.*, 2005	1-3	Skipping of exon 2	Generation of a 12-amino acid protein	None
Kawahara *et. al.*, 2005	9-10	Inclusion of intron 9	Unknown	Unknown
Kawahara *et. al.*, 2005	9	Splices exon 9, 83 nt downstream from stop codon	Unknown	Unknown
Maas and Gommans, 2009	-1-1	Inclusion of exon 0	49-amino acid N-terminal extension	Unknown
Agranat *et. al.*, 2010	7-8	Inclusion of exon 7a	Nonsense-mediated mRNA decay	None

Table 1.1 Alternative splicing sites in human ADAR2 reported in previous studies. Adapted from Fu et. al. (2018).

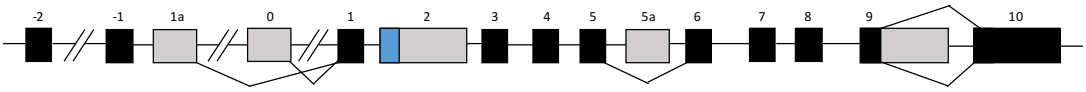

Figure 1.7 Exon-intron organisation of the human *ADAR2* gene.

The human *ADAR2* gene spans ~150 kb of human chromosome 21q22. Exons are numbered from -2 to 10 and showed as filled boxes. Introns and 5' and 3' flanking regions are shown as solid lines. Shaded boxes denote alternatively utilized exons comprising alternative splice sites.

An A-to-I auto-editing event which creates a new 3' splice acceptor site in the intron 1 sequence of ADAR2 results in the addition of 47 nt to the 5' end of exon 2, causing a frameshift in the coding region. This is expected to generate a 9-kDa ADAR protein due to the insertion of a premature translational termination codon (Rueter et. al., 1999). Alternative splicing in exon 5, which causes the incusion of exon 5a, results in another ADAR2 isoform. The alternatively-spliced exon 5a isoform encodes an in-frame AluJ cassette in the catalytic domain, resulting in protein with a twofold reduction in activity (Gerber et. al., 1997). Another splicing event in human ADAR2 mRNA results in the skipping of exon 2, causing a frameshift that inserts a stop codon in exon 3, producing a truncated protein of only 12 amino acids (Kawahara, Ito, Ito, Tsuji, & Kwak, 2005). The insertion of a 30-nt cassette in rats and mice (similar to a 120-nt cassette insertion in humans) results in the generation of two different ADAR isoforms (ADAR2a and ADAR2b). Although both isoforms are equally expressed during neuronal development, the ADAR2b variant is the less active isoform, due to the addition of a 10-aa loop which ultimately interferes with RNA binding, which could explain its lower editing efficiency compared to ADAR2a (Filippini et al., 2018a).

1.2.5 ADAR2 AND GLUA2 Q/R SITE EDITING

ADAR2 edits specific adenosine residues found in RNA hairpins which are normally formed between a portion of an exon that flanks the edited adenosine and sequences in a nearby intron (Higuchi et al., 1993). The Q/R editing sites in mouse *Gria2* and human *GRIA2* transcripts are edited with over 99% efficiency (Sommer et al., 1991).

Adar2 homozygous mice with a targeted deletion of exon 6, which encodes the C-terminal deaminase domain, developed progressive seizures as pups and died by 21 days of age (Higuchi et al., 2000). *Gria2* transcript mutations that prevent dsRNA structure formation required for editing also led to the death of mice, where increased calcium permeability and death of hippocampal neurons were found (Higuchi et al., 1993). *Adar2* mutant pup death is avoided by combining the *Adar2* mutation with a *Gria2* mutant where the arginine residue of the Q/R editing site is introduced in the genomic sequence (Higuchi et al., 2000), thus showing that the Q/R site is the main physiological target of ADAR2 editing.

Glutamate excitotoxicity is an important factor in certain neurodegenerative diseases, such as spinal neurodegeneration in ALS (King et. al., 2016). The expression of ADAR2 is reduced in ALS patient motor neurons and editing downregulation at the Q/R site of GluA2 is seen in ALS patients' motor neurons (Hideyama et al., 2012). The *Adar2* mutant mice die too soon to present more widespread neurodegeneration; nonetheless, *Adar2*-targeted deletion in motor neurons of young mice leads to slow motor neuron degeneration (Hideyama et al., 2010). Vertebrate neuronal cells that are treated with excess glutamate to induce neurotoxicity led to the cleaving of ADAR2 protein by a calcium-activated protease, showing that glutamate excitotoxicity is mediated partly by suppressing GluA2 Q/R site editing (Mahajan et. al., 2011).

1.3 AMYOTROPHIC LATERAL SCLEROSIS

1.3.1 INTRODUCTION

Amyotrophic lateral sclerosis (ALS), also known as Lou Gehrig's disease in the United States of America and motor neuron disease (MND) in the United Kingdom, is a neurodegenerative disease characterised by progressive muscular paralysis reflecting degeneration of motor neurons in the primary motor cortex, corticospinal tracts, brainstem, and spinal cord. The disease gradually starts off with focal weakness, before spreading to most muscles, including the diaphragm. Death normally occurs due to respiratory paralysis 3 to 5 years after disease onset (Brown & Al-Chalabi, 2017). The prevalence of ALS in European populations is projected to be at 2.6-3.0 cases per 100,000 people (van Es et al., 2017). Compared to Alzheimer's disease, the risk of developing ALS peaks at 50-75 years of age and decreases afterwards (van Es et al., 2017).

"Amyotrophy" signifies the atrophy of muscle fibres that are denervated due to degeneration of corresponding anterior horn cells, causing weakness and fasciculations. "Lateral sclerosis" refers to gliosis that replaces degenerated neurons that cause hardening of the corticospinal tract (Rowland & Shneider, 2001). Roughly two-thirds of patients with typical ALS have a spinal form of the disease and present with symptoms linked to focal muscle weakness and wasting. Gradually, spasticity may develop in the weakened atrophic limbs, thus affecting manual dexterity and gait. Most ALS cases are sporadic, whereas 5-10% of cases are familial. In roughly 60-80% of familial ALS patients, large mutation effects can be identified, of which *C9ORF72* (40%), *SOD1* (40%), *FUS* (1-5%) and *TARBDP* (1-5%) are the most common (van Es et al., 2017).

A pathological hallmark of ALS is death of motor neurons in the motor cortex and spinal cord. Neuronal degeneration is more common in ALS with frontotemporal dementia, appearing throughout the frontal and temporal lobes (Brown & Al-Chalabi, 2017). Neuroinflammatory processes such as astroglia, microglia, and oligodendroglial cell proliferation occur alongside motor neuron

degeneration (Kang et al., 2013). One common feature seen in both familial and sporadic ALS is the aggregation of cytoplasmic proteins, notably in the motor neurons. TAR DNA-binding protein 43 (*TDP-43*) is cleaved, hyper-phosphorylated, and mislocalised in the cytoplasm (Neumann et al., 2006). Ubiquitin 2 aggregates are also common, while superoxide dismutase 1 (*SOD1*) are intracytoplasmically deposited in sporadic ALS (Brown & Al-Chalabi, 2017).

The management of ALS has been based on coordinated multidisciplinary care between specialist, community-based therapists and palliative care teams. Even though ALS is deemed incurable, symptoms that arise from the disease are treatable, thus efforts are made to improve life quality and help maintain the patient's autonomy for as long as possible. The general recommendation for improving the quality of ALS patients is by discussing end of life care, respiratory, and nutritional management with patients and relatives at the earliest opportunity (Wijesekera & Leigh, 2009). There is a possibility that ALS patients and their relatives will suffer from depression, hopelessness, and anxiety resulting from the diagnosis or disease progression (Wicks et al., 2007). Hence, psychological support through counselling and palliative care should be offered to both the patients and relatives from early on (Leigh et al., 2003). Non-invasive ventilation increases survival and improves quality of life.

Currently, no cure is available for ALS and only two compounds are available to treat this disease (riluzole and edaravone). Riluzole came to the market as the first FDA (Food and Drug Administration)-approved drug for ALS. It is still unknown what the mechanism of action of riluzole is, but is speculated to block voltage-gated sodium channels of presynaptic neurons, thus reducing glutamatergic neurotransmission (Hardiman et al., 2017). The drug is well-tolerated, but survival of patients was only prolonged by 2-3 months compared to placebo (Lacomblez, Bensimon, Meininger, Leigh, & Guillet, 1996). Edaravone, a drug that can potentially reduce oxidative stress, is now approved by the FDA, but not by the European Medicines Agency (Hardiman et al., 2017). It has been shown to slow disease progression in highly selected patients with early-onset and rapidly-progressing disease (Abe

et al., 2017). However, further studies are necessary to establish whether edaravone would be safe and effective in advance stage ALS patients and to determine if the drug can prolong patient survival (Abe et al., 2017).

1.3.2 MOLECULAR GENETICS

ALS has traditionally been classified either as sporadic (sALS) or familial (fALS). fALS makes up 10-20% of ALS cases and is transmitted classically within families via Mendelian inheritance and is mainly autosomal dominant (Zarei et al., 2015). Most ALS cases (80-90%) are sporadic, which have no clear genetic linkage. Even though more than 30 genes are presented to be linked to ALS, evidence suggests that genetic pleiotropy (where one gene has many phenotypic manifestations) and oligogenic inheritance (where more than one gene determines a phenotypic trait) play a role in the disease (Hardiman et al., 2017). Population studies in those with European descent showed that up to 20% of ALS patients have a family member with either ALS or frontotemporal dementia (familial ALS). Among these, four genes are linked to 70% of all cases of fALS: *C9ORF72*, *TARDBP* (also known as TDP-43, encodes for TAR DNA binding protein), *SOD1* (copper/zinc ion-binding superoxide dismutase), and *FUS* (encodes fusion in sarcoma) (Chiò et al., 2014) (Table 1.2).

fALS	Locus	Inheritance	Mean age at onset	Gene	Protein defective function/protein aggregates	Associated features	References
ALS1/ SOD1	21q22.11	Dominant/ Recessive	47	Superoxide dismutase 1 (*SOD1*)	Protein aggregation, potential gain of redox function, weakened axonal transport, metabolic changes/cytoplasmic inclusions of SOD1, ubiquitin and p62	Lower (LMN) and upper motor neuron (UMN) involvement. Amyotrophy, autonomic and cognitive dysfunction, cerebellar ataxia	(Rosen et al., 1993)
ALS6/ FUS	16p11.2	Dominant/ Recessive	46	Fused in sarcoma (*FUS*)	Altered RNA processing, formation of inclusion bodies/FUS	LMN and UMN involvement, frontotemporal dementia (FTD)	(Vance et al., 2009)
ALS9/ ANG	14q11.1	Dominant	55	Angiogenin (*ANG*)	rRNA transcription, stress granule formation/TDP-43 aggregates	LMN and UMN involvement, FTD, Parkinson's disease	(Van Es et al., 2011)
ALS10/ TARDBP	1p36.22	Dominant/ Recessive (rare)	55	TDP-43 (*TARDBP*)	RNA splicing, formation of protein inclusion bodies, metabolic changes, p62 and TDP-43-positive aggregates	LMN and UMN involvement, FTD	(Gitcho et al., 2009)
ALS12/ OPTN	10p15-p14	Dominant/ Recessive	51	Optineurin (*OPTN*)	Golgi maintenance, membrane trafficking and exocytosis, formation of inclusion bodies	LMN and UMN involvement, FTD	(Maruyama et al., 2010)
C9ORF72/ FTDALS1	9p21.2	Dominant	57	*C9ORF72*	Endosomal trafficking and autophagy, altered C9ORF72 RNA splicing, formation of nuclear RNA foci/TDP-43-positive and -negative aggregates localised in the hippocampus	LMN and UMN involvement, FTD	(DeJesus-Hernandez et al., 2011; Renton et al., 2011)

Table 1.2 Summary of description of genes and loci associated with ALS. Adapted from Zufiria et. al. (2016).

SOD1 mutations, which make up 20% of fALS cases and 5% of sALS cases, cause cytotoxicity but its pathophysiology still remains unclear (Table 1.2) (Kiernan et al., 2011). *TARDBP* and *FUS*, which account or 5% of fALS mutations, play a role in gene expression and regulation processes such as transcription, RNA splicing, transport, and translation (Table 1.2) (Kiernan et al., 2011). *ANG*, a gene responsible for 1% of fALS, codes for an angiogenic factor in response to hypoxia (Table 1.2) (Zarei et al., 2015). Mutations in *OPTN*, a gene involved in open-angle glaucoma, eliminates the inhibition of nuclear factor kappa-beta activation, modifying *OPTN* distribution in the cytoplasm (Table 1.2) (Kiernan et al., 2011). Although *SOD1* and *C9ORF72* mutations most often cause fALS, their frequencies differ across populations (Zarei et al., 2015).

Nearly up to half of fALS cases can be associated with specific genes, where most are apparently rare and highly penetrant *de novo* mutations within affected families. Common variables related to this disease have been identified by genome-wide association studies (He, Mangelsdorf, Fan, Bartlett, & Brown, 2015). Next-generation sequencing (NGS) has also provided a way to map mutations for single gene diseases (He et al., 2015). Both GWAS and NGS have identified genetic variables that are associated with higher risk of developing ALS. Establishing accurate clinical phenotypes of ALS is crucial in the success of GWAS and NGS to prevent false positive results (He et al., 2015).

The genetic mechanisms of sALS is poorly understood. Large and combined GWAS of seemingly sporadic ALS, which analysed disease heritability by allele frequency, insinuate that the genetic risk factors are mainly centred on rare variants (Van Rheenen et al., 2016). This contrasts with diseases associated with high numbers of common variants, such as schizophrenia, which are highly polygenic (Loh et al., 2015). The rare variants which confer risk that might be individual-, family-, and ancestral-specific makes GWAS studies for ALS complicated (Van Rheenen et al., 2016). Whole-genome sequencing comprising a high number of patients and controls will be necessary to completely unravel the genetics behind ALS considering

the disease's genetic architecture. The Project MinE Consortium (www.projectmine.com), launched in 2012, aims to carry out whole-genome sequencing of more than 15,000 ALS patients and 7,500 controls. This is expected to provide better comprehension about the genetic architecture of ALS (Hardiman et al., 2017)

1.3.3 PATHOPHYSIOLOGICAL MECHANISMS

Pathogenic mechanisms that have been suggested for ALS comprise a plethora of changes to the motor neuron microenvironment. This includes the accumulation of protein aggregates, defective RNA processing, oxidative stress, glutamate excitotoxicity, glial dysfunction, neuroinflammation, apoptosis, mitochondrial dysfunction, and metal imbalances (Paez-Colasante, Figueroa-Romero, Sakowski, Goutman, & Feldman, 2015). The presence of intraneuronal aggregates of neurofilaments are apparent in ALS patients, particularly in spinal motor neurons (Paez-Colasante et al., 2015). Alterations in neurotransmitter release and synaptic function are also common to both ALS and FTD (reviewed in Paez-Colasante *et. al.,* 2015). Furthermore, aberrations in RNA-processing protein networks in ALS and other neurodegenerative diseases prompt abnormal RNA regulation and exon splicing (Paez-Colasante et al., 2015). ALS pathogenesis is thus complex, with several causative factors.

1.3.3.1 *SOD1*

The discovery of dominant *SOD1* mutations 20 years ago was the first to demonstrate how linkage analysis can determine the genetic cause of a rare neurodegenerative disease (Rosen et al., 1993). However, only a small number of reliable cases supporting the genetic evidence for the pathogenicity of *SOD1* mutations exist (Andersen, 2006). Nonetheless, population-based studies demonstrate that this gene mutation accounts for ~12% of familial cases and ~1% of sporadic cases (Renton, Chiò, & Traynor, 2014). At least 75 of *SOD1*'s 153 amino acids have been reported to be mutated in ALS and their positions are dispersed throughout the five exons of the gene (Saccon, Bunton-Stasyshyn, Fisher, & Fratta, 2013).

SOD1 is highly conserved, ubiquitously expressed, and makes up 1-2% of total soluble protein in the central nervous system. The gene is made

up of five exons that encode a 153-amino acid metalloenzyme, also known as Cu/Zn superoxide dismutase. The protein localises to the cytoplasm, lysosomes, nucleus, and the mitochondria intermembrane space (Saccon et al., 2013). It binds copper and zinc ions and forms a homodimer which mainly functions as a dismutase that removes dangerous superoxide radicals by metabolising them to molecular oxygen and hydrogen peroxide, thus providing a defence against oxygen toxicity (Saccon et al., 2013). *SOD1* has recently been found to be vital in suppressing respiration and directing energy metabolism by integrating responses to oxygen, glucose and superoxide levels; this function is independent of its oxidative stress functions (Reddi & Culotta, 2013). *SOD1* protein is produced in high quantities that have yet to be explained by known functions, thus, it may also play other neuron-specific and general roles (Reddi & Culotta, 2013).

Many lines of evidence have suggested that *SOD1* mutations cause ALS by a yet unidentified gain of function, although some propose that loss-of-function can also play a secondary role in disease, at least in some cases (Saccon et al., 2013). Many cellular mechanisms have been implicated to be potentially involved in SOD1-fALS pathogenesis. However, distinguishing cause from effect and identifying its critical processes remains a challenge (Redler & Dokholyan, 2013).

No clear consensus has arisen to link *SOD1* mutations to the premature death of motor neurons. Recent understanding has linked genetic mutations to a toxic gain of function of the SOD1 enzyme, with free radical generation that ultimately leads to cell injury and death (Bruijn, Miller, & Cleveland, 2004). Furthermore, mutations in *SOD1* induce conformational instability and misfolding of the SOD1 protein, which results in formation of intracellular aggregates (Zetterström et al., 2007) that inhibit normal proteosomic function, disrupting axonal transport systems and vital cellular functions (Bruijn et al., 2004).

1.3.3.2 TDP-43

A breakthrough event in the understanding of ALS pathogenesis was the finding that TDP-43, a major component of ubiquitin-positive neuronal inclusions, is a pathological hallmark of ALS and frontemporal dementia (FTD) (Neumann et al., 2006). Although questions about whether such aggregates trigger neurodegeneration in ALS has arisen, mutations in TDP-43 were reported in 3% of familial ALS and 1.5% of sporadic ALS (Sreedharan et al., 2008). TDP-43 is a ubiquitously expressed DNA-/RNA-binding protein, which is encoded by *TARDBP* (Ou, Wu, Harrich, Garcia-Martinez, & Gaynor, 1995). It is made up of two RNA recognition motifs, a nuclear localisation sequence (NLS), a nuclear export signal, and a glycine-rich C-terminus that mediates protein-protein interactions (Scotter et. al. 2015). TDP-43 is mainly found in the nucleus, but is also able to undergo nucleocytoplasmic shuttling (Winton et al., 2008). It plays an important role in regulation of RNA splicing and modulation of microRNA biogenesis in the nucleus (Scotter et al., 2015), which requires the glycine-rich C-terminal domain that is able to bind to several members of the heterogenous nuclear ribonucleoprotein (hnRNP) family (Mackenzie & Rademakers, 2008). TDP-43 is capable of regulating the stability of its own mRNA, which provides a mechanism for autoregulating TDP-43 protein levels (Ayala et al., 2010). Aside from TDP-43 RNA, it can also regulate splicing and stability of various other transcripts, thus influencing a large number of cellular processes (Scotter et al., 2015). TDP-43 is generally localised to nuclei of neuronal and some glial cells (Neumann et al., 2006).

TDP-43 was recognised as a main component of ubiquitinated neuronal cytoplasmic inclusions deposited in FTD cortical neurons and ALS spinal motor neurons (Neumann et al., 2006). 97% of both sporadic and familial ALS cases have been shown to be positive for TDP-43 inclusions (Scotter et al., 2015). A common theme seen in neurodegenerative disease is the presence of abnormally phosphorylated and ubiquitinated intracellular insoluble proteins (Lee, Lee, and Trojanowski 2012). Distinctive features of TDP-43 proteinopathies include the mislocalisation of the cognate protein to the cytoplasm, and the loss of its normal nuclear localisation (Lee, Lee, and

Trojanowski 2012). It is still currently unknown which of these features are essential for development of ALS. Thus, all observed features of neurodegenerative diseases with TDP-43 proteinopathies need to be considered when conveying models of disease mechanisms (Lee, Lee, and Trojanowski 2012).

1.3.3.3 *C9ORF72*

An expanded non-coding GGGGCC repeat identified in *C9ORF72* is the most common cause of familial ALS and is also one of the underlying causes to most sporadic ALS cases (DeJesus-Hernandez et al., 2011). This repeat expansion is not just limited to ALS; it also contributes to frontotemporal dementia (FTD) and ALS-FTD, and has been identified in other non-motor diseases such as Alzheimer's disease and Lewy-body dementia (Cooper-Knock, Shaw, & Kirby, 2014).

Although the repeat size shows heterogeneity among patients as well as different tissues within the same individual, the correlation between the number of repeats and the severity of clinical phenotypes is unclear. It has been shown that *C9ORF72* expansion carriers have a higher ALS prevalence, particularly bulbar onset ALS (reviewed by Zufiría et al. 2016). *C9ORF72* is a gene that encodes an uncharacterised protein with no known domains or function, but is highly conserved across species (DeJesus-Hernandez et al., 2011). Despite this, some evidence has shown that the *C9ORF72* protein transcript is involved in endosomal trafficking (Farg et al., 2014). Farg *et. al.* depleted *C9ORF72* expression in SH-SY5Y and Neuro2A cells using siRNA and found that this depletion results in impaired endocytosis and autophagy-mediated trafficking, suggesting its downregulation as a putative pathogenic mechanism (Farg et al., 2014). Studies carried out by DeJesus-Hernandez *et.al.* (2011) suggest multiple potential disease mechanisms are associated with the GGGGCC repeat expansion, which includes a direct effect on *C9ORF72* expression by affecting transcription through a loss-of-function

mechanism and an RNA-mediated gain-of-function mechanism through the generation of toxic RNA foci.

One common characteristic seen in noncoding repeat expansion disorders that has recently gained increased scrutiny is the build-up of RNA fragments made up of the repeated nucleotides as RNA foci in the nucleus and cytoplasm of affected cells (Todd & Paulson, 2010). In some diseases, the RNA foci dysregulate alternative mRNA splicing by sequestering RNA-binding proteins. The presence of such nuclear RNA foci in post-mortem cerebral cortex and spinal cord tissue of *C9ORF72* expanded repeat carriers was confirmed using an oligonucleotide probe specific for the GGGGCC repeat (DeJesus-Hernandez et al., 2011). The hexanucleotide sequence motif predicts the possible binding of several RNA-binding proteins, such as the serine/arginine-rich splicing factor 1 (SRSF1) and the heterozygous nuclear ribonucleoprotein (hnRNP) A2/B1 (Smith et al. 2006; Sofola et al. 2007).

Though further studies are required to illustrate whether these or other RNA-binding proteins are involved in disease pathogenesis, aberrant RNA splicing is a likely mechanism in chromosome 9p-linked FTD/ALS (Brown & Al-Chalabi, 2017). Cells which contain *C9ORF72* repeats, including patient brain and spinal cord neurons, comprise of a prominent nuclear foci of the GGGGCC repeat RNA and the antisense GGCCCC RNA, causing sequestration of essential RNA-binding proteins, such as splicing factors, thus prompting pre-mRNA splicing defects by an RNA toxicity mechanism (Gitler & Tsuiji, 2016). Determining aberrantly spliced RNA targets that are integral in disorders could be pivotal to the discovery of future therapeutic strategies (DeJesus-Hernandez et al., 2011).

1.3.3.4 MICRORNA DYSREGULATION

MicroRNAs (miRNA) are conserved noncoding RNAs that are 22 nucleotides in length. They can individually regulate several hundred targets through RNA-dependent post-transcriptional silencing mechanisms (Schwanhäusser et al., 2008). Conversely, mRNA transcripts can be regulated by many miRNAs (Bartel, 2004). Primary miRNA transcripts (pri-miRNAs) are transcribed in the nucleus, and undergo processing by Drosha (also known as ribonuclease 3) to produce precursor miRNAs (pre-miRNAs) (Y. Lee et al., 2004). Pre-miRNAs are then exported to the cytoplasm and processed by Dicer (an endoribonuclease) to become mature double-stranded miRNAs (Hutvágner et al., 2001). Precursor miRNAs in the human genome are able to modulate many physiological processes, such as neuronal homeostasis and cell differentiation, by elaborate fine-tuning of the transcriptome and proteome (Engels & Hutvagner, 2006; Lau, Lim, Weinstein, & Bartel, 2001; Ponomarev, Veremeyko, Barteneva, Krichevsky, & Weiner, 2011). miRNAs are temporally and differentially expressed among different tissues. miR-138 is confined within the CNS while its precursor is ubiquitously expressed, and miR-9 shows copious neuron-specific expression (Coolen, Katz, & Bally-Cuif, 2013; Mondanizadeh et al., 2015).

In most diseases, differentially expressed miRNAs have been found between both diseased and normal tissue. They are typically subject to change amid the pathogenetic course (Engels & Hutvagner, 2006). Hence, biological pathways altered by miRNA could partially explain complex disorders such as ALS. The implications of miRNA dysregulation have not been entirely clarified in neurodegenerative diseases. It is thus imperative to determine whether dysregulation takes place via transcriptional or post-transcriptional mechanisms, or both. Reduction in TDP-43 can affect RNA processing via interactions with Drosha-containing protein complexes (Honda et al., 2014). Drosha can also interact with other polypeptides, such as TDP-43, AGO2, nuclear pri-miRNAs or cytoplasmic pre-miRNAs to establish an alternative complex with limited processing function (Kawahara & Mieda-Sato, 2012). Reports have shown that TDP-43 mutations leads to differential

expression of mature and functional miRNAs such as miR-132, miR-143 and miR-558 that contribute to ALS pathology (Kye & Gonçalves, 2014). A reduction in TDP-43 led to a deficiency in neurite growth in Neuro2a cells, and this was only recovered by over-expressing miR-132 (Kawahara & Mieda-Sato, 2012). The expression of miR-9 is shown to be reduced in iPSC-derived motor neurons in ALS patients containing *TARDBP* mutations (Zhang et al., 2013).

Recently, FUS/TLS (translocated in sarcoma) has been shown to encourage biogenesis of certain miRNAs by recruiting Drosha to pri-mRNAs. miR-9 regulates axon growth by regulating mRNA translation of microtubule-associated protein 1b (MAP1B), while neuronal morphology and growth are regulated by miR-132 via targeting genes such as acetylcholinesterase and Tau. Neuronal activity triggers miR-134 response by regulating neuronal development and dendritogenesis (reviewed in Kye & Gonçalves, 2014). These results indicate that FUS/TLS mutations could lead to a disruption in miRNA biogenesis and function, thus contributing to pathological phenotypes observed in ALS patients.

Sporadic ALS patients demonstrated a distinctive miRNA expression pattern in white blood cells throughout disease progression. An miRNA profiling data study revealed an increase in miR-338-3p expression, while the expression of seven other miRNAs is reduced in ALS patient leukocytes (De Felice et al., 2012). These findings suggested that disruption to miRNA pathways may be a likely cause or consequence that lead to ALS pathology, which include altered RNA and protein metabolism, cytotoxicity, and impaired structure and signalling at the neuromuscular junction (Figure 1.8) (Paez-Colasante et al., 2015) (Paez-Colasante et al., 2015). Hence, profiling miRNA expression can potentially act as an ALS diagnostic tool (Kye & Gonçalves, 2014).

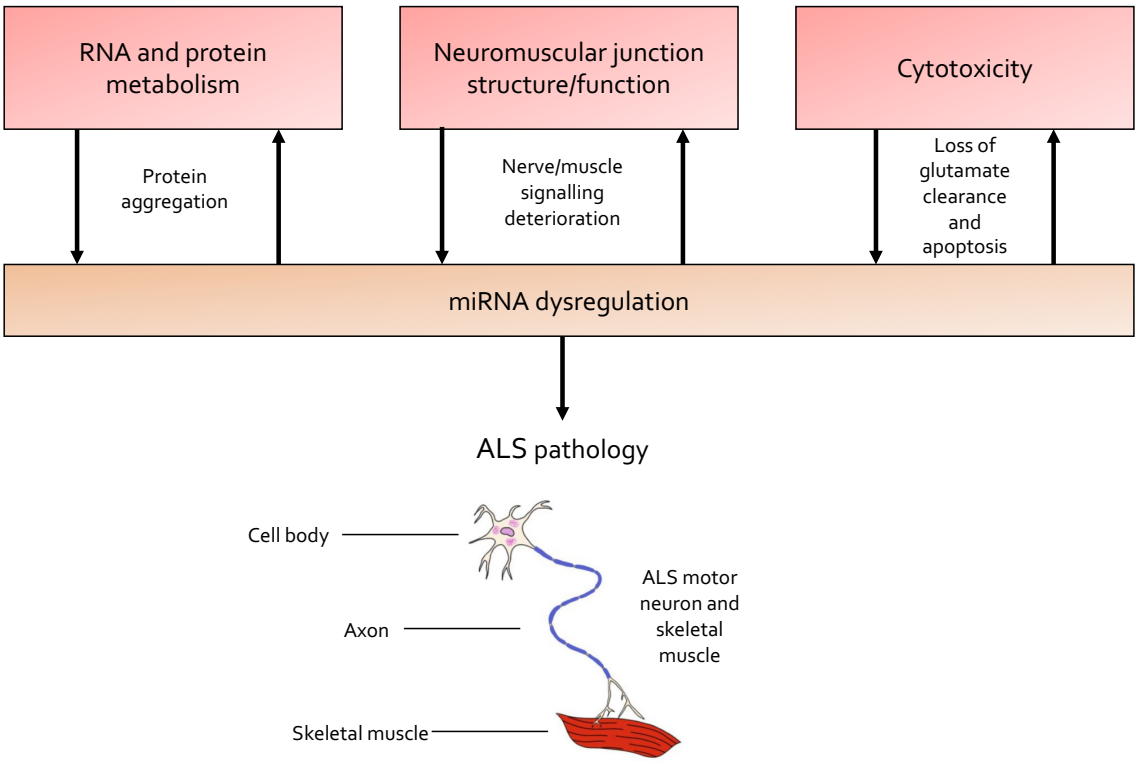

Figure 1.8 Dysregulation of miRNA biogenesis and function.

Dysregulation of miRNA biogenesis and function may be a cause and/or consequence of ALS pathogenesis, which can arise through dysregulation of several cellular pathways. RNA and protein metabolism may be altered by inclusion of cytoplasmic protein aggregates, signalling impairments at the neuromuscular junction, and cell death caused by cytotoxicity linked to excessive glutamate activation.

1.3.3.5 GLUTAMATE-INDUCED EXCITOTOXICITY

Glutamate-induced excitotoxicity has been implicated in ALS pathogenesis. Glutamate is the major excitatory neurotransmitter in the central nervous system and binds to ionotropic N-methyl–D-aspartate (NMDA) receptors and AMPA receptors on the postsynaptic membrane (Heath & Shaw, 2002). Excessive activation of these postsynaptic receptors by glutamate can stimulate neurodegeneration by activating calcium-dependent enzymatic pathways (Regan & Choi, 1991).

Glutamate released from the presynaptic neuron activates ionotropic glutamate receptors present on the postsynaptic neuron during glutamatergic neurotransmission (L. Van Den Bosch, Van Damme, Bogaert, & Robberecht, 2006) (Figure 1.9a). Activation of these glutamate receptors results in Na^+ and Ca^{2+} ion influx into the cell, which leads to depolarisation and ultimately generation of an action potential (Figure 1.9a). Excitotoxicity is neuronal degeneration caused by overstimulation of the glutamate receptors (L. Van Den Bosch et al., 2006) (Figure 1.9b). Olney (1978) first formulated this concept based on the observation that amino acids that induce neuronal death were those known to activate excitatory amino acid receptors. Since then, experimental evidence showed that excitotoxicity could contribute to neuronal damage in stoke, neurotrauma, epilepsy, and a number of neurodegenerative disorders including ALS (Doble, 1999).

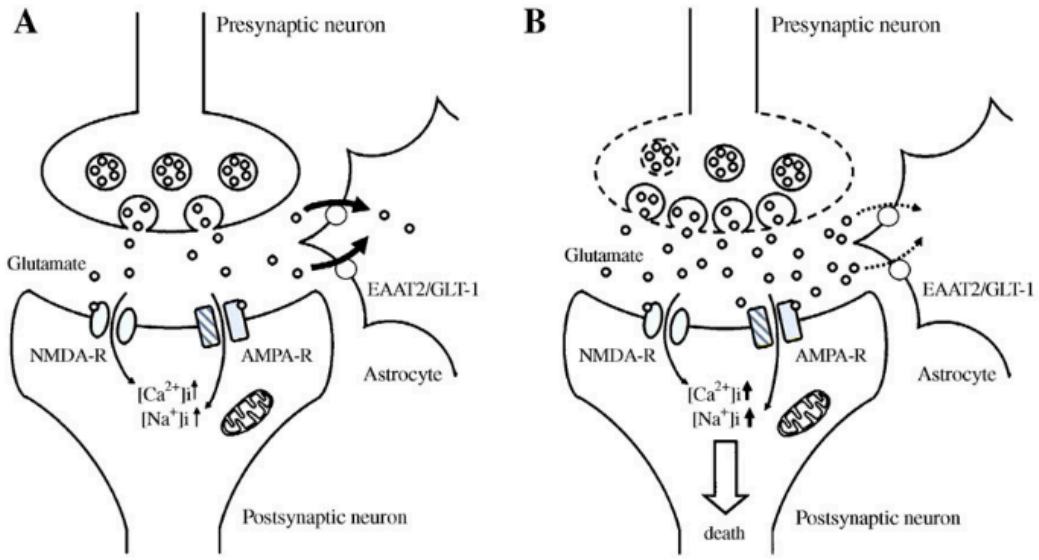

Figure 1.9 Glutamatergic neurotransmission and excitotoxicity.

(A) During normal conditions, glutamate released from the presynaptic neuron activates NMDA and AMPA receptors. This leads to an influx of both Na^+ and Ca^{2+}ions, the depolarisation of the postsynaptic neuron and eventually the generation of an action potential. (B) Excitotoxicity is prompted by an elevation in extracellular glutamate concentration. This can be caused by an increased release of glutamate or defective re-uptake of glutamate into the astrocytes by the EAAT2/GLT-1 transporter. Excessive stimulation of the glutamate receptors causes in increased intracellular concentration of Na^+ and Ca^{2+}ions, resulting in neuronal death. Disintegration of neuronal cells induces a further increase of extracellular glutamate and amplifies the excitotoxic damage. Figure taken from Van Den Bosch et al, 2006.

RNA editing targets are plentiful in the CNS, where proteins involved in synaptic transmission are recoded (Rosenthal & Seeburg, 2012). Editing dysregulation can cause extensive modifications in neuronal signalling, thus inducing severe neurological disorders (Kawahara et al., 2004; Stefan Maas, Kawahara, Tamburro, & Nishikura, 2006). Since RNA editing recodes several glutamate receptor subunits, this process has acute effects on glutamate neurotransmission (Barbon & Barlati, 2011). Under normal physiological conditions, the Q/R site of GluA2 is fully edited, making the AMPA receptors Ca^{2+}-impermeable. Loss of editing at the Q/R site produces an increased influx of Ca^{2+}, leading to epileptic seizures and death in ADAR2-null mice (Miyoko Higuchi et al., 2000). Transient ischemia in humans lowered GluA2 subunit editing and reduced ADAR2 abundance, causing the death of pyramidal neurons (Peng et al., 2006). Moreover, spinal motor neurons of sALS patients showed severely reduced GluA2 Q/R site editing, possibly due to ADAR2 downregulation, thus causing AMPA receptors to be highly permeable to Ca^{2+}. This in turn facilitates the death of motor neurons, as reported in conditional ADAR2 knockout mice (T. Hideyama et al., 2010). Exposing cortical cells to excitotoxic levels of glutamate has also reported to promote ADAR2 cleavage and an ensuing loss of Q/R site editing, leading to excitotoxic cell death (Mahajan et al., 2011).

The most imperative argument for the role of excitotoxicity in ALS is that riluzole, the only drug which is demonstrated to be effective against disease progression in patients, has anti-excitatory properties (Lacomblez et al., 1996). It is currently the only therapy proven in clinical trials to prolong survival of ALS patients (Traynor, Alexander, Corr, Frost, & Hardiman, 2003). Its neuroprotective effect is thought to benefit in many neurodegenerative diseases and amelioration of trauma and stroke (Albo, Pieri, & Zona, 2004). Riluzole slows disease progression and significantly increases survival by a few months. This drug has been shown to inhibit glutamate release due to inactivation of voltage-dependent Na^{+} channels on glutamatergic nerve terminals. Furthermore, evidence has shown that riluzole can also block some of the postsynaptic effects of glutamate by non-competitive inhibition of NMDA and AMPA receptors (Albo et al., 2004).

Motor neurons, both *in vitro* and *in vivo*, are particularly vulnerable to AMPA receptor-mediated excitotoxicity. Intrathecal or intraspinal administration of AMPA receptor agonists induced motor neuron degeneration in animals (Nakamura, Kamakura, & Kwak, 1994). Motor neurons are also proved to be particularly vulnerable to AMPA receptor-mediated excitotoxicity in organotypic rat spinal cord cultures (Saroff et. al., 2000). Direct application of AMPA receptor agonists lead to selective motor neuron loss, which could be prevented by AMPA receptor antagonists.

Likewise, it was established that motor neurons in culture are susceptible to glutamate receptor agonists, particularly those that stimulate AMPA receptors (L. Van Den Bosch & Robberecht, 2000). Ca^{2+} influx through Ca^{2+}-permeable AMPA receptors was shown to be essential for inducing motor neuron death when cultured on an astrocytic feeder layer whereas other neurons were resistant to AMPA receptor over-stimulation (L Van Den Bosch et al., 2002). Little or no effect of NMDA receptor agonists was apparent in these cultured motor neurons (L. Van Den Bosch et al., 2006). Additionally, depolarising these motor neurons by exposing them to a high extracellular K^+ concentration was not sufficient to induce significant cell death (L Van Den Bosch et al., 2002).

Since ADAR2 reduction may likely play a role in motor neuron survival in patients with sporadic ALS, one possible therapeutic strategy is restoring ADAR2 activity in neurons. This was carried out by delivering human ADAR2 cDNA to motor neurons in conditional ADAR knockout (AR2) mice using an adeno-associated virus serotype 9 (AAV9) vector (Yamashita et al., 2013). The vector-based gene delivery prevented ALS phenotype progression, including progressive motor dysfunction. Moreover, the effect of ADAR2 gene delivery was observed even when delivered after the appearance of motor dysfunction (Yamashita et al., 2013).

Another study revealed that homozygous conditional ADAR2-knockout (AR2) mice displayed mislocalisation of TDP-43 from the nucleus to the cytoplasm, where TDP-43 aggregates. This resembles TDP-43 pathology in ADAR2-deficient motor neurons (Yamashita et al., 2012). An *in vitro* calpain

assay further demonstrated that TDP-43 was cleaved specifically by calpain, a Ca^{2+}-dependent cysteine protease, suggesting that calpain-dependent cleavage of TDP-43 is possibly involved in the aetiology of TDP-43 pathology in ALS motor neurons (Yamashita et al., 2012). Oral administration of perampanel, an AMPA receptor antagonist, reduces motor neuron death and TDP-43 mislocalisation in AR2 mice (Akamatsu, Yamashita, Hirose, Teramoto, & Kwak, 2016). The robust effects of perampanel on ADAR2 on AR2 mice suggest that perampanel may have exerted its effects through a Ca^{2+}-permeable AMPA receptor-mediated mechanism (Akamatsu et al., 2016).

Reports have shown that inefficient GluA2 Q/R site editing does not seem to be an underlying mechanism behind ALS cases with *C9ORF72* mutations. Work carried out by (Selvaraj et al., 2018) discovered efficient RNA editing in mutant *C9ORF72* motor neurons with increased Ca^{2+}-permeability. This is consistent with findings in native neurons and familial ALS with SOD1 mutations (Kawahara, Kwak, et al., 2003; Kawahara et al., 2006). Another explanation behind increased Ca^{2+}-permeability include disease-related modifications in AMPA receptor subunit composition. The GluA1 subunit was found to be upregulated in *C9ORF72* mutant motor neurons, which correlates with increased Ca^{2+}-permeability in these cultures (Selvaraj et al., 2018). However, findings reported by (Moore et al., 2019) presented contradictory results, whereby ADAR2 was found to be misloclalised in induced pluripotent stem cells of ALS patients with *C9ORF72* mutations. The mislocalisation of ADAR2 has resulted in RNA editing aberrations of various cellular pathways (Moore et al., 2019), thus suggesting that the repeat expansion of *C9ORF72* does indeed alter RNA processing events.

1.4 ANTISENSE OLIGONUCLEOTIDES

1.4.1 OVERVIEW

Antisense oligonucleotides (ASOs) are synthetic single stranded chains of nucleic acids which are between 8 to 50 nucleotides in length. They bind to RNA through standard Watson-Crick base pairing. ASOs interfere with gene expression by altering RNA function. Subject to sequence and modifications, ASOs can alter RNA function through several distinct mechanisms, thus making them a diverse tool. They can be used to restore protein expression, reduce expression of a toxic protein, or modify mutant proteins to reduce their toxicity (Evers, Toonen, & van Roon-Mom, 2015).

Antisense-mediated gene inhibition was first introduced by Stephenson and Zamecnik in 1978 (Stephenson & Zamecnik, 1978). Using a DNA molecule of 13 nucleotides in length with modifications at the 3′ and 5′ OH moieties, they exhibited inhibition of replication and cell transformation of the Rous sarcoma virus. Modifications to the backbone and sugar component have been made since then, which has improved stability, binding strength and specificity, making ASOs suitable for therapeutic application (Järver, O'Donovan, & Gait, 2014). For some neurodegenerative disorders, such as ALS and spinal muscular atrophy (SMA), antisense oligonucleotide therapy has now advanced from preclinical to clinical stage, aided by the significant widespread distribution and cellular uptake of ASOs once delivered into the brain (Evers et al., 2015).

1.4.2 FUNCTIONAL MECHANISMS

ASOs can be used in different ways to modulate gene expression, depending on the chemistry and target site. One of the major functional mechanisms that can be used in neurodegenerative disorders is RNase H-mediated degradation (Figure 1.10a and b). To induce gene knockdown through RNase H, a strategy using gapmer ASOs has been developed (Figure 1.10a). These consist of a central DNA region with flanking 2'-modified nucleosides. Since the active site of an exonuclease binds only to two or three residues at the 3'- or 5'-end, a short stretch of 2'-modified RNA nucleosides at both ends is sufficient for protection against exonucleases (Teplova et al., 1999). If the target protein enacts important cellular functions, general downregulation would be unfavourable. In such cases, decreasing the mutation-containing protein is preferred. Selective RNase H-mediated degradation can be achieved using antisense oligonucleotide gapmers targeting specific point mutations, structural differences between wild-type and mutant mRNA, or a single nucleotide polymorphism (SNP) that is unique to the mutant RNA (Evers et al., 2015) (Figure 1.10b).

Another functional mechanism used in antisense technology is by interfering with RNA processes via steric hindrance (Figure 1.10c and d). Aside from RNase-mediated breakdown of mRNA, protein levels can also be lowered by inhibiting translation. Suppressing RNA translation to lower protein levels could be attained by ASOs that target the RNA translation initiation site or sterically blocking the binding of RNA protein complexes, such as ribosomal subunits (Kole, Krainer, & Altman, 2012) (Figure 1.10c). Since many RNA processes rely on the recognition sites or secondary structure of RNA molecules, adding short complementary sequences of modified nucleotides can disrupt these processes. The most well-known application of steric hindrance is manipulating splicing events (Van Ommen & Aartsma-Rus, 2013) (Figure 1.8d). Most human genes express more than one mRNA through alternative splicing and this is an important mechanism for gene regulation. There is a very high level of alternative splicing in the brain, and disruption of normal splicing patterns can cause or modify human disease. ASOs can be

used to hinder this naturally occurring regulatory mechanism by targeting splice sites or exonic/intronic inclusion signals that result in skipping or inclusion of the targeted exon and altering the RNA and protein sequence. This can have numerous applications for neurodegenerative disorders, such as switching from a harmful isoform to a less harmful isoform, skipping an aberrantly included exon to restore the normal transcript, removing diseas-causing mutations from genes, or restoring the reading frame by removing a mutated exon (Evers et al., 2015).

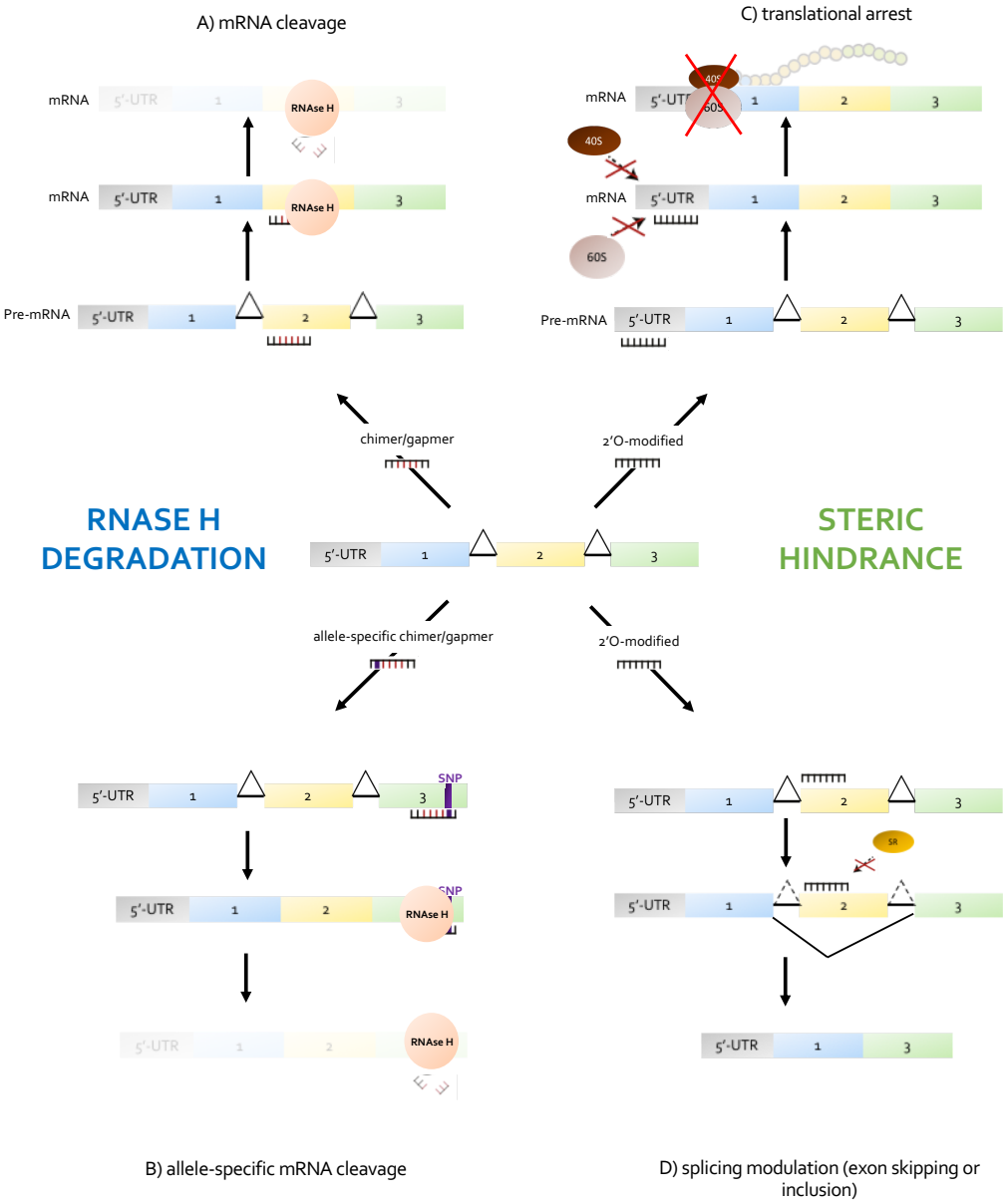

Figure 1.10 Functional mechanisms of antisense oligonucleotides.

ASOs can be used to alter gene expression depending on its chemistry and target site. a) ASO gapmers induce RNase H-mediated breakdown of target RNA. b) RNAse H-mediated breakdown by ASO gapmers that target specific point mutations. c) Suppression of RNA translation by ASOs that target RNA translation start site or sterically hindering binding of RNA binding protein complexes. d) ASOs that bind to splice sites, resulting in exon skipping or inclusion. SR, pre-mRNA splicing machinery. Figure adapted from Evers *et. al.* (2015).

1.4.3 CHEMICAL MODIFICATIONS

ASOs were at first used in the form of synthetic unmodified DNA (Dias & Stein, 2002) (Figure 1.11a). Although effective, these types of oligonucleotides showed susceptibility to degradation by endo- and exonucleases. Thus, it became apparent that their pharmacological profile would have to be improved for ASOs to be used for clinical applications.

First-generation ASOs contain a phosphorothioate (PS)-modified backbone, where a non-bridging oxygen atom in the phosphodiester bond is replaced by a sulphur atom (Figure 1.11c). This modification confers higher resistance against nuclease degradation, giving rise to higher bioavailability of the oligonucleotide. PS-modified ASOs promote RNase-H mediated cleavage of target mRNA. PS modification is the most extensively performed chemical modification of ASOs for loss-of-function studies *in vitro* and *in vivo* for identification and validation of gene targets (Chan, Lim, & Wong, 2006).

To further improve nuclease resistance and increase binding affinity for target mRNA, second-generation ASOs with 2'-sugar modifications were developed (Figure 1.11b). 2'-*O*-Methyl (2'-OMe) and 2'-*O*-Methoxyethyl (2'-MOE) modifications of PS-modified ASOs are the most broadly studied second-generation ASOs (Crooke, 2004). However, 2' sugar modifications do not support RNase H cleavage. To overcome this shortcoming, 'gapmer' ASO structures were developed. They contain 2'-sugar modified residues on either side of a stretch of unmodified PS residues, referred to as the gap. The modified wings improve the binding and stability of the ASO, while the PS gap allows induction of RNase H activity. Binding affinity, and consequently ASO effectiveness, is further improved by using constrained analogs in which the 2' and 4' positions of the sugar are linked. These include locked nucleic acid (LNA) and S-constrained ethyl (cEt) modifications (Southwell, Skotte, Bennett, & Hayden, 2012) (Figure 1.11b).

More radical changes to the backbone have also been developed for non-degradative mechanisms such as translation inhibition or splice modulation, resulting in high resistance to nuclease cleavage but inhibits

cleavage by RNase H. Such ASOs include phosphorodiamidate morpholinos (PMOs), where the furanose moiety is replaced with a morpholine ring connected to the 3' residue through a phosphorodiamidate linkage (Summerton, 1999) (Figure 1.11c). Another example is peptide nucleic acids (PNAs), where a peptide backbone is in place instead of a phosphate backbone (Nielsen, Egholm, Berg, & Buchardt, 1991) (Figure 1.11c). Overall, these chemical alterations greatly enhance pharmacological properties of ASOs, allowing rational design of various and potent therapeutic tools with widespread clinical applications (Southwell et al., 2012).

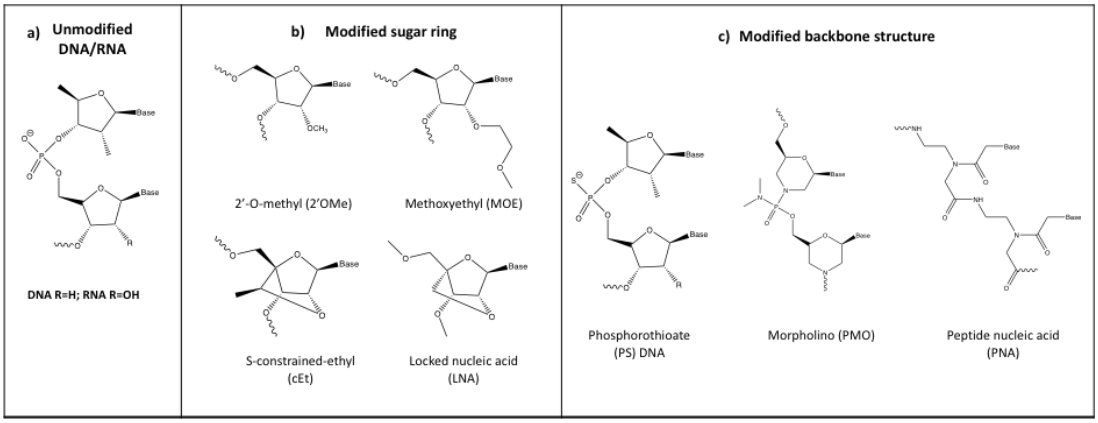

Figure 1.11 Chemical modifications of antisense oligonucleotides.

a) Synthetic unmodified DNA. b) ASOs with modified sugar rings. Alterations to the sugar ring increase target binding affinity to improve pharmacological properties of ASOs. c) ASOs with modified backbone structures. First-generation ASOs contain a PS backbone, whilst more recent modifications resulted in ASOs with a morpholino backbone and a peptide backbone. Alterations to the phosphate backbone increases resistance to nucleases.

1.4.4 PHOSPHORODIAMIDATE MORPHOLINO OLIGONUCLEOTIDES

Phosphorodiamidate morpholino oligonucleotides (PMOs) are synthetic oligonucleotides made up of chains of around 25 subunits that are similar to DNA and RNA oligonucleotides, with a morpholine ring modification instead of a ribose ring (Figure 1.9c). This feature still allows PMOs to undergo Watson-Crick base pairing, but it offers major advantages over conventional oligonucleotides. MOs are particularly resistant to nucleases and are therefore remarkably stable due to its morpholine ring modification. Since they do not carry a negatively charged backbone, they are less likely to undergo non-specific interactions with other components of the cell and may be less toxic as a result (Eisen & Smith, 2008). PMOs do not act through an RNase H mechanism, thus its effects are mainly mediated through steric hindrance of ribosomal assembly, causing translational arrest, or by preventing proper RNA splicing events from occurring (Eisen & Smith, 2008).

1.4.5 ASO APPROACHES FOR NEURODEGENERATIVE DISORDERS

While antisense technology has a long history, ASO drugs have recently shown progress in treating CNS diseases such as spinal muscular atrophy (SMA), Duchenne muscular dystrophy (DMD), and SOD1-related fALS. Further ASO chemistry and design optimisation is needed to enhance tolerability and pharmacology in the CNS. Thorough chemical design and screening of ASOs are essential for effective drug development (Bishop, 2017).

1.4.5.1 ASOS IN SPINAL MUSCULAR ATROPHY

SMA is an autosomal recessive neuromuscular disorder that occurs in infants due to loss and dysfunction of motor neurons in the anterior horn of the spinal cord and lower brain stem. A homozygous deletion of survival motor neuron SMN1 is the main cause of SMA. In humans, two forms of the *SMN* gene exist on each allele: a telomeric form (*SMN1*) and a centromeric form (*SMN2*) (Kolb & Kissel, 2011). *SMN1* gene transcription results in full-length mRNA transcripts that encode the SMN protein. *SMN2* is identical to *SMN1*, aside from a C to T substitution at position 840 which leads to the exclusion of exon 7 during transcription, resulting in a truncated protein and reduced expression of functional SMN protein (Lorson et. al., 2010). Recent therapeutic strategies aim to modify SMN2 splicing by hindering exonic splicing silencers (ESS) or intronic splicing silencers (ISS), thus increasing the inclusion of exon 7. Exon 7 inclusion has been achieved by transfecting fibroblasts with an ASO that blocks an ISS in intron 7 of SMN2 (Singh et. al., 2006), as well as using 2OMe-PS antisense oligonucleotides targeting the 3′ splice site region of exon 8 SMA mouse models (S. R. Lim & Hertel, 2001).

1.4.5.2 ASOS IN DUCHENNE MUSCULAR DUSTROPHY

Other than exon inclusion, ASOs have also been utilised to induce exon skipping as a therapeutic approach for Duchenne muscular dystrophy (DMD), a severe X-linked muscle disease due to mutations in the gene encoding dystrophin. Exon skipping is achieved by masking exon-determining motifs found on frameshift exons to splice them out alongside nearby introns from the pre-mRNA. This helps restore the disrupted reading frame of *DMD* and synthesise shortened Becker muscular dystrophy (BMD)-like dystrophin protein (Jarmin et. al., 2014). Several ASOs designed for DMD treatment have entered clinical trials. Drisapersen, an 18-mer 2'O-methyl phosphorothioate ASO, was designed to target skipping of exon 51. However, drisapersen did not show a statistically significant improvement compared to placebo (Jarmin

et. al., 2014). In another clinical study, eteplirsen, developed by Sarepta Therapeutics, showed significant benefit in walking ability of patients when compared to placebo/delayed controls. Eteplisersen differs from in that it is a 30-mer phosphorodiamidate morpholino oligomer (PMO), hence it is neutrally charged. Eteplirsen was finally granted approval by the US Food and Drug Administration (FDA), thus making the first and currently only FDA-approved drug for DMD (Lim et. al., 2017).

1.4.5.3 ASOS IN ALS

ASOs that have been used in ALS were designed to lower mRNA levels of SOD1 transcripts. Constant infusion of MOE-PS gapmer ASOs into the ventricular system lowered levels of mutant *SOD1* and considerably slowed down disease progression in ALS rodent models (Smith et al., 2006). Phase I studies demonstrated no adverse side effects in patients with SOD1-related fALS following intrathecal injection into the cerebrospinal fluid (Miller et al., 2013). Another recent advance concerning ALS involves targeting the hexanucleotide repeat expansion (GGGGCC) located in the noncoding region of *C9ORF72*. Different types of MOE-PS gapmer ASOs were designed to target exon 2, which is common to all *C9ORF72* transcripts, as well as intron 1 adjacent to the repeat. The ASOs were found to reduce formation of RNA foci in motor neurons differentiated from ALS/FTD patient-derived fibroblasts and induced pluripotent stem cells (Donnelly et al., 2013; Lagier-Tourenne et al., 2013).

1.5 AIMS AND OBJECTIVES

AMPA receptors with an unedited Q/R site at the GluA2 subunit are abnormally permeable to Ca^{2+}, resulting in progressive neuronal death. Dysregulation of RNA editing, which generally occurs in the brain and motor neurons of affected patients with neurodegenerative diseases, can interfere with proper function of glutamate receptors and may be a contributing cause of neuronal death in sporadic ALS (Kawahara et al., 2006). However, the molecular mechanisms and cell death cascade that result in Ca^{2+}-permeable AMPA receptor-mediated cell death remain to be clarified in detail. In this project, we investigate the effects of PMOs on manipulating splicing events of the ADAR enzyme by inducing exon skipping of a 120 bp AluJ cassette, as this cassette has been shown to reduce the catalytic activity of ADAR2. This, in turn, can indirectly improve RNA editing in SH-SY5Y cells. Inducing splicing of the ADAR2 transcript to a more active isoform by using PMOs can increase Q/R site RNA editing levels in SH-SY5Y cells, which endogenously express the GluA2 subunit. Splicing PMOs were designed to target the AluJ cassette (ADAR2 exon 5a), as excluding this cassette has shown to result in a more active isoform of ADAR2 (Gerber et al., 1997). The presence of a more active ADAR2 isoform can hence indirectly improve RNA editing levels, making this a possible therapeutic strategy for sporadic ALS.

Meanwhile, Pin1 and WWP2 have been reported to regulate ADAR2 editing at the Q/R site of GluA2 with opposing effects (Marcucci et al., 2011), suggesting a possible regulatory role of Pin1 and WWP2 in the editing process. Considering that the molecular mechanisms and biological function of underediting in ALS has not been fully elucidated, we then attempted to study the regulation of Pin1 and WWP2 following two separate events: improvement in Q/R site editing and a reduction in editing levels. This will thus provide a better understanding behind the downstream mechanisms behind the pathophysiology of sporadic ALS.

The objectives of this research are:

1. To examine the effects of PMOs on manipulating ADAR2 splicing patterns, and hence RNA editing levels, in SH-SY5Y cells.
2. To study the levels of ADAR2 protein expression in PMO-transfected SH-SY5Y cells.
3. To investigate the regulatory pattern of both Pin1 and WWP2 mRNA and Pin1 protein in SH-SY5Y cells following PMO transfection.
4. To study the effects of PMO transfection on splicing manipulation and gene regulation of Pin1 and WWP2 in differentiated SH-SY5Y cells, which possess a more neuronal-like phenotype.

CHAPTER 2 METHODOLOGY

2.1 PHOSPHORODIAMIDATE MORPHOLINO OLIGONUCLEOTIDES

2.1.1 DESIGN OF PMOS

PMOs used in this project were previously designed by former PhD student, Helena Chaytow. RNA sequences for the human GRIA2 gene and human ADARB1 gene were exported from the Ensembl website (http://www.ensembl.org) in FASTA format (Table 2.1). The sequences were then entered into the MFold website (http://unafold.rna.albany.edu/?q=mfold) in order to predict the RNA secondary structure for both genes. Human Splice Finder (http://www.umd.be/HSF3/) was utilised to provide consensus sequences, splice donor and acceptor sites, and splice enhancer and silencer sequences of exon 6 (which contains the AluJ cassette) and surrounding introns of the ADARB1 gene. The Ensembl transcript number of the gene was inserted and exon 6 was specified for splice site analysis. The graphical output from Human Splice Finder can be seen in Figure 3.2.

Gene	Ensembl Entry Number	Transcript ID
GRIA2	ENSG00000120251	ENST00000348831.9
ADARB1	ENSG00000197381	ENST00000296526.12

Table 2.1 Gene Ensembl entry numbers.

2.1.2 PMO TARGET SITES

The inclusion of the AluJ cassette in the ADAR2 sequence has been shown to reduce RNA editing levels of ADAR2 (Gerber et al., 1997). Hence, PMOs were designed to inhibit the inclusion of the AluJ cassette. The AluJ cassette is a 120 bp sequence that can be found in exon 6 of the ADAR2 gene. The PMOs against AluJ cassette inclusion were designed to target predicted Exon Splice Enhancer (ESE) sites and single-stranded loop structures, which was achieved by using Human Splice Finder (http://www.umd.be/HSF3/). The sequence and its surrounding introns were analysed to predict a suitable secondary structure, which resulted in the design of PMOs 9, 9A and 9B. Inducing exon skipping of the AluJ cassette in SH-SY5Y cells, which results in a more catalytically active isoform of ADAR2, will be able to increase RNA editing levels

PMOs were also designed to disrupt Q/R site editing in cells in order to study its downstream effects. Secondary structures were generated by inputting the sequence of exon 11 and intron 11 of *GRIA2* into MFold, resulting in the design of PMO E1. Sequences of PMOs are shown in Table 2.2.

PMO name	Sequence (5' to 3')
PMO 1 (GRIA2+284+308)	AATGAGAATATGCAGCAAAAACACG
PMO E1 (GRIA2+279+308)	AATGAGAATATGCAGCAAAAACACGGTACC
PMO 9 (AluJ+93+117)	TAGTCCCAGCTCCTTGGAAGGTTGA
PMO 9A (AluJ+94+118)	GTAGTCCCAGCTCCTTGGAAGGTTG
PMO 9B (AluJ+95+119)	TGTAGTCCCAGCTCCTTGGAAGGTT
PMO 10 (AluJ+96+120)	CTGTATCCAGCTCCTTGGAAGGT

Table 2.2 PMO names and sequences

2.1.3 STORAGE OF PMOS

Standard PMOs were supplied as sterile, salt-free, lypophilised solids at 300 nanomoles (Gene Tools LLC, Philomath, OR, USA). 1 mM stock solutions of the PMOs were made by adding 300 µL of nuclease-free water to 300 nanomoles of solid PMO. The PMOs were vortexed to ensure they were readily dissolved. 1 mM stock solutions of PMO were kept at 4°C in sealed containers.

2.2 CELL CULTURE

All cell culture work was carried out using aseptic technique and sterile plasticware inside a class II laminar flow hood.

2.2.1 PROLIFERATION MEDIA FOR SH-SY5Y CELL CULTURE

- Dulbecco's Modified Eagle's Medium – high glucose (Sigma, #D671)
- Foetal Bovine Serum (FBS), 10% final concentration (Gibco, #10500064)
- L-glutamine, 2 mM final concentration (Gibco, #21051040)
- Penicillin-streptomycin, 100 units/mL final concentration (Gibco, #15140122)

The final volume was made up to 500 mL. Culture media was filtered through a sterile 0.45 µM disposable filter (Thermo, #124-0045) before being aliquoted and stored at 4°C.

2.2.2 DIFFERENTIATION MEDIA

- Dulbecco's Modified Eagle's Medium – high glucose (Sigma-, #D671)
- Foetal Bovine Serum (FBS), 1% final concentration (Gibco, #10500064)
- L-glutamine, 2 mM final concentration (Gibco, #21051040)
- Penicillin-streptomycin, 100 units/mL final concentration (Gibco, #15140122)

The final volume was made up to 50 mL and media was stored at 4°C. 1 µM retinoic acid is added to differentiation media prior to differentiating cells.

2.2.3 FREEZING MEDIA

- Dulbecco's Modified Eagle's Medium – high glucose (Sigma, #D671)
- Foetal Bovine Serum (FBS), 10% final concentration (Gibco, #10500064)
- Dimethyl sulfoxide (DMSO), 10 % final concentration (Sigma, #D8418)

Freezing media was made fresh prior to freezing cells at a final volume of 50 mL. Freezing media was stored at 4°C protected from light by covering tubes with aluminum foil.

2.2.4 CELL LINES

The human neuroblastoma SH-SY5Y cell line was purchased from Sigma Aldrich (#94030304-1VL).

2.2.5 THAWING OF FROZEN CELL STOCKS

Frozen cells were retrieved from liquid nitrogen storage and immediately defrosted by submerging the cryovial in a 37°C water bath for 2 minutes. Once defrosted, cells were transferred into a 15 mL tube containing 5 mLs of warm culture media and then spun at 3,000 rpm for 5 minutes to obtain a cell pellet. The media was then aspirated and the cell pellet resuspended in 1 mL of culture media. The cell suspension was next seeded in a T75 cm^3 flask (Corning, #430372). Cells were kept at 37°C and 5% CO_2 and subcultured when they reached 80% confluency.

2.2.6 SUB-CULTURING CELL LINES

Cell confluency was checked daily and sub-cultured once cells were approximately 80% confluent. Growth media was aspirated and cells were washed with pre-warmed 1X phosphate buffered saline (PBS), which is composed of 0.01 M phosphate buffer, 0.0027 M potassium chloride, and 0.137 sodium chloride (Sigma, #P4417). 1 mL of TrypLE (Thermo Fisher #12604021) was then added to detach the cells from the flask and incubated at 37°C and 5% CO_2 for 1 minute. TrypLE activity was then neutralised by adding 9 mL of pre-warmed growth media. Next, cells were centrifuged at 3000 rpm for 5 minutes to obtain a pellet. The media was aspirated and cells were resuspended in 1 mL of pre-warmed growth media, followed by another 9 mL of media to make up 10 mL total solution. A portion of the suspended cells (2 mLs) was then seeded in a new T75 cm^3 flask (Corning, #430372) and a further 10 mL of pre-warmed growth media was added before being incubated at 37°C and 5% CO_2. Cells were sub-cultured when they reached 80% confluency.

2.2.7 CELL DIFFERENTIATION

Prior to plating cells, 12-well plates were first coated with poly-D-lysine (PDL) (0.5 µg/mL in PBS) and incubated for at least 3 hours at 37°C before seeding. Plates were washed with 1X PBS and left to air dry. SH-SY5Y cells were seeded at 60,000 cells per well in a PDL-coated 12-well plate in 500 µL proliferation media. Proliferation media was removed 24 hours post-seeding and cells were washed with 1X PBS before being suspended in 700 µL differentiation media. 350 µL of the medium was replaced every 2 days for a period of 7 days and cell morphology was visualized under a light microscope at the same time points. Cell transfections were carried out at day 6 of differentiation.

2.2.8 CRYOGENIC STORAGE OF CELL LINES

Once cells were 80% confluent, media was aspirated from flasks and cells were washed with 1X PBS. 1 mL of TrypLE was then added to detach cells from the flask, which was followed by incubation at 37°C and 5% CO_2 for 1 minute. 9 mL of pre-warmed growth media was added to inactivate after TrypLE inactivation. Cells were then counted with a haemocytometer, followed by centrifugation at 3000 rpm for 5 minutes to obtain a cell pellet. Cells were resuspended at $1x10^5$ cells per mL in freezing media. Cells were aliquoted at 1 mL per vial in screw-top cryovials and cooled overnight at -80°C, followed by storage in liquid nitrogen.

2.3 PLASMID GROWTH

2.3.1 BACTERIAL TRANSFORMATION

The plasmid expression vector containing the ADAR2 cDNA was kindly provided by the O'Connell group from the University of Edinburgh. The plasmid DNA was transformed and grown in *E. coli* competent cells. NEB 5α competent cells (New England Biolabs) stored at -80°C, were thawed on ice and gently mixed. 50 µL were pipetted into a microcentrifuge tube on ice with 1 µg of plasmid DNA and mixed by flicking before being placed on ice for 30 minutes. The bacteria were then heat shocked at 42°C for 30 seconds and placed on ice for a further 5 minutes. 950 µL of warm SOC media (Thermo Fisher) was added to the microcentrifuge tube which was then placed on a rotating shaker (250 rpm) at 37°C for 60 minutes. Cells were then mixed by flicking and inverting before being streaked on an LB agar plate with 100 µg/mL of ampicillin. Plates were incubated overnight at 37°C.

2.3.2 MAXIPREP OF PLASMID DNA

Large scale preparation of plasmid cDNA was performed using the EndoFree Plasmid Maxi Kit (Qiagen) was used. A single colony was picked from a freshly streaked plate and a starter culture of 5 mL of ampicillin-containing LB medium was inoculated. The culture was incubated for approximately 8 hours at 300 rpm at 37°C. 250 mL of medium was then inoculated with 250 µL of starter culture and grown at 37°C overnight at 300 rpm. The bacterial cells were harvested by centrifugation at 6000 x *g* for 15 minutes at 4°C. The supernatant was discarded and the bacterial pellet was resuspended in 10 mL of Buffer P1. 10 mL of buffer P2 was added and mixed thoroughly by inverting the sealed tube. The mixture was incubated at room temperature for 5 minutes. 10 mL of chilled Buffer P3 was added to the lysate and mixed by inversion. The lysate was poured into the barrel of the QIAfilter Cartridge and incubated at room temperature for 10 minutes. The cap was

removed from the QIAfilter cartridge outlet nozzle. The plunger was gently inserted into the QIAfilter Maxi Cartridge and the cell lysate was filtered into a 50 mL tube. 2.5 mL of Buffer ER was added to the filtered lysate. The contents were mixed by inversion and incubated on ice for 30 minutes. A QIAGEN-tip 500 was equilibrated by applying 10 mL of Buffer QBT and the column was emptied by gravity flow. The filtered lysate was then applied to the QIAGEN-tip and washed with 30 mL of Buffer QC twice. DNA was eluted with 15 mL of Buffer QN and precipitated by adding 10.5 mL of room-temperature isopropanol, followed by centrifugation at 15,000 x *g* for 30 minutes at 4°C. The supernatant was discarded and the pellet washed with 5 mL of 70% ethanol, before another centrifugation at 5,000 rpm for 60 minutes at 4°C. The supernatant was removed and the pellet allowed to air dry for 5 to 10 minutes before being resuspened in 200 µL Buffer TE. The plasmid DNA was the quantified using a NanoDrop spectrophotometer (Thermo Scientific).

2.3.3 RESTRICTION ENZYME DIGEST

Restriction enzyme digests were carried out to validate the correct transformation of the ADAR2 plasmid into the bacteria, according to the ADAR2 gene plasmid map (Figure 2.2). All restriction enzymes used were purchased from Roche. Compatible buffers and digest reaction conditions for each restriction enzyme were found on their respective product pages on the Roche website.

A digestion reaction was typically performed by mixing 0.5 µg of plasmid DNA, 0.5 µL of enzyme, 2 µL of stock buffer solution in a total reaction volume of 20 µL, which was made up with nuclease-free water. Negative control reactions were prepared by excluding the enzyme from the reaction. Digestion reactions were incubated at 37°C for 1 hour. Digestion products were resolved by agarose gel electrophoresis, where 10 µL of the digested plasmid DNA was mixed with 5X loading dye and run on a 1% gel in 1x TAE buffer and visualized under UV trans-illumination.

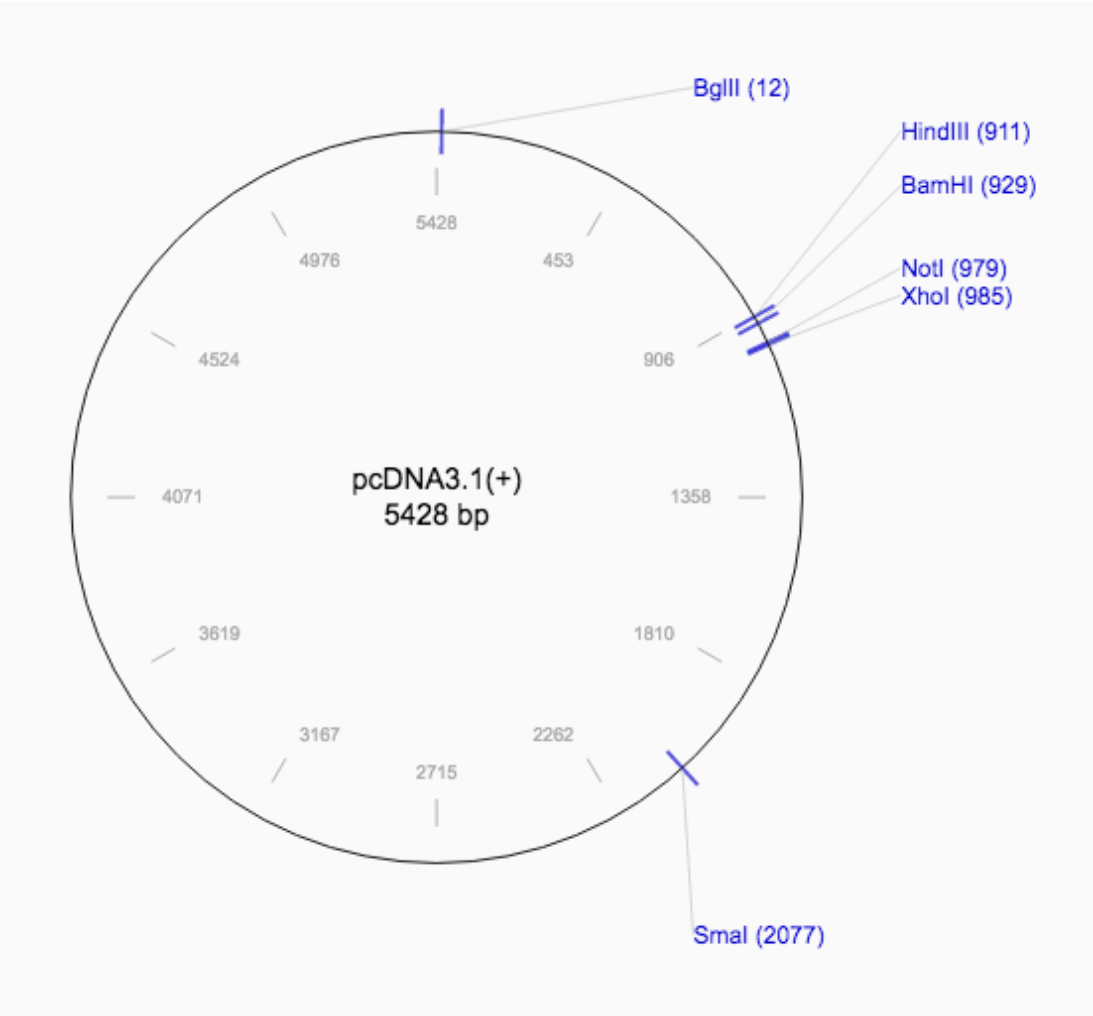

Figure 2.1 Plasmid map of pcDNA3.1 with its multiple cloning sites (MCS).

2.4 CELL TRANSFECTION

2.4.1 LIPOFECTAMINE 2000

SH-SY5Y cells were seeded at a density of 400,000 cells per well in 6-well plates containing 2 mL of proliferation media per well and incubated with 37°C with 5% CO_2. Cells were transfected when 80% confluent. For SH-SY5Y transfection in 6-well plates, a ratio of 1 µL of Lipofectamine 2000 (Thermo Fisher, #11668019) and 1 µg of plasmid DNA per well was used. Lipofectamine 2000 and plasmid DNA were both diluted using 250 µL of serum-free DMEM and incubated at room temperature for 5 minutes. The reagent and plasmid DNA suspensions were mixed together and incubated for another 20 minutes at room temperature to form DNA-lipid complexes. The mixture was then added to the wells and the plate was incubated at 37°C and 5% CO_2. Proliferation media was replaced with fresh media after 4 hours. Cells were then processed 24-48 hours post-transfection. The volumes used were adjusted according to the number of wells to be transfected.

2.4.2 ENDOPORTER

Cells were trypsinised and suspended in media and were seeded in 24-well plates at 200,000 cells per well. Cells were incubated for 24 hours at 37°C in 5% CO_2 before transfection until 80-90% confluent. PMOs were suspended in nuclease-free water to a 1 mM stock concentration and were then stored at 4°C. PMOs were transfected at a range of concentrations, from 0.5-5 µM, as discussed in the results chapters. Prior to transfection, the media was aspirated from each well and replaced with 500 µL of fresh proliferation media. Appropriate volumes of PMO were directly added to the cell media in each well, followed by 6 µM of EndoPorter in DMSO (GeneTools). Plates were swirled to ensure mixing before they were returned to the incubator at 37°C for 24 hours prior to RNA extraction.

2.4.3 PLASMID DNA AND PMO CO-TRANSFECTION

SH-SY5Y cells that were co-transfected with both plasmid DNA and PMO were first seeded at a density of 400,000 cells per well in 6-well plates containing 2 mL proliferation media. Cells were first subjected to plasmid DNA transfection with Lipofectamine 2000, as described in Section 2.4.1. Prior to replacing proliferation media with fresh media after 4 hours of Lipofectamine transfection, cells were transfected with PMOs using EndoPorter, as described in Section 2.4.2.

2.5 RNA EXTRACTION

RNA extraction was carried out using the Promega ReliaPrep RNA Cell Miniprep System (Promega, #Z6011). Media in the wells was removed and wells were washed with 500 µL of ice cold PBS. 250 µL of lysis buffer was added to each well and cells were removed using a cell scraper. 85 µL of 100% isopropanol was added to each lysate and vortexed for 5 seconds to disrupt cell structures. The solution was transferred into a Minicolumn, placed inside a 2 mL collection tube and spun at 14,000 g for 30 seconds. The flow through liquid was discarded and 500 µL RNA wash solution was then added to the column, which was spun at 13,000 g for 30 seconds.

DNase I incubation mix was prepared by combining 24 µL of Yellow Core Buffer, 3 µL of 0.09M $MnCl_2$, and 3 µL of DNase I and mixed by gently pipetting the solution. Samples were incubated with the DNase incubation mix at 20-25°C for 15 minutes. 200 µL of Column Wash Solution was added to the column and spun at 13,000 g for 15 seconds. Next, 500 µL of RNA Wash Solution was added to the sample and spun at 13,000g for 30 seconds. The collection tube was then discarded and the Minicolumn was placed in a new tube. 300 µL of RNA wash solution was added to the sample and was spun at 15,000 g for 2 minutes. The Minicolumn was then transferred to an elution tube. 25 µL of nuclease-free water was added to the Minicolumn membrane

and the sample was spun at 13,000 g for 1 minute to elute the RNA. RNA concentrations were measured using a NanoDrop spectrophotometer (Thermo Scientific).

2.6 POLYMERASE CHAIN REACTION

2.6.1 REVERSE TRANSCRIPTION CDNA SYNTHESIS

1 µg of each DNase-treated total RNA sample was used for cDNA synthesis using the GoScript Reverse Transcriptase kit (Promega, #A5003) according to the manufacturer's instructions. RNA was mixed with Oligo$(dT)_{15}$ (Promega, #C1101) and the final volume was made up to 10 µL with nuclease-free water. Tubes were then heated at 70°C for 5 minutes and left to chill at 4°C for a further 5 minutes. The reverse transcription mix was prepared by combining 4 µL of GoScript 5X Reaction Buffer, 1.2 µL of $MgCl_2$, 0.5 mM of dNTP, 1 µL of GoScript Reverse Transcriptase, where the final volume was made up to 10 µL with nuclease-free water. 5 µL of the RNA mix was then added to the reverse transcription mastermix and placed in a PCR machine with the following heat cycle: annealing at 25°C for 5 minutes, extension at 42°C for one hour, and reverse transcriptase inactivation at 70°C for 15 minutes.

2.6.2 FIRST ROUND AND SECOND ROUND NESTED PCR

For human ADAR2 and GRIA2 gene amplification, two rounds of PCRs were carried out. Primers were obtained from Sigma Aldrich at stock concentrations of 10 µM. Primer stocks were then diluted down to a working concentration of 1 µM for PCR use. Primer target genes and sequences are shown in Table 2.3.

5 µL of cDNA was used for the first round PCR. The GoTaq DNA Polymerase kit (Promega, #M3001) was used. A PCR master mix was

prepared by adding 1x GoTaq Reaction Buffer, 1 mM $MgCl_2$, 0.2 mM of each dNTP, 1 µM of each primer and 0.125 µL of GoTaq DNA Polymerase, where the final volume was made up to 25 µL with nuclease-free water. The PCR was carried out in a G-Storm 482 Thermal Cycler (Gene Technologies, #GS00482) using the following heat steps: 95°C for 3 minutes, 25 cycles of 94°C for 30 seconds, 60°C for 30 seconds and 72°C for 45 seconds, and a final annealing step of 72°C for 10 minutes.

A second round nested PCR was carried out to increase gene amplification of GRIA2 and ADAR2 transcripts. 1 µL of product from first round PCR was added to the PCR master mix as described above. The PCR was performed in a G-Storm 482 Thermal Cycler (Gene Technologies, #GS00482) using the following heat cycle: 95°C for 3 minutes, 18 cycles of 94°C for 30 seconds, 60°C for 30 seconds and 72°C for 45 seconds, and a final annealing step of 72°C for 10 minutes. Samples were then stored at 4°C.

Primer target gene	Sequence (5' to 3')	PCR fragment size (bp)
Human GRIA2	Sense: CAAAGCCCTTCATGAGCCTC	365
	Antisense: CCATGAATGTCCACTTGAGACC	
Human GRIA2 (nested primers)	Sense: GCCTCAGAAGTCCAAACCAG	323
	Antisense: CCATGAATGTCCACTTGAGACC	
ADAR2 AluJ cassette	Sense: ATCCATCTTTCAGAAATCAGAGC	247
	Antisense: TTTGGTCCGTAGCTGTCCTC	
ADAR2 AluJ cassette (nested primers)	Sense: AGGCTGAAGGAGAATGTCCA	127

Table 2.3 Sequences of PCR primers and expected product sizes.

2.7 AGAROSE GEL ELECTROPHORESIS

Agarose gel electrophoresis was used to determine the inclusion of the AluJ cassette and verify the presence of the GRIA2 gene. A 50X stock solution of Tris-acetate-EDTA (TAE) buffer was prepared (242 g Tris base, 57.1 mL glacial acetic acid, 100 mL 500 mM pH 8.0 EDTA made up to 1 L with ddH_2O). 1.5% agarose gels were prepared by adding 0.9 g of agarose to 60 mL of 1X TAE buffer until fully dissolved by heating the mixture in a microwave. 3 µL of SYBR Safe DNA Gel Stain was added to the gel mixture before being poured into a casting tray with a gel comb and left to set. Gels were submerged in 1X TAE buffer in an electrophoresis tank (Bio-Rad). 10 µL of each sample was loaded into wells alongside 5 µL of HyperLadder I (Bioline, #BIO-33025). Gels were run at 90V for 35 minutes and the DNA bands visualized under UV light in a GELDOC system.

2.8 *BBVI* RESTRICTION DIGEST

In order to quantify RNA editing levels in cells, RT-PCR cDNA products of the Q/R editing site were digested with the *BbvI* restriction endonuclease (New England Biolabs). 1 µL SmartCut buffer and 2 µL of *BbvI* (2U/µL) was made up to a total volume of 5 µL mastermix with nuclease-free water. 15 µL of PCR product was then added to the master mix and digest samples were incubated for 1 hour at 37°C. The enzyme was then inactivated by adding 0.1% SDS to each sample and incubated for another 5 minutes at room temperature before adding 5X loading dye. Samples were then run on a 2.5% (w/v) agarose gel at 90 V in 1X TAE buffer for 60 minutes alongside 5 µL Hyperladder I (Bioline).

2.9 DENSITOMETRIC ANALYSIS

Gel images were taken under ultraviolet light using the GELDOC imaging system and saved as JPEG files. Analysis was carried out using the Fiji image processing package (http://fiji.sc/). Each band in the image was highlighted and the fluorescence of each pixel was measured by the software. The mean pixel value was calculated per band, and the background fluorescence was subtracted. Further analysis of the data was then carried out using Microsoft Excel.

2.9.1 ALUJ CASSETTE INCLUSION QUANTIFICATION

Once the fluorescence intensity of each band had been calculated, the relative intensity of AluJ exon-including ADAR2 transcripts to exon-excluding transcripts were compared. Primers used in the PCR targets the exons surrounding the AluJ cassette. ADAR2 transcripts containing the AluJ cassette are of a larger size (247 bp) than transcripts without the AluJ cassette (127 bp). Exon skipping percentages were calculated using the following formula:

$$\frac{Fluorescence\ of\ exon\ skipped\ fragments}{Total\ fluorescence} \times 100\% = Exon\ skipping\ percentage\ in\ cells$$

2.9.2 Q/R SITE EDITING QUANTIFICATION

Editing percentages were calculated using the same method as described above. The relative intensity of edited to unedited DNA was compared, where band sizes were based on the recognition sequence of the *BbvI* restriction enzyme (GC**A**GC). Edited cDNA copies do not contain a recognition sequence for *BbvI* and hence remains undigested and are seen on the gel image as a full-length transcript (323 bp). Unedited cDNA copies are cleaved into two smaller sized fragments (238 bp and 83 bp), as they are digested by *BbvI*. Q/R site editing percentages were calculated using the following formula:

$$\frac{Fluorescence\ of\ edited\ fragments}{Total\ fluorescence} \times 100\% = RNA\ editing\ percentage\ in\ cells$$

2.10 PROTEIN ANALYSIS

2.10.1 REAGENTS AND SOLUTIONS

- DC protein assay (Bio-Rad, #5000111)
- 30% Protogel (Bis-acrylamide solution; National Diagnostics, #EC890)
- Absolute methanol (VWR)
- Marvel Dried Milk Powder
- NuPAGE Sample Reducing Agent (Invitrogen, #NP0009)

Solution	Components
RIPA lysis buffer	150 nM NaCl, 1% Nonidet P-40, 0.5% sodium deoxycholate, 0.1% SDS, 25 mM Tris pH 7.4, 1 protease inhibitor tablet per 10 mL
1X Tris-glycine transfer buffer	25 mM Tris, 192 mM glycine, 10% methanol
1X Tris-glycine running buffer	25 mM Tris, 192 mM glycine, 0.1% SDS; pH 8.3
4X resolving buffer	1.5 M Tris-base, 8 mM EDTA, 0.4% SDS, pH 8.8
4X stacking buffer	0.5 M Tris-base, 8mM EDTA, 0.4% SDS, pH 6.8
1X Tris-buffered saline (TBS)	50 mM Tris base, 150 nM NaCl
1X phosphate-buffered saline (PBS)	1 PBS tablet (Gibco, #003002) dissolved in 500 mL ddH_2O

Table 2.4 Western blot solution recipes

2.10.2 ANTIBODIES

	Antibody	Host	Dilution	Catalog number
Primary	anti-ADAR2	Rabbit	1:100	GeneTex, #GTX114237
	anti-ADAR2	Mouse	1:100	Santa Cruz, #SC-514581
	anti-ADAR2	Mouse	1:100	Santa Cruz, #SC-10012
	anti-Pin1	Mouse	1:100	Santa Cruz, #SC-46660
	anti-β-actin	Mouse	1:5000	Sigma, #A1978
	anti-FLAG	Rabbit	1:1000	Sigma, #F7425
Secondary	anti-rabbit	Goat	1:5000	Cell Signalling, #5151S
	anti-mouse	Goat	1:5000	Cell Signalling, #5470S

Table 2.5 Primary and secondary antibodies used for protein detection.

2.10.3 PROTEIN EXTRACTION

SH-SY5Y and HeLa cells were transfected and treated as previously described is section 2.5. Following 48 hours of Lipofectamine 2000 and EndoPorter transfection, 6-well plates were removed from the incubator and placed on ice. The media was removed and cells were washed with 1X PBS before 100 µL of RIPA lysis buffer was added. Each well was scraped using a cell scraper to detach cells adhering to the bottom of the well. The lysate was

then collected and spun at 13250 rpm for 20 minutes before the supernatant was extracted and stored at -20°C.

2.10.4 DC ASSAY

The concentrations of the protein extracts were determined by using a DC™ (detergent compatible) protein assay (Bio-Rad) as per the manufacturer's instructions. Firstly, known concentrations of bovine serum albumin (BSA) of 0.2-1.5 mg/mL were prepared to use as a standard curve. Next, 20 µL of reagent S was added to each mL of reagent A that was needed for the run in order to form reagent A'. 1 µL of the standards and protein samples were pipetted into each well of a 96-well plate. 25 µL of reagent A' was then added into each well, followed by the addition of reagent B. The plate was then left to stand for 15 minutes before the absorbance was measured in a plate reader at 750 nm.

2.10.5 SAMPLE PREPARATION

Protein lysates were diluted to final concentrations of 1 µg/mL. Each protein sample was prepared to a final volume of 100 µL by diluting the lysate in 25 µL of LDS Sample Buffer (Invitrogen, #NP0008, 4X final), 10 µL NuPAGE Reducing Agent (Invitrogen, #NP0009) and adjusting the volume to 100 µL with molecular grade water. Samples were denatured on a heat-block shaker at 75°C for 8 minutes and kept on ice.

2.10.6 WESTERN BLOTTING

2.10.6.1 SODIUM DODCEYL SULFATE POLYACRYLAMIDE GEL ELECTROPHORESIS (SDS-PAGE)

10% resolving gel solutions were prepared following the recipe shown in Table 2.6. The resolving gel was prepared by casting the solution between two glass-plate cassettes of 1 mm thickness (Mini-PROTEAN Tetra handcast system, Bio-Rad) and overlayed with 100% isopropanol. Once the gel was set, isopropanol was removed by washing with ddH_2O. A 4% stacking gel solution was then prepared and a comb inserted into the glass-plate cassette. Once the stacking gel has set, the glass-plate cassette was transferred into a Mini-PROTEAN Tetra Electrode Assembly, which was then placed into a buffer tank. The chambers were filled with 1X Tris-glycine running buffer and the comb was removed from the stacking gel. 50 µg of protein was loaded into each well alongside 1 µL of BLUeye Prestained Protein Ladder (GeneFlow, #S60024). The gel was then left to run at 125V until the bromophenol blue dye band ran off the gel.

	Resolving gel (10%)	**Stacking gel (4%)**
Buffer	2 mL	1 mL
Protogel	2.6 mL	0.65 mL
ddH_2O	3.4 mL	4.6 mL
TEMED	6 µL	20 µL
10% APS	40 µL	160 µL
Total volume	8 mL	6.25 mL

Table 2.6 Recipes for resolving and stacking gels for SDS-PAGE.

2.10.6.2 PRE-CAST BIS-TRIS SDS-PAGE

10% pre-cast Bis-Tris SDS-PAGE gels (Invitrogen, #NP0303) were used for the detection of Pin1 protein in SH-SY5Y cells. The comb and gel wells were first rinsed with ddH_2O. The white tape located at the bottom of the gel cassette was removed and the gel cassette was then placed in an XCell SureLock Mini-Cell gel running tank. 200 mL of 1X NuPAGE MES SDS Running Buffer (containing 500 µL NuPAGE Antioxidant) was then filled into the upper chamber of the tank. The lower chamber was filed with 600 mL of 1x NuPAGE MES SDS Running Buffer. 50 µg of protein was loaded into each well alongside 1 µL of BLUeye Prestained Protein Ladder (GeneFlow, #S60024). The gel was then left to run at 200V until the bromophenol blue dye band ran off the gel.

2.10.6.3 NITROCELLULOSE MEMBRANE TRANSFER

Following protein electrophoresis, the transfer cassette was assembled. The gel was carefully removed from the glass-plate cassette and placed onto a 0.2 µM pore size nitrocellulose membrane (Amersham, #15249794). The membrane was sandwiched between 2 filter papers (Whatman, and 2 blotting sponges that have been soaked in 1X Tris-glycine transfer buffer. Pressure was applied on the sandwich to remove air bubbles and excess liquid. The transfer cassette was then closed and placed into a transfer tank filled with 1X Tris-glycine transfer buffer and left to run at 10V overnight.

2.10.6.4 IMMUNOBLOTTING

Following protein transfer, the membranes were then blocked with 5% non-fat dried milk in TBS containing 0.05% Tween-20 at a final volume of 5

mL. The membranes were sealed in a plastic bag and agitated for 90 minutes at room temperature. Next, the membranes were incubated with primary antibody diluted in 5% non-fat dried milk in 1X TBS with 0.05% Tween-20 at a final volume of 5 mL overnight at 4°C with gentle agitation. The membranes were then washed twice with 1X TBS for 10 minutes each, followed by incubation with secondary antibody diluted in 5% nonfat dried milk in TBS containing 0.05% Tween-20 at a final volume of 5 mL for 1 hour at room temperature away from light. The two wash steps were repeated and the damp membrane was scanned using the Odyssey CLx Imaging System (LI-COR Biosciences) to visualise the protein bands at 560 nm, 700 nm or 800 nm wavelength. The blots were then stored at -20°C in 1X TBS in sealed bags after scanning.

2.11 QUANTITATIVE REVERSE TRANSCRIPTASE POLYMERASE CHAIN REACTION (QRT-PCR)

For quantitative RT-PCR of mRNAs, 600 ng of RNA was generated using 0.5 µg of random primers (Invitrogen, #48190011) and 0.5 µg oligo(dT) (Promega, #C1101) and the final volume was made up to 10 µL with nuclease-free water. The tubes were then heated at 70°C for 5 minutes and left to chill at 4°C for another 5 minutes. A mastermix was then made up using the GoScript Reverse Transcriptase kit (Promega, #A5003) according to the manufacturer's instructions. RNA was added to 5x GoScript buffer, 2.5 mM $MgCl_2$, 0.5 mM dNTP, 8 units of reverse transcriptase, and the final volume was made up to 15 µL with nuclease-free water. The mixture was incubated in the following RT-PCR cycle: annealing at 25°C for 5 minutes, extension at 42°C for 1 hour, and a final inactivation step of 70°C for 15 minutes. cDNA was then stored at 4°C before use.

The expression levels of target genes were assessed with qRT-PCR using the LightCycler® 480 SYBR Green I Mastermix (Roche, #04887352001). The cDNA produced was first diluted 1:50 in nuclease-free water for the qPCR reactions. 0.5 µM of each forward and reverse primer

(Table 2.8) was added to 5 µL of mastermix before being mixed with diluted cDNA in a 384-well plate. The PCR reaction was conducted at 95°C for 10 minutes, followed by 40 cycles of 95°C for 15 seconds, 60°C for 15 seconds, and 70°C for 15 seconds. All samples were amplified in technical triplicates. Primer sequences were obtained from Primer Bank (https://pga.mgh.harvard.edu/primerbank/) and made by Sigma Aldrich (Table 2.7). The expression levels of β-actin were used as a reference gene. The gene expression levels were defined based on the threshold cycle (Ct), and relative expression levels were calculated using the $2^{-\Delta\Delta Ct}$ method, where fold-change was inferred from Ct level fluctuations of target genes made against reference genes.

Gene	Forward sequence (5'-3')	Reverse sequence (5'-3')
PIN1	TCAGGCCGAGTGTACTACTTC	TCTTCTGGATGTAGCCGTTGA
WWP2	CAAAGCCCAAGGTGCATAATCG	CCAATGCGCTTCCCAGTCT
ACTB	GACGACATGGAGAAAATCTG	ATGATCTGGGTCATCTTCTC

Table 2.7 Primer sequences for genes used in qRT-PCRs.

2.12 DATA ANALYSIS AND STATISTICS

Percentages and ratio-fold changes were calculated on Microsoft Excel from raw values. Calculated values were then inputted in GraphPad Prism 7.0 (GraphPad Software, La Jolla CA, USA) for statistical analysis. Statistical significance was tested using either one-way ANOVA followed by Dunnett's multiple comparison test or unpaired t-test. IC50 and EC50 values were calculated by fitting the Hill equation using GraphPad Prism 7.0. Graphs were

plotted with GraphPad Prism 7.0, where all error bars show standard error of the mean (SEM).

CHAPTER 3 EXON SKIPPING OF THE ALUJ CASSETTE IN SH-SY5Y CELLS AND THE EFFECT ON RNA EDITING

3.1 INTRODUCTION

Alternative splicing refers to the process where exons of primary transcripts are spliced into alternative arrangements, resulting in structurally and functionally different mRNA and protein variants (Siva, Covello, & Denti, 2014). An estimated 70% or more of human multiexon genes undergo alternative splicing (Johnson et al., 2003), and most of these splicing events are regulated in a tissue-specific manner (Clark et al., 2007). The adult human brain expresses more alternatively spliced transcripts compared to any other tissue (Yeo, Holste, Kreiman, & Burge, 2004). Point mutations in a gene can weaken or strengthen splice sites, thus causing modification in splicing events and subsequent disease (Siva et al., 2014). Splicing deficiencies are being increasingly associated with neurodegenerative and neurological diseases, highlighting the need to better comprehend these regulatory processes (Vuong, Black, & Zheng, 2016).

There are two main steps involved in basic splicing events: spliceosome assembly, followed by pre-mRNA splicing. The spliceosome is primarily comprised of U1 and U2 small nuclear ribonucleic proteins (snRNPs), as well as the U4/U5/U6 tri-snRNP. The snRNPs configure and identify the 5' splice site, the branch point sequence, and the 3' splice site. Spliceosome complexes E, A, B and eight evolutionary conserved DExD/H-type RNA-dependent ATPases/helicases assemble in a gradual manner and carry out multiple splicing steps, resulting in exon ligation and intron excision (Y. Wang et al., 2014). Various steps in the pathway are reversible.

Whilst the splicing mechanism has been determined in great detail, it has not yet been fully understood how splice sites are selected (Stamm et al.,

2005). This is due to the degeneracy of regulatory splicing sequences, such as 5' and 3' splice sites, branch points, and exonic/intronic sequence elements, which can only be described as loosely followed consensus sequences (Black, 2003). As a consequence, it is not possible to predict accurate splicing patterns from genomic sequence. A combinatorial regulatory mechanism results from accurate recognition of splice sites *in vivo* (C. W. J. Smith & Valcárcel, 2000). Since splice sites are degenerate, additional sequence elements found in the exon or in adjacent intronic elements assist in their recognition through binding to regulatory proteins, which are subdivided into serine-arginine-rich SR proteins and hnRNPs. The proteins generally bind to RNA weakly. Increased specificity is accomplished by binding multiple proteins to RNA, with the aid of protein-protein interactions. Several regulatory proteins bind to spliceosome components, such as the U1 and U2 snRNP, which defines the 5' splice-site and branch point respectively (Stamm et al., 2005). Considering that splicing factors bind to various weakly conserved sequences, a single factor can regulate numerous target genes. Target genes for the neuron-specific splicing factor NOVA-1 are highly functionally related. These genes were linked to the function of inhibitory synapses, post- and pre-synaptic structures, and signaling and protein synthesis. This implies that a single splicing factor regulates isoform expression of different genes in inhibitory neurons (Stamm et al., 2005).

Splicing processes are regulated by different *cis*- and *trans*-acting factors, which affects splice site selection. Positive *trans*-acting factors, such as SR proteins (serine/arginine-rich family of nuclear phosphoproteins) bind to *cis*-acting elements including exonic splicing enhancers (ESEs) and intronic splicing enhancers (ISEs). Conversely, intronic splicing silencers are bound by negative acting factors, such as heterogenous nuclear ribonucleoproteins (hnRNPs). The association of these elements leads to the promotion or inhibition of spliceosome assembly of weak splice sites (Y. Wang et al., 2014).

Although there is a large potential for errors, splicing processes occur with high fidelity, indicating the extensive involvement of transcript features aside from core splice signals involved in splice site selection. This information is thought to largely derive from the presence of numerous *cis*-regulatory

elements that act as either splicing enhancers or silencers (Z. Wang & Burge, 2008). Enhancer elements play an important role in constitutive splicing, whereas silencer elements are relatively more dominant in alternative splicing (Y. Wang et al., 2014). Aside from the coupling of SR proteins to enhancer elements, SR proteins also interact with U1 snRNP and the 35 kDa subunit of the heterodimeric factor U2AF. $U2AF^{65}$, the second subunit of U2AF, binds splicing factor 1 (SF1) and the pyrimidine tract simultaneously, resulting in recognition and stability of the branch point and polypyrimidine tract sequences (Figure 3.1). Roughly 10-12 serines located in the N-terminal region of the RS domain undergo rapid phosphorylation by the binding of SR-specific protein kinase to SF1 with a remarkably high affinity. This constant cycle of phosphorylation/dephosphorylation of SR proteins aids the transport of SR proteins between the nucleus and cytoplasm, and is crucial for the regulation of alternative splicing by growth signals transduced to the nucleus (Ghosh & Adams, 2011; Twyffels, Gueydan, & Kruys, 2011).

The most common splicing event in mammals is exon skipping, accounting for 40% of alternative splicing events in humans and mice (Sugnet, Kent, Ares, & Haussler, 2004). Exon skipping is the process where an exon cassette is excised from the transcript alongside the flanking introns (Gamazon & Stranger, 2014). Nine splice sites, located at different exons in human ADAR2 pre-mRNA, have been discovered so far. Among these splicing events, five of them are shown to affect the catalytic function of ADAR2 (Li et al., 2015). One such alternative splicing event results in two major ADAR2 isoforms, which differ by the inclusion or exclusion of an *Alu* cassette within the deaminase domain, located between exons 5 and 6 of ADAR2 pre-mRNA. Characterisation of both ADAR2 isoforms showed that they identical substrate specificity. However, inclusion of the *AluJ*-containing exon caused a twofold reduction in ADAR2 activity on a GluA2 R/G site substrate *in vitro* (Gerber et al., 1997). Another major transcript lacking the last two amino acids was isolated and this isoform was found to be catalytically inactive (Lai, Chen, Lee, & Nishikura, 1997).

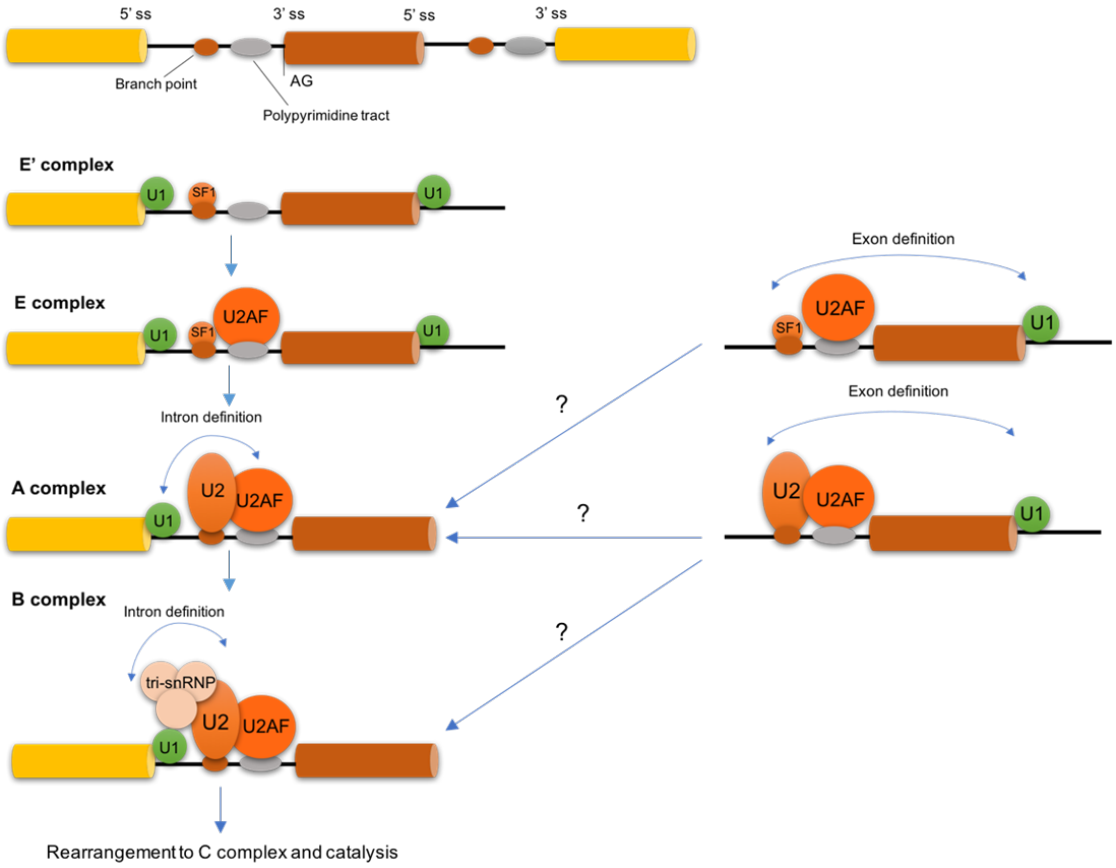

Figure 3.1 Mechanisms of spliceosome assembly.

The process starts with the base pairing of U1 snRNA to the 5' splice site (ss) and the binding of splicing factor 1 (SF1) to the branch point to form the E' complex. The E' complex is converted into the E complex through recruitment of U2 auxiliary factor (U2AF) heterodimer (composed of U2AF65 and U2AF35) to the polypyrimidine tract and 3' terminal AG. The ATP-independent E complex is converted into the ATP-dependent pre-spliceosome A complex by the substitution of SF1 by U2 snRNP at the branch point. Additional recruitment of the U4/U6-U5 tri-snRNP generates the formation of the B complex, containing spliceosomal subunits responsible for pre-mRNA splicing. This is ensued by extensive conformational changes and remodeling, such as the loss of U1 and U4 snRNPs, resulting in the formation of the C complex, the catalytically active spliceosome.

The use of antisense oligonucleotides as agents for downregulation of gene expression is now well-established. Antisense compounds have been developed to manipulate alternative splicing patterns, thus altering both the ratio of different splice variants and gene function (Sazani & Kole, 2003). ASOs that have been designed to bind to splice sites or to ESEs or ISEs causes the masking of these regions, leading to ineffective binding of *trans*-splicing regulatory factors, thus leading to switching between alternative splice isoforms through exon skipping. In principle, ASOs designed to block exonic or intronic splicing silencers (ESSs or ISSs) can also promote exon inclusion in the context of disease-associated exon skipping (Siva et al., 2014). Exon inclusion ASOs has been used in the treatment for spinal muscular atrophy, where the drug Nusinersen promotes inclusion of *SMN2* exon 7 by sequestering the ISS (N. N. Singh, Howell, Androphy, & Singh, 2017). Exon skipping approaches have now been utilized in the treatment of DMD by the drug Eteplirsen, which targets exon 51 of *DMD* (K. R. Q. Lim et al., 2017).

The design of ASOs is vital to effective exon skipping. The optimum length of the ASO is dependent on the antisense chemistry. For example, locked nucleic acid (LNA) oligomers are 8-14mer in length as they are known to have particularly high binding energy, and longer LNAs can form undesirable secondary structures. PMOs however have a lower binding affinity, thus requiring longer sequences (25-30mer) (Shimo, Maruyama, & Yokota, 2017). Other key parameters in designing ASOs include target site selection, mRNA secondary structure, and the melting temperature versus the RNA strand (Aartsma-Rus et al., 2009). Predicting target sequences of the ASO can be carried using in silico tools such as the ESE finder and the RESCUE-ESE. Assessment of off-target effects should also be included in the design process (Shimo et al., 2017).

In this chapter, several different exon skipping PMOs have been used to measure its effectiveness in excluding the AluJ cassette from the final mRNA transcript. These PMOs have previously been tested in HeLa cells that have been transfected with the B13 minigene, which contains a partial fragment of the GluA2 subunit. Transfected HeLa-B13 cells resulted in a 30% increase in Q/R site editing when compared to controls (Chaytow, 2015).

However, we have not examined the efficacy of these PMOs in cells endogenously expressing edited GluA2 and partly replicate neuronal conditions. Human neuroblastoma SH-SY5Y cells were used here as they endogenously express the GluA2 subunit. This cell line is generally used as a neuronal cell model in studies of Parkinson's and Alzheimer's disease since they can be differentiated to resemble dopaminergic neurons (Dwane, Durack, & Kiely, 2013). Following transfection with PMOs, exon skipping levels were calculated and any changes in Q/R site editing levels were measured in the cells. The data presented here shows how PMOs were able to successfully alter exon skipping levels in these cells, consequently increasing Q/R site editing levels. Improving RNA editing levels in cells could be a potential therapeutic strategy for ALS as reduced Q/R site editing has been demonstrated in spinal grey matter and neurons of patients with ALS (Kawahara, Ito, Sun, Kanazawa, & Kwak, 2003; Takuma, Kwak, Yoshizawa, & Kanazawa, 1999). Hence, the work here provides support for the use of ASO exon skipping technology for the treatment of sporadic ALS.

3.2 RESULTS

3.2.1 EFFECTS OF PMOS ON ALUJ CASSETTE INCLUSION

SH-SY5Y cells were transfected with four different PMOs - PMO 9 (AluJ+93+117), PMO 9A (AluJ+94+118), PMO 9B (AluJ+95+119), and PMO 10 (AluJ+96+120) - at concentrations ranging from 0.05 μM to 5 μM for 24 hours. The PMOs were designed to target the exon splice enhancer (ESE) motifs surrounding the AluJ cassette, as this will facilitate exon exclusion (Figure 3.2). Exon splice silencer (ESS) regions were avoided as covering this region could induce exon inclusion (Figure 3.2) The sequence of the PMOs also targets the 25 nucleotides at the 3' end of the exon, thus covering the splice consensus sequence (Figure 3.2).

RNA was harvested from these cells and PCRs were performed to determine the presence of the two different isoforms of ADAR2 present – one containing the AluJ cassette, and one with the AluJ cassette excluded from the final transcript. For AluJ cassette inclusion analysis, nested primers surrounding exons 5 and 7 of the ADAR2 gene, which surrounds the 120 bp AluJ cassette, were used. AluJ cassette inclusion levels were measured by comparing the intensities of PCR fragments that contain the AluJ casstte (247 bp) to those that exclude the cassette (127 bp).

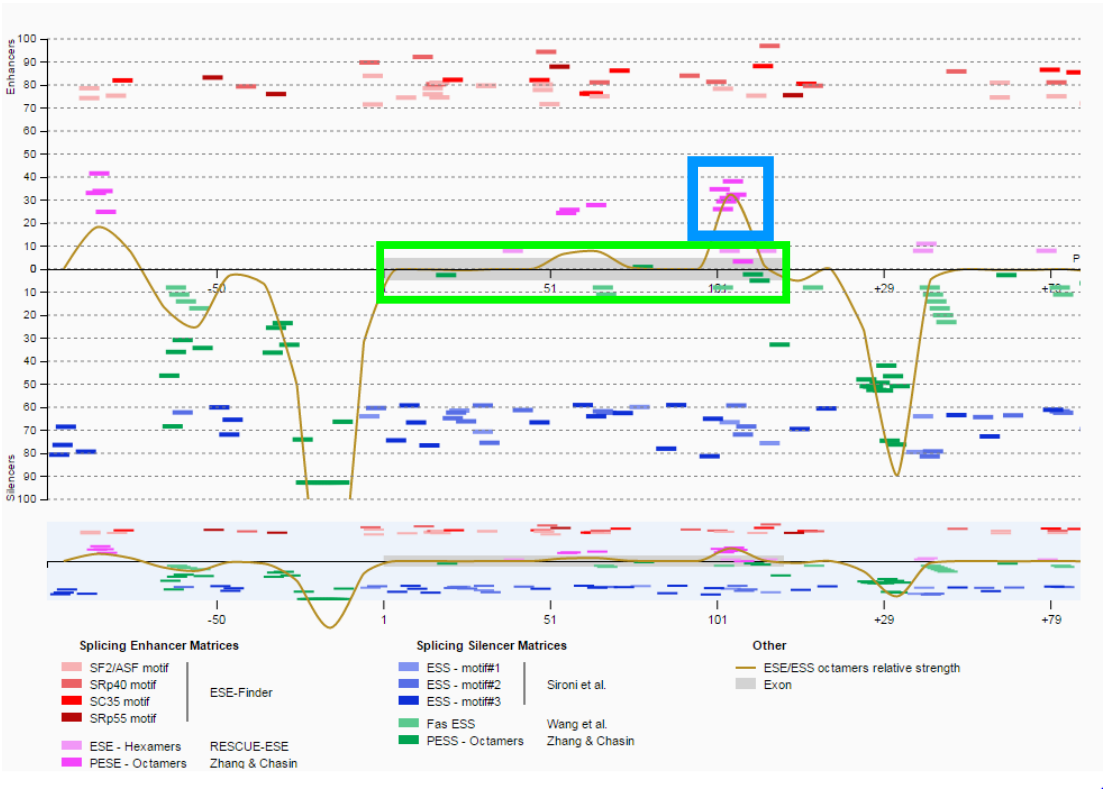

Figure 3.2 Graphical output from Human Splice Finder.

The above figure shows the graphical output of splice enhancer and silencer motifs. The grey box (outlined in green) represents the AluJ cassette-containing exon 6 of *ADARB1* and its surrounding introns. Red and pink boxes represent exon splice enhancer (ESE) regions, while blue and green boxes represent exon splice silencer (ESS) regions. A cluster of ESE binding sites at the 3' end of exon 6 (outlined in blue) indicate potential PMO design targets as covering these sequences may prevent exon inclusion. Yellow peaks above the x-axis illustrate strong ESE regions and yellow troughs below the x-axis illustrate strong ESS regions.

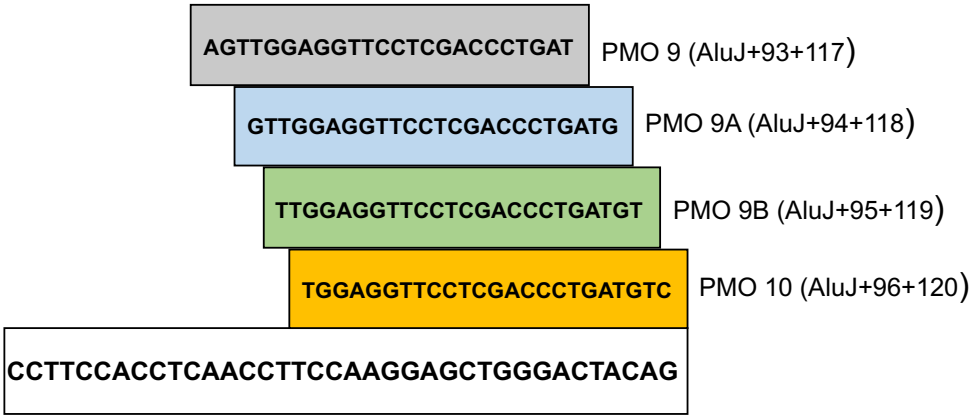

Figure 3.3 Sequences of PMOs that are complementary to the 3' end of the AluJ-containing exon of the ADAR2 gene.

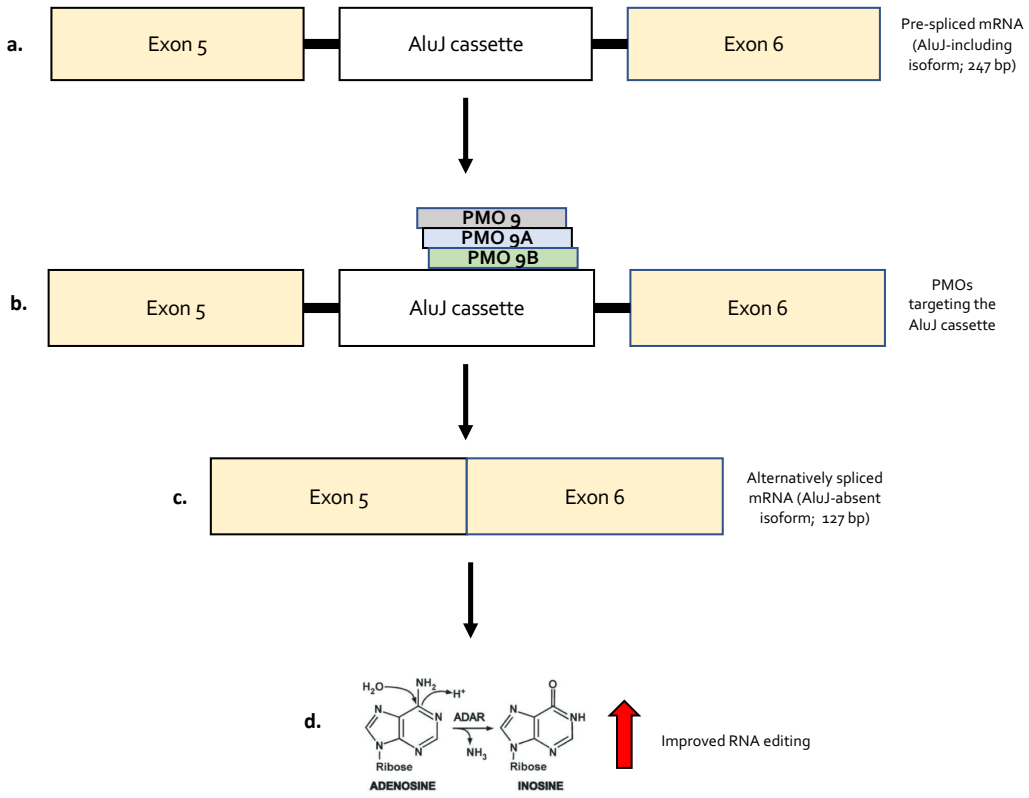

Figure 3.4 Schematic diagram illustrating the outcome of PMO transfection.

a) Pre-spliced mRNA of ADAR2 containing the AluJ cassette. Inclusion of this cassette results in reduced catalytic ADAR2 activity, which can be restored by b) using PMOs that target the AluJ cassette to manipulate ADAR2 splicing by exon skipping. This results in c) an ADAR2 isoform which does not contain the AluJ cassette, hence d) improving RNA editing in SH-SY5Y cells.

3.2.1.1 PMO 9 (ALUJ+93+117)

PMO 9 (AluJ+93+117) was previously tested alongside several other PMOs in HeLa cells, and it was shown to have the strongest effects on cassette exon exclusion. PMO 9 (AluJ+93+117) was then further tested in SH-SY5Y cells to evaluate its ability to promote exon skipping in these cells. SH-SY5Y cells were transfected with PMO 9 (AluJ+93+117) at concentrations varying from 0.05 μM to 5 μM. Concentrations of 50 nM, 100 nM and 300 nM ($p>0.05$) did not show any significant difference in exon inclusion when compared to untreated cells (87.12 ± 1.5%) (Figure 3.5c). Increasing the PMO concentration to 500 nM significantly reduced AluJ cassette inclusion down to 73.56 ± 2.9% (Figure 3.5c). This is apparent in the gel image shown in Figure 3.5a, where the intensity of full-sized transcripts (247 bp) of 100 to 300 nM PMO-transfected samples was stronger than that seen in cassette-excluding transcripts (127 bp).

Treatment with 1 μM of PMO 9 (AluJ+93+117) showed similar levels of exon inclusion to treatment with 500 nM PMO 9 (AluJ+93+117) (71.8 ± 1.6%) (Figure 3.5c). Increasing the concentrations to 2.5 μM and 5 μM showed the strongest effects of PMO 9 (AluJ+93+117) on exon inclusion. 2.5 μM of PMO 9 (AluJ+93+117) reduced exon inclusion levels down to 60.9 ± 0.92%, while 5 μM of PMO 9 (AluJ+93+117) resulted in even lower exon inclusion at 35.1 ± 4.8% (Figure 3.5b). The gel image shown in Figure 3.4b shows how 5 μM of PMO 9 (AluJ+93+117) resulted in similar fragment intensities for both full-sized and cassette-excluding transcripts.

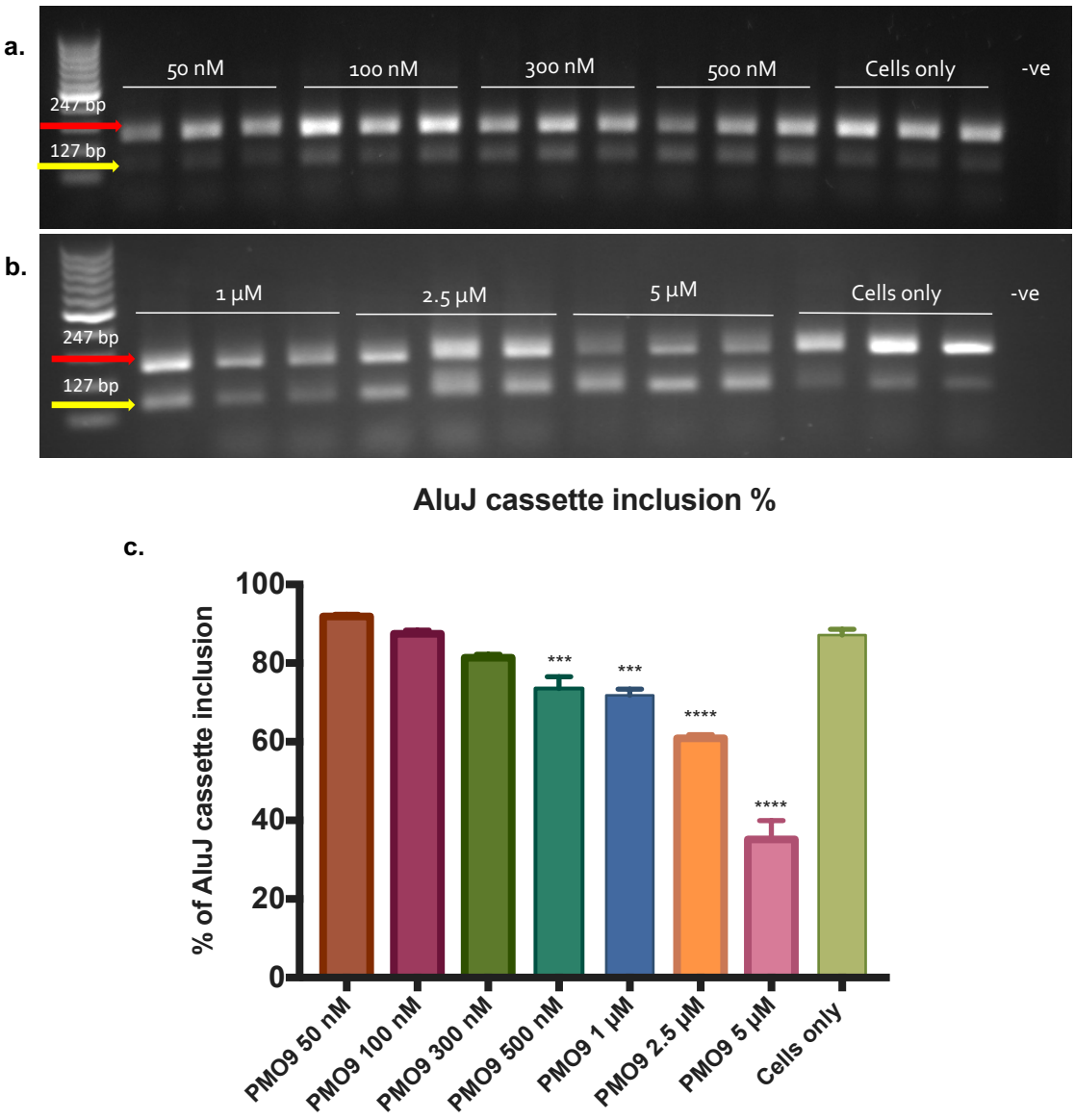

Figure 3.5 The effect of PMO 9 on AluJ insertion in SH-SY5Y cells.

Figure shows images of RT-PCR products of SH-SY5Y cells treated with a) 50-500 nM PMO 9 and b) 1-5 µM PMO 9. c) Bar graph depicting AluJ cassette inclusion percentages in SH-SY5Y cells treated with 0.5-5 µM PMO 9 for 24 hours compared to untreated cells.

Gels were run in a 1.5% agarose gel in 1X TAE buffer against Hyperladder V and visualized under UV light using a GELDOC system. Images were quantified using ImageJ. "-ve" denotes negative control. Sample gel images show the intensity of exon-skipped transcripts (127 bp, yellow arrow) against exon-including transcripts (247 bp, red arrow).

n=3-6, *** = p≤0.001, **** = p≤0.0001. Statistical comparisons were carried out using one-way ANOVA. All data points correspond to mean ± SEM values.

3.2.1.2 PMO 9A (ALUJ+94+118)

Once the effects of PMO 9 (AluJ+93+117) on exon skipping were tested, PMO 9A (AluJ+94+118) was then used to measure its ability to promote exon skipping. PMO 9A (AluJ+94+118) was designed as its sequence covers the end of the 3' end of the AluJ cassette and is shifted one base pair 3' of the sequence of PMO 9 (AluJ+93+117).

Treatment of SH-SY5Y cells with 50-300 nM of PMO 9A (AluJ+94+118) resulted in no significant reduction in AluJ cassette inclusion levels when compared to control cells (88.5 ± 1.5%, $p>0.05$) (Figure 3.6c). 500 nM of PMO 9A (AluJ+94+118) managed to significantly decrease AluJ cassette inclusion down to 81.05±1.4% when compared to untreated samples. The PCR gel image shown in Figure 3.5a shows how both exon-including transcripts (247 bp) have higher fragment intensities than that of exon-skipped transcripts (127 bp) in both transfected and control cells, thus demonstrating that low concentrations of PMO 9 (AluJ+93+117) were ineffective at excluding the AluJ cassette.

Treatment of cells with 1 μM of PMO 9A (AluJ+94+118) managed to significantly decrease AluJ cassette inclusion compared to control cells (64.15 ± 0.6%) (Figure 3.6c). Lower cassette inclusion levels were seen in cells transfected with 2.5 μM PMO 9A (AluJ+94+118) (43.83 ± 3.6%). The strongest effect of PMO 9A (AluJ+94+118) was seen at 5 μM concentration, where near complete exon-skipping levels was achieved, and AluJ cassette inclusion levels decreased down to 4.09 ± 2.3%. The PCR gel image in Figure 3.6b displays how the band intensities of exon-skipped transcripts (127 bp) of 5 μM-treated cells are much higher compared to those of exon-including transcripts (247 bp).

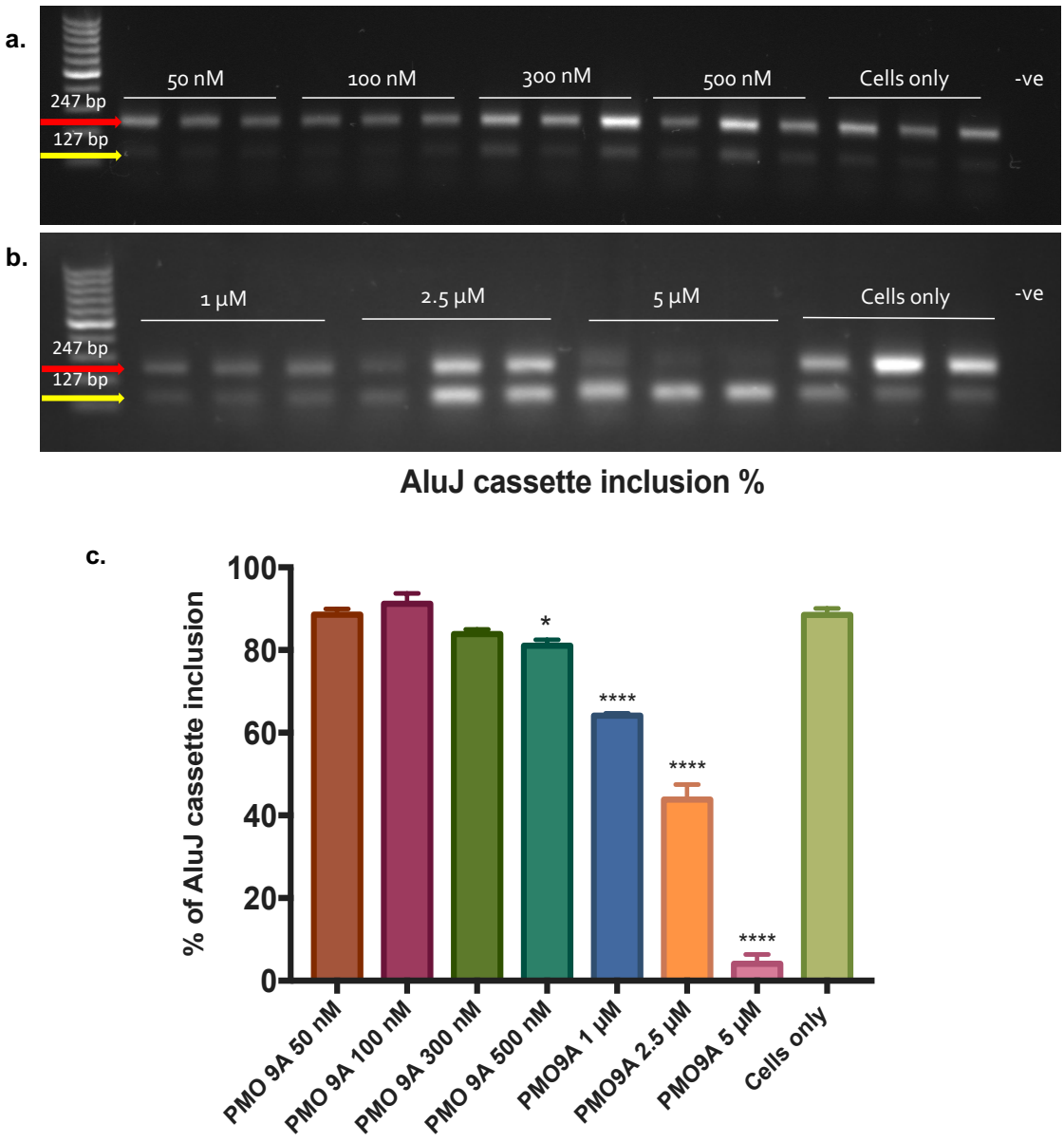

Figure 3.6 The effect of PMO 9A on AluJ insertion in SH-SY5Y cells.

Figure shows gel images of RT-PCR products of SH-SY5Y cells treated with a) 50-500 nM PMO 9A and b) 1-5 µM PMO 9A. c) Bar graph depicting AluJ cassette inclusion percentages in SH-SY5Y cells treated with 0.5-5 µM PMO 9A for 24 hours compared to untreated cells.

Gels were run in a 1.5% agarose gel in 1X TAE buffer against Hyperladder V and visualized under UV light using a GELDOC system. Images were quantified using ImageJ. "-ve" denotes negative control. Sample gel images show the intensity of exon-skipped transcripts (127 bp, yellow arrow) against exon-including transcripts (247 bp, red arrow).

n=3-6, * = $p \leq 0.05$, **** = $p \leq 0.0001$. Statistical comparisons were carried out using one-way ANOVA. All data points correspond to mean ± SEM values.

3.2.1.3 PMO 9B (ALUJ+95+119)

Further to testing PMO 9A (AluJ+94+118), PMO 9B (AluJ+95+119) was also used to measure its effects on cassette exon inclusion as the sequence for this PMO shifts by two base pairs towards the 3' splice site of the cassette from the sequence of PMO 9 (AluJ+93+117). SH-SY5Y cells were transfected with PMO 9B (AluJ+95+119) at the same concentration ranges as previously described. Compared to PMO 9 (AluJ+93+117) and PMO 9A (AluJ+94+118), where a significant decrease in AluJ inclusion was observed even in 500 nM-treated cells, no significant change in AluJ cassette inclusion levels were observed at PMO concentrations of 50 nM to 2.5 μM when compared to control samples (81.99 ± 3.4%, $p>0.05$) (Figure 3.7c). Increasing the PMO concentration to 2.5 μM significantly lowered cassette inclusion levels down to 45.22 ± 2.3%.The most potent effect of PMO 9B (AluJ+95+119) was seen at 5 μM concentration, where AluJ inclusion decreased to 34.2 ± 1.8% (Figure 3.7c). This is similar to thelevels of exon skipping that were observed in PMO 9-transfected cells.

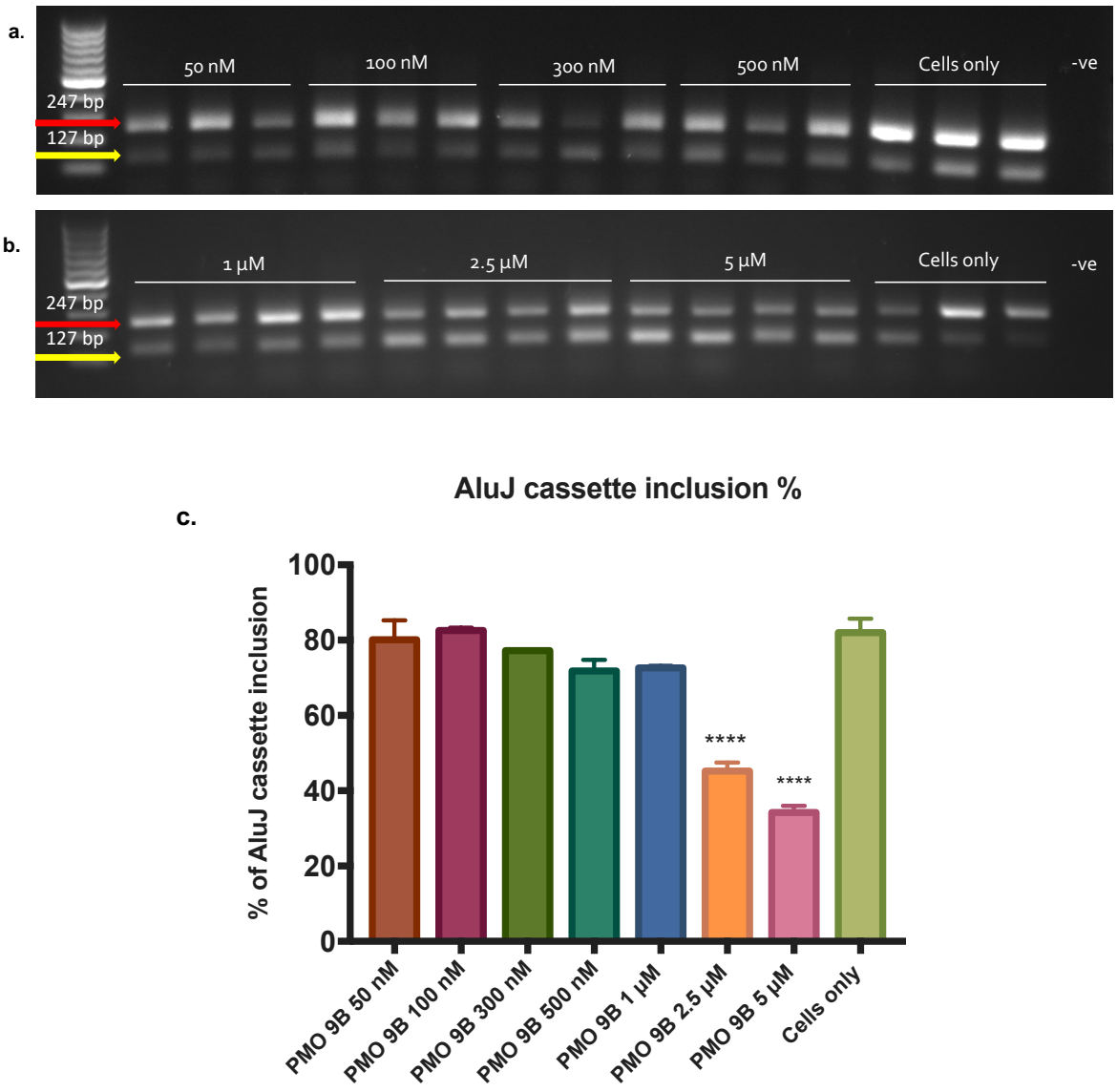

Figure 3.7 The effect of PMO 9B on AluJ insertion in SH-SY5Y cells.

Figure shows gel images of RT-PCR products of SH-SY5Y cells treated with a) 50-500 nM PMO 9B and b) 1-5 µM PMO 9B. c) Bar graph depicting AluJ cassette inclusion percentages in SH-SY5Y cells treated with 0.5-5 µM PMO 9B for 24 hours compared to untreated cells.

Gels were run in a 1.5% agarose gel in 1X TAE buffer against Hyperladder V and visualized under UV light using a GELDOC system. Images were quantified using ImageJ. "-ve" denotes negative control. Sample gel images show the intensity of exon-skipped transcripts (127 bp, yellow arrow) against exon-including transcripts (247 bp, red arrow).

n=3-6, **** = $p \leq 0.0001$. Statistical comparisons were carried out using one-way ANOVA. All data points correspond to mean ± SEM values.

3.2.1.4 PMO 10 (ALUJ+96+120)

In these sets of experiments, PMO 10 (AluJ+96+120) was also used to transfect SH-SY5Y cells as a control PMO. This PMO has previously been tested for its exon skipping abilities and was found to have no effect on cassette exon inclusion levels. The base sequence for PMO 10 (AluJ+96+120) is shifted one base 3' of PMO 9B (AluJ+95+119), thus completely covers the 3' end of the splice site of the AluJ cassette. As seen in the gel images in Figures 3.8a and 3.8b, both full-sized and exon-skipped transcripts have the same intensities in transfected and non-transfected cells, indicating that PMO 10 (AluJ+96+120), even in higher concentrations, was unable to induce any change in AluJ inclusion levels when compared to control cells ($87.08 \pm 3.2\%$). This thus ensures that any alteration in AluJ cassette inclusion levels seen in cells transfected with PMO 9 (AluJ+93+117), PMO 9A (AluJ+94+118), and PMO 9B (AluJ+95+119) were all an effect of the PMOs alone, and not caused by the transfection reagent.

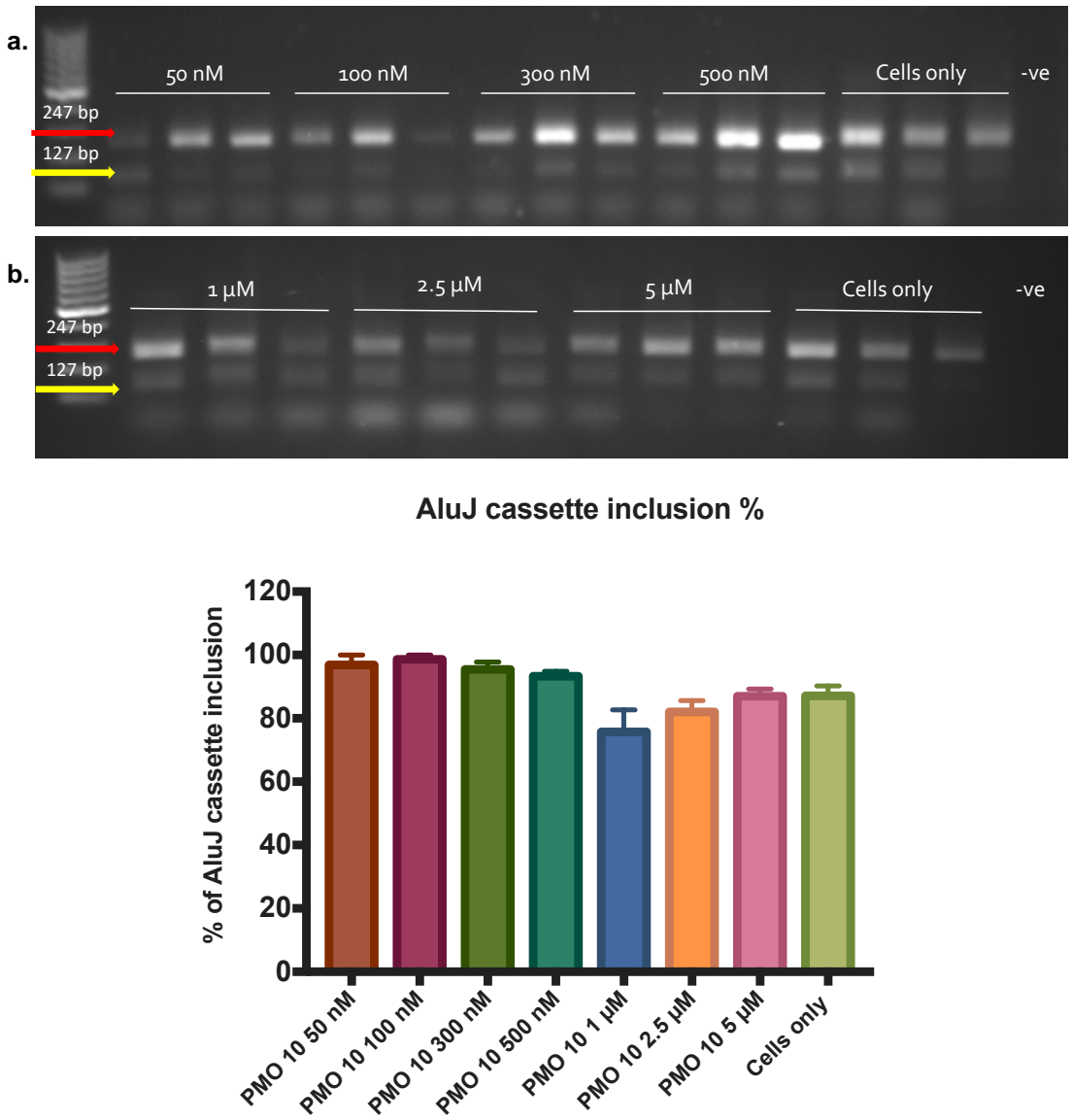

Figure 3.8 The effect of PMO 10 on AluJ insertion in SH-SY5Y cells.

Gel images of RT-PCR products of SH-SY5Y cells treated with a) 50-500 nM PMO 10 and b) 1-5 µM PMO 10. c) Bar graph depicting AluJ cassette inclusion percentages in SH-SY5Y cells treated with 0.5-5 µM PMO 10 for 24 hours compared to untreated cells.

Gels were run in a 1.5% agarose gel in 1X TAE buffer against Hyperladder V and visualized under UV light using a GELDOC system. Images were quantified using ImageJ. "-ve" denotes negative control. Sample gel images show the intensity of exon-skipped transcripts (127 bp, yellow arrow) against exon-including transcripts (247 bp, red arrow).

n=3-6. Statistical comparisons were carried out using one-way ANOVA. All data points correspond to mean ± SEM values.

3.2.1.5 INCREASING CONCENTRATIONS OF PMOS

Since a major difference in exon skipping efficacy was observed between PMO concentrations of 1 μM and 5 μM, the effects of an even higher PMO concentration was investigated to determine whether even higher levels of exon skipping can be attained. SH-SY5Y cells were transfected with 10 μM of PMO and its effects on cassette exon inclusion were compared with cells transfected with 5 μM of PMO. Although the levels of AluJ cassette inclusion in 10 μM-treated samples were reduced slightly compared to those seen in 5 μM-treated samples (Figure 3.9), there was no significant difference in AluJ cassette inclusion levels between the two concentrations.

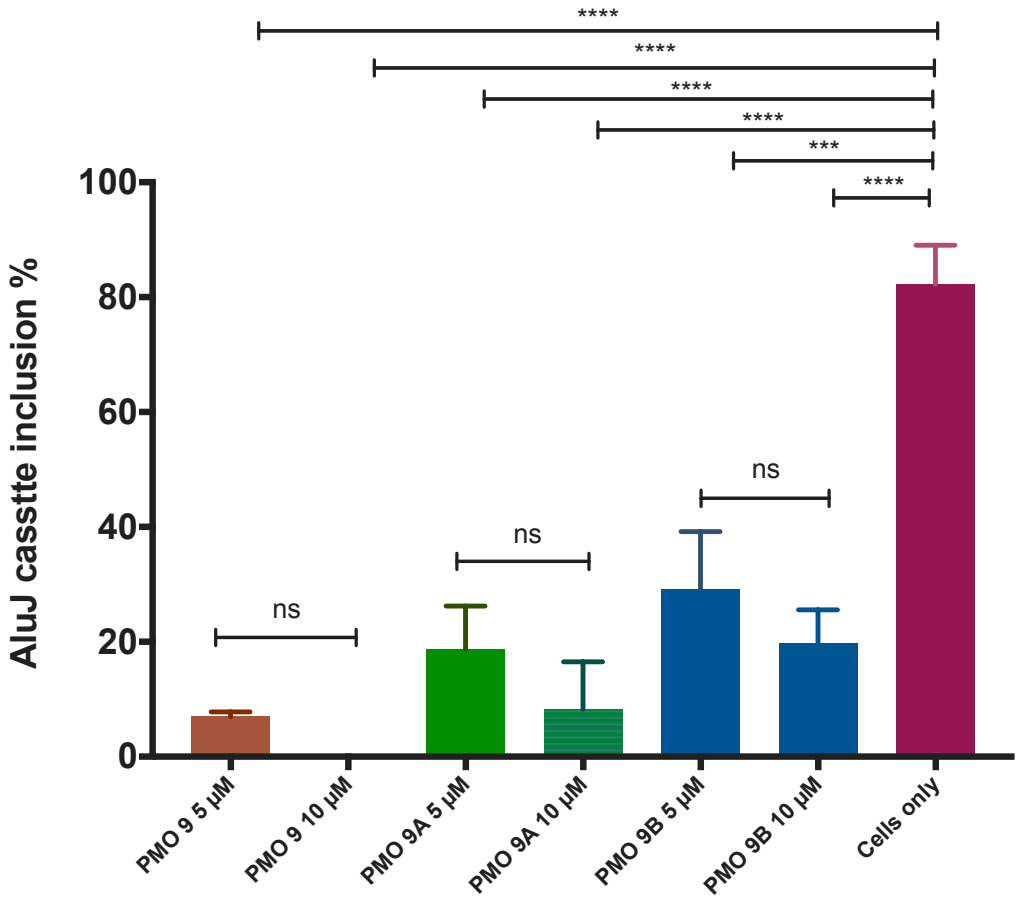

Figure 3.9 Bar graph depicting AluJ cassette inclusion levels in SH-SY5Y cells trated with 5 µM and 10 µM PMO.

n=3-4, *** = p≤0.001, **** = p≤0.0001, . Statistical comparisons were carried out using one-way ANOVA. All data points correspond to mean ± SEM values.

3.2.1.6 INHIBITORY DOSE RESPONSE CURVE FOR ALUJ CASSETTE INCLUSION FOLLOWING PMO TRANSFECTION

Following individual analysis of each PMO and its effects exon skipping, a dose-response curve was plotted in order to calculate the IC_{50} of each PMO (Figure 3.10). The IC_{50} values here represent the concentration of PMO needed to inhibit half of the maximum AluJ cassette inclusion. As PMO 9A (AluJ+94+118) demonstrated the strongest effect on exon skipping, the IC_{50} was found to be the lowest (1.49 $\pm$ 0.15 μM). PMO 9 (AluJ+93+117) had a higher IC_{50} (3.13 $\pm$ 0.42 μM) than PMO 9B (AluJ+95+119) (2.16 $\pm$ 0.33 μM), even though PMO 9 (AluJ+93+117) demonstrated significant exclusion of the AluJ cassette at lower concentrations (500 nM and 1 μM). However, both PMOs resulted in similar AluJ cassette inclusion levels following 5 μM of PMO treatment (35.1 % for PMO 9 (AluJ+93+117) and 34.2% for PMO 9B (AluJ+95+119)). Since PMO 10 (AluJ+96+120) had no effect on exon skipping, it was not possible to calculate the IC_{50} for this PMO.

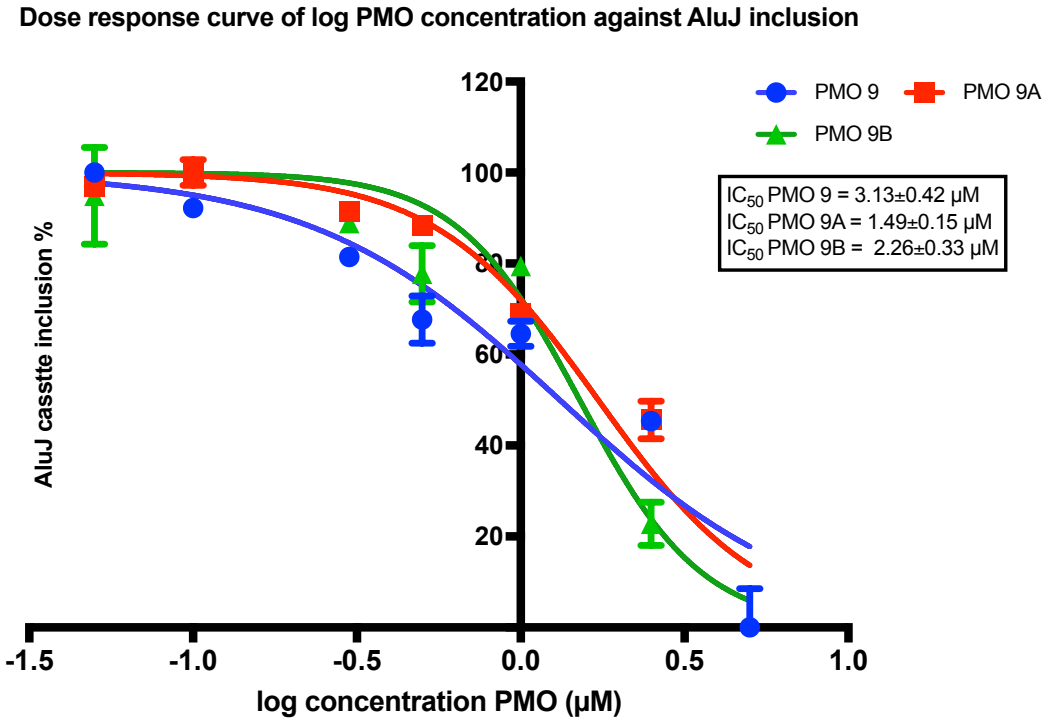

Figure 3.10 Dose response curves of log PMO concentration against AluJ inclusion.

3.2.2 EFFECTS OF EXON SKIPPING ON Q/R SITE EDITING

3.2.2.1 OPTIMISATION OF THE *BBVI* DIGEST RNA EDITING ASSAY

In order to measure Q/R site editing levels in SH-SY5Y cells, a restriction enzyme digest of RT-PCR cDNA products of the Q/R editing site in SH-SY5Y cells was performed using the restriction enzyme *BbvI*. *BbvI* was used in this assay as the enzyme contains the recognition sequence for unedited adenosine in cDNA (GC**A**GC). Thus, the enzyme will then cut unedited transcripts in the cDNA, whilst edited copies will remain uncut as they do not contain the recognition sequence for *BbvI*. This will result in digest products with three different fragment sizes: 323 bp (edited cDNA) and 238 bp and 85 bp (unedited cDNA) (Figure 3.11). 2 units of enzyme were used for each PCR reaction product, followed by an incubation step at 37°C for 1 hour. 10% SDS was initially used to inactivate *BbvI* before running digest products on a gel. However, it was found that this concentration affected migration of DNA in the agarose gel, resulting in smeared bands in both edited and unedited cDNA transcripts (Figure 3.12). Different concentrations of SDS were then tested in order to determine the optimal concentration needed to inactivate *BbvI* (Figure 3.13). It was then found that addition of 1% SDS resulted in sharper, more distinct bands, allowing for Q/R site editing quantification using densitometric analysis with the following equation:

$$\frac{Fluorescence\ of\ edited\ fragments}{Total\ fluorescence} \times 100\% = Editing\ percentage\ in\ cells$$

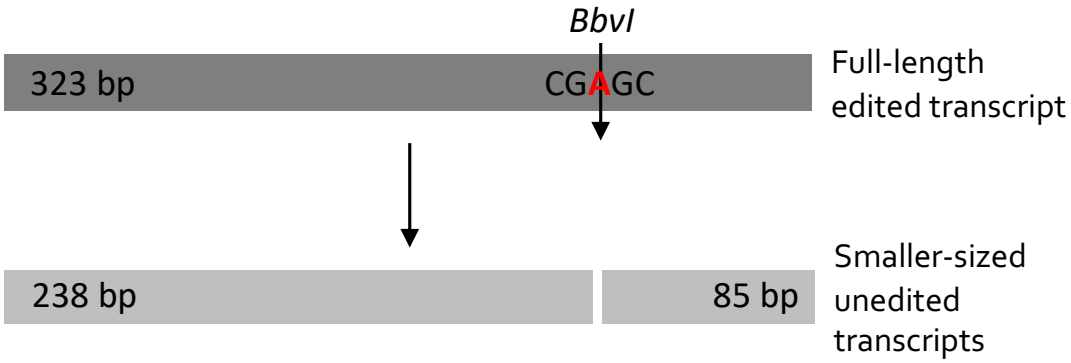

Figure 3.11 Schematic diagram representing cut sites for *BbvI*.

BbvI recognises unedited adenosine. If the sequence is present, it will then be cut by the enzyme, resulting in PCR digest products of two smaller fragments – 238 bp and 85 bp.

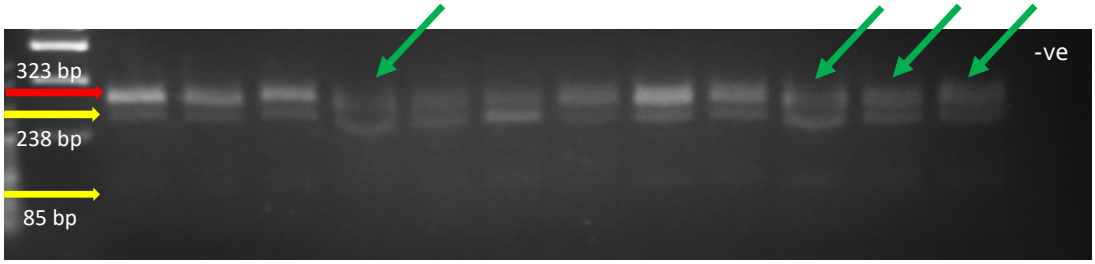

Figure 3.12 Gel image of a *BbvI* digest of SH-SY5Y cells inactivated with 10% SDS.

Smeared bands can be seen in digest products in lanes indicated by green arrows.

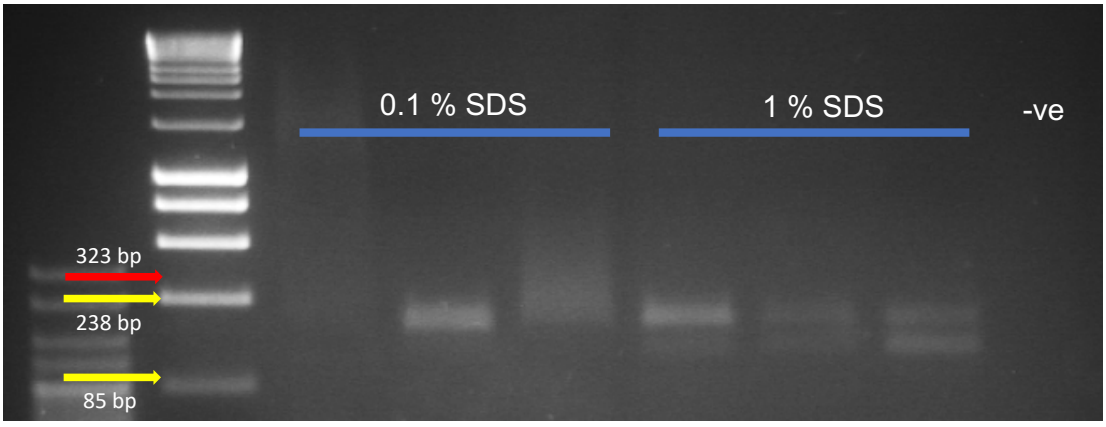

Figure 3.13 Gel image of a *BbvI* digest of SH-SY5Y cells inactivated with 0.1% and 1% SDS.

0.1% SDS resulted in completely indistinct bands whilst 1% SDS resulted in digest products with two distinct fragments.

3.2.2.2 PMO 9 (ALUJ+93+117)

Gerber *et. al.* (1997) previously demonstrated how ADAR2 isoforms that contain a 120 bp AluJ cassette have reduced catalytic activity compared to isoforms that do not contain the cassette. Reduction in the catalytic activity of ADAR2 leads to lower Q/R site editing levels. Hence, inducing alternative splicing using PMOs to promote AluJ cassette inclusion could possibly improve RNA editing levels in SH-SY5Y cells. Following exon skipping PCR assays and analysis of PMO-transfected SH-SY5Y cells, a *BbvI* digest RNA editing assay was performed to measure the effects on exon skipping on Q/R site editing. Q/R site editing levels were normalised to control levels, as shown in Figure 3.14c. No change in editing levels were seen in cells transfected with 50-500 nM of PMO 9 (AluJ+93+117), even though 500 nM PMO 9 (AluJ+93+117) was able to reduce cassette exon inclusion levels. Increased concentrations of PMO 9 (AluJ+93+117), however, significantly increased Q/R site editing levels compared to controls. 1 μM and 2.5 μM PMO 9 (AluJ+93+117) showed similar increase in RNA editing, at 125.7 ± 7.7% and 124.8 ± 2.6%, respectively. Although 5 μM PMO 9 (AluJ+93+117) managed to greatly decrease AluJ cassette inclusion levels compared to 1 μM and 2.5 μM of PMO, the increase in RNA editing is only slightly higher than that observed in 1 and 2.5 μM PMO 9 (AluJ+93+117) (131.7 ± 4.2%).

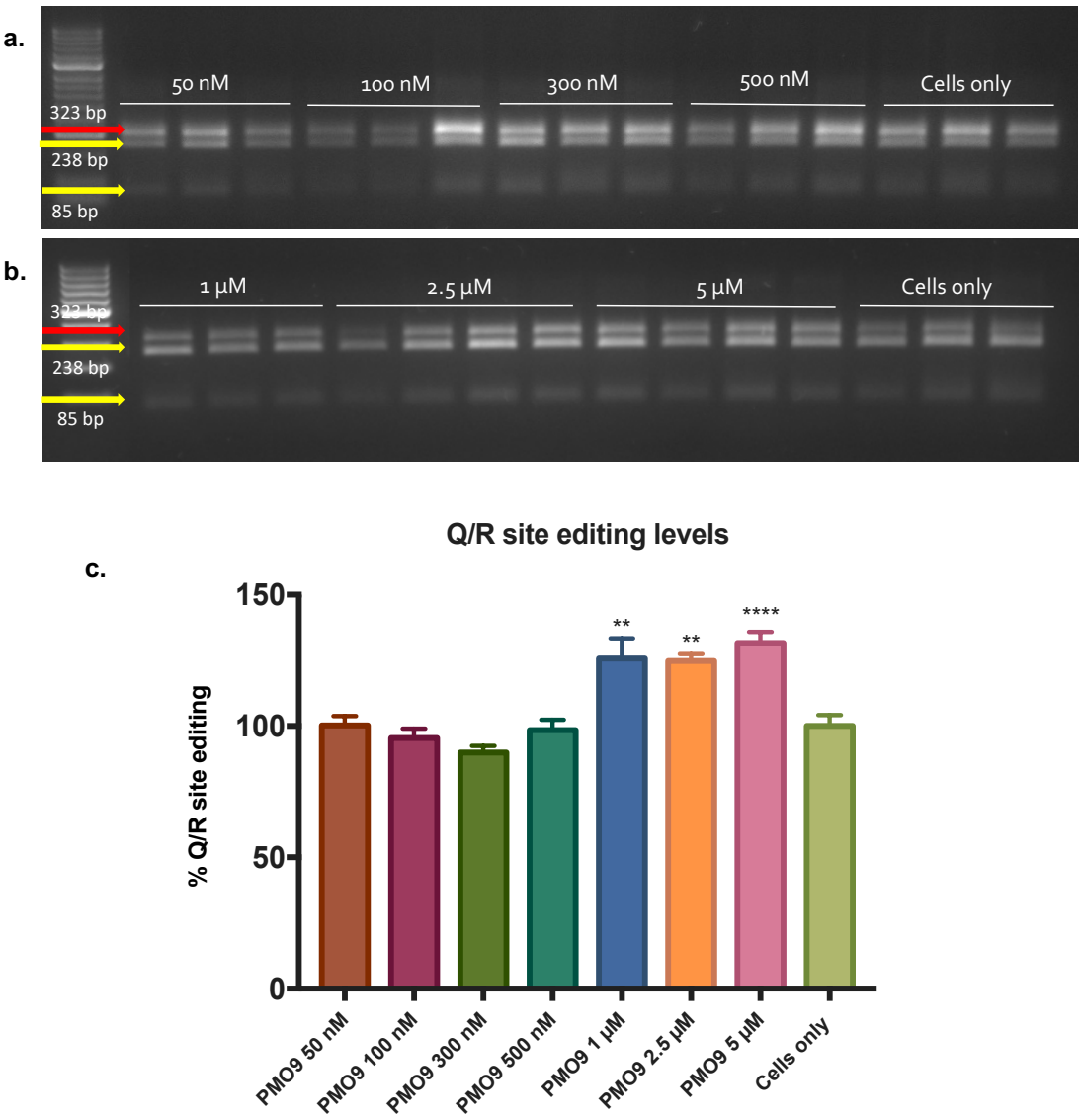

Figure 3.14 The effect of PMO 9 on RNA editing in SH-SY5Y cells.

Figure shows gel images of BbvI digest products of SH-SY5Y cells treated with a) 50-500 nM PMO 9 and b) 1-5 µM PMO 9. c) Bar graph depicting Q/R site editing percentages in SH-SY5Y cells treated with 0.5-5 µM PMO 9 for 24 hours compared to untreated cells.

Gels were run in a 2.5% agarose gel in 1X TAE buffer against Hyperladder V and visualized under UV light using a GELDOC system. Images were quantified using ImageJ. "-ve" denotes negative control. Sample gel images show the intensity of edited transcripts (323 bp, red arrow) against unedited transcripts (238 bp and 85 bp, yellow arrow).

n=3-6, ** = p≤0.01, **** = p≤0.0001. Statistical comparisons were carried out using one-way ANOVA. All data points correspond to mean ± SEM values.

3.2.2.3 PMO 9A (ALUJ+94+118)

Lower concentrations of PMO 9A (AluJ+94+118) did not result in any RNA editing increase in cells (Figure 3.15c). This is expected as the same concentrations (50-300 nM) did not result in AluJ cassette exclusion levels, although as with PMO 9, 500 nM of PMO 9A (AluJ+94+118) did slightly reduce AluJ cassette level inclusion down to 81.05 ± 1.4%. These results demonstrate that the reduction in AluJ cassette levels were too low to improve RNA editing levels in the cells. Higher concentrations of PMO 9A (AluJ+94+118) did however improve RNA editing levels in the cells, where 1 μM transfections increased editing to 166.6 ± 13.8%, and 2.5 μM transfections increased editing to 159.6 ± 3.3%. 5 μM of PMO 9A (AluJ+94+118) resulted in an increase of 167.9 ± 6% in RNA editing. Although 5 μM PMO 9A (AluJ+94+118) showed much higher exon skipping effects than 1 μM and 2.5 μM PMO 9A (AluJ+94+118), the levels of RNA editing among the three concentrations are approximately the same, suggesting that RNA editing levels may have reached saturation in the presence of high levels of AluJ sequence exclusion.

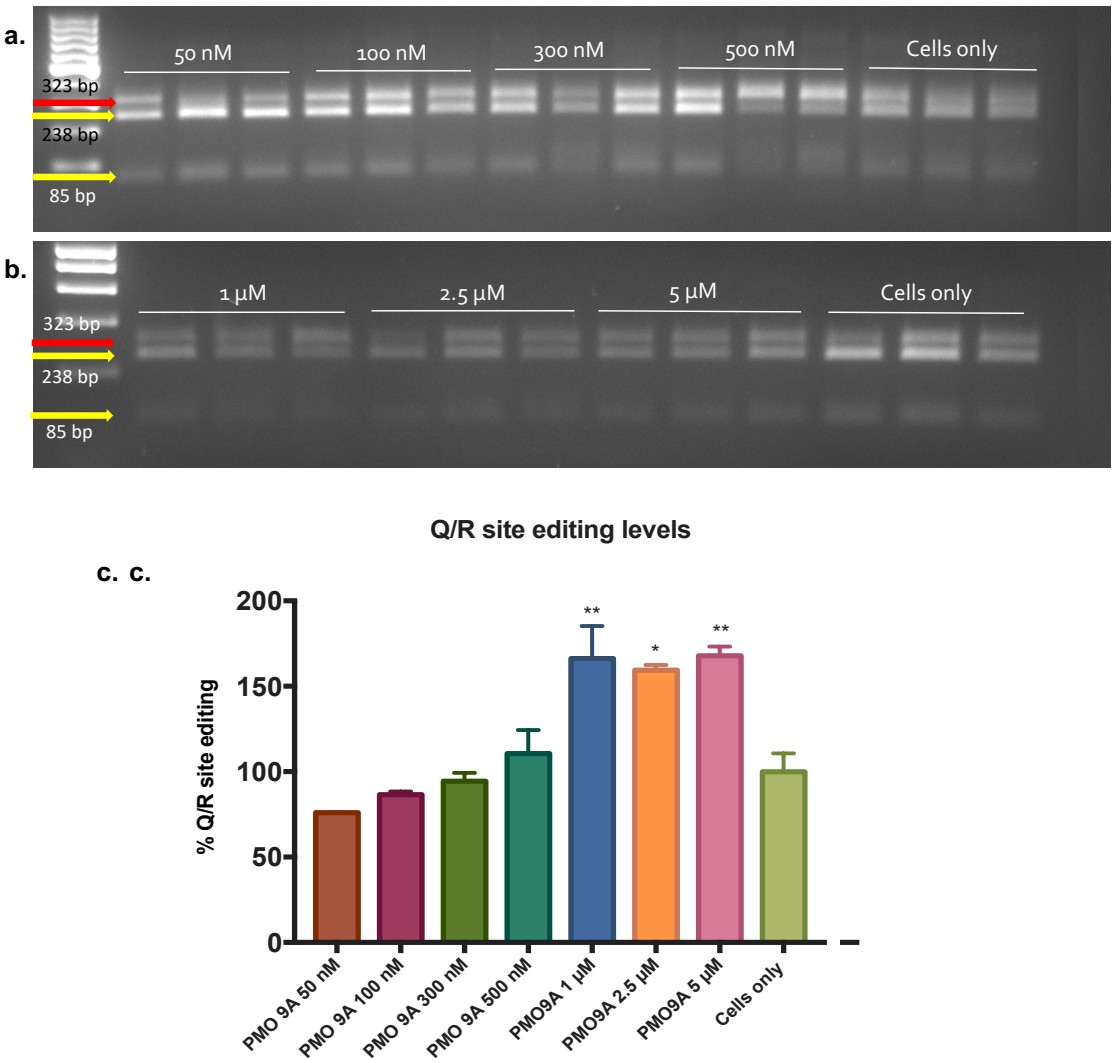

Figure 3.15 The effect of PMO 9A on RNA editing in SH-SY5Y cells.

Figure shows gel images of BbvI digest products of SH-SY5Y cells treated with a) 50-500 nM PMO 9A and b) 1-5 µM PMO 9A. c) Bar graph depicting Q/R site editing percentages in SH-SY5Y cells treated with 0.5-5 µM PMO 9A for 24 hours compared to untreated cells.

Gels were run in a 2.5% agarose gel in 1X TAE buffer against Hyperladder V and visualized under UV light using a GELDOC system. Images were quantified using ImageJ. "-ve" denotes negative control. Sample gel images show the intensity of edited transcripts (323 bp, red arrow) against unedited transcripts (238 bp and 85 bp, yellow arrow).

n=3-6, * = p≤0.05, ** = p≤0.01. Statistical comparisons were carried out using one-way ANOVA. All data points correspond to mean ± SEM values.

3.2.2.4 PMO 9B (ALUJ+95+119)

Compared to PMOs 9 (AluJ+93+117) and 9A (AluJ+94+118), transfection of SH-SY5Y cells with PMO 9B (AluJ+95+119) did not result in any increase in Q/R site editing levels compared to normalised controls ($p>0.05$) (Figure 3.16c). In fact, RNA editing levels remained at roughly the same levels compared to controls, ranging at values from 91.6 ± 5% (50 nM) to 109.3 ± 2% (5 μM). The results were somewhat expected as the effects of PMO 9B (AluJ+95+119) on AluJ cassette inclusion (Figure 3.7) were not as potent as seen with PMOs 9 (AluJ+93+117) and 9A (AluJ+94+118) (Figures 3.5 and 3.6). Although 2.5 μM and 5 μM of PMO 9B (AluJ+95+119) were able to significantly decrease AluJ cassette inclusion (Figure 3.7c), the PMO was unable to result in any improvement on RNA editing levels in these cells.

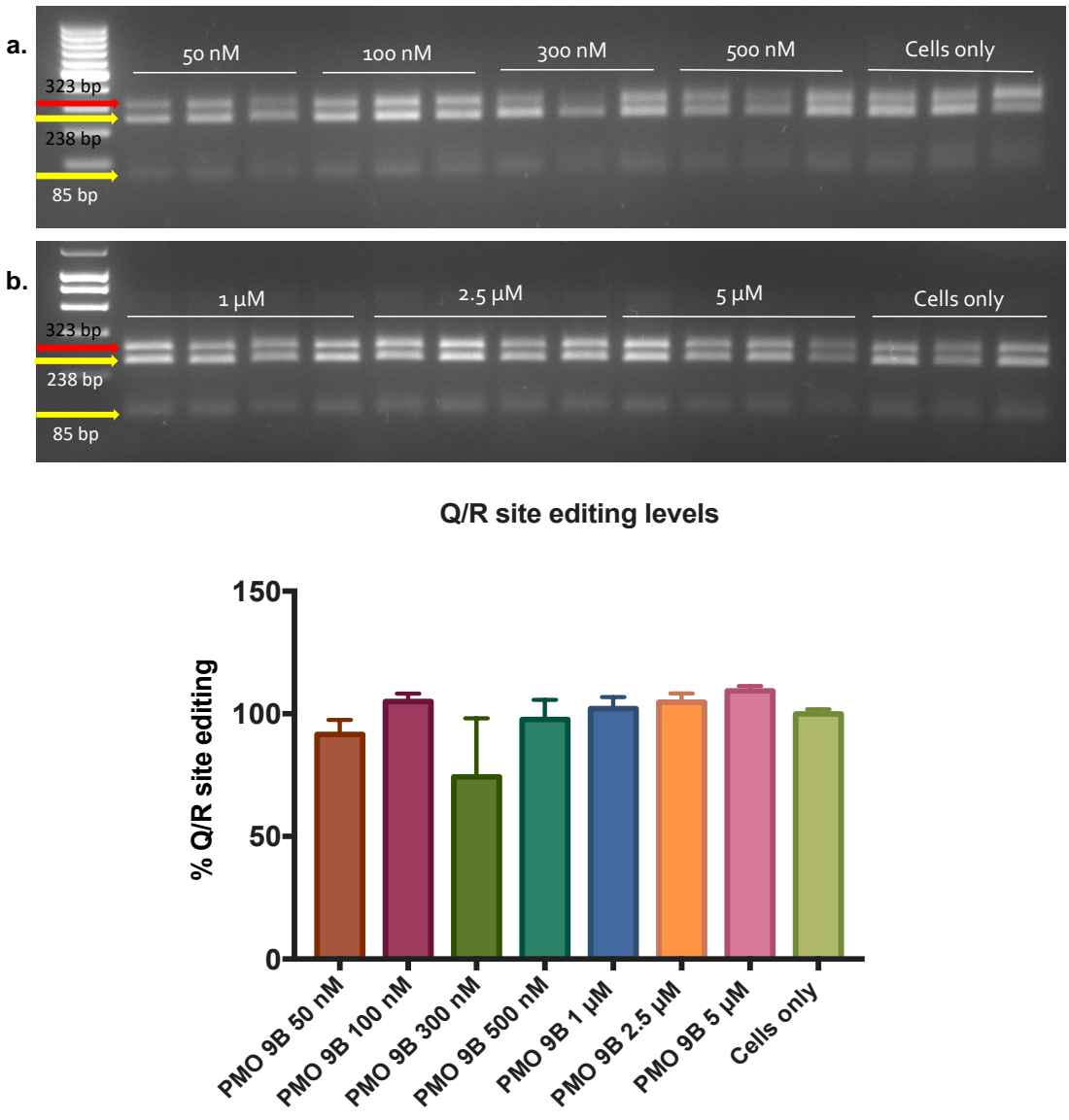

Figure 3.16 The effect of PMO 9B on RNA editing in SH-SY5Y cells.

Figure shows gel images of BbvI digest products of SH-SY5Y cells treated with a) 50-500 nM PMO 9B and b) 1-5 µM PMO 9B. c) Bar graph depicting Q/R site editing percentages in SH-SY5Y cells treated with 0.5-5 µM PMO 9B for 24 hours compared to untreated cells.

Gels were run in a 2.5% agarose gel in 1X TAE buffer against Hyperladder V and visualized under UV light using a GELDOC system. Images were quantified using ImageJ. "-ve" denotes negative control. Sample gel images show the intensity of edited transcripts (323 bp, red arrow) against unedited transcripts (238 bp and 85 bp, yellow arrow).

n=3-6. Statistical comparisons were carried out using one-way ANOVA. All data points correspond to mean ± SEM values.

3.2.2.5 PMO 10 (ALUJ+96+120)

Since PMO 10 (AluJ+96+120) acts as a control PMO and did not have any effect on AluJ cassette inclusion levels, transfection of SH-SY5Y cells with this PMO was not expected to have any change in RNA editing levels as well ($p>0.05$) when compared to normalised controls (Figure 3.17c). Levels of RNA editing remained approximately the same, ranging from $88.11 \pm 4.5\%$ (1 μM) to $95.12 \pm 2.6\%$ (50 nM), with the exception of 100 nM PMO 10 (AluJ+96+120), which reduced editing levels down to $63.85 \pm 4.1\%$, although this could simply be an outlier effect, as seen from the large variability. The levels of RNA editing observed here is consistent with the lack of exon skipping levels previously observed in Figure 3.8c.

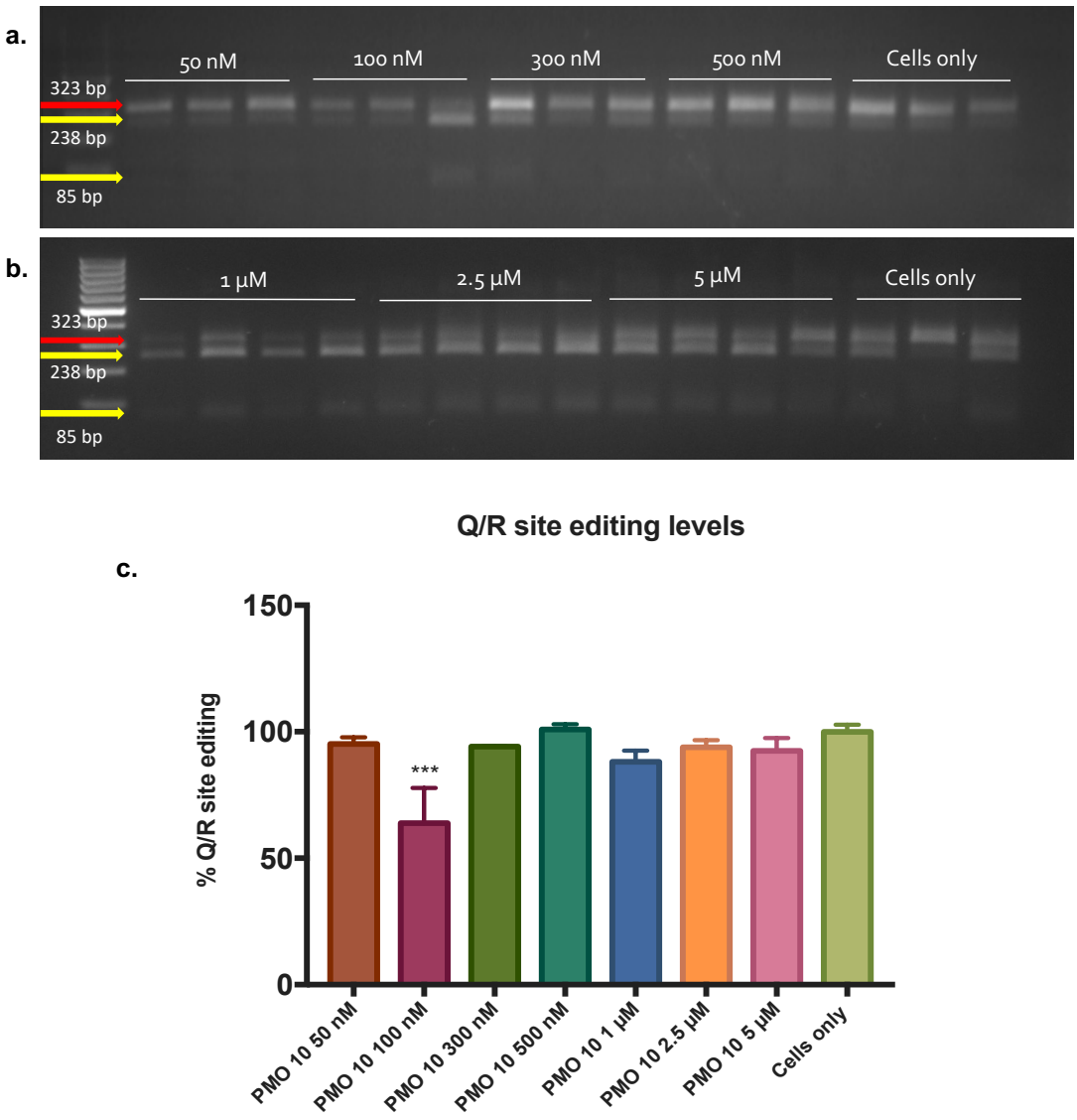

Figure 3.17 The effect of PMO 10 on RNA editing in SH-SY5Y cells.

Figure shows gel images of BbvI digest products of SH-SY5Y cells treated with a) 50-500 nM PMO 10 and b) 1-5 µM PMO 10. c) Bar graph depicting Q/R site editing percentages in SH-SY5Y cells treated with 0.5-5 µM PMO 9B for 24 hours compared to untreated cells.

Gels were run in a 2.5% agarose gel in 1X TAE buffer against Hyperladder V and visualized under UV light using a GELDOC system. Images were quantified using ImageJ. "-ve" denotes negative control. Sample gel images show the intensity of edited transcripts (323 bp, red arrow) against unedited transcripts (238 bp and 85 bp, yellow arrow).

n=3-6, *** = p≤0.001. Statistical comparisons were carried out using one-way ANOVA. All data points correspond to mean ± SEM values.

3.2.2.6 DOSE RESPONSE CURVES FOR RNA EDITING LEVELS FOLLOWING PMO TRANSFECTION

To better compare the effects of PMOs on RNA editing levels, a dose-response curve was plotted to calculate the EC_{50} of each PMO (Figure 3.17). In this context, the EC_{50} values represent the concentration of PMO needed to produce half of the maximum RNA editing levels observed in the cells. As PMO 9A (AluJ+94+118) was able to increase RNA editing levels at 1-5 μM concentrations (Figure 3.15c) and demonstrated the most potent exon skipping effects (Figure 3.6c), the EC_{50} value for PMO 9A (AluJ+94+118) was calculated to be the lowest (0.66 μM). The EC_{50} for PMO 9 (AluJ+93+117) was only slightly higher than that found in PMO 9A (AluJ+94+118) (0.69 μM). This is however indicative of the RNA editing levels observed in PMO 9-treated cells, where a significant increase in editing was seen at the same concentration range (1-5 μM) (Figure 3.14c) as that of PMO 9A-treated cells (Figure 3.15c). PMO 9B (AluJ+95+119) demonstrated a non-sigmoidal relationship, which was expected as this PMO had no effect in improving RNA editing in cells (Figure 3.16c), and its ineffectiveness on RNA editing can be seen on how a sigmoidal curve could not be plotted through the data points (Figure 3.18). Since PMO 10 (AluJ+96+120) had no effect on both exon skipping and RNA editing, the EC_{50} for this PMO could not be calculated.

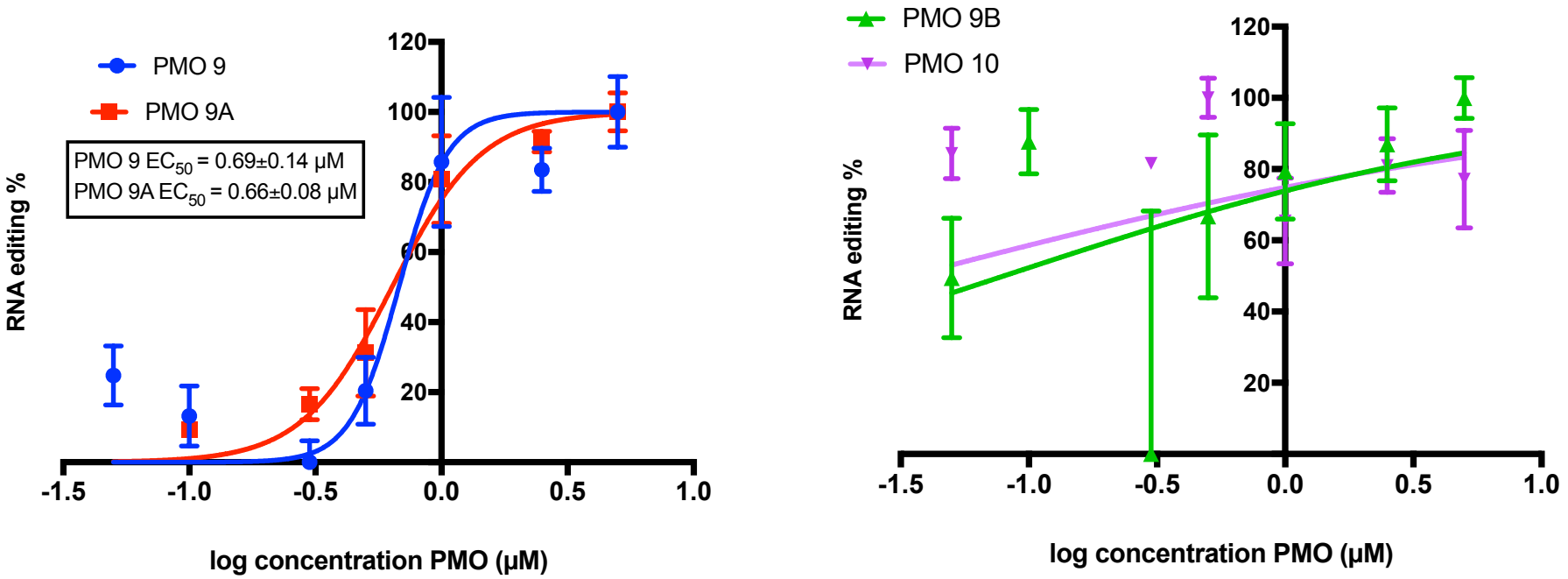

Figure 3.18 Dose-response curves of PMO concentration against RNA editing levels.

3.3 DISCUSSION

The work presented here was performed to investigate the efficacy of the different PMOs designed to exclude the AluJ cassette from the final mRNA transcript of ADAR2, and its subsequent effects on RNA editing levels. The data shown here confirms how PMOs 9 (AluJ+93+117) and 9A (AluJ+94+118) were successful in inducing alternative splicing in these cells and thus increase RNA editing. As the presence of the AluJ cassette was previously reported to reduce the catalytic activity of ADAR2 (Gerber et al., 1997), the exon skipping technique using ASOs was applied here in order to manipulate splicing events in ADAR as to result in an isoform that lacks the AluJ cassette.

Since one of the possible theories behind ALS pathophysiology is underediting at the GluA2 subunit of AMPA receptors, it is essential to validate that a reduction in AluJ cassette levels (which can be found in exon 5a of the ADAR pre-mRNA transcript) can indeed aid in improving RNA editing levels in the GluA2 subunit. In fact, a study carried out by (Li et al., 2015) demonstrated how the relative expression of ADAR transcripts containing the AluJ cassette found in gliomas were higher than that seen in normal human astrocytes (NHAs), thus concluding that an aberrant splicing pattern in ADAR2 pre-mRNA contributes to the downregulation of A-to-I editing in gliomas.

The PMOs tested for exon skipping (9 (AluJ+93+117), 9A (AluJ+94+118) and 9B (AluJ+95+119)) were previously designed in that they all target the 3' end of the AluJ cassette, where the sequences differ by one base pair each. PMO 10 (AluJ+96+120) was used as a control PMO as it was previously found to be ineffective at promoting cassette exon exclusion. PMO 9A (AluJ+94+118) demonstrated the most efficient exon skipping abilities, where a near-complete exon exclusion was found in cells treated with 5 μM of PMO 9A (AluJ+94+118) ($4.09 \pm 2.3\%$). In comparison, PMOs 9 (AluJ+93+117) and 9B (AluJ+95+119) resulted in $35.1 \pm 4.8\%$ and $34.2 \pm 1.8\%$ exon inclusion, respectively, at the same concentration. A dose response curve was plotted to compare the potencies of the PMOs on exon inclusion (Figure 3.10). The

IC_{50} of PMO 9A (AluJ+94+118) was calculated to be the lowest, at 1.49 μM, whilst PMOs 9 (AluJ+93+117) and 9B (AluJ+95+119) had higher IC_{50} values (3.13 μM and 2.16 μM, respectively). At lower concentrations (500 nM and 1 μM), a significant effect on exon skipping was observed with PMOs 9 (AluJ+93+117) and 9A (AluJ+94+118) (Figures 3.5 and 3.6), although this was not the case with PMO 9B (AluJ+95+119), where significant exon skipping effects were seen only at 2.5 μM and 5 μM PMO treatment (Figure 3.7). We have attempted to see whether increasing the PMO concentrations up to 10 μM would result in an even greater exon skipping effect; however, no significant difference in exon skipping levels were calculated between 5 μM and 10 μM PMO concentrations (Figure 3.9), suggesting that there is a saturation effect of the PMOs.

Since the efficacy of the PMOs at inducing AluJ cassette exclusion was established, our hypothesis on how exon skipping can improve RNA editing levels was tested. This was proven in the cases of both PMO 9 (AluJ+93+117) and 9A (AluJ+94+118), where an increase up to 131.7 ± 4.2% was observed in cells compared to normalized controls for PMO 9 (AluJ+93+117), and 167.9 ± 6% editing for PMO 9A (AluJ+94+118). Interestingly, although PMO 9B (AluJ+95+119) managed to exclude the AluJ cassette, no increase in RNA editing was observed. The sequence of PMO 9B (AluJ+95+119) covers the 3' end of the AluJ cassette even further than PMOs 9 and 9A (AluJ+94+118), and is one base pair different than the sequence of PMO 10 (AluJ+96+120), which could possibly indicate that PMOs designed to bind the region towards the end of the AluJ cassette are less effective at improving RNA editing. The inability of PMOs 9B (AluJ+95+119) and 10 (AluJ+96+120) to improve RNA editing can also be seen in the dose response curve drawn in Figure 3.18, where the curves for both PMOs did not produce a good fit.

One thing to note here is how transfections of 1 μM, 2.5 μM, and 5 μM of PMOs resulted in similar levels of RNA editing, even though there is a clear quantifiable difference in exon skipping levels between the increasing concentrations. This also correlates with the very similar EC_{50} values calculated for PMOs 9 (AluJ+93+117) and 9A (AluJ+94+118) (0.69 μM and

0.66 μM respectively) (Figure 3.18), showing that even a substantial difference in the ability of the PMOs to induce exon skipping only results in a marginal increase in RNA editing levels. This trend could be due to low levels of constitutive endogenous expression of ADAR **i**n SH-SY5Y cells, which were confirmed through western blot experiments (discussed in Chapter 4). It seems as if the upper limits on RNA editing through the action of the ADAR enzyme have been reached with this cell model.

Another possible reason behind the small difference in editing levels seen in the cells between the different concentrations, as well as the inability of PMO 9B (AluJ+95+119) to increase editing despite being efficient at exon skipping, is the RNA editing assay used in this study. Restriction enzyme assays are limited in the sense that they rely on the presence of a recognition site for the enzyme, and this site could be formed or destroyed during the A-to-I editing process (Wong, Lyddon, & Dracheva, 2009). Sequencing has also been proven to be successful in assessing A-to-I editing, however, both restriction enzyme assays and sequencing can result in systematic errors in measurements, as they involve multiple steps (Wong et al., 2009). Thus, (Chen et al., 2008) came up with a method to assess editing levels at the Q/R site using a SYBR Green detection-based quantitative PCR (qPCR). (Wong et al., 2009) then invented a novel qPCR assay using TaqMan probes. Their method utilizes two different probes with the same primer pair to distinguish the two transcript variants with a one nucleotide difference at the editing site (**A**→**G**), which is comparable to existing single nucleotide polymorphism (SNP) assays that applies qPCR (Gilbert et al., 2007). The results of their assay have shown how there is less bias in detection of Q/R site editing levels in the GluR5 subunit of the kainate (KA) receptor. when compared to sequencing and the restriction enzyme digest. Hence, employing the TaqMan qPCR method to measure editing levels at the Q/R site of the GluA2 subunit is a possibility.

Alternative ADAR2 splicing events in rats include the insertion of a 30-nt cassette, where, as seen in humans, the presence or absence of this cassettes results in the formation of two different ADAR isoforms (ADAR2a and ADAR2b, respectively). A study performed by (Filippini et al., 2018b)

aimed to characterize the two ADAR isoforms, as well as their expression and RNA editing activity. Their results show a 12% increase in RNA editing levels in ADAR2a compared to ADAR2b at the R/G site of the GluA2 subunit in rat primary cortical neurons, which is a more representative model. This small but significant increase in RNA editing observed is consistent with the findings in this chapter, where even when similar levels of the two ADAR isoforms are detected in the SH-SY5Y cells, the increase in RNA editing still remains approximately the same even at higher exon skipping levels of the AluJ cassette.

The editing efficiency in ALS motor neurons were found to vary between 38% to 75%, whereas editing was complete in control motor neurons (100%) (Kawahara et al., 2004). Quantitative analyses of AMPA receptor mRNA showed that both ALS motor neurons and control motor neurons express similar levels of GluA2 mRNA relative to β-actin expression, indicating that GluA2 mRNA expression is not altered in motor neurons of individuals with ALS (Kawahara, Kwak, et al., 2003). However, this reduction in RNA editing was found to be caused by low levels of ADAR2 expression in ALS motor neurons (Takuto Hideyama et al., 2012). Although SH-SY5Y cells endogenously express low ADAR2 expression levels, an increase in RNA editing was still observed following PMO treatment, thus implying that treatment of ALS motor neurons with PMOs could possibly have a large impact on editing efficiency. However, testing this hypothesis on a more representative and neuronal-like cell model would be ideal. Rats also undergo alternative ADAR splicing events, where an insertion of a 30-nt cassette results in a less active ADAR2 isoform. The splicing isoforms of ADAR2a and ADAR2b have been recently characterised in rat primary neurons (Filippini et al., 2018b), making it a possible cell model to test the effects of the PMOs on RNA editing. Another possibility would be to use patient-specific induced pluripotent stem cells (iPSCs), although currently, only one study has reported the isolation and characterisation of iPSC-derived motor neurons from sporadic ALS cases (S. Lee & Huang, 2017). Expression levels of alternatively-spliced ADAR2 transcripts as well as Q/R site editing levels in iPSCs would however still need to be fully elucidated, and a more effective

way of delivering antisense oligonucleotides into iPSCs would have to be developed.

CHAPTER 4 INVESTIGATING THE EFFECTS OF PMO TRANSFECTION ON ENDOGENOUS AND ARTIFICIAL ADAR2 PROTEIN EXPRESSION IN SH-SY5Y CELLS

4.1 INTRODUCTION

The efficiency of RNA editing at the Q/R site of GluA subunits (specifically human brain GluA2) is correlated to the total amount of ADAR2 mRNA expressed (Kawahara, Ito, et al., 2003). This infers that the levels of ADAR2 mRNA might be one of the regulatory factors behind GluA2 Q/R site RNA editing. However, the amount of total ADAR2 mRNA does not necessarily illustrate its editing activity *in vivo*, since several alternative human ADAR2 mRNA splice variants have been identified (Kawahara et al., 2005). Reports have shown that the ADAR2 gene consists of 14 exons, which includes two 5' untranslated exons (exons -2 and -1) and one 3' untranslated region (UTR) within exons 9 and 10 (Slavov & Gardiner, 2002). Three alternative splice sites have been identified in elementary studies: alternative splicing of exon 5a (incorporation of an Alu cassette) (Gerber et al., 1997); splicing at the long C-terminus and short C-terminus (Lai, Chen, Lee, et al., 1997); and the RNA editing-dependent addition of 47 nucleotides to exon 2 (Rueter et al., 1999). Most splicing variants were generally derived from two main splicing events, where the alternative splice isoforms were classified as ADAR2a to ADAR2f (Lai, Chen, Carter, & Nishikura, 1997; Rueter et al., 1999).

A splicing event that concerns the 5' end of the coding sequence occurs due to a self-editing process, allowing ADAR2 to act in its own pre-mRNA. An alternative 3' acceptor site is created by the conversion of an intronic AA to an AI, which is read as an AG dinucleotide by the splicing machinery. This

acceptor site introduces 47 nucleotides in the transcript, generating a stop codon in the mRNA (Figure 4.1). A truncated and inactive form of the protein is produced (ADAR2e and ADAR2f), adding 82 amino acids in rats and mice (31 amino acids in humans). This self-editing mechanism is meant to have a role in ADAR2 regulation (Rueter et al., 1999). Splicing at the 3' end of the catalytic domain of the protein results in the inclusion of 32 nucleotides in rat and mouse and 120 nucleotides (also known as the AluJ cassette) in humans (Figure 4.1). This splicing event produces two different isoforms of ADAR2, where exclusion of the 120 bp AluJ cassette from the ADAR2 transcript is the more catalytically active isoform of the enzyme (Gerber et al., 1997). The generation of isoforms ADAR2c and ADAR2d occurs at the end of the coding sequence and is only observed in humans, where the insertion of a truncated C terminus forms an isoform with no editing activity (Lai, Chen, Carter, et al., 1997) (Figure 4.1). Additionally, inclusion of exon 0 has been demonstrated to extend the open reading frame by inserting 49 amino acids at the N-terminus, but this isoform is not greatly expressed (Stefan Maas & Gommans, 2009) (Figure 4.1).

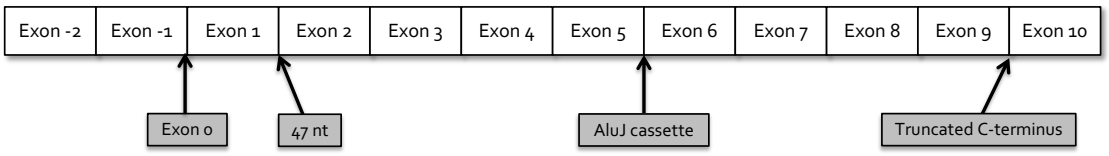

Figure 4.1 Schematic diagram representing possible alternative splicing events in the ADAR2 transcript.

Grey boxes indicate insertions from the intronic sequence. Exon 0 is inserted between exon -1 and exon 1. The 47 nt cassette is inserted at the start of exon 2. The AluJ cassette is inserted between exons 5 and 6. Insertion of a truncated C-terminus occurs at the end of the coding sequence.

Although expression of ADAR proteins and splice forms has not been comprehensively investigated at the protein level, *in situ* hybridisation studies, RT-qPCR, northern blotting, and microarray experiments have shown that ADAR1 and ADAR2, despite being ubiquitously expressed across cell types, are present in differing amounts in individual tissues and cell types (S. Maas & Gommans, 2009). Whilst the developmental expression of ADAR2 protein has been fully elucidated in rat primary neurons (Behm et al., 2017; Filippini et al., 2018b), the endogenous expression of ADAR2 in SH-SY5Y cell lines have not been studied. Data from previous chapters have indicated that PMOs designed to manipulate splicing of the AluJ cassette (PMO 9 (AluJ+93+117) and PMO 9A (AluJ+94+118)) were successfully able to indirectly increase Q/R site RNA editing levels by increasing exon skipping levels in SH-SY5Y cells. However, although there is an increase in exon skipping levels measured in PMO-transfected cells, the improvement in RNA editing levels remain at similar levels between cells transfected with 1-5 μM of PMO. Hence, we studied the expression levels of ADAR2 protein in SH-SY5Y cells to determine its constitutive expression. In this chapter, we assessed the specificity of different antibodies against ADAR2 in cells that have been co-transfected with both the ADAR2 cDNA and PMOs 9 (AluJ+93+117), 9A (AluJ+94+118), and 10 (AluJ+96+120), which were then lysed for protein isolation and western blotting. Cells were also transiently transfected with ADAR2 cDNA as a positive control for ADAR2 protein detection. We have found significantly low expression levels of endogenous ADAR2 in SH-SY5Y cells when compared to ADAR2 cDNA-transfected cells. The results presented here show that despite the high levels of exon skipping observed in PMO-transfected cells, the increase in RNA editing levels have reached saturation as the quantity of ADAR2 in the cells were simply too low.

4.2 RESULTS

4.2.1 TESTING DIFFERENT PRIMARY ANTIBODIES FOR ADAR2 DETECTION

The successful transfection of ADAR2 in SH-SY5Y cells was first verified. Cells were transfected with 2 µg of the ADAR cDNA for 48 hours, followed by protein extraction. As the ADAR2 cDNA is FLAG-tagged at the N-terminal, the expression of the cDNA was confirmed with both anti-ADAR2 C-15 (Santa Cruz) and anti-FLAG (Sigma #F7425) primary antibodies through SDS-PAGE and immunoblotting. Figure 4.2 shows the resulting western blot image of SH-SY5Y cells transfected with ADAR2 cDNA, thus verifying the successful transfection of the ADAR2 cDNA plasmid and protein expression of ADAR2 in the cells.

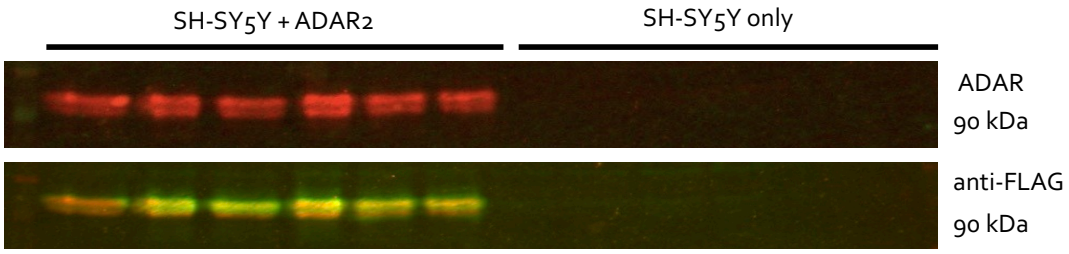

Figure 4.2 Confirmation of ADAR2 transfection in SH-SY5Y cells.

Figure shows western blot gel images of SH-SY5Y cells transfected with 2 µg of ADAR2 cDNA. Immunoblots were incubated with 1:250 ADAR2 C-15 primary antibody (top image) and 1:250 anti-FLAG antibody (bottom image) overnight at 4°C. The transfection was confirmed through visualisation of the blot at 560 nm (bottom image).

In order to examine the expression levels of ADAR2 in SH-SY5Y cells, we first tested three different primary antibodies for optimal ADAR2 detection. Cells were transfected with 2 μg of ADAR2 cDNA for 48 hours, followed by protein extraction. Cells transfected with ADAR2 acted as positive controls, and the detection of ADAR2 protein was compared in the following conditions: cells co-transfected with PMO and ADAR2 cDNA, cells transfected with ADAR2 cDNA only, cells transfected with PMO only and non-transfected cells. The antibodies used for ADAR2 detection can be found in Table 4.1.

Antibody	**Host**	**Company**
ADAR2 C-15	Mouse polyclonal	Santa Cruz, #SC-10012
ADAR2 C-6	Mouse monoclonal	Santa Cruz, #SC-514581
ADAR2 GTX114237	Rabbit polyclonal	GeneTex, #GTX114237

Table 4.1 Primary antibodies used for the detection of ADAR2.

Hand-cast Tris-glycine 10% acrylamide gels were used for SDS-PAGE. Following electrophoresis, blots were all blocked in 2.5% non-fat milk for 1.5 hours. Membranes were then incubated with ADAR2 primary antibodies at a concentration of 1:100 at 4°C overnight. Figure 4.3 shows the gel images of blots incubated with the different antibodies listed in Table 4.1. Non-transfected cells showed very faint ADAR2 signals in the cells following primary antibody incubation, which indicates very low levels of endogenous ADAR2 expression in SH-SY5Y cells. Incubation with ADAR2 C-15 (Santa Cruz) was able to detect ADAR2 signals in ADAR2-transfected cells (Figure 4.3a). The same results were also obtained in blots incubated with ADAR2 GTX (GeneTex) (Figure 4.3c), where slightly more distinct ADAR2 bands were detected compared to ADAR2 C-15 incubation. However, this was not the case for ADAR2 C-6 (Santa Cruz), where no bands were detected in transfected SH-SY5Y cells (Figure 4.3b). Following these findings, we then proceeded to use ADAR2 GTX as the primary antibody for ADAR2 detection in further experiments.

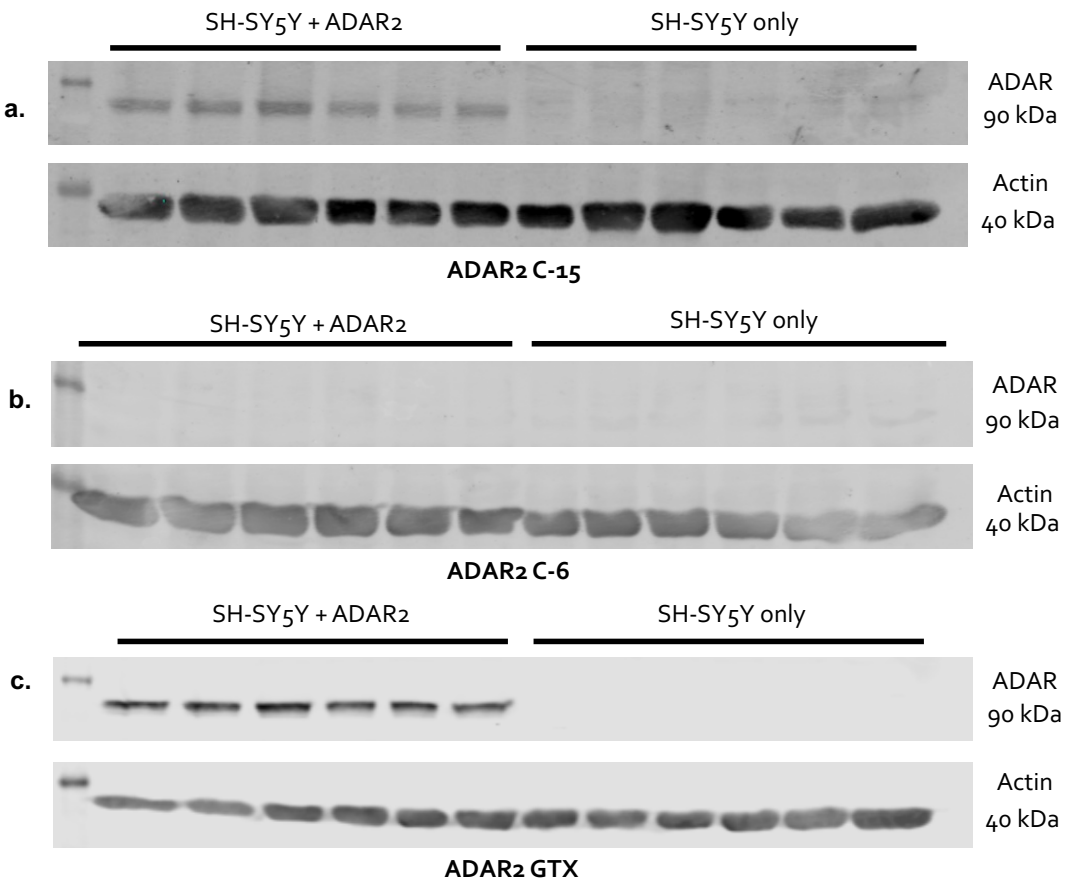

Figure 4.3 Trialling different antibodies for ADAR2 detection.

Figure shows representative western blot gel images for the detection of ADAR2 in transfected and non-transfected SH-SY5Y cells. ADAR2 transfected cells were used as a positive control whilst actin was used as an internal loading control. a) Blots incubated with ADAR2 C-15; b) Blots incubated with ADAR2 C-6; c) Blots incubated with ADAR2 GTX.

Protein samples were run in a 10% Tris-glycine acrylamide gel against BLUeye Prestained Protein Ladder and visualised with the Odyssey CLx Imaging System.

4.2.2 ADAR2 PROTEIN EXPRESSION IN SH-SY5Y CELLS

As previously described in Section 4.2.1, full-length expression of ADAR2 (90 kDa) was confirmed through the use of ADAR2 GTX antibody. The specificity of this antibody was confirmed in cells transfected with 2 µg of ADAR2 cDNA. Since we were attempting to measure differences in ADAR2 expression between PMO-transfected and non-transfected SH-SY5Y cells, cells were subjected to different conditions as follows:

i) Cells co-transfected with both 2 µg of ADAR2 cDNA and 2 µM of PMO using Lipofectamine and EndoPorter;
ii) Cells transfected with only 2 µg of ADAR2 using Lipofectamine;
iii) Cells transfected with only 2 µM of PMO using EndoPorter;
iv) Non-transfected cells.

Protein bands for ADAR2 were detected in cells transfected with ADAR2 cDNA as previously shown in Figure 4.3, however a very weak signal was detected in cell lysates that did not contain a copy of the ADAR2 cDNA (Figures 4.4-4.7). The expression levels of ADAR2 following PMO treatment were compared between the following conditions: ADAR2-transfected cells and non-ADAR2-transfected cells. Levels of ADAR2 expression were normalised to levels of β-actin (40 kDa), which acted as an internal loading control, in order to determine any modification in ADAR2 levels in PMO-transfected cells compared to non-PMO-transfected cells.

4.2.2.1 PMO 9 (ALUJ+93+117)

Since PMO 9 (AluJ+93+117) resulted in reduced AluJ cassette inclusion and increased Q/R site RNA editing levels (as described in Chapter 3), this PMO was then used for protein expression analysis of ADAR2. 2 μM of PMO 9 (AluJ+93+117) was transfected in ADAR2-transfected and non-transfected SH-SY5Y cells. The levels of ADAR2 expression were all normalised to endogenous ADAR2 levels measured in non-transfected cells (Figure 4.4a). The resulting western blot image is depicted in Figure 4.4a. PMO 9-transfected cells had a mean ADAR2 protein expression of 0.73 ± 0.05 (Figure 4.4b). ADAR2 protein expression measured in cells co-transfected with both ADAR2 cDNA and PMO 9 (AluJ+93+117) were revealed to be at 12.98 ± 2.3, whilst cells transfected with only ADAR2 cDNA showed ADAR2 levels to be at 11.93 ± 0.9 (Figure 4.4b). Cultures that were transfected with ADAR2 cDNA all showed significantly higher ADAR2 protein expression compared to non-ADAR2-transfected cells (Figure 4.4b). Statistical analysis suggested that the difference in ADAR2 expression levels between cells transfected with PMO 9 (AluJ+93+117) and non-PMO-transfected cells were not significant ($p>0.05$) in both ADAR2-transfected and non-ADAR2-transfected cells.

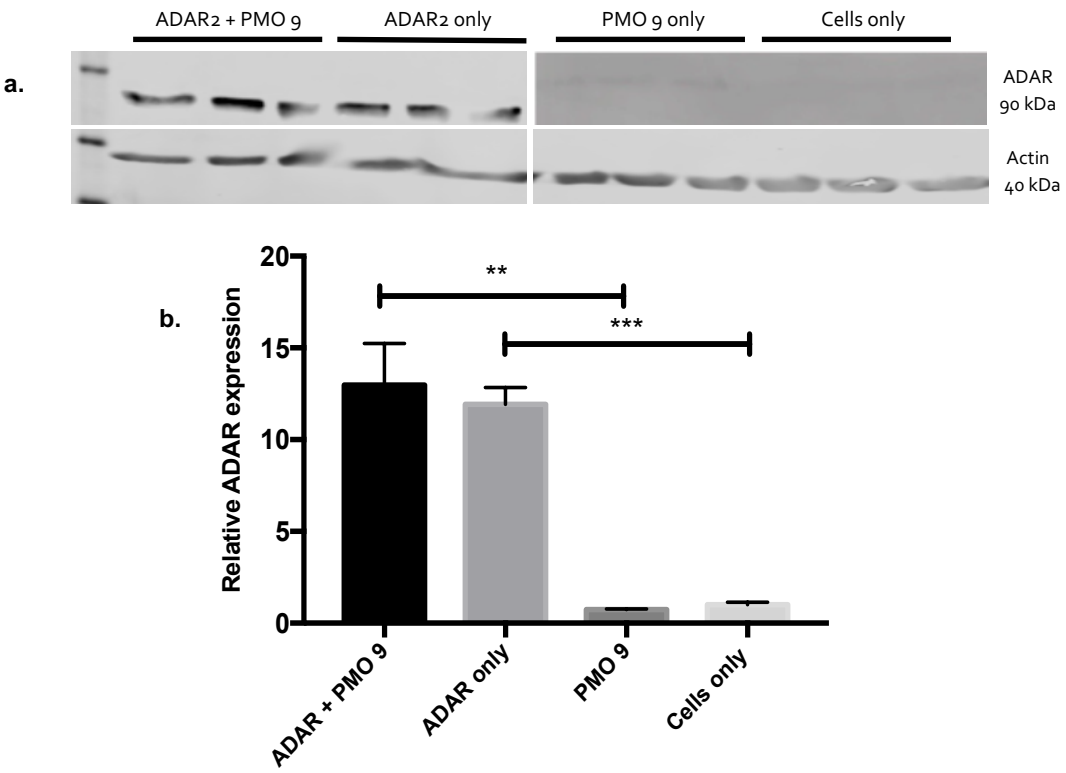

Figure 4.4 Expression of ADAR2 protein in ADAR2- and PMO 9-transfected cells.

Figure shows a) representative western blot gel image of SH-SY5Y cells transfected with ADAR2 and PMO 9. Actin was used as an internal loading control and to normalise expression levels of ADAR2 within each lane; b) Bar graph depicting relative ADAR2 protein expression levels transfected with ADAR2 and PMO 9 compared to non-transfected cells.

Protein samples were run in a 10% Tris-glycine acrylamide gel against BLUeye Prestained Protein Ladder and visualised with the Odyssey CLx Imaging System. Images were quantified using Image Studio 4.0.

n=3, ** = p≤0.01, *** = p≤0.001. Statistical comparisons were carried out using unpaired t-test. All data points correspond to mean ± SEM values.

4.2.2.2 PMO 9A (ALUJ+94+118)

PMO 9A (AluJ+94+118) was also used to measure ADAR2 protein expression as this PMO has also managed to successfully promote AluJ cassette exclusion and henceforth Q/R site RNA editing. The transfection conditions of PMO 9A (AluJ+94+118) were as described in Section 4.2.1. The resulting western blot image is shown in Figure 4.5a. The levels of ADAR2 protein expression in different conditions were all normalised to ADAR2 expression in non-transfected cells (Figure 4.5b). Cells that were transfected with both ADAR2 cDNA and PMO 9A (AluJ+94+118) showed mean ADAR2 protein expression of 14.38 $\pm$ 0.6, whilst mean protein levels in ADAR2-transfected cells were measured to be at 13.76 $\pm$ 0.5 (Figure 4.5b). Cultures transfected with only PMO 9A (AluJ+94+118) resulted in mean ADAR2 protein levels of 1.08 $\pm$ 0.1 (Figure 4.5b). Cultures transfected with ADAR2 cDNA all displayed significantly higher expression of ADAR2 protein compared to their non-ADAR2-transfected counterparts (Figure 4.5b). Treatment with PMO 9A (AluJ+94+118) does not affect ADAR2 expression levels, as supported by statistical analysis, where no significant difference in expression ($p>0.05$) between PMO-transfected and non-PMO-transfected samples were found.

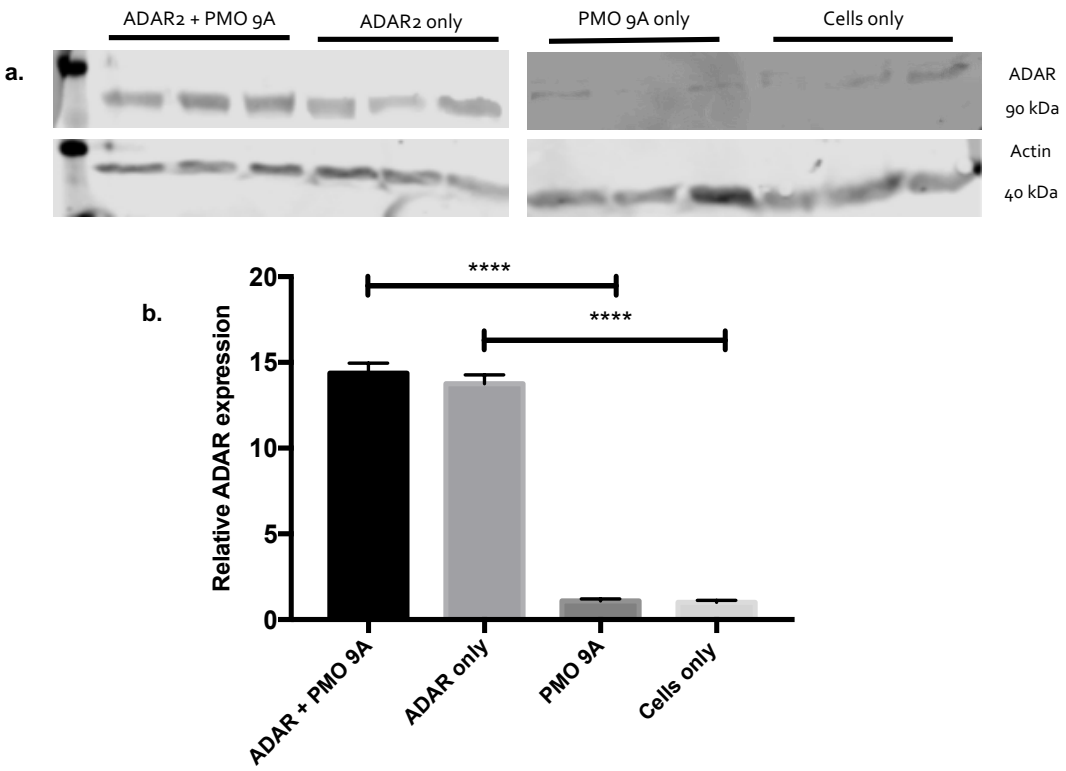

Figure 4.5 Expression of ADAR2 protein in ADAR2- and PMO 9A-transfected cells.

Figure shows a) representative western blot gel image of SH-SY5Y cells transfected with ADAR2 and PMO 9A. Actin was used as an internal loading control and to normalise expression levels of ADAR2 within each lane; b) Bar graph depicting relative ADAR2 protein expression levels transfected with ADAR2 and PMO 9A compared to non-transfected cells.

Protein samples were run in a 10% Tris-glycine acrylamide gel against BLUeye Prestained Protein Ladder and visualised with the Odyssey CLx Imaging System. Images were quantified using Image Studio 4.0.

n=3, **** = p≤0.0001. Statistical comparisons were carried out using unpaired t-test. All data points correspond to mean ± SEM values.

4.2.2.3 PMO 10 (ALUJ+96+120)

As previously mentioned in Chapter 3, PMO 10 (AluJ+96+120) did not promote AluJ cassette exclusion, and hence RNA editing levels did not improve in transfected SH-SY5Y cells. PMO 10 (AluJ+96+120) thus acts as a further control in our protein experiments to ensure that ADAR2 protein expression is not affected by the presence of PMOs. The resulting western blot image is depicted in Figure 4.6a. ADAR2 protein expression levels in differing conditions were normalised to ADAR2 expression in non-transfected cells (Figure 4.6b). Transfection with both ADAR2 and PMO 10 (AluJ+96+120) resulted in mean ADAR2 protein expression levels of 24.7 $\pm$ 3.7 (Figure 4.6b). ADAR2-transfected cells showed mean protein expression of 15.35 $\pm$ 0.3. Mean ADAR2 protein levels in cultures transfected with PMO 10 (AluJ+96+120) were measured to be at 1.03 $\pm$ 0.8 (Figure 4.6b). Cultures transfected with ADAR2 cDNA all showed significantly higher ADAR2 protein expression compared to cultures that do not contain a copy of the ADAR2 cDNA (Figure 4.6b). The difference in ADAR2 protein expression was not statistically significant when comparing levels measured between PMO-transfected and non-PMO-transfected cultures ($p>0.05$).

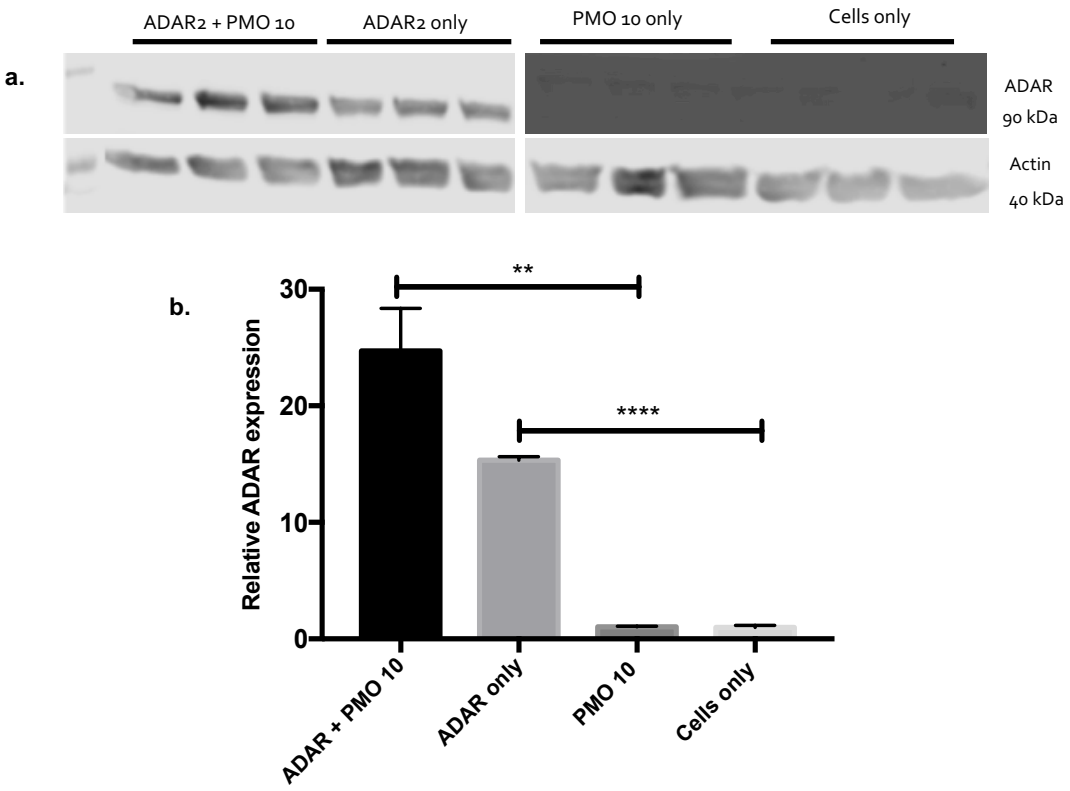

Figure 4.6 Expression of ADAR2 protein in ADAR2- and PMO 10-transfected cells.

Figure shows a) representative western blot gel image of SH-SY5Y cells transfected with ADAR2 and PMO 10. Actin was used as an internal loading control and to normalise expression levels of ADAR2 within each lane; b) Bar graph depicting relative ADAR2 protein expression levels transfected with ADAR2 and PMO 10 compared to non-transfected cells.

Protein samples were run in a 10% Tris-glycine acrylamide gel against BLUeye Prestained Protein Ladder and visualised with the Odyssey CLx Imaging System. Images were quantified using Image Studio 4.0.

n=3, ** = $p \leq 0.01$, **** = $p \leq 0.0001$. Statistical comparisons were carried out using unpaired t-test. All data points correspond to mean ± SEM values.

4.2.2.4 ENDOPORTER

In our PMO experiments, we found that cells co-transfected with PMO and ADAR2 cDNA always displayed slightly higher protein expression compared to cells only transfected with ADAR2 cDNA. We then investigated the possible reason for this effect by examining ADAR2 expression with only EndoPorter without including PMOs. The resulting western blot image is shown in Figure 4.7a. ADAR2 protein levels were all normalised to the expression of ADAR2 protein in non-transfected cells (Figure 4.7b). Transfection of cells with both ADAR2 and EndoPorter resulted in mean protein expression levels of 31.74 $\pm$ 2.5, whilst ADAR2-transfected cells showed mean protein ADAR2 levels of 23.04 $\pm$ 1.5. Protein levels in cultures transfected with EndoPorter were measured to be at 0.95 $\pm$ 0.1. Transfection of ADAR2 cDNA in cells resulted in significantly higher ADAR2 protein expression compared to their non-ADAR2-transfected counterparts. Statistical analysis revealed that ADAR protein expression levels between cells co-transfected with both ADAR2 and EndoPorter were significantly higher than levels measured in ADAR2-transfected cells (Figure 4.7b). This contradicts the results we previously observed in PMO-transfected cells (Figures 4.4-4.6); where cultures that were transfected with both ADAR2 cDNA and PMOs did not result in any significant difference in ADAR2 protein expression when compared against cultures transfected with ADAR2 cDNA. However, the protein expression of ADAR2 in cells transfected with only EndoPorter and non-transfected cells did not result in any significant difference among the two conditions (Figure 4.7b), consistent with the results previously observed (Figures 4.4-4.46).

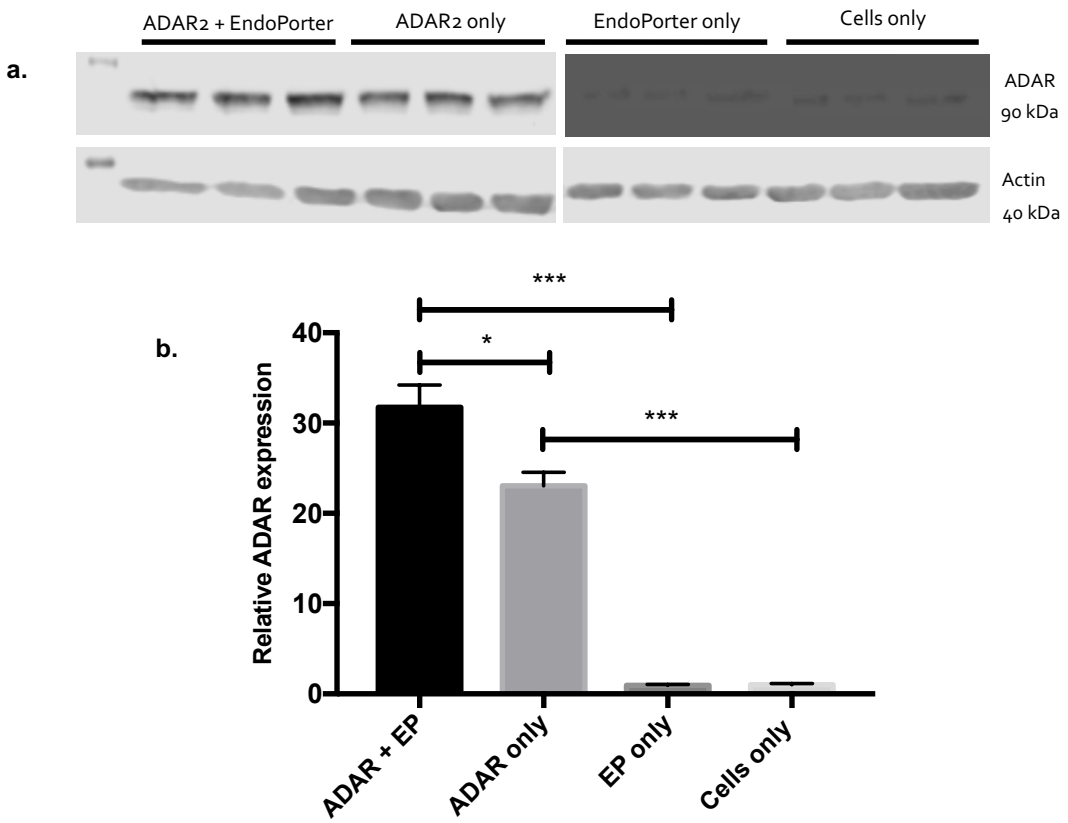

Figure 4.7 Expression of ADAR2 protein in ADAR2- and EndoPorter-transfected cells.

Figure shows a) representative western blot gel image of SH-SY5Y cells transfected with ADAR2 and EndoPorter. Actin was used as an internal loading control and to normalise expression levels of ADAR2 within each lane; b) Bar graph depicting relative ADAR2 protein expression levels transfected with ADAR2 and EndoPorter compared to non-transfected cells.

Protein samples were run in a 10% Tris-glycine acrylamide gel against BLUeye Prestained Protein Ladder and visualised with the Odyssey CLx Imaging System. Images were quantified using Image Studio 4.0.

n=3, * = p≤0.05, *** = p≤0.001. Statistical comparisons were carried out using unpaired t-test. All data points correspond to mean ± SEM values.

4.3 DISCUSSION

Based on the results obtained from ADAR2 protein expression analysis in SH-SY5Y cells, we can conclude that endogenous ADAR2 protein expression in these cells is very low. This is apparent by the very weak expression of ADAR2 in cells that were not transfected with the ADAR2 plasmid, where essentially no signal was detected by the anti-ADAR2 antibody (Figures 4.4a-4.7a). In fact, an ADAR2 signal was only picked up in cells transfected with 2 µg of ADAR2 plasmid. Transfecting SH-SY5Y cells with the ADAR2 plasmid resulted in overall significant increase in ADAR2 protein expression compared to non-transfected SH-SY5Y cells (Figures 4.4b-4.7b). The endogenous ADAR2 levels measured in non-transfected SH-SY5Y cells here corroborates the results we previously observed in Chapter 3. In Chapter 3, we demonstrated that although PMOs 9 (AluJ+93+117) and 9A (AluJ+94+118) were able to result in substantial decrease in ADAR2 RNA expression containing the AluJ cassette in SH-SY5Y cells (Figures 3.5 and 3.6), only a slight (although significant) increase in RNA editing was observed in these cells amongst the different concentrations tested (Figures 3.14 and 3.15). Hence, the marginal increase in RNA editing levels may have been due to the low constitutive ADAR2 expression in the cells, where the effects of the PMOs on increasing RNA editing have reached saturation. The pool of ADAR2 expressed in SH-SY5Y cells were simply not high enough to further improve RNA editing levels.

Since RNA editing requires the formation of an RNA duplex caused by the base-pairing between intron and exon sequences (Bass, 2002), editing is presumed to occur at sites of pre-mRNA transcription prior to splicing (Rueter et al., 1999). This implies that the PMOs are meant to interact with ADAR2 at the pre-mRNA level before the enzyme is translated into protein. Thus, the expression levels of ADAR2 protein should not be altered following transfection with PMOs. Transfection of SH-SY5Y cells with PMOs 9 (AluJ+93+117), 9A (AluJ+94+118), and 10 (AluJ+96+120) did not affect the levels of ADAR2 expression when compared to non-transfected cells (Figures

4.4-4.6). No significant difference was found in ADAR2 protein expression between PMO-transfected cells and non-PMO-transfected cells in ADAR2-transfected cultures as well (Figures 4.4-4.6). However, EndoPorter-transfected cells in cultures that express the ADAR2 plasmid displayed a significant increase in ADAR2 protein expression compared to cultures that were not transfected with EndoPorter (Figure 4.7b). It seems as if the presence of the EndoPorter transfection reagent itself, has somehow increased ADAR2 expression in the cells.

One of the reasons behind the extremely low endogenous levels of ADAR2 protein expressed in SH-SY5Y cells here is the localisation of ADAR2 itself. ADAR2 has been demonstrated to accumulate in the nucleolus (Sansam, Wells, & Emeson, 2003). This occurs in an rRNA-dependent manner and can shuttle between subnuclear compartments rapidly (Sansam et al., 2003). In fact, the translocation of endogenous ADAR2 to the nucleolus from the nucleoplasm corresponds to improved editing of pre-mRNA substrates. This illustrates that the nucleolar localisation of ADAR2 describes an important mechanism that sequesters editing activity from pre-mRNA transcription sites (Sansam et al., 2003). A pool of editing activity is thus accessible for response to changes in the expression of potential RNA substrates, yet concurrently inhibiting aberrant editing activity by maintaining low ADAR2 concentrations in the nucleoplasm (Sansam et al., 2003). In fact, cells that were treated with actinomycin D (which induces translocation of ADAR2) resulted in a 30% increase in the editing of endogenous ADAR2 pre-mRNA. However, no significant alteration was found in ADAR2 protein levels of NIH 3T3 cells treated with actinomycin D (Sansam et al., 2003), similar the results we have obtained here, wherein ADAR protein levels do not change even with improved RNA editing following PMO treatment. This suggests that the nucleolus acts as a site of functional sequestration for the activity of ADAR2 (Sansam et al., 2003). Aside from that, studies carried out in mouse neurons also revealed that although RNA editing increases in developing mouse brain, the protein levels of both ADAR2 isoforms (ADAR2a and ADAR2b) remain consistent and cannot be the major cause for the levels of

increased editing (Behm et al., 2017; Filippini et al., 2018b; Wahlstedt et al., 2009).

Considering that ADAR2 is a nuclear protein, we used radioimmunoprecipitation assay (RIPA) buffer as a lysis buffer for protein extraction, as this buffer is more potent at disrupting nuclear membranes compared to other lysis buffers (Ngoka, 2008). However, protein lysates of SH-SY5Y cells extracted using RIPA buffer still did not enable us to detect sufficient levels of ADAR2 protein. One way to overcome this is by carrying out nuclear fractionisation of SH-SY5Y cells, which separates nuclear fractions from cytosolic fractions (Suzuki, Bose, Leong-Quong, Fujita, & Riabowol, 2010). This will consequently be able to result in better constitutive ADAR2 protein detection in SH-SY5Y cells.

CHAPTER 5 REGULATION OF PIN1 AND WWP2 DURING RNA EDITING

5.1 INTRODUCTION

Protein phosphorylation is an important cellular signalling mechanism which promotes modifications in protein conformation. One common signalling mechanism in cell proliferation and transformation is proline (Pro)-directed serine (Ser)/threonine (Thr) phosphorylation (pSer/Thr-Pro) (Lu & Zhou, 2007). A breakthrough in the insights of the conformational significance of Pro-directed phosphorylation motifs was the discovery of a unique and conserved peptidyl-prolyl *cis/trans* isomerase (PPIase), Pin1 (protein interacting with NIMA (never in mitosis A-1) (Lu, Hanes, & Hunter, 1996). PPIases are evolutionary conserved enzymes which catalyse the *cis/trans* isomerisation of peptidyl-prolyl peptide bonds (Lu & Zhou, 2007). Although several PPIases have been discovered, currently, Pin1 is the only one known to specifically target the pSer/ Thr-Pro sequence (Driver, Zhou, & Lu, 2015). The specificity of Pin1 derives from its two-domain structure. The double-trytophan (WW) domain binds only to specific pSer/Thr-Pro motifs, while the PPIase domain catalyses the conformational change (Driver et al., 2015) (Figure 5.1).

The identification of Pin1 resulted in the hypothesis of a new signalling mechanism, by which Pin1 regulates substrate post-phosphorylation conformation to further control protein function (Ranganathan, Lu, Hunter, & Noel, 1997). Ensuing studies showed that Pin1-catalysed conformational regulation has a significant impact on many vital proteins involved in cell growth regulation, genotoxic and other stress responses, immune response, germ cell development, neuronal differentiation, and survival (Lu & Zhou, 2007).

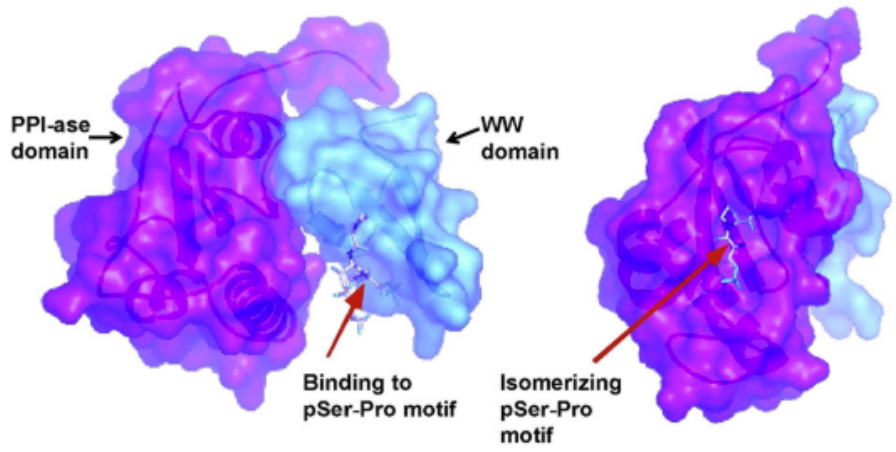

Figure 5.1 Two-domain structure of Pin1.

Pin1 has risen as a novel molecular timer that regulates its numerous targets at various steps of a given cellular process to synergistically control the amplitude and duration of a cellular response or process. Essentially, Pin1 is highly regulated at numerous levels and its deregulation plays a role in a rising number of pathological conditions, such as cancer, Alzheimer's disease (AD), ageing, asthma, and microbial infection (Lu & Zhou, 2007). In cancers, Pin1 was found to be overexpressed in human cancer tissues, including breast, prostate, lung, and colon cancer (Bao et al., 2004). Pin1 promotes oncogenesis by activating various oncogenes or growth enhancers and by inactivating a large number of tumour suppressors or growth inhibitors (T. H. Lee, Pastorino, & Lu, 2011). In contrast, Pin1 plays a protective role against AD, where reduced Pin1 expression correlates with increased vulnerability during neurodegeneration. Knockdown of Pin1 expression in mice results in an AD type age-dependent neurodegeneration, causing increased phosphorylated tau levels and increased APP pathogenic processing and insoluble β-amyloid (Liou et al., 2003). The same can also be found in ageing, where Pin1-deficient mice eventually display extensive premature ageing phenotypes compared to wild-type mice, such as reduced body size, retina atrophy, motor coordination and behavioural defects, and accelerated telomere loss (T. H. Lee, Pastorino, et al., 2011). Recent studies demonstrated that phosphorylation-independent prolyl isomerisation functions as a molecular timer to modulate several biological and pathological processes,

namely cell signalling, ion channel gating, gene expression, and phage infection (Lu & Zhou, 2007).

Pin1 has been shown to interact with ADAR2 as a positive regulator essential for the nuclear localisation and stability of ADAR2, where it binds to the amino-terminus of ADAR2 in a phosphorylation dependent manner. ADAR2 protein is more labile and will mislocalise to the cytoplasm when Pin1 is absent, resulting in its inability to edit pre-mRNAs and thus decreasing Q/R and R/G site editing in GluA2 transcripts. Hence, Pin1 is a positive regulator of ADAR2 editing activity (Marcucci et al., 2011).

Protein ubiquitination is a post-translational modification that regulates various cellular processes such as protein turnover, trafficking, sub-cellular localisation, transcriptional function, and DNA repair mechanisms (Kerscher, Felberbaum, & Hochstrasser, 2006). Ubiquitin conjugation comprises a series of events sequentially catalysed by E1 (ubiquitin-activating), E2 (ubiquitin-conjugating), and E3 (ubiquitin ligase) enzymes. E3 ligases are sub-divided into RING type and HECT domain ligases (Chantry, 2011). Within the HECT E3 sub-division contains a small group known as the Nedd4 superfamily. Nedd4 E3s contain a HECT ligase domain as well as a membrane-targeting Ca^{2+}/phospholipid-binding C2 and up to four WW (double tryptophan) domains. WW domains interact with PPXY, phosphor-Ser-Pro and Pro-Arg motifs. They are mainly responsible for the recruitment of specific target substrates. These features make Nedd4 E3s not only functionally diverse, but also makes them a suitable therapeutic target by disrupting specific substrate recruitment (Chantry, 2011).

Although several specific substrates have been identified for individual Nedd4 family members (Rotin & Kumar, 2009), their biological and pathological roles are still not well understood. However, there have been recent reports that feature novel functional roles for one member of the Nedd4 family, the WWP2 E2 ligase. Knockout studies reveal main developmental roles for WWP2 in craniofacial development and chondrogenesis, while molecular approaches uncovered two new WWP2 substrates, PTEN and Smads, that are associated with critical oncogenic signalling pathways

responsible for cell survival and epithelial-to-mesenchymal transition (EMT), respectively (Chantry, 2011). Additionally, the characterisation of two new WWP2 isoforms, WWP2-N and WWP2-C, highlights novel intra-molecular mechanisms that control WWP2 biological activity (Soond & Chantry, 2011). WWP2 has also been identified as a negative regulator of ADAR2 activity, where increased WWP2 expression results in reduced ADAR2 protein levels (Marcucci et al., 2011).

Since both Pin1 and WWP2 were found to regulate GluA2 Q/R site editing in an opposing manner (Marcucci et al., 2011), work here was carried out to investigate whether increased RNA editing in SH-SY5Y cells (which was attained through transfections with PMO 9 (AluJ+93+117) and 9A (AluJ+94+118)) through the exclusion of the AluJ cassette plays a role in the regulation of both Pin1 and WWP2 gene expression. Furthermore, whilst WWP2 negatively regulates RNA editing, it is not known how a reduction in RNA editing (due to steric hindrance of the Q/R editing site) can affect the expression of either regulatory protein. Hence, we also studied how transfecting SH-SY5Y cells with PMOs that inhibit RNA editing influence both Pin1 and WWP2 gene expression. Additionally, since Pin1 expression levels were altered at the mRNA level, we also attempted to measure the expressional changes in Pin1 protein levels following PMO transfection.

5.2 RESULTS

5.2.1 VALIDATION OF RT-QPCR PRIMER TARGET GENES

Reverse transcriptase-quantitative PCR (RT-qPCR) was the method utilised in this chapter to study the expression levels of Pin1 and WWP2 in SH-SY5Y cells. Prior to carrying out qPCRs on transfected cells, the primers used for the PCR were first validated to ensure target gene specificity and efficiency. Primer sequences for Pin1 (PrimerBank ID: 336285452c1) and WWP2 (PrimerBank ID: 5902156a1) were obtained from PrimerBank (https://pga.mgh.harvard.edu/primerbank/) (Figure 5.2). PrimerBank primers are compatible with SYBR Green I detection methods (as described in Section 2.11) and primers were designed based on an algorithm previously used to design oligonucleotide probes for DNA microarrays (Spandidos, Wang, Wang, & Seed, 2009). All primer sequences from this database have been validated through qPCR as well as sequencing and agarose gel electrophoresis (X. Wang, Spandidos, Wang, & Seed, 2012). An agarose gel electrophoresis was performed on PCR products of SH-SY5Y cells to ensure that no multiple PCR product bands and primer dimers were formed. Distinct PCR products of the expected sizes were detected using both sets of primers (Figure 5.3).

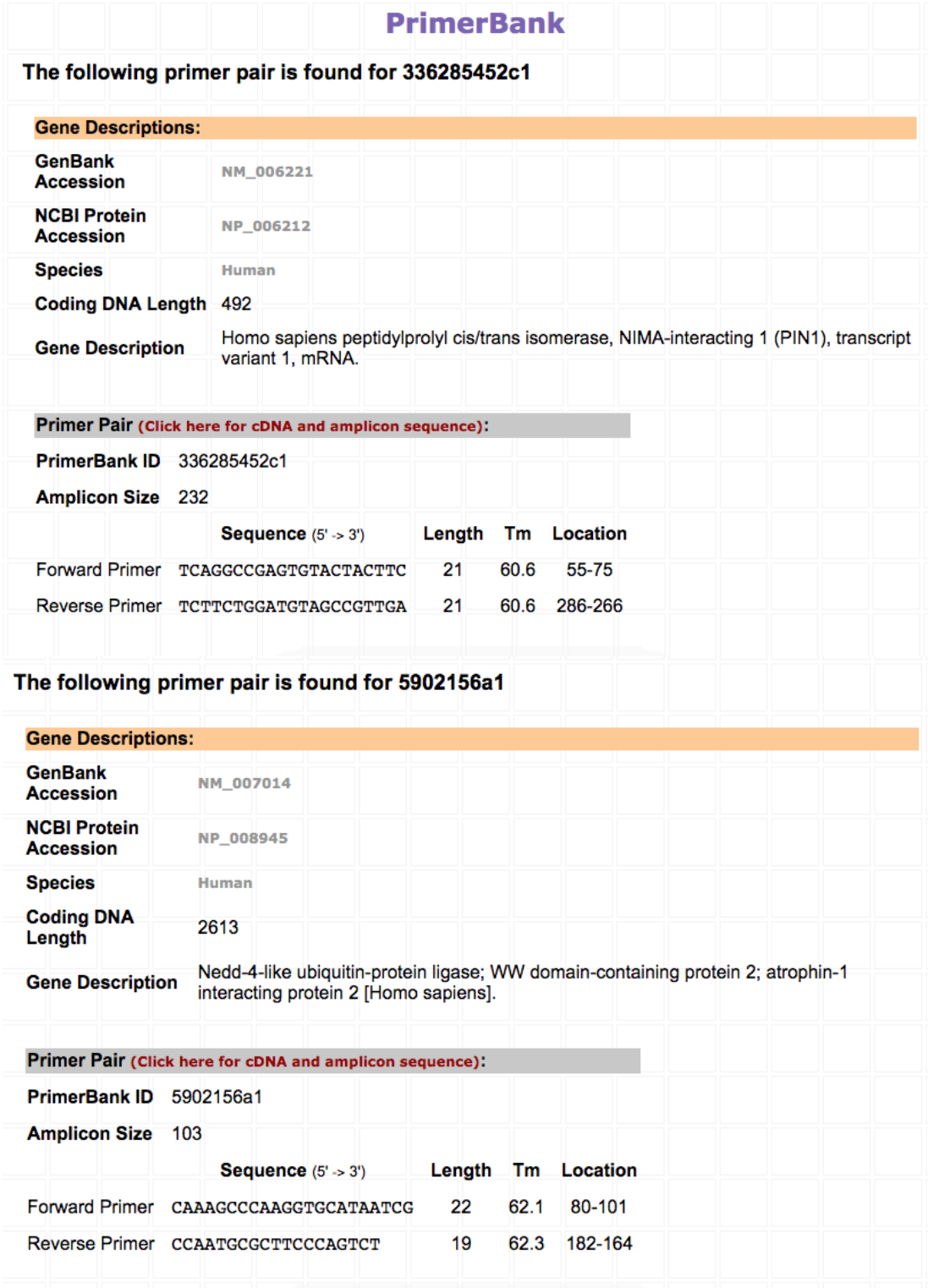

PrimerBank

The following primer pair is found for 336285452c1

Gene Descriptions:	
GenBank Accession	NM_006221
NCBI Protein Accession	NP_006212
Species	Human
Coding DNA Length	492
Gene Description	Homo sapiens peptidylprolyl cis/trans isomerase, NIMA-interacting 1 (PIN1), transcript variant 1, mRNA.

Primer Pair (Click here for cDNA and amplicon sequence):

PrimerBank ID 336285452c1

Amplicon Size 232

	Sequence (5' -> 3')	Length	Tm	Location
Forward Primer	TCAGGCCGAGTGTACTACTTC	21	60.6	55-75
Reverse Primer	TCTTCTGGATGTAGCCGTTGA	21	60.6	286-266

The following primer pair is found for 5902156a1

Gene Descriptions:	
GenBank Accession	NM_007014
NCBI Protein Accession	NP_008945
Species	Human
Coding DNA Length	2613
Gene Description	Nedd-4-like ubiquitin-protein ligase; WW domain-containing protein 2; atrophin-1 interacting protein 2 [Homo sapiens].

Primer Pair (Click here for cDNA and amplicon sequence):

PrimerBank ID 5902156a1

Amplicon Size 103

	Sequence (5' -> 3')	Length	Tm	Location
Forward Primer	CAAAGCCCAAGGTGCATAATCG	22	62.1	80-101
Reverse Primer	CCAATGCGCTTCCCAGTCT	19	62.3	182-164

Figure 5.2 Primer sequences and PrimerBank IDs.

Figure shows the sequences and PrimerBank IDs for Pin1 (left) and WWP2 (right) obtained from https://pga.mgh.harvard.edu/primerbank/.

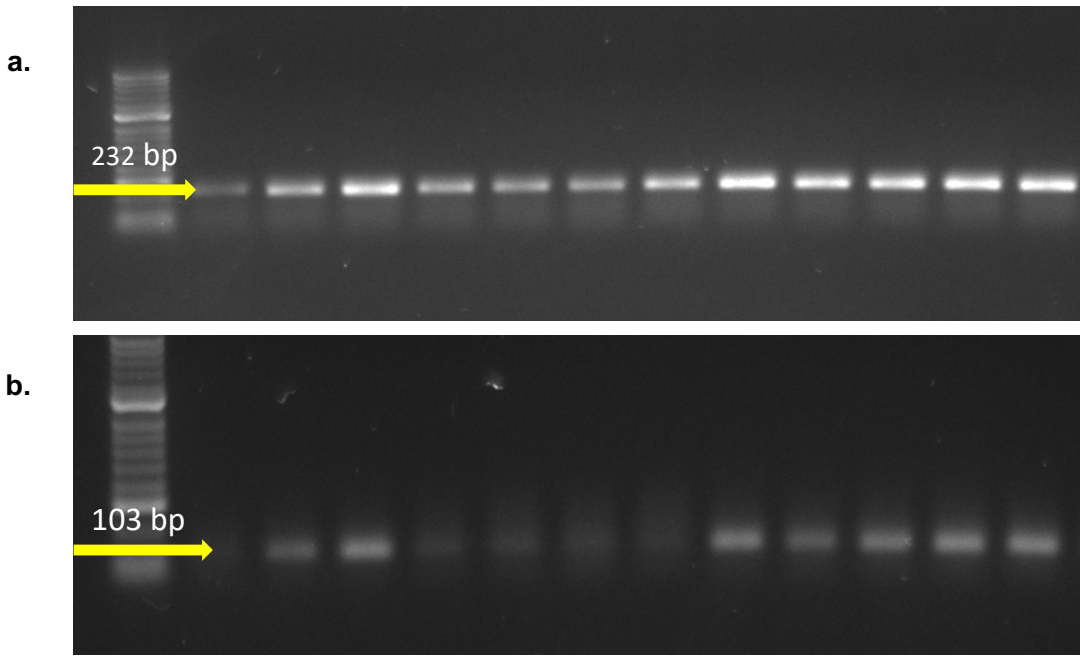

Figure 5.3 Validation of Pin1 and WWP2 RT-qPCR primers.

a) Gel image RT-PCR products of control SH-SY5Y cells amplified with Pin1 primers. The yellow arrow denotes the expected band size for Pin1 (232 bp). b) Gel image RT-PCR products of control SH-SY5Y cells amplified with WWP2 primers. The yellow arrow denotes the expected band size for WWP2 (103 bp).

Gels were run in a 1.5% agarose gel in 1X TAE buffer against Hyperladder V and visualised under UV light using a GELDOC system.

5.2.2 QUANTIFYING PIN1 AND WWP2 EXPRESSION FOLLOWING EXCLUSION OF THE ALUJ CASSETTE

Once the primer sets for Pin1 and WWP2 were validated, the primers were then utilised for qPCR experiments. We investigated whether a reduction in AluJ cassette incorporation in SH-SY5Y cells influences the expression of Pin1 and WWP2 following transfection of PMOs 9 (AluJ+93+117), 9A (AluJ+94+118) and 10 (AluJ+96+120). qPCRs were performed on cells that have been transfected with 5 μM of each PMO, with β-actin used as a housekeeping reference gene. Transfection of SH-SY5Y cells with 5 μM of PMO 9 (AluJ+93+117) increased the level of Pin1 mRNA (11.52 ± 2.1 fold-change vs cells only) (Figure 5.4a) while the mRNA levels of WWP2 were reduced (0.41 ± 0.08 fold-change vs cells only) (Figure 5.4b). Similar results were observed with 5 μM PMO 9A-transfected cells, where an increase in Pin1 mRNA expression was detected (6.26 ± 0.7 fold-change vs cells only) (Figure 5.3c), whereas a downregulation in WWP2 mRNA expression was observed (0.17 ± 0.04 fold-change vs cells only) (Figure 5.4d). Transfections with 5 μM of PMO 10 (AluJ+96+120), however, did not result in any significant fold-change in both Pin1 (0.81 ± 0.02 fold-change vs cells only) (Figure 5.4e) and WWP2 expression (0.82 ± 0.3 fold-change vs cells only) (Figure 5.4f) compared to control cells. The change in both Pin1 and WWP2 expression here are consistent with the results obtained in Chapter 3, where an increase in RNA editing levels caused by a reduction in AluJ cassette incorporation plays a role in the regulation of both Pin1 and WWP2 expression levels. Pin1 mRNA expression showed significant upregulation following PMO 9 (AluJ+93+117) and 9A (AluJ+94+118) treatment while WWP2 mRNA expression was significantly downregulated.

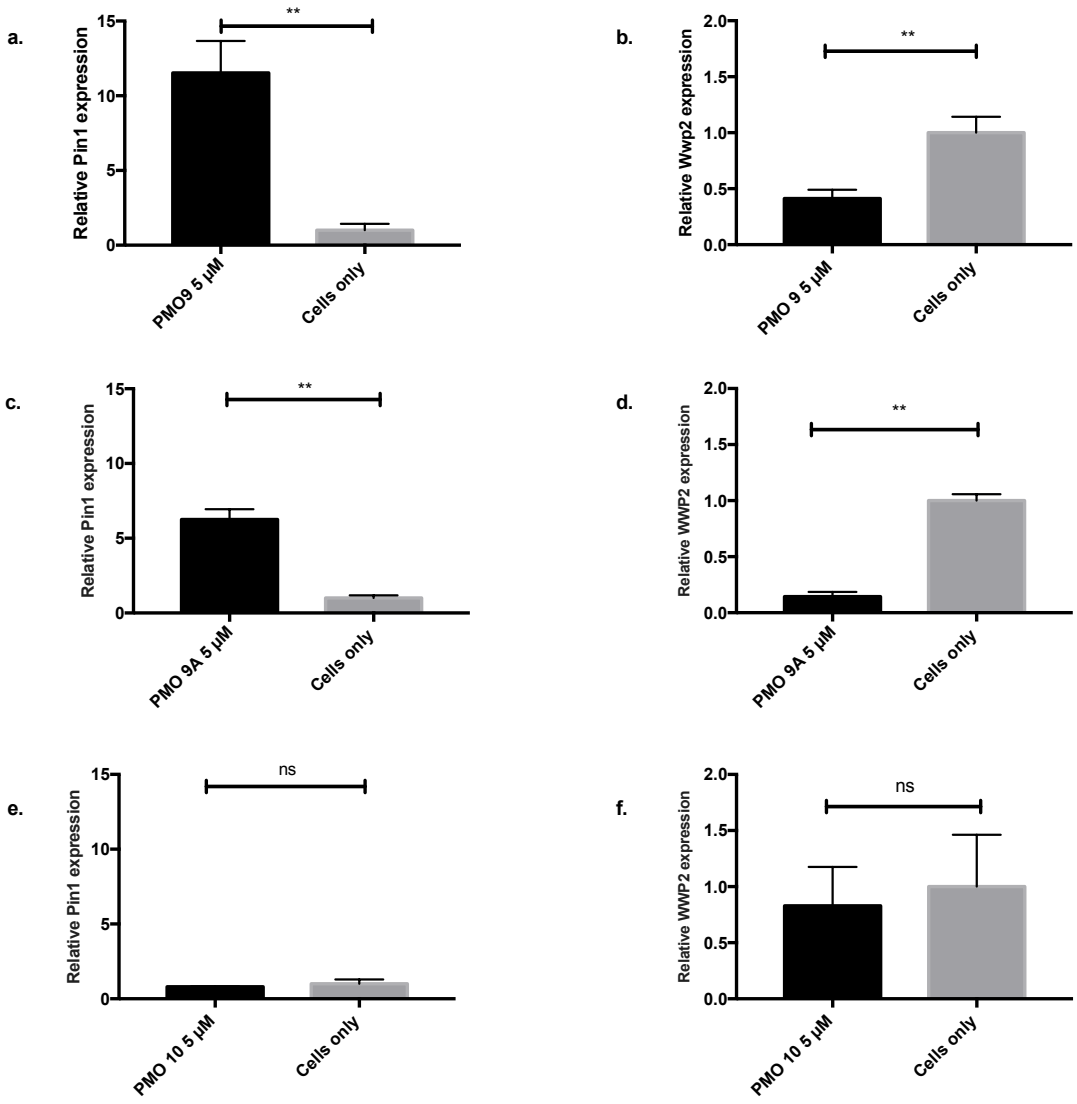

Figure 5.4 Pin1 and WWP2 expression in SH-SY5Y cells.

RT-qPCR analysis of mRNA isolated from cells transfected with 5 µM of PMOs 9, 9A and 10. Bar graphs **a** and **b** show expression levels of Pin1 and WWP2 in PMO 9-transfected cells; bar graphs **c** and **d** show expression levels of Pin1 and WWP2 in PMO 9A-transfected cells; and bar graphs **e** and **f** show expression levels of Pin1 and WWP2 in PMO 10-transfected cells.

Expression of Pin1 and WWP2 was assessed using the LightCycler 480 (Roche) and reactions were performed using the LightCycler SYBR Green I Mastermix (Roche). The expression levels of β-actin were used as a reference gene. The gene expression levels were defined based on the threshold cycle (Ct), and relative expression levels were calculated using the $2^{-\Delta\Delta Ct}$ method. Measurements were made from three separate transfections in triplicate.

n=3-4, * = p≤0.05, ** = p≤0.01. Statistical comparisons were carried out using an unpaired t-test. All data points correspond to mean ± SEM values.

5.2.3 DISRUPTING Q/R SITE EDITING IN SH-SY5Y CELLS

In this section, PMOs that were designed to disrupt the internal secondary structure of GluA2 RNA via steric hindrance were utilised. These PMOs are therefore able to inhibit GluA2 Q/R site editing in SH-SY5Y cells, which resembles low editing efficiency in motor neurons of ALS patients (Kwak & Kawahara, 2005). Since the downstream effects of disrupted Q/R site editing in ALS is still largely unknown, using PMOs to sterically inhibit editing could be used to study regulatory changes at the molecular level, thus giving a better understanding on the pathophysiology of ALS.

Two PMOs were used for these sets of experiments: first, PMO E1 (GRIA2+279+308), which covers the double-stranded region located around the Q/R site of GluA2; second, PMO 1 (GRIA2+284+308), which is used as a control PMO as it has previously been shown to have no effect on RNA editing levels (Chaytow, 2015). Both PMOs were designed to complement the Exon Complementary Sequence located in intron 11 of *GRIA2* (Figure 5.5). SH-SY5Y cells were transfected with 5 μM of PMOs E1 and 1 for 24 hours, and its effects on both AluJ cassette inclusion and RNA editing, as well as Pin1 and WWP2 expression, were assessed.

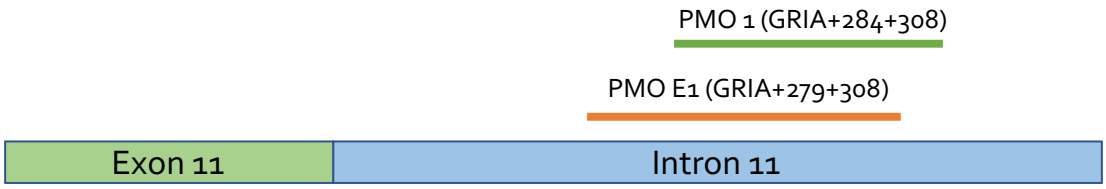

Figure 5.5 Schematic diagram showing the PMO binding positions on intron 11 of *GRIA2*.

5.2.3.1 EFFECT OF Q/R SITE EDITING DISRUPTION ON ALUJ INSERTION AND RNA EDITING

AluJ cassette inclusion in RT-PCR products of cells treated with PMOs E1 (GRIA2+279+308) and 1 (GRIA2+284+308) were quantified to determine whether transfection with these PMOs will result in any changes in exon skipping levels. Figure 5.6 shows the results of the RT-PCR. As expected, treatment with 5 µM of both PMO E1 (GRIA2+279+308) and PMO 1 (GRIA2+284+308) did not result in any reduction in AluJ cassette inclusion levels compared to control cells ($p>0.05$).

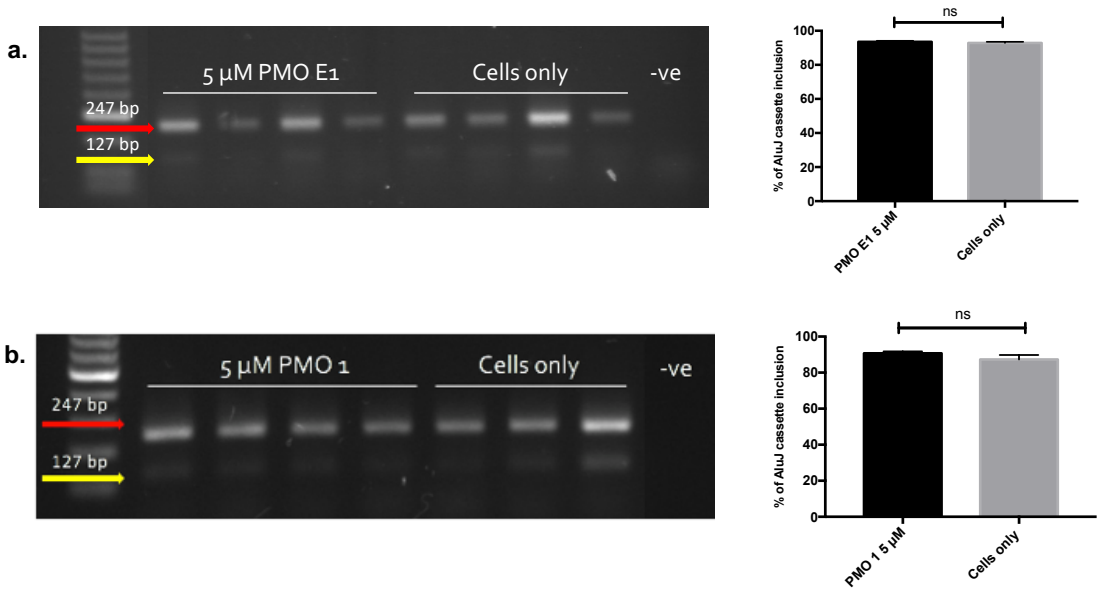

Figure 5.6 The effect of PMO E1 and PMO 1 on AluJ insertion in SH-SY5Y cells.

Figure shows a sample gel image of a) RT-PCR products of SH-SY5Y cells transfected with 5 µM of PMO E1 (left) and a bar graph depicting AluJ cassette inclusion percentages (right) and *b)* RT-PCR products of SH-SY5Y cells transfected with 5 µM of PMO 1 (left) and a bar graph depicting AluJ cassette inclusion percentages (right).

Gels were run in a 1.5% agarose gel in 1X TAE buffer against Hyperladder V and visualized under UV light using a GELDOC system. Images were quantified using ImageJ. "-ve" denotes negative control. Sample gel images show the intensity of exon-skipped transcripts (127 bp, yellow arrow) against exon-including transcripts (247 bp, red arrow).

n=4. Statistical comparisons were carried out using unpaired t-test. All data points correspond to mean ± SEM values.

Since PMO E1 (GRIA2+279+308) was designed to disrupt Q/R site editing in the GluA2 subunit, the editing levels in cells transfected with this PMO significantly decreased to 41.53 ± 1.5% when compared to control cells (Figure 5.7a). RNA editing levels in cells transfected with PMO 1 (GRIA2+284+308) remained approximately the same compared to non-transfected cells (p>0.05) (Figure 5.7b). This is in agreement with previous findings (Chaytow, 2015).

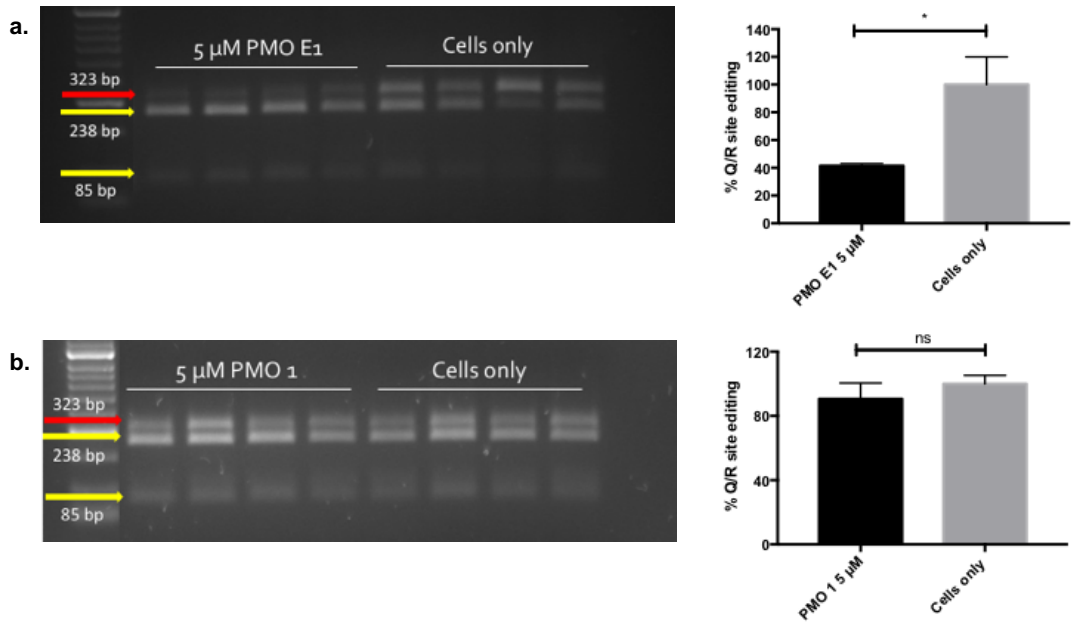

Figure 5.7 The effect of PMO E1 and PMO 1 on RNA editing in SH-SY5Y cells.

Figure shows a sample gel image of a) BbvI digest products of SH-SY5Y cells transfected with 5 µM of PMO E1 (left) and a bar graph depicting Q/R site editing percentages in SH-SY5Y cells (right) and b) BbvI digest products of SH-SY5Y cells transfected with 5 µM of PMO 1 (left) *and* a bar graph depicting Q/R site editing percentages in SH-SY5Y cells (right).

Gels were run in a 2.5% agarose gel in 1X TAE buffer against Hyperladder V and visualized under UV light using a GELDOC system. Images were quantified using ImageJ. "-ve" denotes negative control. Sample gel images show the intensity of edited transcripts (323 bp, red arrow) against unedited transcripts (238 bp and 85 bp, yellow arrow).

n=4, * = p≤0.05. Statistical comparisons were carried out using unpaired t-test. All data points correspond to mean ± SEM values.

5.2.3.2 EFFECT OF Q/R SITE EDITING DISRUPTION ON PIN1 AND WWP2 EXPRESSION

The mRNA levels of Pin1 and WWP2 were then evaluated in PMO E1- and PMO 1-transfected cells. Pin1 mRNA levels in PMO E1-transfected cells showed no significant difference in expression compared to control cells (1.74 ± 0.4 fold-change vs cells only) (Figure 5.8a), even though a reduction in RNA editing levels were observed. WWP2 mRNA levels did, however, significantly increase following PMO E1 (GRIA2+279+308) transfection (2.01 ± 0.2 fold-change vs cells only) (Figure 5.8b). Since PMO 1 (GRIA2+284+308) did not have any effect on RNA editing levels, no difference in both Pin1 (1.44 ± 0.2 fold-change vs cells only) and WWP2 (1.19 ± 0.2 fold-change vs cells only) expression were observed in transfected cells compared to controls (Figures 5.8c and 5.8d).

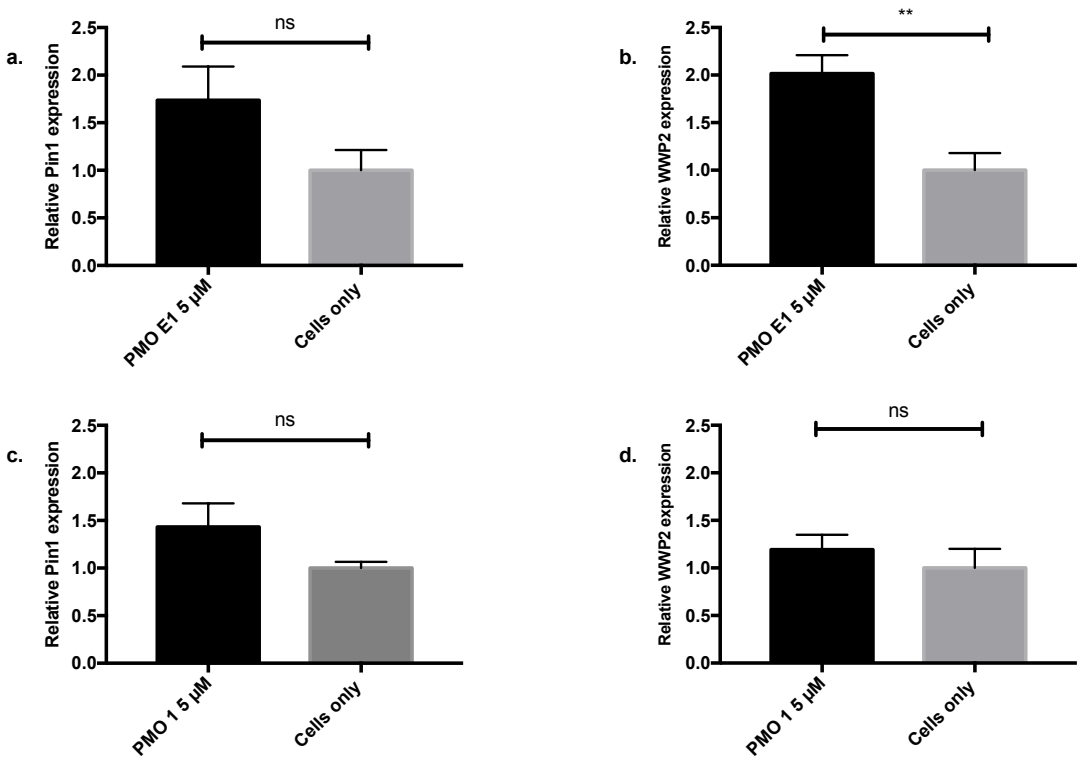

Figure 5.8 Pin1 and WWP2 expression in PMO E1- and PMO 1-transfected SH-SY5Y cells.

RT-qPCR analysis of mRNA isolated from cells transfected with 5 µM of PMO E1 and PMO 1. Bar graphs **a** and **b** show expression levels of Pin1 and WWP2 in PMO E1-transfected cells; bar graphs **c** and **d** show expression levels of Pin1 and WWP2 in PMO 1-transfected cells.

Expression of Pin1 and WWP2 was assessed using the LightCycler 480 (Roche) and reactions were performed using the LightCycler SYBR Green Mastermix (Roche). The expression levels of β-actin were used as a reference gene. The gene expression levels were defined based on the threshold cycle (Ct), and relative expression levels were calculated using the $2^{-\Delta\Delta Ct}$ method. Measurements were made from three separate transfections in triplicate.

n=4, ** = p≤0.01. Statistical comparisons were carried out using unpaired t-test. All data points correspond to mean ± SEM values.

5.2.4 OVEREXPRESSION OF ADAR2 IN SH-SY5Y CELLS

A study carried out by Hideyama and colleagues (2010) demonstrated that ADAR2-knockout mice resulted in death of motor neurons. Furthermore, ADAR2 expression was also found to be downregulated in motor neurons of ALS patients, indicating that ADAR2 downregulation is involved in the pathology of neuronal death in ALS (Takuto Hideyama et al., 2012). Hence, restoration of ADAR2 activity could be a possible therapeutic strategy for ALS, where gene delivery of ADAR2 was shown to prevent ALS phenotype progression (Yamashita et al., 2013). HeLa cells transfected with ADAR2 cDNA showed a significant increase in RNA editing levels compared to non-ADAR-transfected HeLa cells (Chaytow, 2015). Here, we have transfected SH-SY5Y cells with an ADAR2 cDNA plasmid (provided by the O'Connell lab) to identify whether RNA editing levels can be improved, and how RNA editing activity in ADAR2-transfected cells affects the expression of both Pin1 and WWP2.

5.2.4.1 EFFECT OF ADAR2 OVEREXPRESSION ON ALUJ CASSETTE INCLUSION AND RNA EDITING

The delivery of ADAR2 cDNA to motor neurons has been shown to restore its activity to a level that is sufficient for improved Q/R site editing (Yamashita et al., 2013). We then tested whether increasing ADAR2 expression in SH-SY5Y cells can increase RNA editing levels. SH-SY5Y cells were transfected with 2 µg of ADAR2 plasmid over a period of 24 hours. Overexpression of ADAR2 cDNA in SH-SY5Y cells resulted in the expression of ADAR2 without the AluJ cassette, whist control samples displayed typical AluJ cassette levels (Figure 5.9).

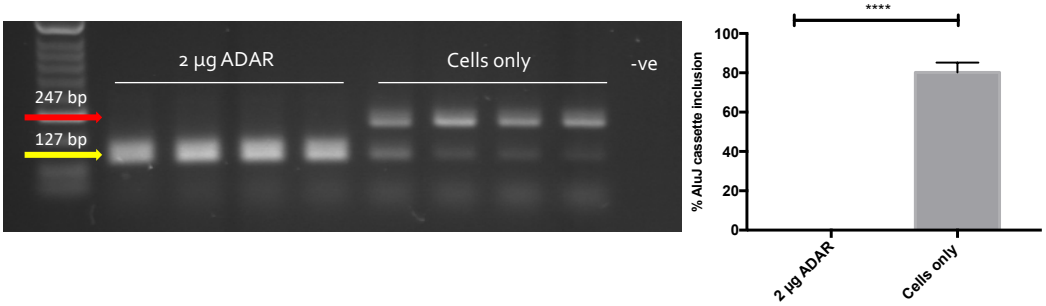

Figure 5.9 The effect of ADAR2 overexpression on AluJ insertion in SH-SY5Y cells.

Figure shows a sample gel image of RT-PCR products of SH-SY5Y cells transfected with 2 µg of ADAR2 plasmid (left) and a bar graph depicting AluJ cassette inclusion percentages in SH-SY5Y cells transfected with 2 µg of ADAR2 plasmid for 24 hours compared to non-transfected cells (right).

Gels were run in a 1.5% agarose gel in 1X TAE buffer against Hyperladder V and visualized under UV light using a GELDOC system. Images were quantified using ImageJ. "-ve" denotes negative control. Sample gel images show the intensity of exon-skipped transcripts (127 bp, yellow arrow) against exon-including transcripts (247 bp, red arrow).

n=4, **** = $p \leq 0.0001$. Statistical comparisons were carried out using unpaired t-test. All data points correspond to mean ± SEM values.

In order to examine the effects of ADAR2 overexpression on RNA editing, a *BbvI* RNA editing digest was then performed. However, no improvement in RNA editing levels were observed in ADAR2-transfected cells when compared to controls (103.2 ± 2.5% vs cells only) ($p>0.05$) (Figure 5.10).

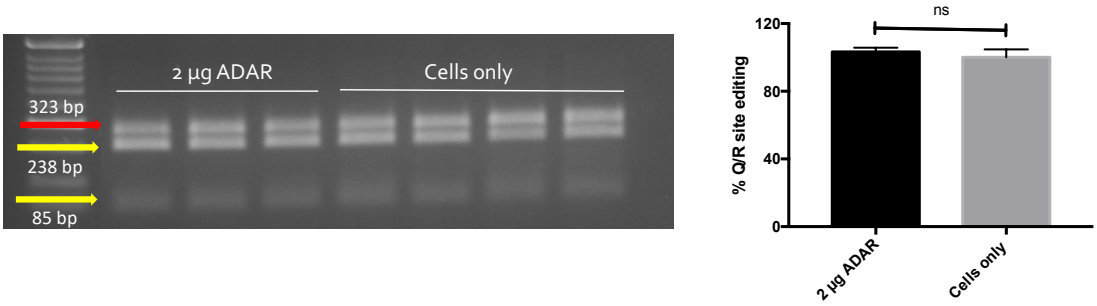

Figure 5.10 The effect of ADAR2 overexpression on RNA editing in SH-SY5Y cells.

Figure shows a sample gel image of BbvI digest products of SH-SY5Y cells transfected with 2 µg of ADAR plasmid (left) and a bar graph depicting Q/R site editing percentages in SH-SY5Y cells in SH-SY5Y cells transfected with 2 µg of ADAR2 plasmid for 24 hours compared to non-transfected cells (right).

Gels were run in a 2.5% agarose gel in 1X TAE buffer against Hyperladder V and visualized under UV light using a GELDOC system. Images were quantified using ImageJ. "-ve" denotes negative control. Sample gel images show the intensity of edited transcripts (323 bp, red arrow) against unedited transcripts (238 bp and 85 bp, yellow arrow).

n=3-4. Statistical comparisons were carried out using unpaired t-test. All data points correspond to mean ± SEM values.

5.2.4.2 EFFECT OF ADAR2 OVEREXPRESSION ON PIN1 AND WWP2 REGULATION

Next, we proceeded to examine whether there were any changes in both Pin1 and WWP2 expression in ADAR2-transfected cells when compared to controls. Since no improvement in RNA editing levels were observed in ADAR2-transfected cells, we examined whether the expression of these genes would be affected by the overexpression of ADAR2 protein. Therefore an RT-qPCR was performed to evaluate the underlying cause behind the lack in RNA editing improvement. Figure 5.11 shows the outcomes of the RT-qPCR. In SH-SY5Y cells, overexpression of ADAR2 did not result in any changes in Pin1 mRNA levels (1.09 ± 0.39 fold-change vs cells only) (Figure 5.11a). Similarly, no significant difference in WWP2 mRNA levels were observed between the two sets of conditions (0.83 ± 0.14 fold-change vs cells only) (Figure 5.11b) The results obtained indicated that Pin1 and WWP2 regulation is indeed influenced by RNA editing in cells, and not necessarily directly caused by the expression of a more catalytically active ADAR2 isoform.

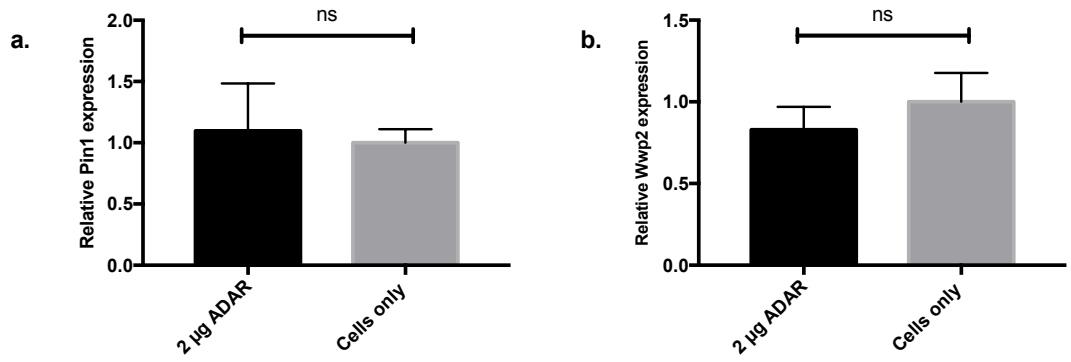

Figure 5.11 Pin1 and WWP2 expression in ADAR2-transfected SH-SY5Y cells.

RT-qPCR analysis of mRNA isolated from cells transfected with 2 µg of ADAR2 plasmid. Expression of Pin1 and WWP2 was assessed using the LightCycler 480 (Roche) and reactions were performed using the LightCycler SYBR Green Mastermix (Roche). The expression levels of β-actin were used as a reference gene. The gene expression levels were defined based on the threshold cycle (Ct), and relative expression levels were calculated using the $2^{-\Delta\Delta Ct}$ method. Measurements were made from three separate transfections in triplicate.

n=3-4. Statistical comparisons were carried out using unpaired t-test. All data points correspond to mean ± SEM values.

5.2.5 PIN1 PROTEIN EXPRESSION IN SH-SY5Y CELLS

The RT-qPCR results obtained in Sections 5.2.1 to 5.2.4 describes the regulatory expression of Pin1 mRNA in SH-SY5Y cells in PMO-transfected cells. Cells that were transfected with PMO 9 (AluJ+93+117) showed upregulation in Pin1 mRNA expression compared to non-transfected cells (Figure 5.4a), whilst PMO 10 (AluJ+96+120) did not have any effect on Pin1 mRNA expression (Figure 5.4e). Hence, we decided to determine whether any alterations of Pin1 expression at the protein level will be observed following transfection with PMO 9 (AluJ+93+117) and PMO 10 (AluJ+96+120). SH-SY5Y cells were transfected with 2 μM PMO for 48 hours, after which cells were lysed for protein extracts and western blotting. 10% pre-cast Bis-Tris SDS-PAGE gels were used for the detection of Pin1 protein in cell lysates. Blots were then incubated with 1:100 concentration of anti-Pin1 primary antibody for the detection of Pin1 signals in the cells. Primary antibody incubation was carried out overnight at 4°C.

The protein expression of Pin1 in PMO-transfected cells was then normalised to endogenous Pin1 levels of SH-SY5Y cells. Figure 5.12a depicts the resulting western blot image of cells transfected with PMO 9 (AluJ+93+117). Transfection with PMO 9 (AluJ+93+117) did not result in any significant change in mean Pin1 protein expression compared to non-transfected cells (0.75±0.08 vs cells only) (Figure 5.12b). This is in contrast with the fold-change in Pin1 mRNA levels observed in Figure 5.4a, where a significant increase in Pin1 mRNA expression was measured. The mean protein expression in PMO 10-transfected cells was then compared to non-transfected cells. The resulting western blot image of PMO 10-transfected cells is shown in Figure 5.13a. In line with results we observed in Figure 5.3e, no significant difference in Pin1 protein expression was measured amongst PMO 10-transfected and non-transfected cells (0.65±0.07 vs cells only) (Figure 5.13b).

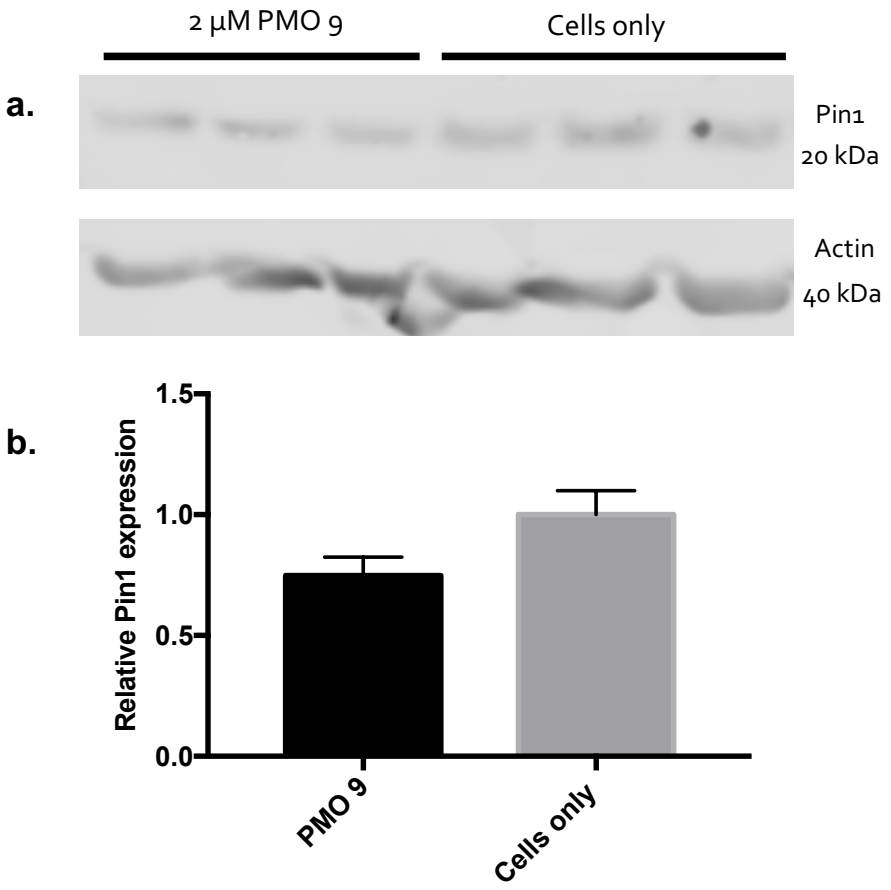

Figure 5.12 Expression of Pin1 protein in PMO 9-transfected cells.

Figure shows a) representative western blot gel image of SH-SY5Y cells transfected with 2 µM PMO 9. Actin was used as an internal loading control and to normalise expression levels of Pin1 within each lane; b) Bar graph depicting relative Pin1 protein expression levels transfected with PMO 9 compared to non-transfected cells.

Protein samples were run in a 10% pre-cast Bis-Tris acrylamide gel against BLUeye Prestained Protein Ladder and visualised with the Odyssey CLx Imaging System. Images were quantified using Image Studio 4.0.

n=3. Statistical comparisons were carried out using unpaired t-test. All data points correspond to mean ± SEM values.

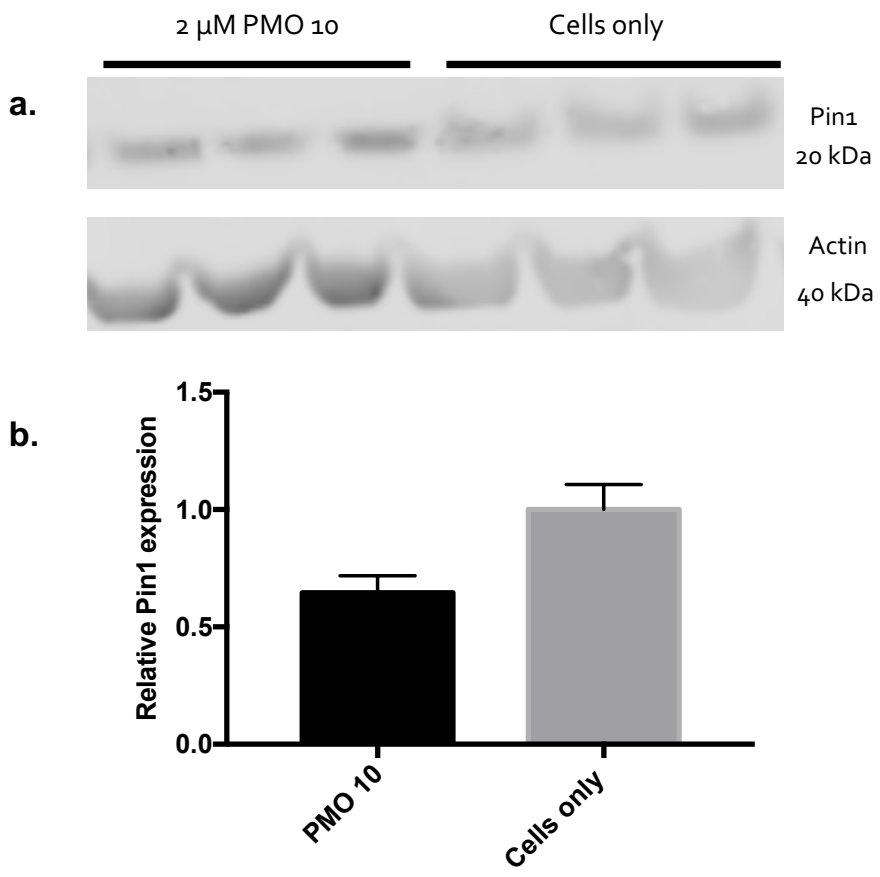

Figure 5.13 Expression of Pin1 protein in PMO 10-transfected cells.

Figure shows a) representative western blot gel image of SH-SY5Y cells transfected with 2 µM PMO 10. Actin was used as an internal loading control and to normalise expression levels of Pin1 within each lane; b) Bar graph depicting relative Pin1 protein expression levels transfected with PMO 10 compared to non-transfected cells.

Protein samples were run in a 10% pre-cast Bis-Tris acrylamide gel against BLUeye Prestained Protein Ladder and visualised with the Odyssey CLx Imaging System. Images were quantified using Image Studio 4.0.

n=3. Statistical comparisons were carried out using unpaired t-test. All data points correspond to mean ± SEM values.

5.3 DISCUSSION

5.3.1 HOW IMPROVING AND DISRUPTING Q/R SITE EDITING AFFECTS PIN1 AND WWP2 EXPRESSION

At the outset of this study, we had hypothesised that alterations in RNA editing levels induced by PMO transfection in SH-SY5Y cells could be correlated to the levels of both Pin1 and WWP2 expression. Any downstream effects on GluA2 function is therefore considered to be the consequence of this ADAR2-caused regulation of Pin1 and WWP2 (Marcucci et al., 2011). A study carried out by (Marcucci et al., 2011) has demonstrated that ADAR2 protein levels and catalytic activity are regulated correlatively by Pin1 in a positive fashion, whilst WWP2 is negatively regulated (Figure 5.14). The results of our RT-qPCRs have shown that this is indeed the case for both PMO 9- and PMO 9A-transfected cells (Figure 5.4), as the gene expression of both Pin1 and WWP2 showed regulatory alteration as a result of improved RNA editing (as discussed in Chapter 3). As expected, no change in Pin1 and WWP2 expression was observed in PMO 10-transfected cells (Figure 5.4), further confirming that an increase in ADAR2 catalytic activity (hence also RNA editing) is required to induce any regulatory expressional changes in Pin1 and WWP2.

The data presented in section 5.2.2 shows that there is significant upregulation in Pin1 levels in PMO 9 and 9A-transfected cells, which is likely as the result of increased ADAR2 catalytic activity, indirectly caused by decreased AluJ cassette inclusion levels. Conversely, WWP2 levels were significantly downregulated in these cells. Pin1 post-translationally regulates ADAR2-specific editing, and so the interaction between these two proteins is dependent on the phosphorylation of a Ser/Thr-Pro motif located in the N-terminal region of ADAR2 (Marcucci et al., 2011). It is possible that a developmentally-timed phosphorylation event stimulates an ADAR2 conformational change, which in turn prompts its stabilisation in the nucleus (Behm et al., 2017). Hence, in the case of PMO 9 and 9A-transfected cells, the high relative expression levels of Pin1 in these cells may have triggered

ADAR2 stabilisation which led to the increase in RNA editing (Figure 5.14). It is still crucial to further understand how this feedback mechanism operates – is the PMO transfection itself causing the increase in Pin1 expression, thus leading to the phosphorylation and transport of ADAR2 in the nucleus, eliciting RNA editing? Or is the increased expression of Pin1 simply due to the presence of a more catalytically active ADAR isoform? As aforementioned, WWP2 has been reported to negatively regulate ADAR2 activity and Q/R site editing. Since PMO 9 and 9A-transfected cells have shown increased RNA editing levels, the mRNA levels of WWP2 are relatively lower in these cells compared to controls (Figure 5.4). WWP2 triggers ADAR2 degradation by poly-ubiquitination (Marcucci et al., 2011). However, when WWP2 is unable to bind to ADAR2, a high level of accumulated ADAR2 in the cytoplasm is observed (Marcucci et al., 2011). The localisation of ADAR2 into the nucleus, which results in increased RNA editing (Sansam et al., 2003), is reported to be stabilised by Pin1 (Marcucci et al., 2011). Hence, it would be worth looking into the localisation of ADAR2, Pin1, and WWP2 following PMO transfection in the cells. This can further clarify how the levels and localisation of WWP2 plays a role in the translocation of ADAR2 between the cytoplasm and the nucleus.

When transfected with PMO E1 (GRIA2+279+308), a reduction in RNA editing levels was observed (Figure 5.7b), which in turn resulted in a significant increase in WWP2 mRNA expression compared to control cells (Figure 5.8b). No significant difference was seen in Pin1 mRNA levels in these cells (Figure 5.8a). Pin1 catalytic activity is essential in order to localise and stabilise ADAR2 in the nucleus. ADAR2 becomes unstable and will pool in the cytoplasm when Pin1 is absent, causing the interaction of ADAR2 with WWP2, resulting in its subsequent degradation by the proteasome (Marcucci et al., 2011). This directly results in the reduction of both Q/R site and R/G site editing in the GluA2 subunit. The results presented in Section 5.2.3.1 confirms, in part, that a regulatory feedback mechanism may exist between WWP2 expression and Q/R site editing activity. This decrease in Q/R site editing in the cells may have been due to the cytoplasmic accumulation of ADAR2 in the cells, making ADAR2 accessible for degradation by WWP2 (Figure 5.14). Cytoplasmic

mature ADAR mRNAs or miRNAs are no longer substrates for A-to-I editing, making them more susceptible to WWP2 degradation (Behm et al., 2017). Although PMO E1 (GRIA2+279+308) has been designed to sterically hinder Q/R site editing in these cells, there may be another regulatory mechanism involved in the disruption pathway that has somehow caused ADAR2 to be aggregated in the cytoplasm. Most ADAR2 substrates must be edited in their premature nuclear transcript state since the editing reaction requires the presence of intronic sequences for the formation of necessary double-stranded structures (Behm et al., 2017), which have been disrupted by the actions of PMO E1 (GRIA2+279+308). Ultimately, further experiments need to be performed to determine the localisation of WWP2 in cells after transfection with PMO E1 (GRIA2+279+308).

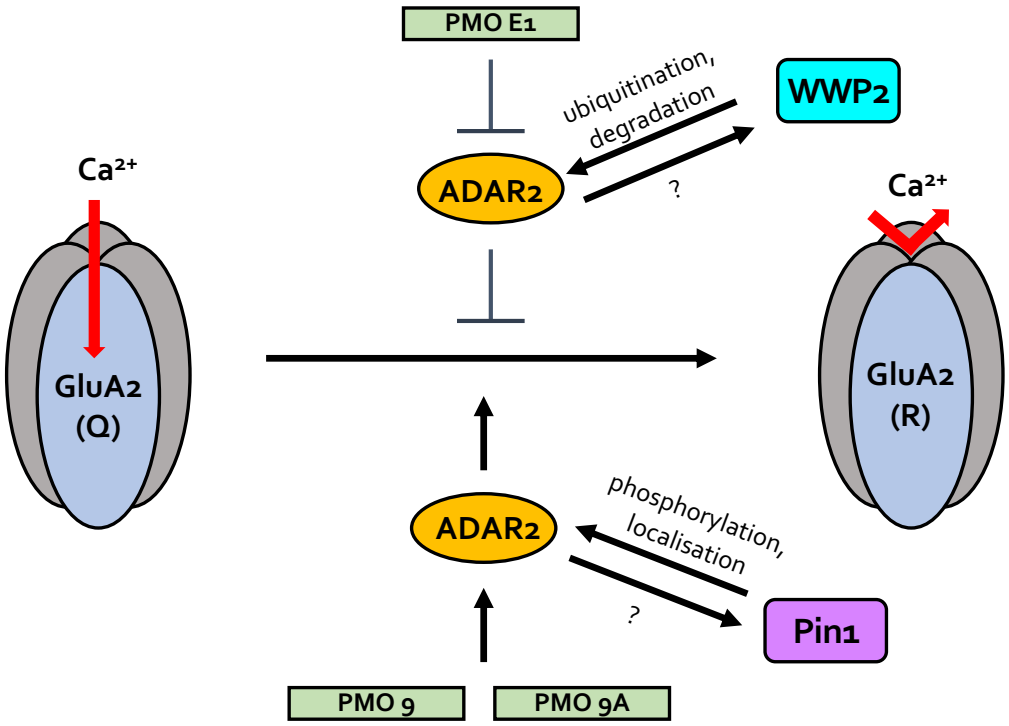

Figure 5.14 Possible regulatory mechanisms behind Pin1 and WWP2 expression following PMO transfection and altered RNA editing.

One of the positive regulators of ADAR2 localisation is importin-α4 (Behm et al., 2017). Importins are a type of karyopherin that transports protein molecules into the nucleus by binding to the nuclear localisation sequence (NLS) (Görlich, Prehn, Laskey, & Hartmann, 1994). It is also worth studying to find out whether expression of importin-α4 is affected by PMO treatment. Essentially, using PMO E1 (GRIA2+279+308) in SH-SY5Y cells is ideal for the study of downstream effects of acutely disrupting Q/R site editing, considering that there are still various factors and regulatory processes involved in the expression and function of both negative and positive regulators of ADAR2 transport, and subsequently RNA editing efficiency. Would the expression levels of WWP2, or Pin1, have any direct effects on GluA2 subunit trafficking into the synapse? This would ultimately aid in the understanding as to how and why the reduction in Q/R site editing occurs in ALS motor neurons in the first place, and possibly allow us to discover more therapeutic targets for disease treatment. Similarly, the same regulatory processes can also be studied by utilising PMOs that enhance Q/R site editing, therefore allowing insights into the downstream effects of PMO treatment for ALS.

5.3.2 EFFECT OF ADAR OVEREXPRESSION ON PIN1 AND WWP2 LEVELS

One possible strategy of gene therapy for ALS is by enhancing ADAR2 activity in mouse motor neurons by using adeno-associated virus serotype 9 (AAV9) as a vector to deliver the ADAR2 gene (Yamashita et al., 2013). The results obtained in this study demonstrated the restoration of ADAR2 activity in ADAR-deficient anterior horn cells (AHCs) of ADAR2 knockout mice (AR2) caused exogenous ADAR2 expression to a level that is satisfactory to edit Q/R sites of essentially all GluA2 mRNAs expressed in AR2 mice, which subsequently prevented progressive motor dysfunction (Yamashita et al., 2013). The motor neurons of AR2 mice were notably rescued from death through the normalisation of TDP-43 expression (Yamashita et al., 2013). Accordingly, we hypothesised that by transfecting SH-SY5Y cells with a copy of the ADAR2 cDNA, Q/R site editing in these cells will be restored and possibly increased. However, the opposite result was observed.

Although increasing ADAR2 levels in SH-SY5Y cells completely altered the detection of certain ADAR2 splice variants in the cells (Figure 5.9) (presumably due to overexpression of the ADAR2 cDNA), there was no increase observed in RNA editing levels compared to non-transfected cells (Figure 5.10). It is interesting, then, that whilst the more catalytically-active ADAR2 isoform was conferred by the transient overexpression of ADAR2, for some reason, this was translated differentially in terms of Q/R site editing levels observed in ADAR2-transfected cells.

Seeing as transfection with different PMOs resulted in altered expression levels of Pin1 and WWP2 (as discussed in Sections 5.2.2 and 5.2.3), we proceeded to examine if Pin1 and WWP2 levels were altered in ADAR2-transfected cells. RT-qPCR analysis has revealed how Pin1 and WWP2 levels show similar expressional profiles in both ADAR2-transfected and control cells. The results here somewhat corroborate the editing levels observed in Figure 5.10, which explains that the lack of improvement in Q/R site editing is consistent with the unaffected levels of both Pin1 and WWP2

mRNA. This also further supports the RT-qPCR results of PMO 10-transfected cells (Figures 5.4e and 5.4f), whereby unvarying AluJ splicing and subsequent unaltered ADAR2 catalytic activity does not have any regulatory effect on Pin1 and WWP2 levels.

ADARs deaminate adenosines mainly found in base-paired RNA. The ability of ADARs to deaminate substrates is due to the fact that the dsRNA-binding domains (dsRBDs) of ADARs essentially recognise target RNAs by shape instead of sequence (Deffit & Hundley, 2016). Initial biochemical experiments have identified that binding of ADARs to dsRNA and editing are two distinct events (Kallman, Sahlin, & Ohman, 2003). The immediate structure that surrounds the editing site is crucial, whereby a purine located opposite to the binding site has a negative effect on both editing selectivity and efficiency (Kallman et al., 2003). In the pre-mRNA of GluA2, the unique position of the second dsRBD of ADAR2 (located near two bulged bases adjacent to the R/G editing site), may contribute to the adenine selected for editing (Nishikura, 2010). This editing-site selectivity of ADAR1 and ADAR2 may be mediated by functional interactions between monomers of ADAR1 and ADAR2, since these interactions can possibly position specific adenosine residues relative to the ADAR catalytic center (Nishikura, 2010). Aside from that, studies in the neurons of developing mice have shown that although editing increases during development, the rise in Q/R site editing does not correlate with ADAR2 expression, which have been found to be constant throughout development (Wahlstedt et al., 2009). It seems that simply increasing ADAR2 expression alone cannot improve RNA editing levels. Instead, other factors, such as regulatory and competing proteins, RNA helicases, or the local RNA environment itself may be the underlying cause behind editing level regulation (Licht, Kapoor, Mayrhofer, & Jantsch, 2016).

Many genes display “isoform switching” under experimental or physiological perturbation (Trapnell et al., 2013). However, the levels of ADAR1-dependent editing and transcript expression were found to be uncorrelated (I. X. Wang et al., 2013). For instance, *IKZF3,* a transcription factor that regulates proliferation and differentiation of B lymphocytes, demonstrated increased expression levels following ADAR1 knockdown, whist

its editing levels decreased. Conversely, both the editing and expression levels of *CENPN* (a gene essential for kinetochore assembly) decreased after ADAR1 knockdown. The position and number of edited sites in the transcript did not correspond to expressional changes ensuing ADAR1 knockdown. These results indicate that ADAR proteins affect editing and gene expression independently (I. X. Wang et al., 2013).

A change in the conformation of ADAR2 may also explain the results we obtained. Pin1 functions to isomerise a specific proline from the *cis* to *trans* conformation or *vice versa* (Ranganathan et al., 1997). Nearly all biological processes necessitate proline to be in the *trans* conformation. However, when a protein undergoes translation, the choice in conformation is subject to the surrounding amino acids. Hence, if there is a pool of ADAR2 that is unphosphorylated, it will not be a Pin1 substrate, making the protein not fully active (Marcucci et al., 2011). There may be enough Pin1 present, but the kinase essential for Pin1-binding site phosphorylation is limited, hence the transfected ADAR2 here may be inactive as it still requires phosphorylation and subsequent Pin1 activity. For instance, ADAR2 is well-expressed in undifferentiated NT2 cells; but for efficient Q/R site editing to occur, NT2 cells need to undergo differentiation. This arises without any considerable alteration in ADAR2 expression, suggesting that a post-translational regulatory mechanism is involved (Lai, Chen, Lee, et al., 1997). Moreover, the ADAR2 cDNA transfected in the cells was only left incubated for 24 hours, which may not be sufficient enough time for all of the ADAR2 to be effectively phosphorylated and be transported into the nucleus, where it will become more active. It is therefore worth optimising the protocol by adjusting certain conditions, such as increasing transfection times, as well as increasing concentrations of the ADAR2 cDNA plasmid.

5.3.3 PIN1 PROTEIN EXPRESSION IN SH-SY5Y CELLS

Our RT-qPCR findings has revealed that PMO 9-transfected cells show increased levels of Pin1 mRNA expression, which is a result of improved RNA editing in these cells (Figure 5.4a). PMO 10-transfected cells did not result in any change in Pin1 expression (Figure 5.4e) as this PMO did not show any effects on excluding AluJ cassette expression in SH-SY5Y cells. The protein expression profiles of Pin1 were then studied in both PMO 9- and PMO 10-transfected cells to observe whether any changes in expression occurred. Considering that Pin1 mRNA levels improved in PMO 9-transfected cells, we expected to see an increase in Pin1 protein levels as well. However, no significant alteration in mean Pin1 protein expression was found in these cells (Figure 5.12). This is in contrast to findings presented by (Behm et al., 2017), where western blot analysis revealed that Pin1 expression increased during maturation of developing neurons (13 DIV) compared to 1-3 DIV neurons. The increased Pin1 protein expression is concurrent with the increase in RNA editing levels found in cultured primary neurons as they mature (Behm et al., 2017). Pin1 and ADAR2 localisation was detected in the nucleus of mature neurons, whereby a striking increase in the number of interactions between the two proteins was observed at 13 DIV. It was established that the nuclear import of ADAR2 is mediated by the gradual increase in importin−α4 expression during development, and ADAR2 localisation is further stabilised by increased Pin1 expression, resulting in a rise in editing levels (Behm et al., 2017).

The lack of increase in Pin1 protein expression may be due to the weak correlation between mRNA and protein expression profiles. Differential studies in mRNA expression essentially assume that mRNA expressional changes are most likely mediated by corresponding changes in protein levels (Koussounadis, Langdon, Um, Harrison, & Smith, 2015). However, genome-wide correlation between mRNA and protein expression levels are notoriously poor, accounting for roughly 40% of explanations across various studies (Vogel & Marcotte, 2012). The discrepancy is generally associated with levels of regulation between transcript and protein product (Maier, Güell, & Serrano,

2009). However, certain classes of genes have higher correlations, such as secreted proteins (only requires transcription when needed); cell cycle genes (which are time dependent; and bacterial genes optimised for quick translation (Koussounadis et al., 2015).

Whilst the nucleotide sequence of a gene determines the sequence of its mRNA product, and subsequently the sequence of an mRNA determines the amino acid sequence of the resulting polypeptide, a significant relationship takes place between the transcript concentration and the protein concentration derived from a specific locus (Yansheng Liu, Beyer, & Aebersold, 2016). Systematic studies that have quantified transcripts and proteins at genomic scales show the importance of various processes beyond transcript concentration that contribute to protein expression levels (McManus, Cheng, & Vogel, 2015). These processes include 1) rate of translation, as they are significantly influenced by the mRNA sequence ; 2) modulation of translation rates, which occurs through the protein binding to regulatory elements on the transcript, binding of non-coding RNAs, or relative transcript availability; 3) modulation of a protein's half-life; 4) protein synthesis delay; and 5) transport of proteins (Yansheng Liu et al., 2016). Hence, direct comparisons between protein and mRNA expression from the same location or the same cell type may not be applicable.

In the case of Pin1 protein expression, the lack of correlation between the mRNA levels and protein levels observed may be due to the fact that proteins have very contrasting half-lives, as a consequence of varied protein synthesis and degradation (Greenbaum, Colangelo, Williams, & Gerstein, 2003). Protein turnover can differ substantially depending on several factors; where the cell can control the degradation or synthesis rates of a given protein. Significant heterogeneity is even observed within proteins with similar functions (Greenbaum et al., 2003). Since we have transfected the cells with PMO 9 (AluJ+93+117) for only 48 hours before protein isolation, the incubation time may have not been long enough for Pin1 to be translated into protein, resulting in no significant difference in Pin1 protein expression in PMO 9-transfected cells compared to non-transfected cells. However, we have observed that incubation of cells for 72 hours has resulted in significant cell

death, which is likely caused by cell over-confluency and prolonged exposure to EndoPorter. Therefore, optimisation of a protocol for Pin1 protein detection is worth performing in order to measure any changes in protein expression levels in cells following PMO 9 (AluJ+93+117) transfection.

CHAPTER 6 THE EFFECTS OF ANTISENSE OLIGONUCLEOTIDES IN DIFFERENTIATED SH-SY5Y CELLS

6.1 INTRODUCTION

The subjects of neurobiology and neuroscience have been vastly improved due to the use of *in vitro* model systems. Cultured cells allow researchers to characterise protein function and the molecular mechanisms behind certain biological occurrences, which in turn aids in the understanding of disease and infection pathology and carry out preliminary drug testing (Shipley, Mangold, & Szpara, 2016). *In vitro* cell culture models are often used for the study of neurotoxin properties and the development of novel therapeutic compounds for disease management, where the neuroblastoma SH-SY5Y cell line has frequently been utilised to study the pathogenesis of neurodegeneration and drug screening (Cheung et al., 2009). This is due to the ability of the cells to mimic both morphological and biochemical characteristics of primary neurons (Shastry, Basu, & Rajadhyaksha, 2001).

Although proliferative SH-SY5Y cells are extensively used as a model for neurodegenerative diseases, these cells are usually locked in an early neuronal differentiation stage, as they lack many neuron-defining features, such as neuronal morphology, inhibited cell division, and expression of neuronal markers (Agholme, Lindström, Kgedal, Marcusson, & Hallbeck, 2010). As a result, proliferative SH-SY5Y cells do not represent a wholly suitable model for studying molecular and cellular mechanisms of neurodegenerative diseases (Lopes et al., 2010). While primary neurons are a more apt cell model for neurological disease study, its use for general screening is limited as it contains mixed cell populations (Shastry et al., 2001). Furthermore, they are notoriously difficult to transfect and standard transfection techniques are not suitable for neuronal work, hence requiring the

testing and optimisation of other methods, such as calcium-phosphate transfection or electroporation (Karra & Dahm, 2010).

The differentiation of SH-SY5Y cells into a more mature, neuron-like phenotype has added numerous benefits in neuroscience research. Cell differentiation allows the capacity for extensive expansion of cells before differentiation, with relative easiness and lower cost compared to culturing primary neurons (Kovalevich & Langford, 2013). Undifferentiated SH-SY5Y cells rapidly proliferate and appear to be non-polarised with very few and short neurites, growing in clumps (Shipley et al., 2016). When differentiated, these cells decrease in proliferation, extend long and branched neurites, and polarise in some cases (Kovalevich & Langford, 2013). The removal of the neurotrophin brain-derived neurotrophic factor (BDNF) results in cellular apoptosis, suggesting that the survival of differentiated SH-SY5Y cells depends on trophic factors, akin to mature neurons (Encinas et al., 2000). Depending on media conditions, SH-SY5Y cells can be differentiated into different adult neuronal phenotypes, such as cholinergic, adrenergic, or dopaminergic neurons (Xie, Hu, & Li, 2010), making these cells practical for a multitude of neurobiological experiments. Additionally, the cell cycle in undifferentiated SH-SY5Y cells and other frequently used cell lines can radically fluctuate. Hence, cell differentiation can synchronise the cell cycle to generate a homogenous neuronal cell population (Encinas et al., 2000).

Numerous publications have demonstrated that SH-SY5Y cells are able to attain neuron-like phenotype with neurite outgrowth and branching when treated with all-*trans*-retinoic acid (RA) (Lopes et al., 2010). Retinoic acid is a derivative of vitamin A, which has been identified to contain potent growth-inhibiting and cellular differentiating-promoting features (Kovalevich & Langford, 2013). RA is vital in embryonic development and growth and differentiation maintenance of epithelial, fibroblastic, and myelomonocytic cells (Lopes et al., 2010). RA governs cellular differentiation processes through alteration of expression of several RA-responsive genes by activating retinoic acid/retinoic nuclear receptors (RARs and RXRs) (Lopes et al., 2010). The transition from proliferating precursor cell to post-mitotic differentiated cell is regulated by RA *in vitro*, where it was also shown to downregulate mRNA of

various differentiation-inhibiting transcription factors (López-Carballo, Moreno, Masiá, Pérez, & Barettino, 2002).

As we have previously studied and quantified the effects of PMOs in undifferentiated cells, we next proceeded to characterise the effects of the same PMOs in differentiated SH-SY5Y cells. Since differentiated cells possess more neuronal-like characteristics, these cells have a more appropriate neuronal environment which is suitable to study the effects of PMOs on both splicing manipulation and henceforth RNA editing. In this chapter, we show that we have successfully differentiated the SH-SY5Y cell line through treatment with RA. The cells were then successfully transfected with PMOs 9 and 9A, since these two PMOs were demonstrated to have a positive effect on both exon skipping and RNA editing. Next, the expression levels of Pin1 and WWP2 were quantified to determine whether any change in RNA editing plays a role in their regulatory expression.

6.2 RESULTS

6.2.1 OPTIMISATION OF A DIFFERENTIATION PROTOCOL

Our first step was to ensure that the SH-SY5Y cell line could be successfully differentiated following treatment with RA. Differentiated cells are expected to show decreased proliferation and show long, neurite-like projections (Kovalevich & Langford, 2013). Any changes in morphology were confirmed through microscopic visualisation. Cells were seeded at a concentration of 60,000 cells per well in a 6-well plate and were left to grow in differentiation media, which contained reduced serum (1% FBS) and 1 μM RA. Media was changed every two days and cells were visualised under a light microscope at the same time points.

In order to determine the optimum conditions for successful cell differentiation, SH-SY5Y cells were all subjected to different conditions as follows:

i) Cells grown in plates coated with 0.5 μg/mL poly-D-lysine (PDL) and differentiation media;
ii) Cells grown in plates coated with 0.5 μg/mL PDL which were left to grow in proliferation media for 24 hours before being replaced with differentiation media;
iii) Cells grown in non-coated plates in differentiation media.

The different conditions were tested as previous work carried out on differentiating SH-SY5Y cells have shown that different plate coatings can influence the morphological and biochemical characteristics of differentiated SH-SY5Y cells (Pedrioli, 2015). The neurite length of the cells day 5 post-plating were measured and compared between each condition. RNA was then extracted from the cells and used for cDNA synthesis, followed by exon skipping and RNA editing PCRs to measure endogenous exon skipping and RNA editing levels in differentiated cells.

The microscope images shown in Figure 6.1 revealed that cells cultured in PDL with differentiation media, PDL with proliferation media replaced with

differentiation media, and non-coated plates showed variation in neurite projection length at Day 5. Neurite-like projections were more apparent in cells cultured in PDL with proliferation media replaced with differentiation media (Figure 6.1b) compared to cells cultured in other conditions (Figures 6.1a and 6.1c). Cells cultured in PDL with proliferation replaced with differentiation media resulted in mean neurite lengths of 105.9 ± 5.7 μm, whilst the mean neurite lengths of cells cultured in PDL with differentiation media were 59.0 ± 2.8 μm. (Figure 6.2) Cells cultured in non-coated plates demonstrated the shortest mean neurite lengths (44.1 ± 2.1 μm) (Figure 6.2).

Conditions	Day 1	Day 5
a) PDL + differentiation media	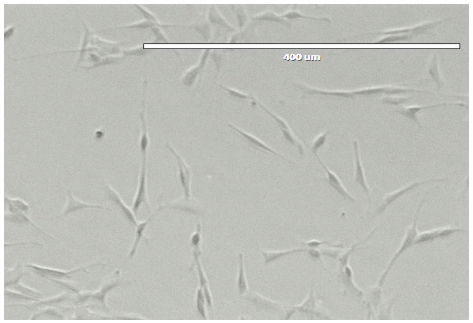	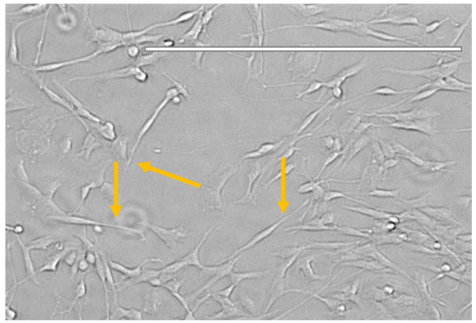
b) PDL + differentiation media + proliferation media	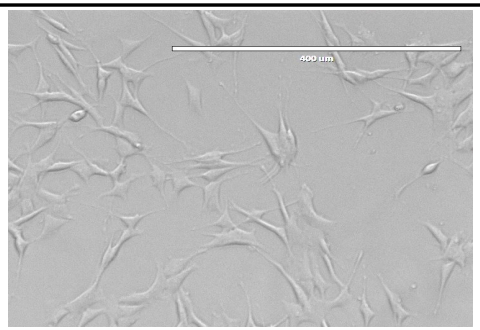	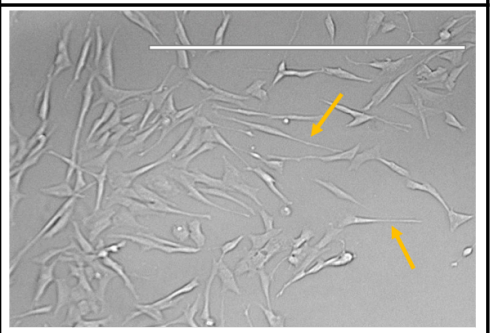
c) Differentiation media only	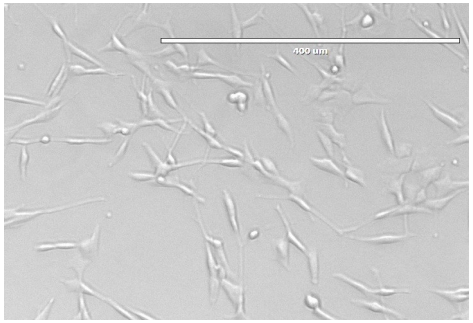	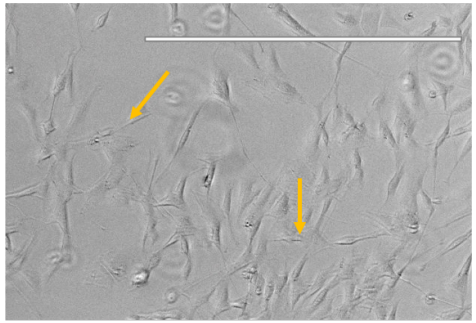

Figure 6.1 Effect of differentiation conditions on SH-SY5Y cell morphology.

Figure shows microscope images of SH-SY5Y cells in varying differentiation conditions at Day 1 and Day 5 Neurite projections are indicated by orange arrows. Scale bars represent 400 µm.

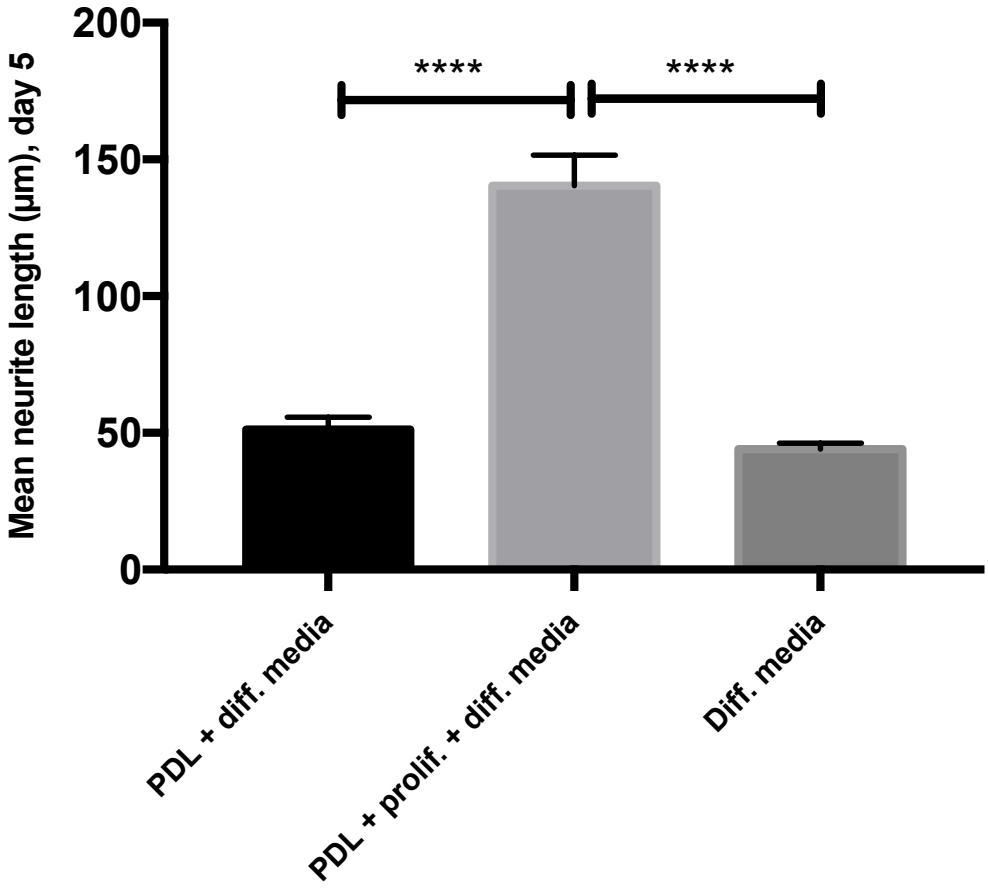

Figure 6.2 Mean neurite lengths of SH-SY5Y cells in differentiation conditions.

Bar graph shows the mean lengths of neurite projections from SH-SY5Y cells in differentiation conditions at Day 5.

Neurite lengths were quantified using NeuronJ. For each condition, the neurite lengths of n>6 cells were measured.

**** = p≤0.0001. Statistical comparisons were carried out using one-way ANOVA. All data points correspond to mean ± SEM values.

Following morphological analysis, we proceeded to compare and analyse any difference in both AluJ cassette inclusion and RNA editing levels among the three different conditions. Figure 6.2 shows the results obtained from the two PCR assays carried out. AluJ cassette inclusion levels remain similar between the three different conditions (Figure 6.2a), ranging between 76.4 ± 3.3% to 89.9 ± 2.3%. The AluJ cassette inclusion levels measured in differentiated cells were similar to the levels observed in proliferating cells (70.9 ± 2.4%) (Figure 6.3b). Interestingly, although the levels of AluJ cassette inclusion were similar between these samples, a variation in RNA editing levels were observed (Figure 6.4b). Cells cultured in PDL with differentiation media showed RNA editing levels of 43.8 ± 5.7%. Cells cultured in PDL with proliferation media and replaced with differentiation media displayed significantly higher RNA editing levels (93.9 ± 6%), while cells cultured in non-coated plates have shown RNA editing levels of 75.5 ± 12.3%. Differentiated cells cultured in PDL with proliferation media replaced with differentiation media as well as cells cultured in differentiation media both show a significant increase in RNA editing levels compared to proliferating cells (38.9 ± 1.9%) (Figure 6.4b). The high editing levels (at nearly 100%) observed in cells cultured in PDL with proliferation media replaced with differentiation media is noteworthy as these levels are reflective of a neuronal phenotype, as editing at the Q/R site in neurons virtually occur at 100% efficiency throughout life (Sasaki, Yamashita, Hideyama, & Kwak, 2014). Since cells cultured in PDL with proliferation media replaced with differentiation media demonstrated the most neuronal-like phenotype (longest neurite projections and highest RNA editing levels), we proceeded to use these conditions in subsequent differentiation experiments.

a.

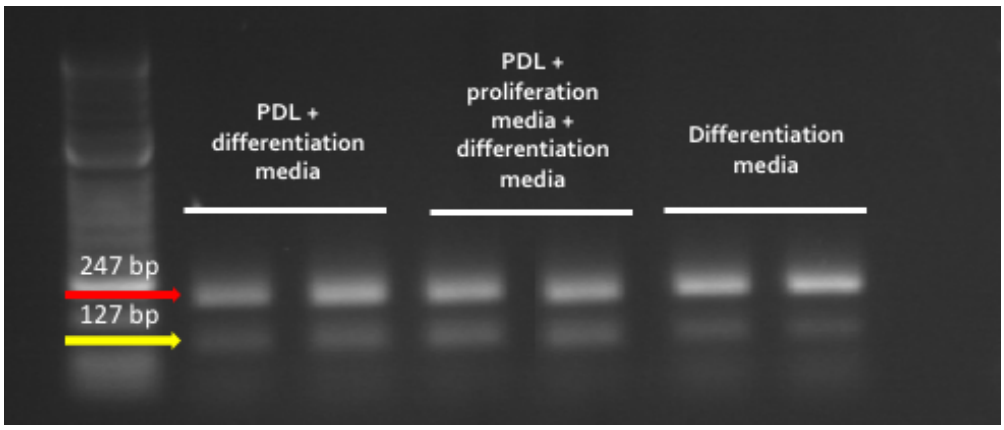

b.

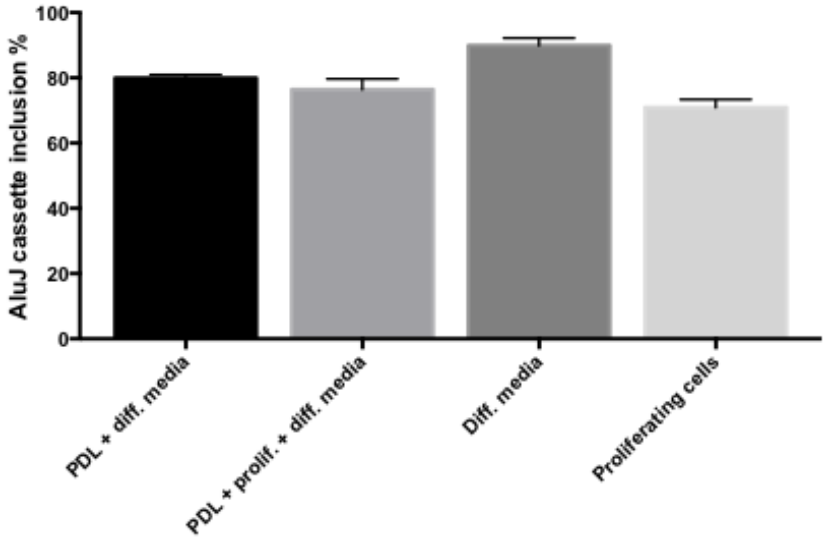

Figure 6.3 Effect of differentiation conditions on AluJ insertion in SH-SY5Y cells.

Figure shows a sample gel image of a) RT-PCR products from SH-SY5Y cells under varying differentiation conditions and b) a bar graph depicting AluJ cassette inclusion levels after differentiation.

Gels were run in a 1.5% agarose gel in 1X TAE buffer against Hyperladder V and visualized under UV light using a GELDOC system. Images were quantified using ImageJ. Sample gel image shows the intensity of exon-skipped transcripts (127 bp, yellow arrow) against exon-including transcripts (247 bp, red arrow).

n=3.. Statistical comparisons were carried out using one-way ANOVA. All data points correspond to mean ± SEM values.

a.

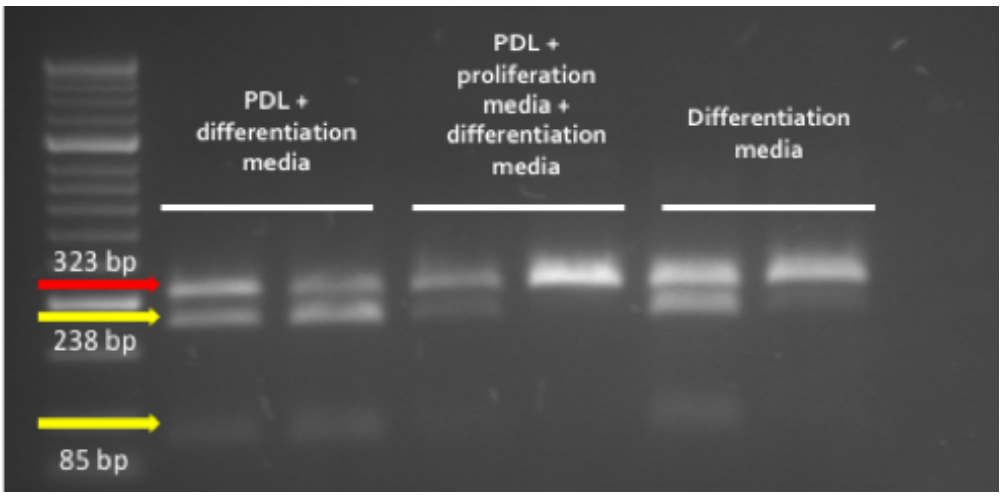

b.

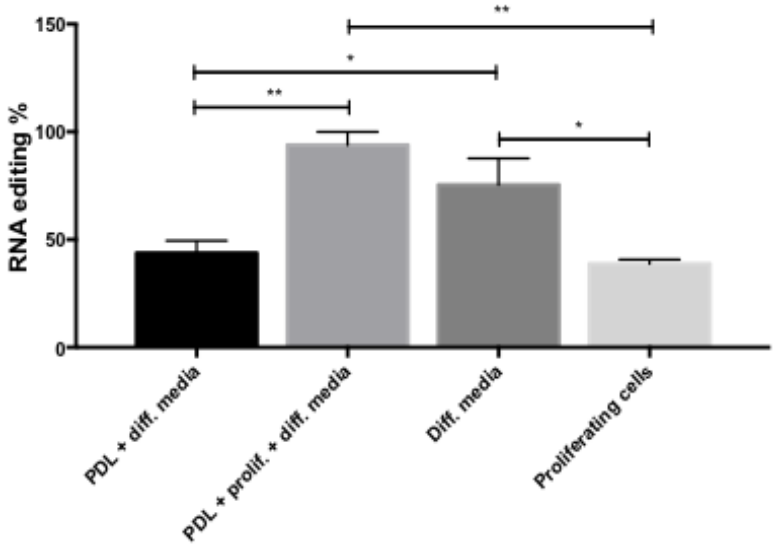

Figure 6.4 Effect of differentiation conditions on RNA editing in SH-SY5Y cells.

Figure shows a sample gel image of a) BbvI digest products of differentiated SH-SY5Y cells in varying conditions and b) a bar graph depicting Q/R site editing percentages after differentiation.

Gels in were run in a 2.5% agarose gel in 1X TAE buffer against Hyperladder V and visualized under UV light using a GELDOC system. Images were quantified using ImageJ. Sample gel image shows the intensity of edited transcripts (323 bp, red arrow) against unedited transcripts (238 bp and 85 bp, yellow arrow).

n=3, * = p≤0.05, ** = ≤0.01. Statistical comparisons were carried out using one-way ANOVA. All data points correspond to mean ± SEM values.

Once we determined the optimum conditions for cell differentiation, we then assessed morphological changes between RA-treated cells and non-RA-treated cells, which act as undifferentiated controls. In the undifferentiated state, SH-SY5Y cells are morphologically characterised by neuroblast-like, non-polarised cell bodies with few, truncated projections (Kovalevich & Langford, 2013). Both RA-treated and non-RA-treated cells were seeded on PDL-coated plates at 60,000 cells per well. 350 µL of differentiation media was replaced at 2 day intervals for 7 days and morphological changes were visualised under a microscope. The neurite lengths of differentiated cells were compared to those measured in undifferentiated cells. Figure 6.5 shows the morphology of both differentiated and undifferentiated cells over the course of 7 days. Identical cell morphology was observed in both cell populations at Day 1 of differentiation, and the neurite projections were measured to be at similar lengths (Figure 6.6). By Day 3, a more distinct difference in morphology was observed in differentiated cells, reflected by the significant increase in neurite length compared to undifferentiated cells (Figure 6.6). Undifferentiated cells were also observed to possess a more rounded cell body compared to differentiated cells (Figure 6.5). Differentiated cells continued to develop a more neuron-like phenotype, and the neurite projections continued to increase in length up to Day 7 (Figures 6.5 and 6.6). The mean neurite lengths of differentiated cells at Day 7 were measured to be at 198.9 ± 17 µM, whilst the mean neurite lengths of undifferentiated cells were significantly lower (93.2 ± 4.4 µM) (Figure 6.6). Differentiated cells also proliferated at a much lower rate compared to undifferentiated cells (Figure 6.5). Control cells did not show any significant increase in mean neurite length from Day 1 to Day 7 (Figure 6.6) and continued to proliferate up to Day 7 (Figure 6.5). The bar graph in Figure 6.4 shows how the mean length of neurite projections of differentiated cells are significantly higher compared to undifferentiated cells.

Conditions	PDL and retinoic acid	PDL only
Day 1	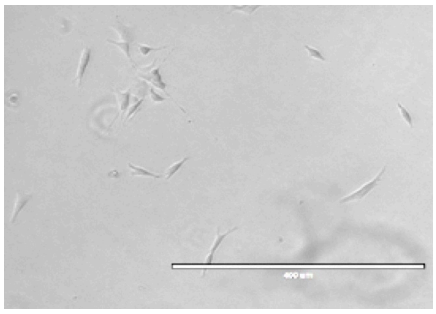	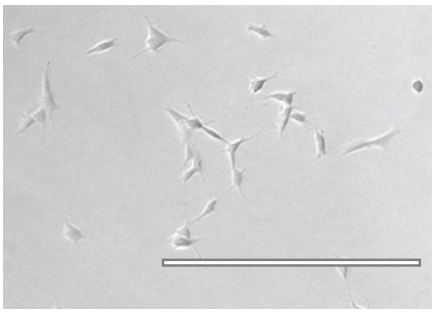
Day 3	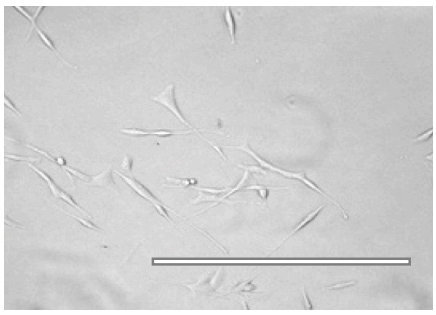	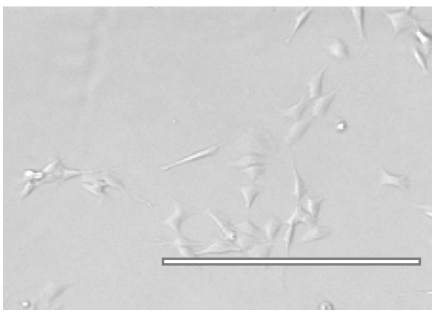
Day 5	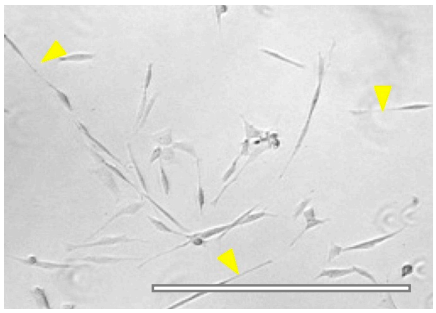	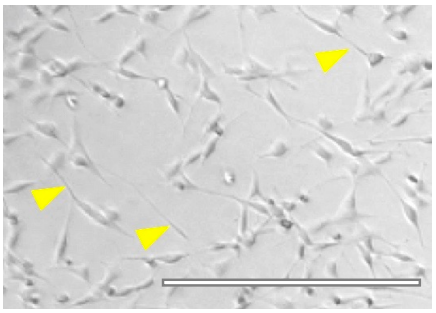
Day 7	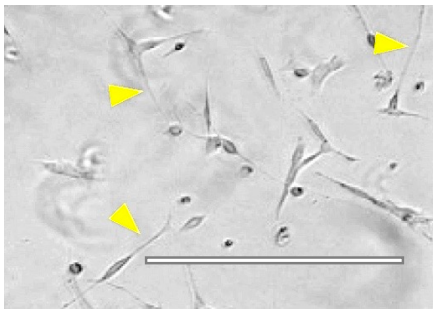	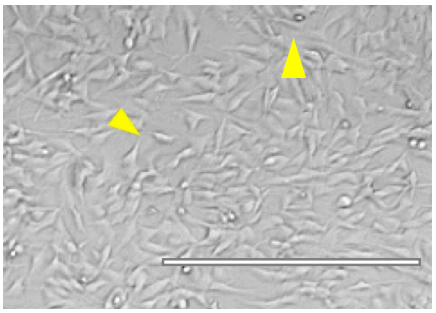

Figure 6.5 Comparison of cell morphology between differentiated and undifferentiated SH-SY5Y cells.

Figure shows microscope images of SH-SY5Y cells cultured in RA-treated media (left panel) and non-RA-treated media (right panel) for 7 days. Neurite projections are indicated by yellow arrows. Scale bars represent 400 µm.

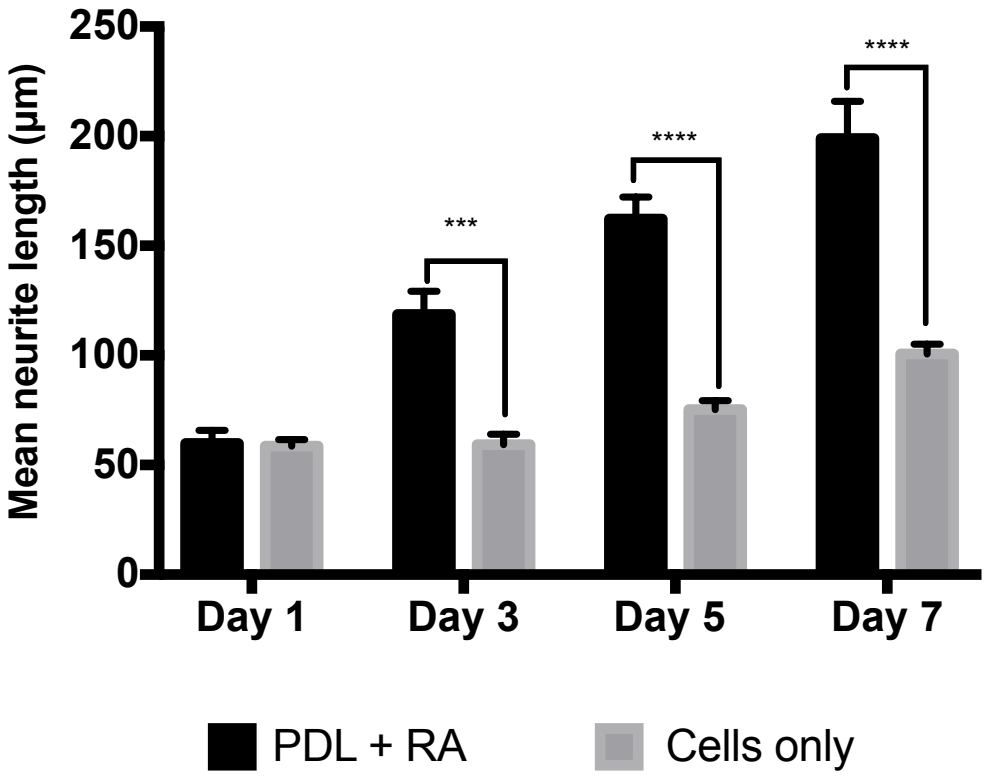

Figure 6.6 Comparison of mean neurite lengths between differentiated and undifferentiated SH-SY5Y cells.

Figure shows the mean lengths of neurite projections from SH-SY5Y cultured in RA-treated media (black bars) and non-RA-treated media (grey bars) for 7 days.

RA; retinoic acid. Neurite lengths were quantified using NeuronJ. For each condition, the neurite lengths of n>6 cells were measured. *** = p≤0.001, **** = p≤0.0001 . Statistical comparisons were carried out using student's paired t-test. All data points correspond to mean ± SEM values.

6.2.2 EFFECTS OF PMO 9 AND PMO 9A ON ALUJ CASSETTE INCLUSION AND RNA EDITING IN DIFFERNTIATED CELLS

SH-SY5Y cells were cultured according to the conditions described in the previous section. 5 μM of PMOs 9 (AluJ+93+117) and 9A (AluJ+94+118) were used to transfect these cells and their effects were compared to two different control conditions: differentiated cells (cultured in RA-treated media) and undifferentiated cells (cultured in proliferation media). Cells were transfected at Day 6 of differentiation. RNA was when harvested at Day 7 of differentiation and exon skipping and RNA editing PCR assays were performed. Figure 6.7 shows the difference in AluJ cassette insertion between transfected and non-transfected cells. Both RA-treated and undifferentiated cells showed similar AluJ cassette inclusion levels (84.24 ± 0.5% and 77.78 ± 1.6%, respectively). Transfection with both PMO 9 (AluJ+93+117) and 9A (AluJ+94+118) resulted in significant reduction of AluJ cassette inclusion when compared to both controls. PMO 9 (AluJ+93+117) lowered AluJ cassette inclusion levels to 32.93 ± 4.8%, while AluJ cassette inclusion was reduced to 37.1 ± 1.2% in PMO 9A-transfected cells.

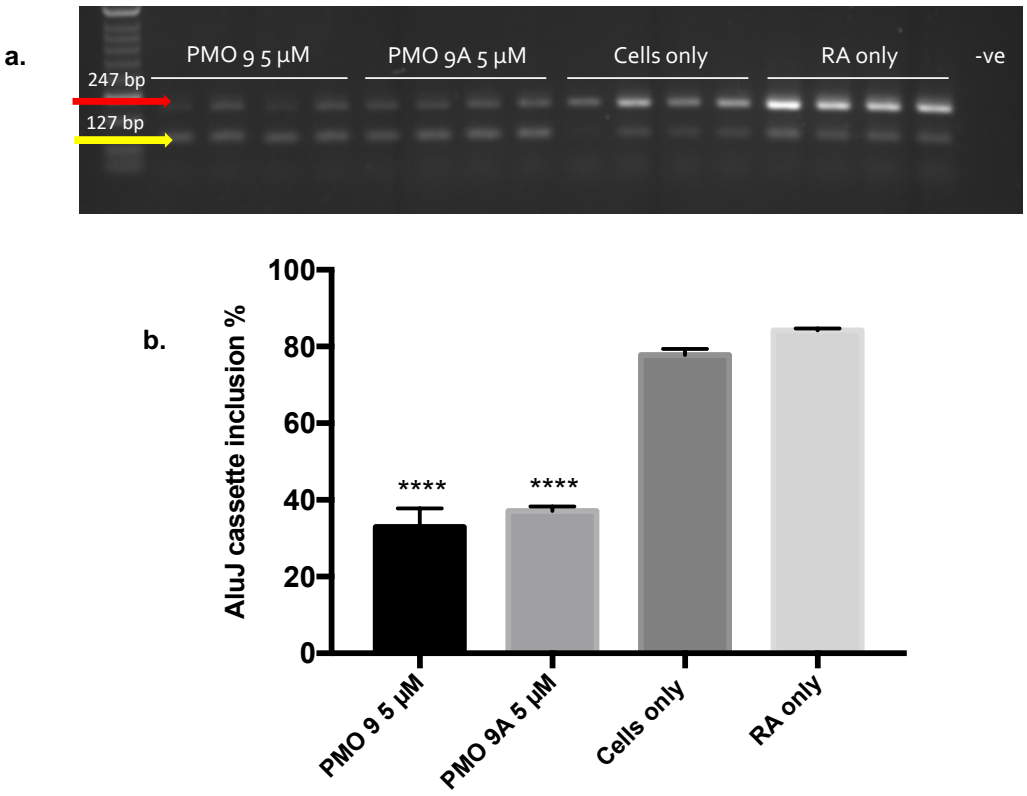

Figure 6.7 The effect of PMO 9 and PMO 9A on AuJ insertion in differentiated SH-SY5Y cells.

Figure shows a) a representative gel image of RT-PCR products of differentiated SH-SY5Y cells treated with 5 µM PMO 9 and PMO 9A and b) bar graph depicting AluJ cassette inclusion percentages in differentiated SH-SY5Y cells treated with 5 µM PMO 9 and PMO 9A for 24 hours compared to RA-treated cells and undifferentiated cells.

Gels were run in a 1.5% agarose gel in 1X TAE buffer against Hyperladder V and visualized under UV light using a GELDOC system. Images were quantified using ImageJ. "-ve" denotes negative control. Sample gel images show the intensity of exon-skipped transcripts (127 bp, yellow arrow) against exon-including transcripts (247 bp, red arrow).

RA, retinoic acid. n=3-4, **** = p≤0.0001. Statistical comparisons were carried out using one-way ANOVA. All data points correspond to mean ± SEM values.

A *BbvI* RNA editing assay was then carried out to assess the RNA editing levels in the cells. The RNA editing percentages calculated in differentiated cells (both transfected with PMOs and non-transfected cells) were normalised to the levels measured in undifferentiated cells. Figure 6.8 shows the RNA editing levels of these cells. PMO 9-transfected cells improved RNA editing levels up to 151.3 ± 6.1%, whilst transfection with PMO 9A (AluJ+94+118) increased RNA editing up to 133.2 ± 10.9%, which was expected as low AluJ cassette inclusion was observed (Figure 6.5). RA-treated cells also showed higher levels of RNA editing (162.6 ± 10.9%), reflective of the results previously described in Section 6.2.1 (Figure 6.4b). All three conditions displayed a significant increase in RNA editing compared to undifferentiated cells (Figure 6.8b). However, since RA-treated cells displayed high baseline levels of RNA editing, statistical analysis revealed no significant difference in editing levels between PMO-transfected cells and RA-treated cells ($p>0.05$) (Figure 6.8b).

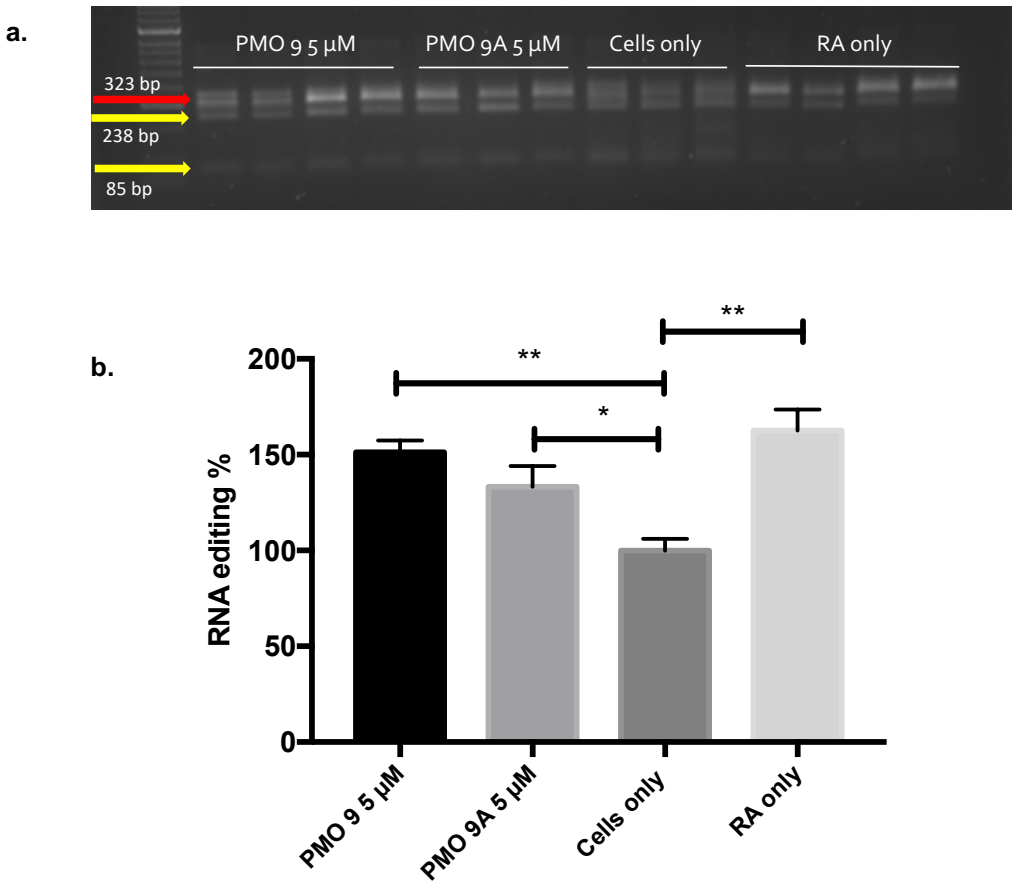

Figure 6.8 The effect of PMO 9 and PMO 9A on RNA editing in differentiated SH-SY5Y cells.

Figure shows a) a representative gel image of RT-PCR products of differentiated SH-SY5Y cells treated with 5 µM PMO 9 and PMO 9A and b*)* bar graph depicting RNA editing percentages in differentiated SH-SY5Y cells treated with 5 µM PMO 9 and PMO 9A for 24 hours compared to RA-treated cells and undifferentiated cells.

Gels were run in a 2.5% agarose gel in 1X TAE buffer against Hyperladder V and visualized under UV light using a GELDOC system. Images were quantified using ImageJ. Sample gel images show the intensity of edited transcripts (323 bp, red arrow) against unedited transcripts (238 bp and 85 bp, yellow arrow).

RA; retinoic acid. n=3-4, * = p≤0.05, ** = p≤0.01. Statistical comparisons were carried out using one-way ANOVA. All data points correspond to mean ± SEM values.

6.2.3 PIN1 AND WWP2 EXPRESSION IN DIFFERENTIATED SH-SY5Y CELLS

Once the effects of PMOs on AluJ inclusion and RNA editing in differentiated cells were assessed, the mRNA levels of Pin1 and WWP2 were then evaluated in PMO 9- and PMO 9A-transfected cells. In addition to examining the regulation of Pin1 and WWP2 in PMO-transfected cells, we also sought to study the regulatory levels of Pin1 and WWP2 in differentiated SH-SY5Y cells. The relative expression levels of both Pin1 and WWP2 were normalised to levels measured in undifferentiated cells, with β-actin used as a housekeeping reference gene. As the increase in RNA editing resulting from PMO treatment have consistently resulted in upregulation or downregulation of Pin1 and WWP2, respectively (previously discussed in Chapter 5), the same outcomes were expected in differentiated cells, which can be seen in Figure 6.9.

Transfection of differentiated SH-SY5Y cells with 5 μM PMO 9 (AluJ+93+117) increased the level of Pin 1 mRNA (6.98 ± 0.8 fold-change vs cells only) (Figure 6.9a) while the mRNA levels of WWP2 were reduced (0.34 ± 0.05 fold-change vs cells only) (Figure 6.9b). The levels of Pin1 mRNA measured in PMO 9-transfected cells compared to RA-only treated cells did result in any significant change in expression ($p>0.05$) (Figure 6.9a). The same outcome was also observed in WWP2 mRNA levels of PMO 9-transfected and RA-treated cells ($p>0.04$) (Figure 6.9b). PMO 9A-transfected cells also displayed comparable patterns in both Pin1 and WWP2 expression levels to PMO 9-transfected cells, where Pin1 expression increased (9.24 ± 2.4 fold-change vs cells only) (Figure 6.9c), and a downregulation in WWP2 levels was detected (0.23 ± 0.02 fold-change vs cells only) (Figure 6.9d). No significant difference in both Pin1 and WWP2 mRNA levels were calculated between PMO 9A (AluJ+94+118) and RA-treated cells (Figures 6.9c and d).

Overall, differentiated SH-SY5Y cells (cultured in RA-treated media) also displayed the same patterns of Pin1 and WWP2 expression as PMO-transfected cells. Pin1 mRNA expression was upregulated (6.66 ± 1.2 fold-change vs cells only) (Figure 6.9a and c), whilst a reduction in WWP2 levels was observed (0.18 ± 0.02 fold-change vs cells only) (Figure 6.9b and d). The results procured here reflect the outcomes of previous findings – the regulation of Pin1 and WWP2 in undifferentiated cells, where similar mRNA expression levels were observed (reviewed in Chapter 5), and increased Pin1 and decreased WWP2 expression are consistent with the increased RNA editing levels observed in PMO-transfected and RA-treated cells (Figure 6.9).

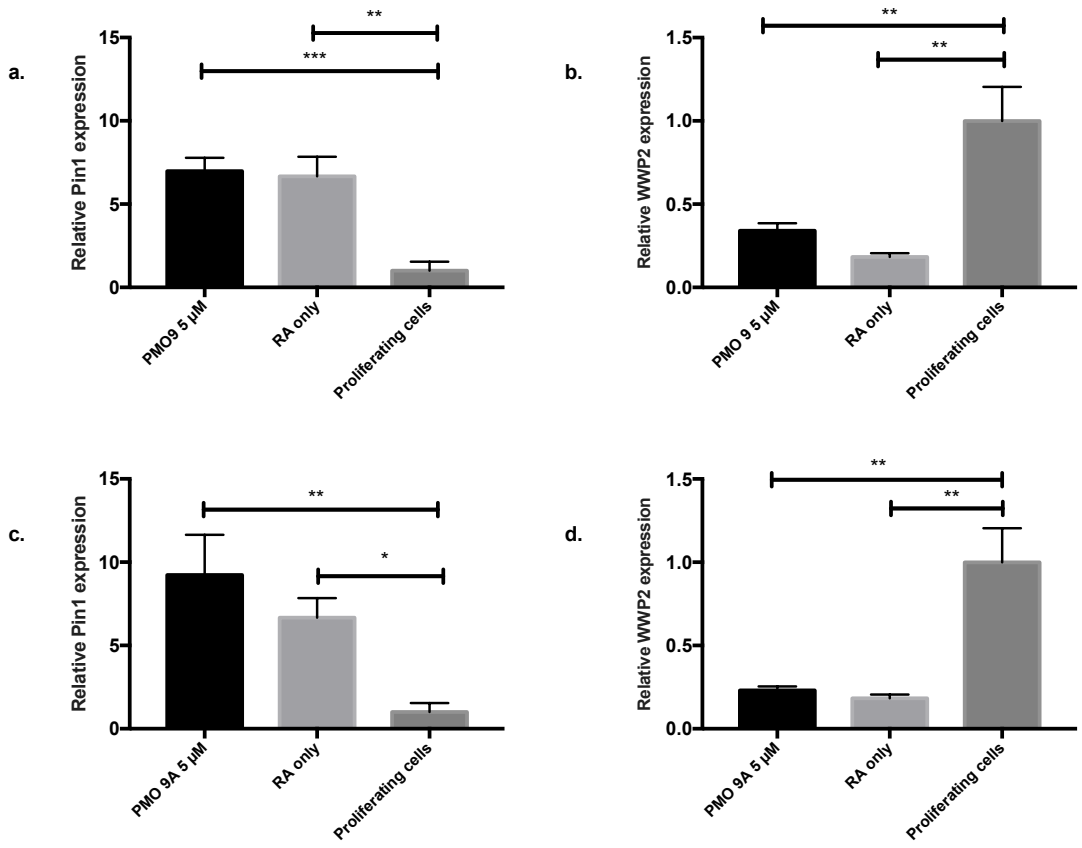

Figure 6.9 Pin1 and WWP2 mRNA expression in differentiated SH-SY5Y cells.

qRT-PCR analysis of mRNA isolated from differentiated SH-SY5Y cells transfected with 5 µM of PMOs 9 and 9A. Bar graphs **a** and **b** show expression levels of Pin1 and WWP2 in PMO 9-transfected cells; and bar graphs **c** and **d** show expression levels of Pin1 and WWP2 in PMO 9A-transfected cells.

Expression of Pin1 and WWP2 was assessed using the LightCycler 480 (Roche) and reactions were performed using the LightCycler SYBR Green I Mastermix (Roche). The expression levels of β-actin were used as a reference gene. The gene expression levels were defined based on the threshold cycle (Ct), and relative expression levels were calculated using the $2^{-\Delta\Delta Ct}$ method. Measurements were made from three separate transfections in triplicate.

RA; retinoic acid. n=4, * = p≤0.05, ** = p≤0.01, *** = p≤0.001. Statistical comparisons were carried out using one-way ANOVA. All data points correspond to mean ± SEM values.

Additionally, we also compared the effects of both PMO 9 (AluJ+93+117) and PMO 9A (AluJ+94+118) on the mRNA expression of Pin1 and WWP2 in both proliferating and differentiated cells. In Chapter 5, we transfected proliferating SH-SY5Y cells with 5 μM of PMOs 9 and 9A and found increased levels in Pin1 mRNA expression (Figures 5.3a and c) whilst WWP2 expression were reduced (Figures 5.3b and d). The fold-change values of the genes compared to non-transfected proliferating cells are listed in Table 6.1. In the case of both proliferating and differentiated cells, transfection with PMO 9 (AluJ+93+117) has resulted in upregulation of Pin1 expression (Figure 6.8a). Furthermore, Pin1 expression is significantly higher in PMO 9-transfected proliferating cells compared to PMO 9-transfected differentiating cells (Figure 6.10a). WWP2 mRNA levels also showed significant reduction in expression in both proliferating and differentiated cells compared with non-transfected proliferating cells (Figure 6.10b). Both proliferating and differentiated cells transfected with PMO 9A (AluJ+94+118) showed significant increase in Pin1 expression compared to non-transfected proliferating cells (Figure 6.10c). Consistent with results seen in PMO 9-transfected cells, significant downregulation of WWP2 mRNA levels were observed in PMO 9A-transfected cells (Figure 6.10d). Contrary to the results observed in Pin1 mRNA levels of PMO 9-transfected cells, statistical analysis did not show any significant difference in WWP2 mRNA levels between proliferating and differentiated cells transfected with PMO9 and either Pin1 and WWP2 mRNA levels between proliferating and differentiated cells transfected with PMO9A ($p>0.05$) (Figures 6.10b, c, and d).

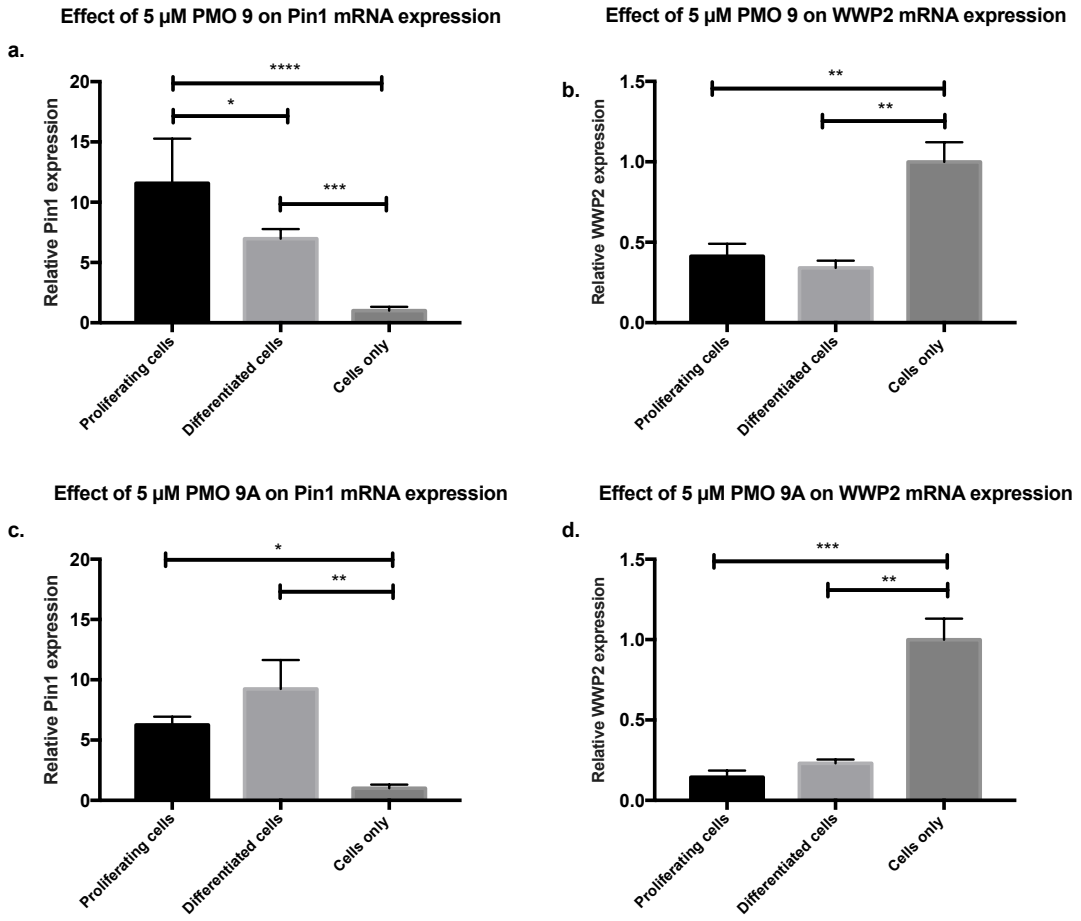

Figure 6.10 Comparison of Pin1 and WWP2 mRNA expression in proliferating and differentiated SH-SY5Y cells.

qRT-PCR analysis of mRNA isolated from proliferating and differentiated SH-SY5Y cells transfected with 5 µM of PMOs 9 and 9A. 'Cells only' refers to non-transfected proliferating cells. Bar graphs **a** and **b** show expression levels of Pin1 and WWP2 in PMO 9-transfected cells; and bar graphs **c** and **d** show expression levels of Pin1 and WWP2 in PMO 9A-transfected cells.

Expression of Pin1 and WWP2 was assessed using the LightCycler 480 (Roche) and reactions were performed using the LightCycler SYBR Green I Mastermix (Roche). The expression levels of β-actin were used as a reference gene. The gene expression levels were defined based on the threshold cycle (Ct), and relative expression levels were calculated using the $2^{-\Delta\Delta Ct}$ method. Measurements were made from three separate transfections in triplicate.

RA; retinoic acid. n=4, * = p≤0.05, ** = p≤0.01, *** = p≤0.001, **** = p≤0.0)01. Statistical comparisons were carried out using one-way ANOVA. All data points correspond to mean ± SEM values.

Fold-change in expression			
PMO transfected	**Gene**	**Proliferating cells**	**Differentiated cells**
PMO 9	**Pin1**	11.58 ± 3.7	6.98 ± 0.8
	WWP2	0.41 ± 0.08	0.34 ± 0.05
PMO 9A	**Pin1**	6.26 ± 0.7	9.24 ± 2.4
	WWP2	0.14 ± 0.04	0.23 ± 0.02

Table 6.1 Fold-change values of Pin1 and WWP2 mRNA expression in both proliferating and differentiated cells.

6.3 DISCUSSION

Although animal models more precisely imitate certain characteristics of a disease, there are some disadvantages to using them, such as time, cost and ethics. Many variables in a live animal can affect the study of different mechanisms. Cell culture models are advantageous in that they are easier to perform and repeat experiments, whilst also being time- and cost-saving. Thus, cell models are a good candidate for preliminary studies of the efficiency of various substances, more so when a more controlled setting is essential. In this chapter, we attempted to differentiate SH-SY5Y cells into a more neuronal-like cell model as differentiated cells possess both morphological and biochemical likenesses to human neurons. SH-SY5Y cells were cultured in RA-treated media in three different conditions: PDL-coated plates with differentiation media, PDL-coated plates with proliferation media replaced with differentiation media, and non-coated plates. When compared to undifferentiated cells, differentiated SH-SY5Y cells expressed longer, neurite-like projections (Figures 6.3 and 6.4). Differentiated cells cultured in PDL with proliferation media replaced with differentiation media also demonstrated near-complete RNA editing (Figure 6.2b), a biochemical characteristic that is reflective of neurons, since near 100% editing at the Q/R site of neurons is essential for normal GluA2 receptor function (S Maas, Patt, Schrey, & Rich, 2001). Differentiation of cells also promotes a reduction in proliferation rate (Figure 6.3), due to the withdrawing of cells from the cell cycle (Kovalevich & Langford, 2013).

Whilst the effects of PMOs on AluJ cassette inclusion and RNA editing in proliferating SH-SY5Y cells has been established, it was still not known whether morphological or biochemical changes affects these two processes. RNA isolated from differentiated cells were analysed following transfection with PMOs 9 and 9A. The inclusion of the AluJ cassette in ADAR2 transcripts were measured in both PMO-transfected and RA-treated cells at Day 7 of cell differentiation. As expected, transfection with PMOs 9 and 9A resulted in the reduction of AluJ cassette expression in cells when compared to

undifferentiated cells and RA-treated cells (32.93 ± 4.8% and 37.1 ± 1.2%, respectively) (Figure 6.5). The levels of AluJ cassette inclusion following transfection with PMO 9 (AluJ+93+117) in differentiated cells (32.93 ± 4.8%) (Figure 6.5) are similar to those measured in undifferentiated cells (32.93 ± 4.8%) (Figure 3.4). However, PMO 9A (AluJ+94+118) did not manage to decrease AluJ cassette levels in differentiated cells (37.1 ± 1.2%) as much as in undifferentiated cells at the same concentration (4.09 ± 2.3%) (Figure 3.5). In fact, whilst PMO 9A (AluJ+94+118) demonstrated to be most effective at exon skipping in undifferentiated cells (discussed is Section 3.3), the exon skipping efficacies of both PMO 9 (AluJ+93+117) and PMO 9A (AluJ+94+118) are similar in differentiated SH-SY5Y cells (Figure 6.5). It seems as if the morphological and biochemical changes in differentiated SH-SY5Y cells have prevented PMO 9A (AluJ+94+118) from binding as efficiently to the ADAR2 transcript, although the reasoning behind this is uncertain. The endogenous AluJ cassette insertion levels in RA-treated cells were also compared to undifferentiated cells (Figure 6.5). The AluJ cassette inclusion levels in RA-treated cells (84.24 ± 0.5%) did not significantly differ to AluJ cassette inclusion in undifferentiated cells (77.78 ± 1.6%) ($p>0.05$).

The RNA editing levels in differentiated cells were then assessed following PMO transfection. Since we have previously hypothesised that promoting AluJ cassette inclusion can indirectly increase Q/R site editing, we observed the same results in PMO-transfected differentiated cells (Figure 6.6). Since PMO 9 (AluJ+93+117) showed greater exon skipping efficacy in differentiated cells, the RNA editing levels improved to 151.3 ± 6.1% compared to normalised controls. The RNA editing levels measured were slightly higher compared to those calculated in PMO 9A-transfected cells (133.2 ± 10.9%). Again, the results obtained here slightly differs to our observations in Chapter 3, where PMO 9A (AluJ+94+118) resulted in higher increase in RNA editing levels compared to PMO 9 (AluJ+93+117). Considering that higher levels of AluJ cassette inclusion were known to result in reduced Q/R site RNA editing levels, it was therefore interesting to see that RNA editing levels in RA-treated cells (162.6 ± 10.9%) were higher than the levels quantified in undifferentiated cells. This further confirms that the high endogenous Q/R site editing levels in

differentiated SH-SY5Y cells is comparable to the high editing levels generally observed in neurons.

Since RA-treated cells demonstrated high levels of RNA editing despite incorporating higher levels of the AluJ cassette when compared to PMO-transfected cells, it was worth assessing whether Pin1 and WWP2 levels are regulated in differentiated cells. As discussed in Chapter 4, Pin1 acts a positive regulator for ADAR2 activity while WWP2 acts in a negative manner. Transfecting cells with PMOs 9 and 9A resulted in the upregulation in Pin1 mRNA levels (Figures 6.7a and 6.7c), as expected. The levels of WWP2 expression were reduced (Figures 6.7b and 6.7d), which additionally highlights the regulatory mechanism of both Pin1 and WWP2 expression with regards to Q/R site RNA editing. Investigation of Pin1 and WWP2 expression levels in RA-treated cells revealed the same expression patterns of the two genes previously observed in PMO-transfected cells, where we detected increased Pin1 and reduced WWP2 expression (Figures 6.7e and 6.7f). The expressional patterns of both Pin1 and WWP2 mRNA observed in RA-treated cells here are reflective of the high RNA editing levels that were measured in these cells (Figure 6.6), thus further confirming a possible regulatory mechanism in Pin1 and WWP2 expression during Q/R site editing.

It is therefore interesting to discern the possible underlying reasons behind the high endogenous RNA editing levels seen in differentiated cells, despite the fact that the cells displayed higher AluJ cassette inclusion and were not transfected with PMOs. Alternative splicing of the AluJ cassette may perform a key function in regulating editing activity *in vivo* at specific nucleotide sites (Paupard, O'Connell, Gerber, & Zukin, 1999). The human analog of the AluJ cassette insertion in rats is an alternative splicing event rat in ADAR2 pre-mRNA as a 30-nt insertion in their carboxy terminal catalytic domains, which yields isoforms that differ in their editing efficiency (Gerber et al., 1997; Lai, Chen, Carter, et al., 1997). Studies have demonstrated almost parallel temporal and spatial expression patterns of the two rat isoforms, though the expression of the 30-nt cassette-containing isoform appears more abundant (Filippini et al., 2018b; Paupard et al., 1999). In fact, another study has shown that expression of the normal transcript of Adarb1 appears to be at constant

levels throughout mouse brain development (Wahlstedt et al., 2009). Taken together, the results obtained by Paupard et. al., Wahlstedt et. al. and Filippini et. al. corroborates with the expression levels of the two ADAR2 isoforms we see in RA-treated cells (Figure 6.5). These data indicate that both splicing isoforms are required for normal neuronal function (Filippini et al., 2018b).

The editing levels measured in RA-treated cells (Figure 6.6) could be an indicator of a self-editing process of ADAR, whereby a new 3' splice acceptor site is created (modifying adenosine-adenosine to adenosine-inosine) in the intronic sequence of the ADAR2 mRNA (Li et al., 2015). Editing of ADAR2 pre-mRNA increases throughout rat brain development (Behm et al., 2017; Hang, Tohda, & Matsumoto, 2008); however, this editing activity does not correlate with ADAR expression levels, illustrating the presence of other regulatory mechanisms which regulate editing activity (Behm & Öhman, 2016). A study performed by (Filippini et al., 2018b) demonstrated increased self-editing process during primary neuron maturation in rat CNS. The self-editing process is additionally characterized by the parallel expression of ADAR2 isoforms containing 47-nt cassette, whereby inclusion of this cassette results in a truncated, less active isoform of the ADAR2 protein (Rueter et al., 1999). ADAR2 self-editing has also been demonstrated to take place in pre-mRNA during early development of primary neurons, followed by a gradual increase of editing levels during maturation (Behm et al., 2017; Hang et al., 2008). The expression of the less active ADAR2 isoform seems to contradict the increased editing levels reported during development, but fine-tuning ADAR2 activity (from self-editing) is essential for appropriate neuronal development. The increase of the inactive ADAR2 isoform may represent an autoregulatory mechanism where ADAR2 can prevent its own overactivity to avoid unwarranted and inappropriate RNA editing for numerous ADAR2 substrates throughout the CNS (Feng et al., 2006).

We have previously showed in Chapter 5 how Pin1 and WWP2 levels are regulated by ADAR2 during Q/R site RNA editing, where improved RNA editing in SH-SY5Y cells was a result of transfection with PMOs 9 and 9A. Similar expression levels were obtained in differentiated SH-SY5Y cells (Figures 6.7a-d). The same expressional patterns of Pin1 and WWP2 were

also measured in RA-treated cells (Figures 6.7e and f). The increase in RNA editing levels in maturing primary neurons has been attributed to the accumulation of ADAR2 in the nucleus during neuronal development (Behm et al., 2017). Accumulation of ADAR2 in the nucleus is essential for its interaction with Pin1 (Marcucci et al., 2011). Western blot analysis has previously revealed that Pin1 expression in developing neurons is expressed at low levels 1-3 DIV, and expression increased up to 13 DIV during maturation (Behm et al., 2017). The high RNA editing levels in RA-treated cells (Figure 6.6), which may also have been caused by the high expression levels of Pin1 in the cells (Figure 6.7e), could be attributed to the increasing accumulation of Pin1 in the nucleus. Additionally, other substrates for ADAR2 also exist, such as importin-α4, which mediates the nuclear import of ADAR2 (Behm & Öhman, 2016).

Pin1 regulates many proteins and processes within the cell. However, Pin1 itself is regulated by phosphorylation, inhibiting its activity (T. H. Lee, Chen, et al., 2011). (Marcucci et al., 2011) hypothesised that Pin1 acts at the core of a regulatory network, where any defects in normal biological processes leads to a reduction in Pin1 activity. This can eventually result in reduced ADAR2 activity with an ensuing reduction in the Q/R site editing of GluA2 transcripts, causing increased calcium permeability of AMPA receptors. This influx of calcium can ultimately induce excitotoxic neuronal death. Hence, 100% editing at the Q/R site of the GluA2 subunit may be a regulatory measure that indicates healthy neuronal function (Marcucci et al., 2011).

6.4 CONCLUSION

To conclude, the work in this chapter demonstrates that PMOs 9 (AluJ+93+117) and 9A (AluJ+94+118) are able to be successfully transfected into a more neuronal-like cell model, thus inducing alternative splicing of the AluJ cassette. What is interesting of note here is how we have observed high endogenous RNA editing levels in differentiated cells, which have been previously studied by (Lai, Chen, Lee, et al., 1997), where a rise in GluA2 Q/R site editing become progressively increased during neuronal differentiation of NT2 cells. Since editing levels are already high in differentiated cells, it would be worth attempting RNAi-induced gene knockdown of ADAR2 or Pin1 in differentiated cells in order to disrupt Q/R site editing, allowing us to quantify the effects of PMO 9 (AluJ+93+117) and 9A on improving RNA editing in differentiated cells. This can be followed by eventually testing PMOs 9 (AluJ+93+117) and 9A (AluJ+94+118) in neurons.

CHAPTER 7 DISCUSSION

7.1 ADAR2 SPLICING AND RNA EDITING

ADAR2, the enzyme responsible for the editing at the Q/R site of the GluA2 subunit of AMPA receptors, can exist as multiple splice variants. The insertion of a 120 bp AluJ cassette results in an ADAR2 isoform with reduced catalytic activity. PMOs 9, 9A, and 9B were designed to manipulate splicing of ADAR2 in order to exclude the AluJ cassette from the final transcript, resulting in a more active isoform of ADAR2. The expression of the ADAR2 isoform that does not express the AluJ cassette resulted in increased RNA editing levels in SH-SY5Y cells, highlighting the importance of alternative splicing in cells for normal cell function, as well as the correlation between ADAR2 activity and the role it plays in RNA editing.

Aside from RNA editing, ADARs also play a role during several key steps of miRNA maturation (Tomaselli et al., 2013). The maturation steps of both pre-miRNA and miRNA can be disrupted by ADARs that can sequester or edit the RNAs with crucial effects (Tomaselli, Locatelli, & Gallo, 2014). Although ADARs are deaminase enzymes, they can also serve as RNA-binding proteins due to the presence of RNA-binding domains. Hence, ADARs have been shown to bind to various transcripts without editing them (Klaue, Källman, Bonin, Nellen, & Öhman, 2003). Consequently, the binding of ADAR2 to pri-376a was shown to sufficiently inhibit its processing by Drosha, which is independent of ADAR2 editing activity (Heale et al., 2009). Additionally, the involvement of A-to-I editing in the heterochromatic silencing mechanism, where ADAR regulates gene silencing in *Drosophila*, has been reported (Savva et al., 2013). This data reveals additional roles carried out by ADAR enzymes and a global role for RNA editing in regulating gene expression (Savva et al., 2013). Considering that ADAR enzymes perform various roles, it is therefore expected that the many different cell pathways can be influenced by ADARs. ADAR activity is differentially regulated and spatiotemporally controlled (Tomaselli et al., 2014). Hence, aberrant RNA

editing profiles can be seen in different human diseases, such as neurological and neurodegenerative diseases (schizophrenia, depression, Alzheimer's disease, ALS), epilepsy, systemic lupus erythematosus (SLE), and cancers (Tomaselli et al., 2014).

In the case of ALS, deficiency in RNA editing at GluA2 Q/R site causes AMPA receptors to be permeable to Ca^{2+}, leading to exaggerated Ca^{2+} influx and death of motor neurons (Figure 7.1). ADAR2 protein is cleaved by a calcium-activated protease in vertebrate neuronal cells treated with excess glutamate, suggesting that glutamate excitotoxicity is partly mediated by the suppression of GluA2 Q/R site editing (Mahajan et al., 2011). The expression and editing state of GluA2 appears to act as a gatekeeper that can switch the phenotype of cells between two states, differing by their vulnerability to toxicity (Buckingham, Kwak, Jones, Blackshaw, & Sattelle, 2008). Hence, the question is, what is the adaptive advantage of a mechanism whereby an error in that mechanism can cause massive loss of motor neurons? Recent evidence has shown that this may be to allow regulation of ADAR2 RNA editing of glutamate receptor transcripts in response to neuronal excitation. GluA2 RNA editing modifies residues at surface interfaces and influences tetrameric receptor assembly (Greger & Esteban, 2007). Glutamate receptors that contain unedited Q/R site subunits can undergo intracellular membrane transport to the cell surface adjacent to synapses more effectively (Gallo, Vukic, Michalík, O'Connell, & Keegan, 2017). Q/R site subunits that have been edited aggregate in the endoplasmic reticulum and may be destroyed prior to arriving at the cell surface; giving rise to the possibility that the evolution of ADAR2 editing is to deter glutamate signalling by synaptic scaling in response to general neuronal excitation (Gallo et al., 2017). This is vital for neuronal synaptic plasticity response in both AMPA and kainate receptors (Evans, Gurung, Wilkinson, Stephens, & Henley, 2017). However, it is still unclear whether the effects of editing on membrane trafficking involves other receptor classes or edited proteins (Gallo et al., 2017).

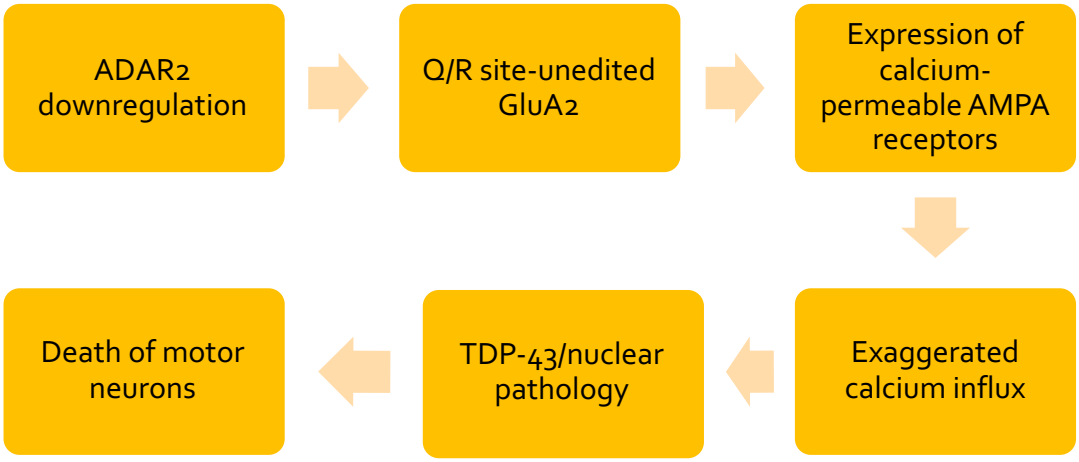

Figure 7.1 Proposed cell death cascade of motor neurons in sporadic ALS by Yamashita et. al. (2017).

Several antisense oligonucleotide therapies are under development for non-neurodegenerative disorders. Most notably, Eteplirsen, an exon-skipping ASO designed for the treatment of Duchenne muscular dystrophy (DMD), was granted accelerated approval by the US Food and Drug Administration (FDA) in September 2016 (K. R. Q. Lim et al., 2017). However, attaining sufficient levels of ASO distribution in the target organ and establishing high cellular uptake is a major issue (Evers et al., 2015). Neurodegenerative disorders are at an advantage here, as ASOs are readily taken up by neurons and glia once reaching the nervous system (Evers et al., 2015). The uptake is suggested to happen through nucleic acid channels, but little is still known about the exact cellular uptake mechanism (Evers et al., 2015). Vascular barriers in the nervous system prevents the ASOs from entering the periphery, hence no rapid excretion or breakdown by the kidney or liver will occur, allowing the ASO to reach clinically effective concentrations (Evers et al., 2015). The use of ASOs that interfere with pre-mRNA splicing has prominently been researched for spinal muscular atrophy (SMA), where the inclusion of exon 7 is increased by blocking the exonic splicing silencers (ESS) and intronic splicing silencers (ISS) to modulate the splicing of *SMN2*. ASOs have also been applied to correct the ratio of tau protein isoforms as a possible treatment for frontotemporal dementia (FTD) (Peacey, Rodriguez, Liu, & Wolfe, 2012). Tau

interacts with microtubules through its microtubule binding repeat domains encoded by exons 9 to 12. Tau isoforms with or without exon 10 (named the 3R and 4R isoforms, respectively) is produced by alternative splicing of exon 10 (Peacey et al., 2012). The ratio of 4R to 3R tau in healthy human brain is generally around 1. In FTD patients, however, the 4R to 3R ratio is shifted towards more exon 10-containing 4R, resulting in the formation of intracellular neurofibrillary tangles (Peacey et al., 2012). MAPT (microtubule associated protein tau) minigenes co-transfected with PNA ASOs targeting the 5' splice site of exon 10 inhibited exon 10 inclusion, shifting the 4R to 3R ratio towards higher 3R tau level (Peacey et al., 2012). Considering that ASOs have been thoroughly researched and utilised to correct aberrant pre-mRNA splicing in other diseases, using ASOs for exon skipping to correct ADAR2 splicing to improve RNA editing has the potential for us in ALS therapy. Overall, we have shown that both PMO 9 (AluJ+93+117) and PMO 9A (AluJ+94+118) are both efficient and inducing exon skipping in SH-SY5Y cells, although at different degrees. Although only mild effects on RNA editing were observed in PMO-transfected SH-SY5Y cells, this slight increase may be sufficient to safeguard motor neurons against excitotoxicity. This can be determined by studying the effects of glutamate overstimulation on cell viability in PMO-transfected cells.

7.2 PIN1 REGULATION DURING RNA EDITING

Although our understanding of the amount and extent of RNA editing has increased rapidly, how the process is physiologically regulated is less well-understood. It has been established that the same RNA transcript located in different regions of the brain is subjected to variable editing levels (Walkley & Li, 2017). Aside from ADAR editing enzymes themselves, only a small number of proteins that modulate RNA editing have been identified. Protein structural studies have revealed candidates for the alteration of ADAR protein function. The catalytic domain of ADAR2 comprises of inositol hexakiphosphate (IP_6), an integral structure required for efficient editing activity (Macbeth et al., 2005). One curious postulation is that the formation of elevated IP_6 from phospholipase C (PLC) following activation of 5-HT_{2c} may increase nascent ADAR2 protein activity and account for some of the feedback onto 5-HT_{2c} receptor editing (Schmauss, Zimnisky, Mehta, & Shapiro, 2010). Nevertheless, additional work is needed to establish whether levels of IP_6 in neurons are rate-limiting for ADAR2 activity (Penn, Balik, & Greger, 2013). ADAR protein function and abundance have also been shown to be regulated by post-translational modifications such as SUMOylation, phosphorylation-dependent propyl isomerisation, and ubiquitination (Penn et al., 2013). Moreover, it has been suggested that dynamic associations of ADARs with subcellular compartments are controlled as a way to sequester functional ADARs away from their nuclear targets. For example, editing site activity increases when ADAR2 is translocated to the nucleolus (Sansam et al., 2003).

One regulator that has been found to influence ADAR2 expression is CREB (cAMP-response element-binding protein), which can induce ADAR2 expression in hippocampal CA1 neurons in rat brain following transient ischemic insults (Peng et al., 2006). More recent evidence revealed that JNK1 (c-Jun Amino-Terminal Kinase 1) acts as a vital component in mediating glucose-responsive upregulation of ADAR2 expression in pancreatic β-cells, suggesting the functional relationship between the JNK1 pathway and the nutrient-sensing actions of ADAR2-mediated RNA editing in professional

secretory cells (Yang et al., 2012). Extensive profiling of A-to-I editing sites in human samples from the Genotype-Tissue Expression (GTEx) project recently identified AIMP2 (aminoacyl TRNA synthase complex interacting multifunctional protein 2) as a novel negative regulator of RNA editing, as its expression is negatively correlated with overall editing levels in thousands of samples (Tan et al., 2017). Further experiments and analyses in myoblasts suggests that AIMP2 partly functions by blocking ADAR1-mediated RNA editing, which was demonstrated to be essential for myoblast-to-myotube transition (Tan et al., 2017). The identification of Pin1 and WWP2 as regulators of ADAR2 activity were revealed when *Pin1*$^{-/-}$ mouse embryonic fibroblasts show ADAR2 mislocalisation in the cytoplasm and reduced GluA2 Q/R and R/G site editing, suggesting that Pin1 is required for the nuclear localisation and stability of ADAR2 (Marcucci et al., 2011). WWP2 was shown to negatively regulate ADAR2 activity by binding to ADAR2 and catalysing its ubiquitination and subsequent degradation (Marcucci et al., 2011). The involvement of these genes indicates that ADAR and other regulators can alter the editing efficiency observed at a given locus (Figure 7.2).

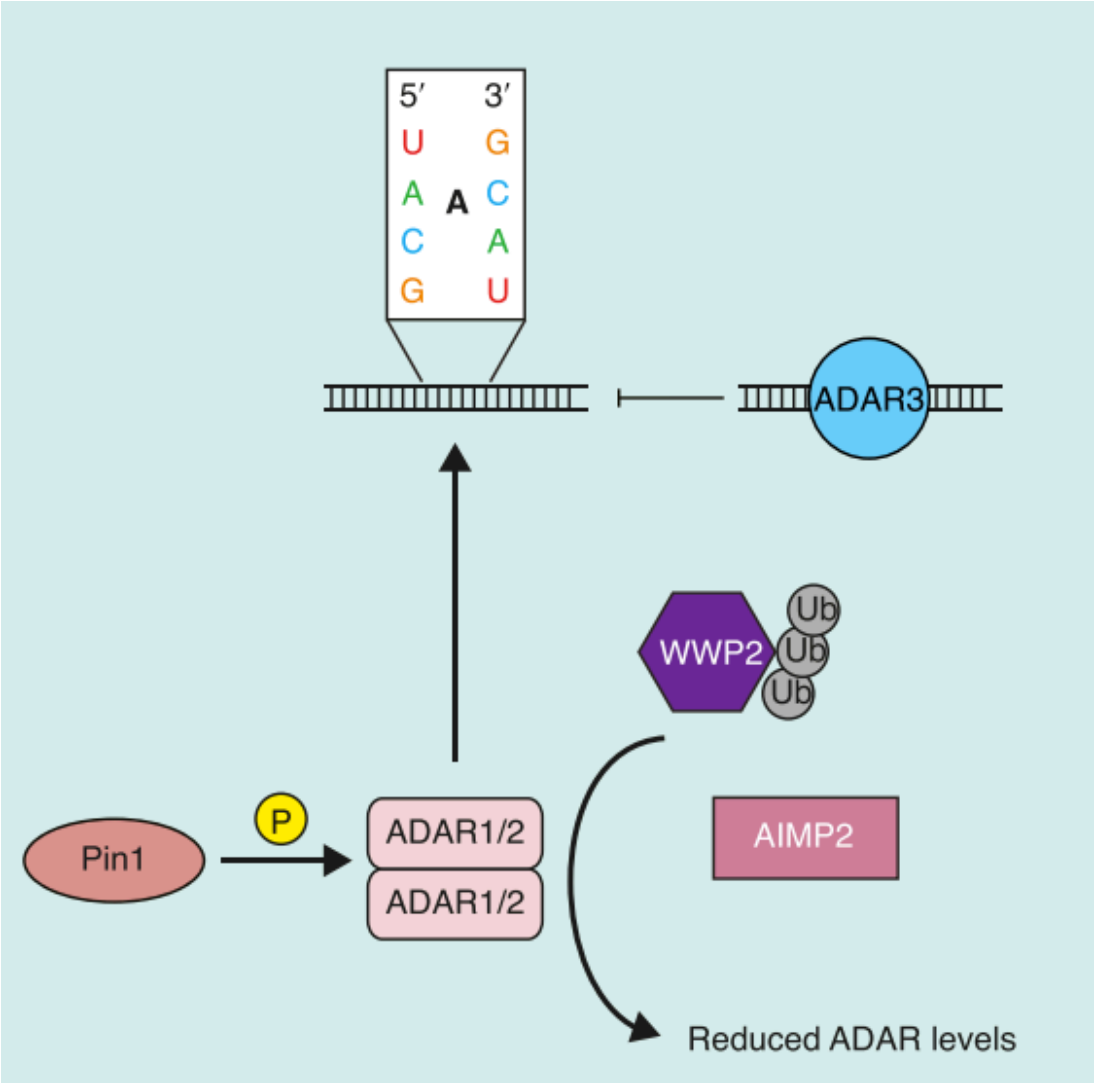

Figure 7.2 *Trans* regulation of A-to-I editing.

Trans regulation can either enhance editing, such as with Pin1 phosphorylation of ADAR, or reduce editing, as happens with WWP2 (ADAR ubiquitination) or AIMP2 (decreases overall ADAR1 levels). Figure taken from Walkley and Li (2017).

Based on our findings, we have shown that Pin1 mRNA levels show significant increase in expression in both PMO 9- and PMO 9A-transfected cells when compared to non-transfected cells. Conversely, WWP2 mRNA levels show reduced expression in PMO 9- and PMO 9A-transfected cells. Similarly, when cells were transfected with PMO E1 (which was designed to disrupt Q/R site editing), WWP2 mRNA levels showed increased expression. The results we obtained corroborates the findings by (Marcucci et al., 2011), whereby the higher Pin1 mRNA levels were found to act as a positive regulator for ADAR2 activity, since PMO 9 (AluJ+93+117) and PMO 9A (AluJ+94+118) transfected cells showed improved Q/R site RNA editing levels compared to control cells. Further Pin1 and WWP2 mRNA experiments were also performed in differentiated SH-SY5Y cells. Once SH-SY5Y cells have reached the differentiated state, the cells possess more neuronal-like properties, such as near-complete Q/R site editing levels, as opposed to the RNA editing levels measured in proliferating cells. This was an interesting observation as both differentiated and proliferating cells displayed similar levels of AluJ cassette inclusion in the cells. The expression levels of Pin1 mRNA in differentiated cells were also similar to those measured in PMO-transfected cells, thus implying that the increase in Pin1 mRNA that we have observed in PMO-transfected cells was, in fact, due to increased RNA editing, and not necessarily only caused by the expression of a more active ADAR2 isoform without the AluJ cassette.

Functionally, Pin1 plays a key role in various cellular processes, such as the cell cycle, cell signalling, transcription and splicing, DNA damage response, germ cell development and neuronal survival (Lu & Zhou, 2007). Pin1 also uses several mechanisms to regulate several targets and various steps of a cellular process to synergise and drive the cell in one direction (T. H. Lee, Pastorino, et al., 2011). Hence, the regulation of prolyl isomerisation catalysed by Pin1 may function as a timing mechanism, which enables the cell to turn phosphoprotein function on or off with great efficiency during dynamic cellular processes (T. H. Lee, Pastorino, et al., 2011). The deregulation of Pin1 has an essential role in many pathological conditions, particularly premature ageing, cancer, and Alzheimer's disease (T. H. Lee, Pastorino, et al., 2011).

Levels of soluble Pin1 are decreased in AD patient brains compared with age-matched control brains (Lu et. al. 1999) and Pin1 expression is reduced in neurons that are vulnerable for tauopathy (Liou et al., 2003), suggesting a protective role played by Pin1 and that a reduction in Pin1 levels might account for neurodegeneration.

Seeing its involvement in cancer and AD, Pin1 can be a used as a diagnostic marker and therapeutic tool for these diseases. Overexpression of Pin1 in postnatal neurons effectively prevented neurodegeneration in AD mouse models. A possible approach to treat neurodegeneration and AD is by preventing Pin1 downregulation by the brain-specific transcription factor AP4, or increasing Pin1 function in disease-affected neurons by inhibiting the oxidation of Pin1. However, since the effects of Pin1-based therapies depend on the individual's specific nature of neurodegeneration or neural biochemistry, further work is required to establish when and where targeting Pin1 would it a viable therapeutic target (Driver et al., 2015).

7.3 FUTURE WORK

In this thesis, we have demonstrated that alternative splicing of ADAR2 was successfully manipulated in SH-SY5Y cells, which endogenously express the GluA2 subunit. The effects of the PMOs were also studied in differentiated cells, which contain a more neuronal phenotype. Hence, it is worth testing the effects of the PMOs in primary neurons, as the ADAR2 splicing variants in rats have just been recently characterized (Filippini et al., 2018a) (Figure 7.3). However, this work would still require an optimization of a PMO transfection protocol for primary neurons, as they are notoriously difficult to transfect. The effects of PMOs on cell viability can also be studied by overstimulation of glutamate in PMO-transfected cells, and by visualizing the number of neurons expressing Ca^{2+}-permeable AMPA receptors by cobalt uptake staining (Kuner, 2005; Ludo Van Den Bosch et al., 2000) (Figure 7.3).

Since we have characterized Pin1 mRNA levels in PMO-transfected cells, the same experiments can also be performed in human iPSCs during differentiation. It is also worth investigating whether there are other factors contributing to the increase in RNA editing during SH-SY5Y differentiation. Additionally, it would also be interesting to study the effects of elevated and disrupted editing on miRNA dysregulation (such as miR-132, miR-143 and miR-55), since the implication of miRNA dysregulation has not yet been fully elucidated in neurodegenerative disorders. Additionally, the effects of PMOs on other genes known to regulate ADAR2 activity (CREB and AIMP) can also be examined (Figure 7.3). We have shown that excluding the AluJ cassette from the final ADAR2 transcript can indirectly improve Q/R site editing. Future studies can determine if other editing sites can also be affected by expressing a more catalytically active ADAR2 isoform. Thus, the effects of PMOs on other Q/R editing sites can also be studied, such as the GluK1 and GluK2 subunits of kainate receptors (Figure 7.3), which can provide a better understanding of the impact of improved or reduced RNA editing in the genome.

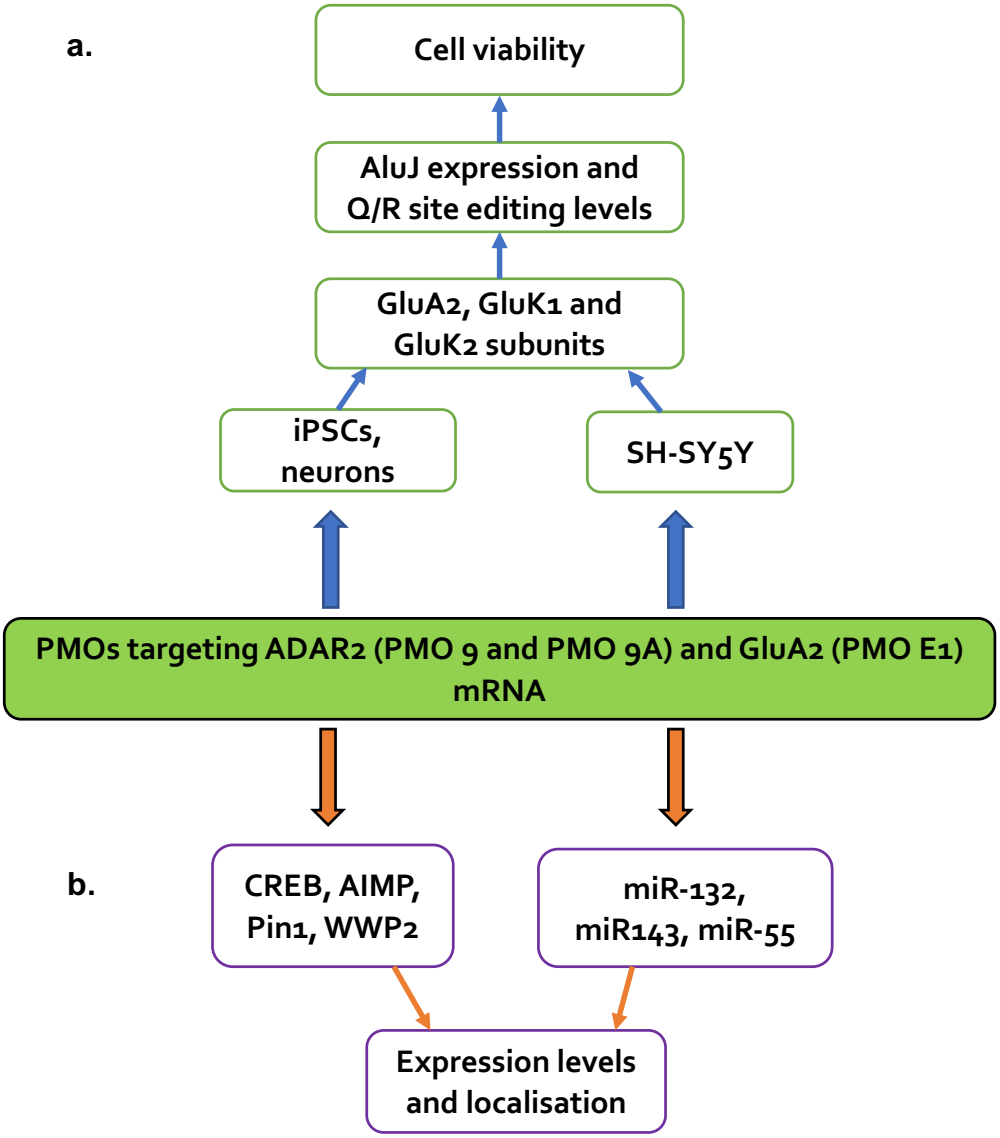

Figure 7.3 Summary of proposed future work to be performed.

a) PMOs can be further used in different cell lines (iPSCs, rat neurons) and can be used to study other Q/R editing sites (GluK1 and GluK2) to investigate AluJ cassette expression and Q/R site editing. Cells can be further tested for viability following glutamate overstimulation. b) The effects of PMO transfection in cells can be studied by measuring expression levels of CREB, AIMP and miRNAs. Additionally, the localization of CREB, AIMP, Pin1 and WWP2 (whether localized in the nucleolus or cytoplasm) can be tested.

BIBLIOGRAPHY

Aartsma-Rus, A., van Vliet, L., Hirschi, M., Janson, A. A. M., Heemskerk, H., de Winter, C. L., … van Ommen, G. J. B. (2009). Guidelines for antisense oligonucleotide design and insight into splice-modulating mechanisms. *Molecular Therapy*, *17*(3), 548–553. https://doi.org/10.1038/mt.2008.205

Abe, K., Aoki, M., Tsuji, S., Itoyama, Y., Sobue, G., Togo, M., … Yoshino, H. (2017). Safety and efficacy of edaravone in well defined patients with amyotrophic lateral sclerosis: a randomised, double-blind, placebo-controlled trial. *The Lancet Neurology*, *16*(7), 505–512. https://doi.org/10.1016/S1474-4422(17)30115-1

Agholme, L., Lindström, T., Kgedal, K., Marcusson, J., & Hallbeck, M. (2010). An in vitro model for neuroscience: Differentiation of SH-SY5Y cells into cells with morphological and biochemical characteristics of mature neurons. *Journal of Alzheimer's Disease*, *20*(4), 1069–1082. https://doi.org/10.3233/JAD-2010-091363

Akamatsu, M., Yamashita, T., Hirose, N., Teramoto, S., & Kwak, S. (2016). The AMPA receptor antagonist perampanel robustly rescues amyotrophic lateral sclerosis (ALS) pathology in sporadic ALS model mice. *Scientific Reports*, *6*(1), 28649. https://doi.org/10.1038/srep28649

Albo, F., Pieri, M., & Zona, C. (2004). Modulation of AMPA receptors in spinal motor neurons by the neuroprotective agent riluzole. *Journal of Neuroscience Research*, *78*(2), 200–207. https://doi.org/10.1002/jnr.20244

Andersen, P. M. (2006). Amyotrophic lateral sclerosis associated with mutations in the CuZn superoxide dismutase gene. *Curr Neurol Neurosci Rep*, *6*(1), 37–46.

Ayala, Y. M., De Conti, L., zquez, S. E. eacute ndira A. ntilde o-V. aacute, Dhir, A., Romano, M., Ambrogio, A. D. apos, … Baralle, F. E. (2010). TDP-43 regulates its mRNA levels through a negative feedback loop. *The EMBO Journal*, *30*(2), 277–288. https://doi.org/10.1038/emboj.2010.310

Bao, L., Kimzey, A., Sauter, G., Sowadski, J. M., Lu, K. P., & Wang, D. G. (2004). Prevalent Overexpression of Prolyl Isomerase Pin1 in Human Cancers. *American Journal of Pathology*, *164*(5), 1727–1737. https://doi.org/10.1016/S0002-9440(10)63731-5

Barbon, A., & Barlati, S. (2011). Glutamate receptor RNA editing in health and disease. *Biochemistry (Moscow)*, *76*(8), 882–889. https://doi.org/10.1134/s0006297911080037

Bartel, D. P. (2004). MicroRNAs: Genomics, Biogenesis, Mechanism, and Function. *Cell*, *116*(2), 281–297. https://doi.org/10.1016/S0092-8674(04)00045-5

Bass, B. L. (2002). RNA editing by adenosine deaminases that act on RNA. *Annual Review of Biochemistry*, 3377. https://doi.org/10.1093/nar/gkx050

Bass, B. L., & Weintraub, H. (1987). A developmentally regulated activity that unwinds RNA duplexes. *Cell*, *48*(4), 607–613. https://doi.org/10.1016/0092-8674(87)90239-X

Bass, B. L., & Weintraub, H. (1988). An unwinding activity that covalently modifies its double-stranded RNA substrate. *Cell*, *55*(6), 1089–1098. https://doi.org/10.1016/0092-8674(88)90253-X

Bassani, S., Valnegri, P., Beretta, F., & Passafaro, M. (2009). The GLUR2 subunit of AMPA receptors: Synaptic role. *Neuroscience*, *158*(1), 55–61. https://doi.org/10.1016/j.neuroscience.2008.10.007

Behm, M., & Öhman, M. (2016). RNA Editing: A Contributor to Neuronal Dynamics in the Mammalian Brain. *Trends in Genetics*, *32*(3), 165–175. https://doi.org/10.1016/j.tig.2015.12.005

Behm, M., Wahlstedt, H., Widmark, A., Eriksson, M., & Öhman, M. (2017). Accumulation of nuclear ADAR2 regulates adenosine-to-inosine RNA editing during neuronal development. *Journal of Cell Science*, *130*(4), 745–753. https://doi.org/10.1242/jcs.200055

Benne, R., Van Den Burg, J., Brakenhoff, J. P. J., Sloof, P., Van Boom, J. H.,

& Tromp, M. C. (1986). Major transcript of the frameshifted coxll gene from trypanosome mitochondria contains four nucleotides that are not encoded in the DNA. *Cell*, *46*(6), 819–826. https://doi.org/10.1016/0092-8674(86)90063-2

Bishop, K. M. (2017). Progress and promise of antisense oligonucleotide therapeutics for central nervous system diseases. *Neuropharmacology*, *120*, 56–62. https://doi.org/10.1016/j.neuropharm.2016.12.015

Black, D. L. (2003). Mechanisms of Alternative Pre-Messenger RNA Splicing. *Annual Review of Biochemistry*, *72*(1), 291–336. https://doi.org/10.1146/annurev.biochem.72.121801.161720

Brett, D., Pospisil, H., Valcárcel, J., Reich, J., & Bork, P. (2002). Alternative splicing and genome complexity. *Nature Genetics*, *30*(1), 29–30. https://doi.org/10.1038/ng803

Brown, R. H., & Al-Chalabi, A. (2017). Amyotrophic Lateral Sclerosis. *New England Journal of Medicine*, *377*(2), 162–172. https://doi.org/10.1056/NEJMra1603471

Bruijn, L. I., Miller, T. M., & Cleveland, D. W. (2004). Unraveling the Mechanisms Involved in Motor Neuron Degeneration in Als. *Annual Review of Neuroscience*, *27*(1), 723–749. https://doi.org/10.1146/annurev.neuro.27.070203.144244

Buckingham, S. D., Kwak, S., Jones, a. K., Blackshaw, S. E., & Sattelle, D. B. (2008). Edited GluR2, a gatekeeper for motor neurone survival? *BioEssays*, *30*(11–12), 1185–1192. https://doi.org/10.1002/bies.20836

Burnashev, N., Monyer, H., Seeburg, P. H., & Sakmann, B. (1992). Divalent ion permeability of AMPA receptor channels is dominated by the edited form of a single subunit. *Neuron*, *8*(1), 189–198. https://doi.org/10.1016/0896-6273(92)90120-3

Chan, J. H. P., Lim, S., & Wong, W. S. F. (2006). Antisense oligonucleotides: From design to therapeutic application. *Clinical and Experimental Pharmacology and Physiology*, *33*(5–6), 533–540.

https://doi.org/10.1111/j.1467-9248.2006.00620.x

Chantry, A. (2011). WWP2 ubiquitin ligase and its isoforms: New biological insight and promising disease targets. *Cell Cycle*, *10*(15), 2437–2439. https://doi.org/10.4161/cc.10.15.16874

Chaytow, H. A. (2015). *Development of an Antisense Oligonucleotide-Based Method to Manipulate RNA Editing of AMPAR Subunits*. Royal Holloway, University of London.

Chen, Y. C., Kao, S. C., Chou, H. C., Lin, W. H., Wong, F. H., & Chow, W. Y. (2008). A real-time PCR method for the quantitative analysis of RNA editing at specific sites. *Analytical Biochemistry*, *375*(1), 46–52. https://doi.org/10.1016/j.ab.2007.12.037

Cheung, Y. T., Lau, W. K. W., Yu, M. S., Lai, C. S. W., Yeung, S. C., So, K. F., & Chang, R. C. C. (2009). Effects of all-trans-retinoic acid on human SH-SY5Y neuroblastoma as in vitro model in neurotoxicity research. *NeuroToxicology*, *30*(1), 127–135. https://doi.org/10.1016/j.neuro.2008.11.001

Chiò, A., Battistini, S., Calvo, A., Caponnetto, C., Conforti, F. L., Corbo, M., … Tanel, R. (2014). Genetic counselling in ALS: Facts, uncertainties and clinical suggestions. *Journal of Neurology, Neurosurgery and Psychiatry*, *85*(5), 478–485. https://doi.org/10.1136/jnnp-2013-305546

Clark, T. A., Schweitzer, A. C., Chen, T. X., Staples, M. K., Lu, G., Wang, H., … Blume, J. E. (2007). Discovery of tissue-specific exons using comprehensive human exon microarrays. *Genome Biology*, *8*(4). https://doi.org/10.1186/gb-2007-8-4-r64

Coolen, M., Katz, S., & Bally-Cuif, L. (2013). miR-9: a versatile regulator of neurogenesis. *Frontiers in Cellular Neuroscience*, *7*(November), 220. https://doi.org/10.3389/fncel.2013.00220

Cooper-Knock, J., Shaw, P. J., & Kirby, J. (2014). The widening spectrum of C9ORF72-related disease; Genotype/phenotype correlations and potential modifiers of clinical phenotype. *Acta Neuropathologica*, *127*(3),

333–345. https://doi.org/10.1007/s00401-014-1251-9

Crooke, S. T. (2004). Progress in Antisense Technology. *Annual Review of Medicine*, *55*(1), 61–95. https://doi.org/10.1146/annurev.med.55.091902.104408

Dawson, T. R., Sansam, C. L., & Emeson, R. B. (2003). Structure and Sequence Determinants Required for the RNA Editing of ADAR2 Substrates. *Journal of Biological Chemistry*, *279*(6), 4941–4951. https://doi.org/10.1074/jbc.M310068200

De Felice, B., Guida, M., Guida, M., Coppola, C., De Mieri, G., & Cotrufo, R. (2012). A miRNA signature in leukocytes from sporadic amyotrophic lateral sclerosis. *Gene*, *508*(1), 35–40. https://doi.org/10.1016/j.gene.2012.07.058

Deffit, S. N., & Hundley, H. A. (2016). To edit or not to edit: Regulation of ADAR editing specificity and efficiency. *Wiley Interdisciplinary Reviews: RNA*, *7*(1), 113–127. https://doi.org/10.1002/wrna.1319

DeJesus-Hernandez, M., Mackenzie, I. R., Boeve, B. F., Boxer, A. L., Baker, M., Rutherford, N. J., … Boylan, K. (2011). Expanded GGGGCC hexanucleotide repeat in non-coding region of C9ORF72 causes chromosome 9p-linked frontotemporal dementia and amyotrophic lateral sclerosis, *72*(2), 245–256. https://doi.org/10.1016/j.neuron.2011.09.011.Expanded

Desterro, J. M. P., Keegan, L. P., Lafarga, M., Berciano, M. T., O'Connell, M. A., & Carmo-Fonseca, M. (2003). Dynamic association of RNA-editing enzymes with the nucleolus. *Journal of Cell Science*, *116*(9), 1805–1818. https://doi.org/10.1242/jcs.00371

Dias, N., & Stein, C. a. (2002). Antisense Oligonucleotides : Basic Concepts and Mechanisms. *Cancer Research*, 347–355.

Doble, A. (1999). The Role of Excitotoxicity in Neurodegenerative Disease. *Pharmacology & Therapeutics*, *81*(3), 163–221. https://doi.org/10.1016/S0163-7258(98)00042-4

Donnelly, C. J., Zhang, P.-W., Pham, J. T., Haeusler, A. R., Mistry, N. A., Vidensky, S., … Rothstein, J. D. (2013). RNA Toxicity from the ALS/FTD C9ORF72 Expansion Is Mitigated by Antisense Intervention. *Neuron*, *80*(2), 415–428. https://doi.org/10.1016/j.neuron.2013.10.015

Driver, J. A., Zhou, X. Z., & Lu, K. P. (2015). Pin1 dysregulation helps to explain the inverse association between cancer and Alzheimer's disease. *Biochimica et Biophysica Acta - General Subjects*, *1850*(10), 2069–2076. https://doi.org/10.1016/j.bbagen.2014.12.025

Dwane, S., Durack, E., & Kiely, P. A. (2013). Optimising parameters for the differentiation of SH-SY5Y cells to study cell adhesion and cell migration. *BMC Research Notes*, *6*(1), 366. https://doi.org/10.1186/1756-0500-6-366

Eisen, J. S., & Smith, J. C. (2008). Controlling morpholino experiments: don't stop making antisense. *Development*, *135*(10), 1735–1743. https://doi.org/10.1242/dev.001115

Encinas, M., Iglesias, M., Liu, Y., Wang, H., Cefia, V., Gallego, C., & Comella, X. (2000). Sequential Treatment of SH-SY5Y Cells with Retinoic Acid and Brain-Derived Neurotrophic Factor Gives Rise to Fully Differentiated, Neurotrophic Factor-Dependent, Human Neuron-Like Cells. *Journal of Neurochemistry*, *75*(3), 991–1003. https://doi.org/10.1046/j.1471-4159.2000.0750991.x

Engels, B. M., & Hutvagner, G. (2006). Principles and effects of microRNA-mediated post-transcriptional gene regulation. *Oncogene*, *25*(46), 6163–6169. https://doi.org/10.1038/sj.onc.1209909

Evans, A. J., Gurung, S., Wilkinson, K. A., Stephens, D. J., & Henley, J. M. (2017). Assembly, Secretory Pathway Trafficking, and Surface Delivery of Kainate Receptors Is Regulated by Neuronal Activity. *Cell Reports*, *19*(12), 2613–2626. https://doi.org/10.1016/j.celrep.2017.06.001

Evers, M. M., Toonen, L. J. A., & van Roon-Mom, W. M. C. (2015). Antisense oligonucleotides in therapy for neurodegenerative disorders. *Advanced*

Drug Delivery Reviews, *87*, 90–103. https://doi.org/10.1016/j.addr.2015.03.008

Farg, M. A., Sundaramoorthy, V., Sultana, J. M., Yang, S., Atkinson, R. A. K., Levina, V., … Atkin, J. D. (2014). C9ORF72, implicated in amytrophic lateral sclerosis and frontotemporal dementia, regulates endosomal trafficking. *Human Molecular Genetics*, *23*(13), 3579–3595. https://doi.org/10.1093/hmg/ddu068

Feng, Y., Sansam, C. L., Singh, M., & Emeson, R. B. (2006). Altered RNA editing in mice lacking ADAR2 autoregulation. *Molecular and Cellular Biology*, *26*(2), 480–488. https://doi.org/10.1128/MCB.26.2.480-488.2006

Filippini, A., Bonini, D., Giacopuzzi, E., La Via, L., Gangemi, F., Colombi, M., & Barbon, A. (2018a). Differential enzymatic activity of rat ADAR2 splicing variants is due to altered capability to interact with RNA in the deaminase domain. *Genes*, *9*(2). https://doi.org/10.3390/genes9020079

Filippini, A., Bonini, D., Giacopuzzi, E., La Via, L., Gangemi, F., Colombi, M., & Barbon, A. (2018b). Differential Enzymatic Activity of Rat ADAR2 Splicing Variants Is Due to Altered Capability to Interact with RNA in the Deaminase Domain. *Genes*, *9*(2), 79. https://doi.org/10.3390/genes9020079

Gallo, A., Vukic, D., Michalík, D., O'Connell, M. A., & Keegan, L. P. (2017). ADAR RNA editing in human disease; more to it than meets the I. *Human Genetics*, *136*(9), 1265–1278. https://doi.org/10.1007/s00439-017-1837-0

Gamazon, E. R., & Stranger, B. E. (2014). Genomics of alternative splicing: Evolution, development and pathophysiology. *Human Genetics*, *133*(6), 679–687. https://doi.org/10.1007/s00439-013-1411-3

George, C. X., & Samuel, C. E. (1999). Human RNA-specific adenosine deaminase ADAR1 transcripts possess alternative exon 1 structures that initiate from different promoters, one constitutively active and the other interferon inducible. *Proceedings of the National Academy of Sciences*,

96(8), 4621–4626. https://doi.org/10.1073/pnas.96.8.4621

George, Cyril X., Wagner, M. V., & Samuel, C. E. (2005). Expression of interferon-inducible RNA adenosine deaminase ADAR1 during pathogen infection and mouse embryo development involves tissue-selective promoter utilization and alternative splicing. *Journal of Biological Chemistry*, *280*(15), 15020–15028. https://doi.org/10.1074/jbc.M500476200

Gerber, A., O'Connell, M. A., & Keller, W. (1997). Two forms of human double-stranded RNA-specific editase 1 (hRED1) generated by the insertion of an Alu cassette. *RNA*, *3*(5), 453–463.

Ghosh, G., & Adams, J. A. (2011). Phosphorylation mechanism and structure of serine-arginine protein kinases. *FEBS Journal*, *278*(4), 587–597. https://doi.org/10.1111/j.1742-4658.2010.07992.x

Gilbert, M. T. P., Sanchez, J. J., Haselkorn, T., Jewell, L. D., Lucas, S. B., Van Marck, E., … Worobey, M. (2007). Multiplex PCR with minisequencing as an effective high-throughput SNP typing method for formalin-fixed tissue. *Electrophoresis*, *28*(14), 2361–2367. https://doi.org/10.1002/elps.200600589

Gitler, A. D., & Tsuiji, H. (2016). There has been an awakening: Emerging mechanisms of C9orf72 mutations in FTD/ALS. *Brain Research*, *1647*, 19–29. https://doi.org/10.1016/j.brainres.2016.04.004

Görlich, D., Prehn, S., Laskey, R. A., & Hartmann, E. (1994). Isolation of a protein that is essential for the first step of nuclear protein import. *Cell*, *79*(5), 767–778. https://doi.org/10.1016/0092-8674(94)90067-1

Greenbaum, D., Colangelo, C., Williams, K., & Gerstein, M. (2003). Comparing protein abundance and mRNA expression levels on a genomic scale. *Genome Biology*, *4*(9). https://doi.org/10.1021/bp990004b

Greger, I. H., & Esteban, J. A. (2007). AMPA receptor biogenesis and trafficking. *Current Opinion in Neurobiology*, *17*(3), 289–297. https://doi.org/10.1016/j.conb.2007.04.007

Hang, P. N. T., Tohda, M., & Matsumoto, K. (2008). Developmental changes in expression and self-editing of adenosine deaminase type 2 pre-mRNA and mRNA in rat brain and cultured cortical neurons. *Neuroscience Research*, *61*(4), 398–403. https://doi.org/10.1016/j.neures.2008.04.007

Hardiman, O., Al-Chalabi, A., Chio, A., Corr, E. M., Logroscino, G., Robberecht, W., … van den Berg, L. H. (2017). Amyotrophic lateral sclerosis. *Nature Reviews Disease Primers*, *3*, 17071. https://doi.org/10.1038/nrdp.2017.71

He, J., Mangelsdorf, M., Fan, D., Bartlett, P., & Brown, M. A. (2015). Amyotrophic Lateral Sclerosis Genetic Studies. *The Neuroscientist*, *21*(6), 599–615. https://doi.org/10.1177/1073858414555404

Heale, B. S. E., Keegan, L. P., McGurk, L., Michlewski, G., Brindle, J., Stanton, C. M., … O'Connell, M. a. (2009). Editing independent effects of ADARs on the miRNA/siRNA pathways. *The EMBO Journal*, *28*(20), 3145–3156. https://doi.org/10.1038/emboj.2009.244

Heath, P. R., & Shaw, P. J. (2002). Update on the glutamatergic neurotransmitter system and the role of excitotoxicity in amyotrophic lateral sclerosis. *Muscle & Nerve*, *26*(4), 438–458. https://doi.org/10.1002/mus.10186

Hideyama, T., Yamashita, T., Suzuki, T., Tsuji, S., Higuchi, M., Seeburg, P. H., … Kwak, S. (2010). Induced Loss of ADAR2 Engenders Slow Death of Motor Neurons from Q/R Site-Unedited GluR2. *Journal of Neuroscience*, *30*(36), 11917–11925. https://doi.org/10.1523/JNEUROSCI.2021-10.2010

Hideyama, Takuto, Yamashita, T., Aizawa, H., Tsuji, S., Kakita, A., Takahashi, H., & Kwak, S. (2012). Profound downregulation of the RNA editing enzyme ADAR2 in ALS spinal motor neurons. *Neurobiology of Disease*, *45*, 1121–1128. https://doi.org/10.1016/j.nbd.2011.12.033

Higuchi, M, Single, F. N., Köhler, M., Sommer, B., Sprengel, R., & Seeburg, P. H. (1993). RNA editing of AMPA receptor subunit GluR-B: a base-

paired intron-exon structure determines position and efficiency. *Cell*, *75*(7), 1361–1370. https://doi.org/10.1016/0092-8674(93)90622-W

Higuchi, Miyoko, Maas, S., Single, F. N., Hartner, J., Rozov, A., Burnashev, N., … Seeburg, P. H. (2000). Point mutation in an AMPA receptor gene rescues lethality in mice deficient in the RNA-editing enzyme ADAR2. *Nature*, *406*(6791), 78–81. https://doi.org/10.1038/35017558

Hogg, M., Paro, S., Keegan, L. P., & O'Connell, M. a. (2011). *RNA Editing by Mammalian ADARs*. *Advances in Genetics* (1st ed., Vol. 73). Elsevier Inc. https://doi.org/10.1016/B978-0-12-380860-8.00003-3

Honda, D., Ishigaki, S., Iguchi, Y., Fujioka, Y., Udagawa, T., Masuda, A., … Sobue, G. (2014). The ALS/FTLD-related RNA-binding proteins TDP-43 and FUS have common downstream RNA targets in cortical neurons. *FEBS Open Bio*, *4*, 1–10. https://doi.org/10.1016/j.fob.2013.11.001

Hutvágner, G., McLachlan, J., Pasquinelli, A. E., Bálint, E., Tuschl, T., & Zamore, P. D. (2001). A cellular function for the RNA-interference enzyme Dicer in the maturation of the let-7 small temporal RNA. *Science (New York, N.Y.)*, *293*(5531), 834–838. https://doi.org/10.1126/science.1062961

Irimia, M., Denuc, A., Ferran, J. L., Pernaute, B., Puelles, L., Roy, S. W., … Marfany, G. (2012). Evolutionarily conserved A-to-I editing increases protein stability of the alternative splicing factor Nova1. *RNA Biology*, *9*(1), 12–21. https://doi.org/10.4161/rna.9.1.18387

Isaac, J. T. R., Ashby, M., & McBain, C. J. (2007). The Role of the GluR2 Subunit in AMPA Receptor Function and Synaptic Plasticity. *Neuron*, *54*(6), 859–871. https://doi.org/10.1016/j.neuron.2007.06.001

Jarmin, S., Kymalainen, H., Popplewell, L., & Dickson, G. (2014). New developments in the use of gene therapy to treat Duchenne muscular dystrophy. *Expert Opin. Biol. Ther*, *14*(2), 209–230. https://doi.org/10.1517/14712598.2014.866087

Järver, P., O'Donovan, L., & Gait, M. J. (2014). A Chemical View of

Oligonucleotides for Exon Skipping and Related Drug Applications. *Nucleic Acid Therapeutics*, *24*(1), 37–47. https://doi.org/10.1089/nat.2013.0454

Johnson, J. M., Castle, J., Garrett-Engele, P., Kan, Z., Loerch, P. M., Armour, C. D., … Shoemaker, D. D. (2003). Genome-Wide Survey of Human Alternative Pre-mRNA Splicing with Exon Junction Microarrays. *Science*, *302*(5653), 2141–2144. https://doi.org/10.1126/science.1090100

Kallman, A. M., Sahlin, M., & Ohman, M. (2003). ADAR2 A->I editing: site selectivity and editing efficiency are separate events. *Nucleic Acids Research*, *31*(16), 4874–4881. https://doi.org/10.1093/nar/gkg681

Kang, S. H., Li, Y., Fukaya, M., Lorenzini, I., Cleveland, D. W., Ostrow, L. W., … Bergles, D. E. (2013). Degeneration and impaired regeneration of gray matter oligodendrocytes in amyotrophic lateral sclerosis. *Nature Neuroscience*, *16*(5), 571–579. https://doi.org/10.1038/nn.3357

Karra, D., & Dahm, R. (2010). Transfection Techniques for Neuronal Cells. *Journal of Neuroscience*, *30*(18), 6171–6177. https://doi.org/10.1523/JNEUROSCI.0183-10.2010

Kawahara, Y., Ito, K., Ito, M., Tsuji, S., & Kwak, S. (2005). Novel splice variants of human ADAR2 mRNA: Skipping of the exon encoding the dsRNA-binding domains, and multiple C-terminal splice sites. *Gene*, *363*, 193–201. https://doi.org/10.1016/j.gene.2005.07.028

Kawahara, Y., Ito, K., Sun, H., Aizawa, H., Kanazawa, I., & Kwak, S. (2004). Glutamate receptors: RNA editing and death of motor neurons. *Nature*, *427*(6977), 801. https://doi.org/10.1038/427801a

Kawahara, Y., Ito, K., Sun, H., Kanazawa, I., & Kwak, S. (2003). Low editing efficiency of GluR2 mRNA is associated with a low relative abundance of ADAR2 mRNA in white matter of normal human brain. *European Journal of Neuroscience*, *18*(1), 23–33. https://doi.org/10.1046/j.1460-9568.2003.02718.x

Kawahara, Y., Kwak, S., Sun, H., Ito, K., Hashida, H., Aizawa, H., …

Kanazawa, I. (2003). Human spinal motoneurons express low relative abundance of GluR2 mRNA: an implication for excitotoxicity in ALS. *Journal of Neurochemistry*, *85*(3), 680–689. https://doi.org/10.1046/j.1471-4159.2003.01703.x

Kawahara, Y., & Mieda-Sato, A. (2012). TDP-43 promotes microRNA biogenesis as a component of the Drosha and Dicer complexes. *Proceedings of the National Academy of Sciences of the United States of America*, *109*(9), 3347–3352. https://doi.org/10.1073/pnas.1112427109

Kawahara, Y., Sun, H., Ito, K., Hideyama, T., Aoki, M., Sobue, G., … Kwak, S. (2006). Underediting of GluR2 mRNA, a neuronal death inducing molecular change in sporadic ALS, does not occur in motor neurons in ALS1 or SBMA. *Neuroscience Research*, *54*(1), 11–14. https://doi.org/10.1016/j.neures.2005.09.006

Kerscher, O., Felberbaum, R., & Hochstrasser, M. (2006). Modification of Proteins by Ubiquitin and Ubiquitin-Like Proteins. *Annual Review of Cell and Developmental Biology*, *22*(1), 159–180. https://doi.org/10.1146/annurev.cellbio.22.010605.093503

Kiernan, M. C., Vucic, S., Cheah, B. C., Turner, M. R., Eisen, A., Hardiman, O., … Zoing, M. C. (2011). Amyotrophic lateral sclerosis. *The Lancet*, *377*(9769), 942–955. https://doi.org/10.1016/S0140-6736(10)61156-7

King, A. E., Woodhouse, A., Kirkcaldie, M. T. K., & Vickers, J. C. (2016). Excitotoxicity in ALS: Overstimulation, or overreaction? *Experimental Neurology*, *275*, 162–171. https://doi.org/10.1016/j.expneurol.2015.09.019

Klaue, Y., Källman, A. M., Bonin, M., Nellen, W., & Öhman, M. (2003). Biochemical analysis and scanning force microscopy reveal productive and nonproductive ADAR2 binding to RNA substrates. *Rna*, *9*(7), 839–846. https://doi.org/10.1261/rna.2167603

Kolb, S. J., & Kissel, J. T. (2011). Spinal Muscular Atrophy: A Timely Review. *Arch Neurol.*, *68*(8). https://doi.org/10.1038/jid.2014.371

Kole, R., Krainer, A. R., & Altman, S. (2012). RNA therapeutics: beyond RNA interference and antisense oligonucleotides. *Nature Reviews Drug Discovery*, *11*(2), 125–140. https://doi.org/10.1038/nrd3625

Koussounadis, A., Langdon, S. P., Um, I. H., Harrison, D. J., & Smith, V. A. (2015). Relationship between differentially expressed mRNA and mRNA-protein correlations in a xenograft model system. *Scientific Reports*, *5*(June), 1–9. https://doi.org/10.1038/srep10775

Kovalevich, J., & Langford, D. (2013). Considerations for the use of SH-SY5Y neuroblastoma cells in neurobiology. *Methods Mol Biol*, *1078*, 9–21. https://doi.org/10.1007/978-1-62703-640-5

Kuner, R. (2005). Mechanisms of Disease: Motoneuron Disease Aggravated by Transgenic Expression of a Functionally Modified AMPA Receptor Subunit. *Annals of the New York Academy of Sciences*, *1053*(1), 269–286. https://doi.org/10.1196/annals.1344.024

Kwak, S., & Kawahara, Y. (2005). Deficient RNA editing of GluR2 and neuronal death in amyotropic lateral sclerosis. *Journal of Molecular Medicine*, *83*(2), 110–120. https://doi.org/10.1007/s00109-004-0599-z

Kye, M. J., & Gonçalves, I. do C. G. (2014). The role of miRNA in motor neuron disease. *Frontiers in Cellular Neuroscience*, *8*(January), 1–8. https://doi.org/10.3389/fncel.2014.00015

Lacomblez, L., Bensimon, G., Meininger, V., Leigh, P. ., & Guillet, P. (1996). Dose-ranging study of riluzole in amyotrophic lateral sclerosis. *The Lancet*, *347*, 1425–1431. https://doi.org/10.1016/S0140-6736(96)91680-3

Lagier-Tourenne, C., Baughn, M., Rigo, F., Sun, S., Liu, P., Li, H.-R., … Ravits, J. (2013). Targeted degradation of sense and antisense C9orf72 RNA foci as therapy for ALS and frontotemporal degeneration. *Proceedings of the National Academy of Sciences of the United States of America*, *110*(47), E4530-9. https://doi.org/10.1073/pnas.1318835110

Lai, F., Chen, C. X., Carter, K. C., & Nishikura, K. (1997). Editing of glutamate

receptor B subunit ion channel RNAs by four alternatively spliced DRADA2 double-stranded RNA adenosine deaminases. *Mol Cell Biol*, *17*(5), 2413–2424. Retrieved from http://www.ncbi.nlm.nih.gov/cgi-bin/Entrez/referer?http://www.ncbi.nlm.nih.gov/htbin-post/Omim/getmim?field=medline_uid&search=9111310

Lai, F., Chen, C. X., Lee, V. M., & Nishikura, K. (1997). Dramatic increase of the RNA editing for glutamate receptor subunits during terminal differentiation of clonal human neurons. *J Neurochem*, *69*(1), 43–52.

Lau, N. C., Lim, L. P., Weinstein, E. G., & Bartel, D. P. (2001). An abundant class of tiny RNAs with probable regulatory roles in Caenorhabditis elegans. *Science (New York, N.Y.)*, *294*(5543), 858–862. https://doi.org/10.1126/science.1065062

Lee, E. B., Lee, V. M. Y., & Trojanowski, J. Q. (2012). Gains or losses: Molecular mechanisms of TDP43-mediated neurodegeneration. *Nature Reviews Neuroscience*, *13*(1), 38–50. https://doi.org/10.1038/nrn3121

Lee, S., & Huang, E. J. (2017). Modeling ALS and FTD with iPSC-derived neurons. *Brain Research*, *1656*, 88–97. https://doi.org/10.1016/j.brainres.2015.10.003

Lee, T. H., Chen, C. H., Suizu, F., Huang, P., Schiene-Fischer, C., Daum, S., … Lu, K. P. (2011). Death-Associated Protein Kinase 1 Phosphorylates Pin1 and Inhibits Its Prolyl Isomerase Activity and Cellular Function. *Molecular Cell*, *42*(2), 147–159. https://doi.org/10.1016/j.molcel.2011.03.005

Lee, T. H., Pastorino, L., & Lu, K. P. (2011). Peptidyl-prolyl cis-trans isomerase Pin1 in ageing, cancer and Alzheimer disease. *Expert Reviews in Molecular Medicine*, *13*(May), 1–26. https://doi.org/10.1017/S1462399411001906

Lee, Y., Kim, M., Han, J., Yeom, K. H., Lee, S., Baek, S. H., & Kim, V. N. (2004). MicroRNA genes are transcribed by RNA polymerase II. *Embo J*, *23*(20), 4051–4060. https://doi.org/10.1038/sj.emboj.7600385\r7600385

[pii]

Leigh, P. N., Abrahams, S., Al-Chalabi, a, Ampong, M., Goldstein, L. H., Johnson, J., … Willey, E. (2003). The management of motor neurone disease. *Journal of Neurology, Neurosurgery, and Psychiatry*, *74 Suppl 4*, iv32–iv47. https://doi.org/10.1136/jnnp.74.suppl_4.iv32

Li, Z., Tian, Y., Tian, N., Zhao, X., Du, C., Han, L., & Zhang, H. (2015). Aberrant alternative splicing pattern of ADAR2 downregulates adenosine-to-inosine editing in glioma. *Oncology Reports*, *33*(6), 2845–2852. https://doi.org/10.3892/or.2015.3907

Licht, K., Kapoor, U., Mayrhofer, E., & Jantsch, M. F. (2016). Adenosine to Inosine editing frequency controlled by splicing efficiency. *Nucleic Acids Research*, 1–11. https://doi.org/10.1093/nar/gkw325

Lim, K. R. Q., Maruyama, R., & Yokota, T. (2017). Eteplirsen in the treatment of Duchenne muscular dystrophy. *Drug Design, Development and Therapy*, *11*, 533–545. https://doi.org/10.2147/DDDT.S97635

Lim, S. R., & Hertel, K. J. (2001). Modulation of Survival Motor Neuron Pre-mRNA Splicing by Inhibition of Alternative 3' Splice Site Pairing. *Journal of Biological Chemistry*, *276*(48), 45476–45483. https://doi.org/10.1074/jbc.M107632200

Liou, Y. C., Sun, A., Ryo, A., Zhou, X. Z., Yu, Z. X., Huang, H. K., … Lu, K. P. (2003). Role of the prolyl isomerase Pin1 in protecting against age-dependent neurodegeneration. *Nature*, *424*(6948), 556–561. https://doi.org/10.1038/nature01832

Liu, Yansheng, Beyer, A., & Aebersold, R. (2016). On the Dependency of Cellular Protein Levels on mRNA Abundance. *Cell*, *165*(3), 535–550. https://doi.org/10.1016/j.cell.2016.03.014

Liu, Yong, George, C. X., Patterson, J. B., & Samuel, C. E. (1997). Functionally distinct double-stranded RNA-binding domains associated with alternative splice site variants of the interferon-inducible double- stranded RNA-specific adenosine deaminase. *Journal of Biological Chemistry*,

272(7), 4419–4428. https://doi.org/10.1074/jbc.272.7.4419

Loh, P. R., Bhatia, G., Gusev, A., Finucane, H. K., Bulik-Sullivan, B. K., Pollack, S. J., … Price, A. L. (2015). Contrasting genetic architectures of schizophrenia and other complex diseases using fast variance-components analysis. *Nature Genetics*, *47*(12), 1385–1392. https://doi.org/10.1038/ng.3431

Lopes, F. M., Schröder, R., Júnior, M. L. C. da F., Zanotto-Filho, A., Müller, C. B., Pires, A. S., … Klamt, F. (2010). Comparison between proliferative and neuron-like SH-SY5Y cells as an in vitro model for Parkinson disease studies. *Brain Research*, *1337*, 85–94. https://doi.org/10.1016/j.brainres.2010.03.102

López-Carballo, G., Moreno, L., Masiá, S., Pérez, P., & Barettino, D. (2002). Activation of the phosphatidylinositol 3-kinase/Akt signaling pathway by retinoic acid is required for neural differentiation of SH-SY5Y human neuroblastoma cells. *Journal of Biological Chemistry*, *277*(28), 25297–25304. https://doi.org/10.1074/jbc.M201869200

Lorson, C. L., Rindt, H., & Shababi, M. (2010). Spinal muscular atrophy: Mechanisms and therapeutic strategies. *Human Molecular Genetics*, *19*(R1), 111–118. https://doi.org/10.1093/hmg/ddq147

Lu, K. P., Hanes, S. D., & Hunter, T. (1996). A human peptidyl-prolyl isomerase essential for regulation of mitosis. *Letters to Nature*, *380*(April), 544–547.

Lu, K. P., & Zhou, X. Z. (2007). The prolyl isomerase PIN1: A pivotal new twist in phosphorylation signalling and disease. *Nature Reviews Molecular Cell Biology*, *8*(11), 904–916. https://doi.org/10.1038/nrm2261

Maas, S., & Gommans, W. M. (2009). Identification of a selective nuclear import signal in adenosine deaminases acting on RNA. *Nucleic Acids Research*, *37*(17), 5822–5829. https://doi.org/10.1093/nar/gkp599

Maas, S, Patt, S., Schrey, M., & Rich, A. (2001). Underediting of glutamate receptor GluR-B mRNA in malignant gliomas. *Proceedings of the National*

Academy of Sciences of the United States of America, *98*(25), 14687–14692. https://doi.org/10.1073/pnas.251531398

Maas, Stefan, & Gommans, W. M. (2009). Novel Exon of Mammalian ADAR2 Extends Open Reading Frame. *PLoS ONE*, *4*(1), e4225. https://doi.org/10.1371/journal.pone.0004225

Maas, Stefan, Kawahara, Y., Tamburro, K. M., & Nishikura, K. (2006). A-to-I RNA editing and human disease. *RNA Biology*, *3*(1), 1–9. https://doi.org/10.4161/rna.3.1.2495

Macbeth, M. R., Schubert, H. L., VanDemark, A. P., Lingam, A. T., Hill, C. P., & Bass, B. L. (2005). Inositol Hexakiphosphate Is Bound in the ADAR2 Core and Required for RNA Editing. *Science*, *309*, 1534–1539.

Mackenzie, I. R. A., & Rademakers, R. (2008). The role of TDP-43 in amyotrophic lateral sclerosis and frontotemporal dementia. *Current Opinion in Neurology*, *21*(6), 693–700. https://doi.org/10.1097/WCO.0b013e3283168d1d

Mahajan, S. S., Thai, K. H., Chen, K., & Ziff, E. (2011). Exposure of neurons to excitotoxic levels of glutamate induces cleavage of the RNA editing enzyme, adenosine deaminase acting on RNA 2, and loss of GLUR2 editing. *Neuroscience*, *189*, 305–315. https://doi.org/10.1016/j.neuroscience.2011.05.027

Maier, T., Güell, M., & Serrano, L. (2009). Correlation of mRNA and protein in complex biological samples. *FEBS Letters*, *583*(24), 3966–3973. https://doi.org/10.1016/j.febslet.2009.10.036

Mannion, N., Arieti, F., Gallo, A., Keegan, L. P., & O'Connell, M. A. (2015). New Insights into the Biological Role of Mammalian ADARs; the RNA Editing Proteins. *Biomolecules*, *5*(4), 2338–2362. https://doi.org/10.3390/biom5042338

Marcucci, R., Brindle, J., Paro, S., Casadio, A., Hempel, S., Morrice, N., … O'Connell, M. a. (2011). Pin1 and WWP2 regulate *GluR2* Q/R site RNA editing by ADAR2 with opposing effects. *The EMBO Journal*, *30*(20),

4211–4222. https://doi.org/10.1038/emboj.2011.303

McManus, J., Cheng, Z., & Vogel, C. (2015). Next-generation analysis of gene expression regulation--comparing the roles of synthesis and degradation. *Molecular BioSystems*, *11*(10), 2680–2689. https://doi.org/10.1039/c5mb00310e

Miller, T. M., Pestronk, A., David, W., Rothstein, J., Simpson, E., Appel, S. H., … Cudkowicz, M. E. (2013). An antisense oligonucleotide against SOD1 delivered intrathecally for patients with SOD1 familial amyotrophic lateral sclerosis: A phase 1, randomised, first-in-man study. *The Lancet Neurology*, *12*(5), 435–442. https://doi.org/10.1016/S1474-4422(13)70061-9

Mondanizadeh, M., Arefian, E., Mosayebi, G., Saidijam, M., Khansarinejad, B., & Hashemi, S. M. (2015). MicroRNA-124 regulates neuronal differentiation of mesenchymal stem cells by targeting Sp1 mRNA. *Journal of Cellular Biochemistry*, *116*(6), 943–953. https://doi.org/10.1002/jcb.25045

Moore, S., Alsop, E., Lorenzini, I., Starr, A., Rabichow, B. E., Mendez, E., … Sattler, R. (2019). ADAR2 mislocalization and widespread RNA editing aberrations in C9orf72-mediated ALS/FTD. *Acta Neuropathologica*, *138*(1), 49–65. https://doi.org/10.1007/s00401-019-01999-w

Mu, Y., Otsuka, T., Horton, A. C., Scott, D. B., & Ehlers, M. D. (2003). Activity-dependent mRNA splicing controls ER export and synaptic delivery of NMDA receptors. *Neuron*, *40*(3), 581–594. https://doi.org/10.1016/S0896-6273(03)00676-7

Nakamura, R., Kamakura, K., & Kwak, S. (1994). Late-onset selective neuronal damage in the rat spinal cord induced by continuous intrathecal administration of AMPA. *Brain Research*, *654*(2), 279–285. https://doi.org/0006-8993(94)90490-1 [pii]

Neumann, M., Sampathu, D. M., Kwong, L. K., Truax, A. C., Micsenyi, M. C., Chou, T. T., … Lee, V. M.-Y. (2006). Ubiquitinated TDP-43 in

Frontotemporal Lobar Degeneration and Amyotrophic Lateral Sclerosis. *Science*, *314*(5796), 130–133. https://doi.org/10.1002/ana.21425.Phosphorylated

Ngoka, L. C. M. (2008). Sample prep for proteomics of breast cancer: Proteomics and gene ontology reveal dramatic differences in protein solubilization preferences of radioimmunoprecipitation assay and urea lysis buffers. *Proteome Science*, *6*, 1–24. https://doi.org/10.1186/1477-5956-6-30

Nielsen, P. E., Egholm, M., Berg, R. H., & Buchardt, O. (1991). Sequence-selective recognition of DNA by strand displacement with a thymine-substituted polyamide. *Science (New York, N.Y.)*, *254*(5037), 1497–1500. https://doi.org/10.1126/science.1962210

Nishikura, K. (2010). Functions and Regulation of RNA Editing by ADAR Deaminases. *Annual Review of Biochemistry*, *79*(1), 321–349. https://doi.org/10.1146/annurev-biochem-060208-105251

Orlandi, C., la Via, L., Bonini, D., Mora, C., Russo, I., Barbon, A., & Barlati, S. (2011). AMPA receptor regulation at the mRNA and protein level in rat primary cortical cultures. *PLoS ONE*, *6*(9). https://doi.org/10.1371/journal.pone.0025350

Ou, S.-H. I., Wu, F., Harrich, D., Garcia-Martinez, L. F., & Gaynor, R. B. (1995). Cloning and Characterization of a Novel Cellular Protein, TDP-43, That Binds to Human Immunodeficiency Virus Type 1 TAR DNA Sequence Motifs. *J. Virol.*, *69*(6), 3584–3596.

Paez-Colasante, X., Figueroa-Romero, C., Sakowski, S. a, Goutman, S. a, & Feldman, E. L. (2015). Amyotrophic lateral sclerosis: mechanisms and therapeutics in the epigenomic era. *Nature Reviews. Neurology*, *11*(5), 266–279. https://doi.org/10.1038/nrneurol.2015.57

Patterson, J. B., & Samuel, C. E. (1995). Expression and regulation by interferon of a double-stranded-RNA-specific adenosine deaminase from human cells: evidence for two forms of the deaminase. *Molecular and*

Cellular Biology, *15*(10), 5376–5388. https://doi.org/10.1128/MCB.15.10.5376

Paupard, M. C., O'Connell, M. a., Gerber, a. P., & Zukin, R. S. (1999). Patterns of developmental expression of the RNA editing enzyme rADAR2. *Neuroscience*, *95*(3), 869–879. https://doi.org/10.1016/S0306-4522(99)00431-5

Peacey, E., Rodriguez, L., Liu, Y., & Wolfe, M. S. (2012). Targeting a pre-mRNA structure with bipartite antisense molecules modulates tau alternative splicing. *Nucleic Acids Research*, *40*(19), 9836–9849. https://doi.org/10.1093/nar/gks710

Pedrioli, G. (2015). *Characterization of differentiated human neuroblastoma SH-SY5Y cell line*. Royal Holloway, University of London.

Peng, P. L., Zhong, X., Tu, W., Soundarapandian, M. M., Molner, P., Zhu, D., … Lu, Y. (2006). ADAR2-Dependent RNA Editing of AMPA Receptor Subunit GluR2 Determines Vulnerability of Neurons in Forebrain Ischemia. *Neuron*, *49*(5), 719–733. https://doi.org/10.1016/j.neuron.2006.01.025

Penn, A. C., Balik, A., & Greger, I. H. (2013). Reciprocal regulation of A-to-I RNA editing and the vertebrate nervous system. *Frontiers in Neuroscience*, *7*(7 APR), 1–6. https://doi.org/10.3389/fnins.2013.00061

Ponomarev, E. D., Veremeyko, T., Barteneva, N., Krichevsky, A. M., & Weiner, H. L. (2011). MicroRNA-124 promotes microglia quiescence and suppresses EAE by deactivating macrophages via the C/EBP-α-PU.1 pathway. *Nature Medicine*, *17*(1), 64–70. https://doi.org/10.1038/nm.2266

Ranganathan, R., Lu, K. P., Hunter, T., & Noel, J. P. (1997). Structural and functional analysis of the mitotic peptidyl-prolyl isomerase Pin1 suggests that substrate recognition is phosphorylation dependent. *Cell*, *89*, 875–886. Retrieved from http://dx.doi.org/10.1016/S0092-8674(00)80273-1

Reddi, A. R., & Culotta, V. C. (2013). SOD1 integrates signals from oxygen and glucose to repress respiration. *Cell*, *152*(1–2), 224–235.

https://doi.org/10.1016/j.cell.2012.11.046

Redler, R. L., & Dokholyan, N. V. (2013). *The Complex Molecular Biology of Amyotrophic Lateral Sclerosis (ALS)*. *Prog. mol. biol. transl. sci* (Vol. 107). https://doi.org/10.1016/B978-0-12-385883-2.00002-3.The

Regan, R. F., & Choi, D. W. (1991). Glutamate neurotoxicity in spinal cord cell culture. *Neuroscience*, *43*(2–3), 585–591. https://doi.org/10.1016/0306-4522(91)90317-H

Renton, A. E., Chiò, A., & Traynor, B. J. (2014). State of play in amyotrophic lateral sclerosis genetics. *Nature Neuroscience*, *17*(1), 17–23. https://doi.org/10.1038/nn.3584

Rosen, D. R., Siddique, T., Patterson, D., Figlewicz, D. A., Sapp, P., Hentati, A., … Deng, H. X. (1993). Mutations in Cu/Zn superoxide dismutase gene are associated with familial amyotrophic lateral sclerosis. *Nature*, *362*(6415), 59–62. https://doi.org/10.1038/362059a0

Rosenthal, J. J. C., & Seeburg, P. H. (2012). A-to-I RNA Editing: Effects on Proteins Key to Neural Excitability. *Neuron*, *74*(3), 432–439. https://doi.org/10.1016/j.neuron.2012.04.010

Rotin, D., & Kumar, S. (2009). Physiological functions of the HECT family of ubiquitin ligases. *Nature Reviews Molecular Cell Biology*, *10*(6), 398–409. https://doi.org/10.1038/nrm2690

Rowland, L. P., & Shneider, N. A. (2001). Amyotrophic Lateral Sclerosis. *New England Journal of Medicine*, *344*(22), 1688–1700. https://doi.org/10.1056/NEJM200105313442207

Rueter, S. M., Dawson, T. R., & Emeson, R. B. (1999). Regulation of alternative splicing by RNA editing, *399*(May), 75–80.

Saccon, R. A., Bunton-Stasyshyn, R. K. A., Fisher, E. M. C., & Fratta, P. (2013). Is SOD1 loss of function involved in amyotrophic lateral sclerosis? *Brain*, *136*(8), 2342–2358. https://doi.org/10.1093/brain/awt097

Sans, N., Vissel, B., Petralia, R. S., Wang, Y.-X., Chang, K., Royle, G. a, …

Wenthold, R. J. (2003). Aberrant formation of glutamate receptor complexes in hippocampal neurons of mice lacking the GluR2 AMPA receptor subunit. *The Journal of Neuroscience : The Official Journal of the Society for Neuroscience*, *23*(28), 9367–9373. https://doi.org/23/28/9367 [pii]

Sansam, C. L., Wells, K. S., & Emeson, R. B. (2003). Modulation of RNA editing by functional nucleolar sequestration of ADAR2. *Proceedings of the National Academy of Sciences of the United States of America*, *100*(24), 14018–14023. https://doi.org/10.1073/pnas.2336131100

Santos, S. D., Carvalho, A. L., Caldeira, M. V., & Duarte, C. B. (2009). Regulation of AMPA receptors and synaptic plasticity. *Neuroscience*, *158*(1), 105–125. https://doi.org/10.1016/j.neuroscience.2008.02.037

Saroff, D., Delfs, J., Kuznetsov, D., & Geula, C. (2000). Selective vulnerability of spinal cord motor neurons to non-NMDA toxicity. *Neuroreport*, *11*(5), 1117–1121. Retrieved from http://www.ncbi.nlm.nih.gov/entrez/query.fcgi?cmd=Retrieve&db=PubMed&dopt=Citation&list_uids=10790892

Sasaki, S., Yamashita, T., Hideyama, T., & Kwak, S. (2014). Unique nuclear vacuoles in the motor neurons of conditional ADAR2-knockout mice. *Brain Research*, *1550*, 36–46. https://doi.org/10.1016/j.brainres.2014.01.006

Savva, Y. A., Jepson, J. E. C., Chang, Y. J., Whitaker, R., Jones, B. C., St Laurent, G., … Reenan, R. A. (2013). RNA editing regulates transposon-mediated heterochromatic gene silencing. *Nature Communications*, *4*, 1–11. https://doi.org/10.1038/ncomms3745

Sazani, P., & Kole, R. (2003). Therapeutic potential of antisense oligonucleotides as modulators of alternative splicing. *Journal of Clinical Investigation*, *112*(4), 481–486. https://doi.org/10.1172/JCI200319547

Schmauss, C., Zimnisky, R., Mehta, M., & Shapiro, L. P. (2010). The roles of phospholipase C activation and alternative ADAR1 and ADAR2 pre-

mRNA splicing in modulating serotonin 2C-receptor editing in vivo. *Rna*, *16*(9), 1779–1785. https://doi.org/10.1261/rna.2188110

Schwanhäusser, B., Selbach, M., Thierfelder, N., Rajewsky, N., Khanin, R., & Fang, Z. (2008). Widespread changes in protein synthesis induced by microRNAs. *Nature*, *455*(7209), 58–63. https://doi.org/10.1038/nature07228

Scotter, E. L., Chen, H. J., & Shaw, C. E. (2015). TDP-43 Proteinopathy and ALS: Insights into Disease Mechanisms and Therapeutic Targets. *Neurotherapeutics*, *12*(2), 352–363. https://doi.org/10.1007/s13311-015-0338-x

Selvaraj, B. T., Livesey, M. R., Zhao, C., Gregory, J. M., James, O. T., Cleary, E. M., … Chandran, S. (2018). C9ORF72 repeat expansion causes vulnerability of motor neurons to Ca2+-permeable AMPA receptor-mediated excitotoxicity. *Nature Communications*, *9*(1). https://doi.org/10.1038/s41467-017-02729-0

Shastry, P., Basu, A., & Rajadhyaksha, M. S. (2001). Neuroblastoma cell lines - A versatile in vitro model in neurobiology. *Intern. J. Neuroscience*, *108*(020), 109–126.

Shepherd, J. D., & Huganir, R. L. (2007). The cell biology of synaptic plasticity: AMPA receptor trafficking. *Annu Rev Cell Dev Biol*, *23*, 613–643. https://doi.org/10.1146/annurev.cellbio.23.090506.123516

Shimo, T., Maruyama, R., & Yokota, T. (2017). Designing Effective Antisense Oligonucleotides for Exon Skipping. In *Duchenne Muscular Dystrophy: Methods and Protocols* (Vol. 1687, pp. 143–155). https://doi.org/10.1016/j.nmd.2013.06.373

Shimokawa, T., Mohammed Ferdous-Ur Rahman, Tostar, U., Sonkoly, E., Ståhle, M., Pivarcsi, A., … Zaphiropoulos, P. G. (2013). RNA editing of the GLI1 transcription factor modulates the output of Hedgehog signaling. *RNA Biology*, *10*(2), 321–333. https://doi.org/10.4161/rna.23343

Shipley, M. M., Mangold, C. A., & Szpara, M. L. (2016). Differentiation of the

SH-SY5Y Human Neuroblastoma Cell Line. *Journal of Visualized Experiments*, (108), 1–11. https://doi.org/10.3791/53193

Singh, N. K., Singh, N. N., Androphy, E. J., & Singh, R. N. (2006). Splicing of a critical exon of human Survival Motor Neuron is regulated by a unique silencer element located in the last intron. *Society*, *26*(4), 1333–1346. https://doi.org/10.1128/MCB.26.4.1333

Singh, N. N., Howell, M. D., Androphy, E. J., & Singh, R. N. (2017). How the discovery of ISS-N1 led to the first medical therapy for spinal muscular atrophy. *Gene Therapy*, *24*(9), 520–526. https://doi.org/10.1038/gt.2017.34

Siva, K., Covello, G., & Denti, M. A. (2014). Exon-skipping antisense oligonucleotides to correct missplicing in neurogenetic diseases. *Nucleic Acid Therapeutics*, *24*(1), 69–86. https://doi.org/10.1089/nat.2013.0461

Slavov, D., & Gardiner, K. (2002). Phylogenetic comparison of the pre-mRNA adenosine deaminase ADAR2 genes and transcripts: conservation and diversity in editing site sequence and alternative splicing patterns. *Gene*, *299*(1–2), 83–94. https://doi.org/S0378111902010168 [pii]

Smith, C. W. J., & Valcárcel, J. (2000). Alternative pre-mRNA splicing: the logic of combinatorial control. *Trends in Biochemical Sciences*, *0004*(August), 381–388. https://doi.org/10.1016/S0968-0004(00)01604-2

Smith, P. J., Zhang, C., Wang, J., Chew, S. L., Zhang, M. Q., & Krainer, A. R. (2006). An increased specificity score matrix for the prediction of SF2/ASF-specific exonic splicing enhancers. *Human Molecular Genetics*, *15*(16), 2490–2508. https://doi.org/10.1093/hmg/ddl171

Smith, R. a, Miller, T. M., Yamanaka, K., Monia, B. P., Condon, T. P., Hung, G., … Cleveland, D. W. (2006). Antisense oligonucleotide therapy for neurodegenerative disease. *J Clin Invest*, *116*(8), 2290–2296. https://doi.org/10.1172/JCI25424.2290

Sofola, O. A., Jin, P., Qin, Y., Duan, R., Liu, H., de Haro, M., … Botas, J. (2007). RNA-Binding Proteins hnRNP A2/B1 and CUGBP1 Suppress

Fragile X CGG Premutation Repeat-Induced Neurodegeneration in a Drosophila Model of FXTAS. *Neuron*, *55*(4), 565–571. https://doi.org/10.1016/j.neuron.2007.07.021

Solomon, O., Oren, S., Safran, M., Deshet-Unger, N., Akiva, P., Jacob-Hirsch, J., … Eyal, E. (2013). Global regulation of alternative splicing by adenosine deaminase acting on RNA (ADAR). *Rna*, *19*(5), 591–604. https://doi.org/10.1261/rna.038042.112

Sommer, B., Kohler, M., Sprengel, R., & Seeburg, P. H. (1991). RNA editing in brain controls a determinant of ion flow in glutamate-gated channels. *Cell*, *67*(1), 11–19. https://doi.org/0092-8674(91)90568-J [pii]

Soond, S. M., & Chantry, A. (2011). Selective targeting of activating and inhibitory Smads by distinct WWP2 ubiquitin ligase isoforms differentially modulates TGFB signalling and EMT. *Oncogene*, *30*(21), 2451–2462. https://doi.org/10.1038/onc.2010.617

Southwell, A. L., Skotte, N. H., Bennett, C. F., & Hayden, M. R. (2012). Antisense oligonucleotide therapeutics for inherited neurodegenerative diseases. *Trends in Molecular Medicine*, *18*(11), 634–643. https://doi.org/10.1016/j.molmed.2012.09.001

Spandidos, A., Wang, X., Wang, H., & Seed, B. (2009). PrimerBank: A resource of human and mouse PCR primer pairs for gene expression detection and quantification. *Nucleic Acids Research*, *38*(SUPPL.1), 792–799. https://doi.org/10.1093/nar/gkp1005

Sreedharan, J., Blair, I. P., Tripathi, V. B., Hu, X., Vance, C., Rogelj, B., … Shaw, C. E. (2008). TDP-43 mutations in familial and sporadic amyotrophic lateral sclerosis. *Science*, *249*(March), 1668–1672. https://doi.org/10.1126/science.1154584

Stamm, S., Ben-Ari, S., Rafalska, I., Tang, Y., Zhang, Z., Toiber, D., … Soreq, H. (2005). Function of alternative splicing. *Gene*, *344*, 1–20. https://doi.org/10.1016/j.gene.2004.10.022

Stephenson, M. L., & Zamecnik, P. C. (1978). Inhibition of Rous sarcoma viral

RNA translation by a specific oligodeoxyribonucleotide. *Proc Natl Acad Sci U S A*, *75*(1), 285–288. https://doi.org/10.1073/pnas.75.1.285

Sugnet, C. W., Kent, W. J., Ares, M., & Haussler, D. (2004). Transcriptome and Genome Conservation of Alternative Splicing Events in Humans and Mice. In *Pacific Symposium on Biocomputing* (Vol. 77, pp. 66–77). https://doi.org/10.1142/9789812704856_0007

Summerton, J. (1999). Morpholino antisense oligomers: The case for an RNase H-independent structural type. *Biochimica et Biophysica Acta - Gene Structure and Expression*, *1489*(1), 141–158. https://doi.org/10.1016/S0167-4781(99)00150-5

Suzuki, K., Bose, P., Leong-Quong, R. Y., Fujita, D. J., & Riabowol, K. (2010). REAP: A two minute cell fractionation method. *BMC Research Notes*, *3*(1), 294. https://doi.org/10.1186/1756-0500-3-294

Takuma, H., Kwak, S., Yoshizawa, T., & Kanazawa, I. (1999). Reduction of GluR2 RNA editing, a molecular change that increases calcium influx through AMPA receptors, selective in the spinal ventral gray of patients with amyotrophic lateral sclerosis. *Annals of Neurology*, *46*(6), 806–815. https://doi.org/10.1002/1531-8249(199912)46:6<806::AID-ANA2>3.0.CO;2-S

Tan, M. H., Li, Q., Shanmugam, R., Piskol, R., Kohler, J., Young, A. N., … Li, J. B. (2017). Dynamic landscape and regulation of RNA editing in mammals. *Nature*, *550*(7675), 249–254. https://doi.org/10.1038/nature24041

Teplova, M., Wallace, S. T., Tereshko, V., Minasov, G., Symons, a M., Cook, P. D., … Egli, M. (1999). Structural origins of the exonuclease resistance of a zwitterionic RNA. *Proceedings of the National Academy of Sciences of the United States of America*, *96*(25), 14240–14245. https://doi.org/10.1073/pnas.96.25.14240

Todd, P. K., & Paulson, H. L. (2010). RNA-mediated neurodegeneration in repeat expansion disorders. *Annals of Neurology*, *67*(3), 291–300.

https://doi.org/10.1002/ana.21948

Tomaselli, S., Bonamassa, B., Alisi, A., Nobili, V., Locatelli, F., & Gallo, A. (2013). ADAR enzyme and miRNA story: A nucleotide that can make the difference. *International Journal of Molecular Sciences*, *14*(11), 22796–22816. https://doi.org/10.3390/ijms141122796

Tomaselli, S., Locatelli, F., & Gallo, A. (2014). The RNA editing enzymes ADARs: Mechanism of action and human disease. *Cell and Tissue Research*, *356*(3), 527–532. https://doi.org/10.1007/s00441-014-1863-3

Trapnell, C., Hendrickson, D. G., Sauvageau, M., Goff, L., Rinn, J. L., & Pachter, L. (2013). Differential analysis of gene regulation at transcript resolution with RNA-seq. *Nature Biotechnology*, *31*(1), 46–53. https://doi.org/10.1038/nbt.2450

Traynor, B. J., Alexander, M., Corr, B., Frost, E., & Hardiman, O. (2003). An outcome study of riluzole in amyotrophic lateral sclerosis: A population-based study in Ireland, 1996-2000. *Journal of Neurology*, *250*(4), 473–479. https://doi.org/10.1007/s00415-003-1026-z

Twyffels, L., Gueydan, C., & Kruys, V. (2011). Shuttling SR proteins: More than splicing factors. *FEBS Journal*, *278*(18), 3246–3255. https://doi.org/10.1111/j.1742-4658.2011.08274.x

Van Den Bosch, L., & Robberecht, W. (2000). Different receptors mediate motor neuron death induced by short and long exposures to excitotoxicity. *Brain Research Bulletin*, *53*(4), 383–388. https://doi.org/10.1016/S0361-9230(00)00371-3

Van Den Bosch, L., Van Damme, P., Bogaert, E., & Robberecht, W. (2006). The role of excitotoxicity in the pathogenesis of amyotrophic lateral sclerosis. *Biochimica et Biophysica Acta (BBA) - Molecular Basis of Disease*, *1762*(11–12), 1068–1082. https://doi.org/10.1016/j.bbadis.2006.05.002

Van Den Bosch, L, Van Damme, P., Vleminckx, V., Houtte, E. Van, Lemmens, G., Missiaen, L., … Robberecht, W. (2002). An α-mercaptoacrylic acid

derivative (PD150606) inhibits selective motor neuron death via inhibition of kainate-induced Ca 2+ influx and not via calpain inhibition. *Neuropharmacology*, *42*, 706–713. Retrieved from www.elsevier.com/locate/neuropharm

Van Den Bosch, Ludo, Vandenberghe, W., Klaassen, H., Houtte, E. Van, Robberecht, W., Van Houtte, E., & Robberecht, W. (2000). Ca2+-permeable AMPA receptors and selective vulnerability of motor neurons. *Journal of the Neurological Sciences*, *180*(1–2), 29–34. https://doi.org/10.1016/S0022-510X(00)00414-7

van Es, M. A., Hardiman, O., Chio, A., Al-Chalabi, A., Pasterkamp, R. J., Veldink, J. H., & van den Berg, L. H. (2017). Amyotrophic lateral sclerosis. *The Lancet*, *6736*(17), 1–15. https://doi.org/10.1016/S0140-6736(17)31287-4

Van Ommen, G. J. B., & Aartsma-Rus, A. (2013). Advances in therapeutic RNA-targeting. *New Biotechnology*, *30*(3), 299–301. https://doi.org/10.1016/j.nbt.2013.01.005

Van Rheenen, W., Shatunov, A., Dekker, A. M., McLaughlin, R. L., Diekstra, F. P., Pulit, S. L., … Veldink, J. H. (2016). Genome-wide association analyses identify new risk variants and the genetic architecture of amyotrophic lateral sclerosis. *Nature Genetics*, *48*(9), 1043–1048. https://doi.org/10.1038/ng.3622

Vogel, C., & Marcotte, E. M. (2012). Insights into the regulation of protein abundance from proteomic and transcriptomic analyses. *Nature Reviews Genetics*, *13*(4), 227–232. https://doi.org/10.1038/nrg3185

Vuong, C. K., Black, D. L., & Zheng, S. (2016). The neurogenetics of alternative splicing. *Nature Reviews. Neuroscience*, *17*(5), 265–281. https://doi.org/10.1038/nrn.2016.27

Wahlstedt, H., Daniel, C., Enstero, M., & Ohman, M. (2009). Large-scale mRNA sequencing determines global regulation of RNA editing during brain development. *Genome Research*, *19*(6), 978–986.

https://doi.org/10.1101/gr.089409.108

Walkley, C. R., & Li, J. B. (2017). Rewriting the transcriptome: adenosine-to-inosine RNA editing by ADARs. *Genome Biology*, *18*(1), 205. https://doi.org/10.1186/s13059-017-1347-3

Wang, E. T., Sandberg, R., Luo, S., Khrebtukova, I., Zhang, L., Mayr, C., … Burge, C. B. (2008). Alternative isoform regulation in human tissue transcriptomes. *Nature*, *456*(7221), 470–476. https://doi.org/10.1038/nature07509

Wang, I. X., So, E., Devlin, J. L., Zhao, Y., Wu, M., & Cheung, V. G. (2013). *ADAR Regulates RNA Editing, Transcript Stability, and Gene Expression*. *Cell Reports* (Vol. 5). The Authors. https://doi.org/10.1016/j.celrep.2013.10.002

Wang, X., Spandidos, A., Wang, H., & Seed, B. (2012). PrimerBank: A PCR primer database for quantitative gene expression analysis, 2012 update. *Nucleic Acids Research*, *40*(D1), 1144–1149. https://doi.org/10.1093/nar/gkr1013

Wang, Y., Liu, J., Huang, B., Xu, Y., Li, J., Huang, L., … Wang, X. (2014). Mechanism of alternative splicing and its regulation (Review). *Biomedical Reports*, 152–158. https://doi.org/10.3892/br.2014.407

Wang, Z., & Burge, C. B. (2008). Splicing regulation: From a parts list of regulatory splicing elemets to an integrated splicing code. *RNA*, *14*(617), 802–813. https://doi.org/10.1261/rna.876308.802

Weier, H. U. G., George, C. X., Greulich, K. M., & Samuel, C. E. (1995). The interferon-inducible, double-stranded RNA-specific adenosine deaminase gene (DSRAD) maps to human chromosome 1q21.1-21.2. *Genomics*, *30*(2), 372–375. https://doi.org/10.1006/geno.1995.0034

Wicks, P., Abrahams, S., Masi, D., Hejda-Forde, S., Leigh, P. N., & Goldstein, L. H. (2007). Prevalence of depression in a 12-month consecutive sample of patients with ALS. *European Journal of Neurology*, *14*(9), 993–1001. https://doi.org/10.1111/j.1468-1331.2007.01843.x

Wijesekera, L. C., & Leigh, P. N. (2009). Amyotrophic lateral sclerosis. *Orphanet Journal of Rare Diseases*, *4*(1), 3. https://doi.org/10.1186/1750-1172-4-3

Winton, M. J., Igaz, L. M., Wong, M. M., Kwong, L. K., Trojanowski, J. Q., & Lee, V. M. Y. (2008). Disturbance of nuclear and cytoplasmic TAR DNA-binding protein (TDP-43) induces disease-like redistribution, sequestration, and aggregate formation. *Journal of Biological Chemistry*, *283*(19), 13302–13309. https://doi.org/10.1074/jbc.M800342200

Wisden, W., & Seeburg, P. H. (1993). Mammalian ionotropic glutamate receptors. *Curr Opin Neurobiol*, *3*(3), 291–298. https://doi.org/10.1016/0959-4388(93)90120-N

Wong, K., Lyddon, R., & Dracheva, S. (2009). TaqMan-based, real-time quantitative polymerase chain reaction method for RNA editing analysis. *Analytical Biochemistry*, *390*(2), 173–180. https://doi.org/10.1016/j.ab.2009.04.011

Wright, A., & Vissel, B. (2012). The essential role of AMPA receptor GluR2 subunit RNA editing in the normal and diseased brain. *Frontiers in Molecular Neuroscience*, *5*(April), 1–13. https://doi.org/10.3389/fnmol.2012.00034

Xie, H., Hu, L., & Li, G. Y. (2010). SH-SY5Y human neuroblastoma cell line: in vitro cell model of dopaminergic neurons in Parkinson's disease. *Chin Med J*, *123*(8), 1086–1092. https://doi.org/10.3760/cma.j.issn.0366-6999.2010.08.021

Yamashita, T., Chai, H. L., Teramoto, S., Tsuji, S., Shimazaki, K., Muramatsu, S. I., & Kwak, S. (2013). Rescue of amyotrophic lateral sclerosis phenotype in a mouse model by intravenous AAV9-ADAR2 delivery to motor neurons. *EMBO Molecular Medicine*, *5*, 1710–1719. https://doi.org/10.1002/emmm.201302935

Yamashita, T., Hideyama, T., Hachiga, K., Teramoto, S., Takano, J., Iwata, N., … Kwak, S. (2012). A role for calpain-dependent cleavage of TDP-43

in amyotrophic lateral sclerosis pathology. *Nature Communications*, *3*, 1307. https://doi.org/10.1038/ncomms2303

Yang, L., Huang, P., Li, F., Zhao, L., Zhang, Y., Li, S., … Liu, Y. (2012). c-Jun amino-terminal kinase-1 mediates glucose-responsive upregulation of the RNA editing enzyme ADAR2 in pancreatic beta-cells. *PloS One*, *7*(11), 1–11. https://doi.org/10.1371/journal.pone.0048611

Yeo, G., Holste, D., Kreiman, G., & Burge, C. B. (2004). Variation in alternative splicing across human tissues. *Genome Biology*, *5*(10), 1–15.

Zarei, S., Carr, K., Reiley, L., Diaz, K., Guerra, O., Altamirano, P., … Chinea, A. (2015). A comprehensive review of amyotrophic lateral sclerosis. *Surgical Neurology International*, *6*(1), 171. https://doi.org/10.4103/2152-7806.169561

Zetterström, P., Stewart, H. G., Bergemalm, D., Jonsson, P. A., Graffmo, K. S., Andersen, P. M., … Marklund, S. L. (2007). Soluble misfolded subfractions of mutant superoxide dismutase-1s are enriched in spinal cords throughout life in murine ALS models. *Proceedings of the National Academy of Sciences of the United States of America*, *104*(35), 14157–14162. https://doi.org/10.1073/pnas.0700477104

Zhang, Z., Almeida, S., Lu, Y., Nishimura, A. L., Peng, L., Sun, D., … Gao, F. B. (2013). Downregulation of MicroRNA-9 in iPSC-Derived Neurons of FTD/ALS Patients with TDP-43 Mutations. *PLoS ONE*, *8*(10). https://doi.org/10.1371/journal.pone.0076055

Zinshteyn, B., & Nishikura, K. (2010). Adenosine-to-inosine RNA editing. *Wiley Interdiscip Rev Syst Biol Med*, *1*(2), 202–209. https://doi.org/10.1002/wsbm.10.Adenosine-to-inosine

Zufiría, M., Gil-Bea, F. J., Fernández-Torrón, R., Poza, J. J., Muñoz-Blanco, J. L., Rojas-García, R., … de Munain, A. L. (2016). ALS: A bucket of genes, environment, metabolism and unknown ingredients. *Progress in Neurobiology*. https://doi.org/http://dx.doi.org/10.1016/j.pneurobio.2016.05.004